CHANGES IN MOLECULAR INTEGRITY OF CHLOROPLAST DNA AND MITOCHONDRIAL DNA IN MAIZE

Rachana A. Kumar

A dissertation

submitted in partial fulfillment of the

requirements for the degree of

Doctor of Philosophy

University of Washington

2014

Reading Committee:

Arnold J. Bendich, Chair

Elizabeth Van Volkenburgh

Takato Imaizumi

Program Authorized to Offer Degree:

Biology

University Of Washington

ABSTRACT

Changes in molecular integrity of chloroplast DNA and mitochondrial DNA in maize

Rachana A. Kumar

Chair of the Supervisory Committee:

Professor Arnold J. Bendich

Biology

Genome copy number is typically two for the nucleus in diploid plants and animals, regardless of developmental or environmental changes, and nuclear DNA is stable. For genomes in mitochondria and chloroplasts, I report that their copies and their DNA integrity change greatly during development in maize. In order to accurately determine organellar genome number, I devise new experimental procedures to overcome limitations of the standard PCR-based methods. First, I describe a new experimental procedure to avoid the confusing influence of nuclear-located organellar DNA (orgDNA) sequences on authentic orgDNA using the PCR. The procedure includes designing organelle-specific primers using bioinformatics methods and methylation-sensitive PCR. In addition to copy number determination, this procedure should be useful in a wide range of applications, including phylogenetic and functional analyses, as well as in a clinical setting. Further, I devise a novel long-PCR method to quantify DNA damage, molecular integrity, copy number, and amount of repair for both plastid DNA and mitochondrial

DNA during maize leaf development. I find a developmental increase in orgDNA damage and molecules with impediments that prevent amplification by *Taq* polymerase, with light causing the greatest change. I also find a hundred- to a thousand-fold decrease in functional copies of orgDNA during leaf development. I suggest that the changes in molecular integrity of orgDNA during development are due to oxidative stress from energy metabolism that damages orgDNA. As leaves develop, the maintenance of high-copy orgDNA lessens, damage persists, and orgDNA is degraded. Furthermore, I confirm a hypothesis that oxidative stress causes DNA damage by studying differences in orgDNA between mesophyll and bundle sheath cells. Higher ROS levels occur in mesophyll due to the light-dependent reactions of photosynthesis. When compared to mesophyll cells, bundle sheath cells have less orgDNA damage and a higher percentage of unimpeded orgDNA. In addition, the orgDNA is more fragmented in mesophyll than bundle sheath cells. The data indicate that higher levels of ROS in mesophyll than bundle sheath cause orgDNA damage. The similar trend in orgDNA properties (copies, damage, and repair) for both plastid DNA and mitochondrial DNA suggests inter-organellar signaling and common regulation by nuclear genes.

Table of Contents

List of Figures

List of Tables

DEDICATION

I dedicate this dissertiation work to my husband, Ajay kumar, who has been a constant source of support and encouragement.

ACKNOWLEDGEMENTS

I am grateful to have had enormous support during my tenure as a PhD student. I would like to express my appreciation to my advisor, Dr. Arnold Bendich for believing in me. He encouraged me to think independently and critically. I am thankful for his support and accommodating me while I was fulfilling my maternal duties.

I am grateful to have an excellent mentor and friend as Dr. Delene Oldenburg. She was always available and willing to help me with my projects. I truly appreciate her time, ideas and critical discussions. Her feedback on my experiments was instrumental in optimizing and troubleshooting techniques. She is a great listener and a good critic! I also appreciate her collegiality that helped me flourish as an independent scientist and made my stay in the lab very enjoyable. Here, I would also like to thank my lab mates, Anna Kovac, Andy Nam, Akiko Carver, and Vihn-Thuy for fun times, discussions and laughs. This was very refreshing and helpful during stressful times.

I would like to thank my first advisor in grad school, Dr. Veronica Di Stilio. She trained me in scientific skills as well as provided lab space and supplies for my experiments throughout. I would like to thank my committee, Dr. Elizabeth Volkenburgh and Dr. Takato Imazumi for their useful comments on my research projects. Liz has always been very encouraging and offered great personal as well as professional advice.

Many people in the department were helpful in various aspects of my projects and navigating through grad school. I would like to thank Dave Hurley for technical assistance, Doug Ewing for help on growing maize, and Bruce Godfrey for providing technical support with instruments. Finally, I would like to thank Judy Farrow and Marissa Adamczyk for helping me

with grad school requirements.

I am thankful to my long time mentor and role model, Dr. Hema Sane, for passing her passion for science and her enthusiasm on to me. I am grateful to her for providing a strong foundation in science which was critical for my research. She has guided me over the years, inspiring me to follow my love for science and pursue a PhD. I am very fortunate to have a loving and supportive husband, Ajay Kumar, whose constant motivation made this accomplishment possible. He also provided his computer expertise that was very helpful during my dissertation work. I would also like to thank a newly added member of my family, Ishan Kumar, for allowing me to finish my thesis writing.

Finally, I would like to thank Dr. Charles Laird and Judy Laird for opening their hearts and providing my family a home away from home.

Chapter 1

DISTINGUISHING AUTHENTIC MITOCHONDRIAL AND PLASTID DNAS FROM SIMILAR DNA SEQUENCES IN THE NUCLEUS USING THE POLYMERASE CHAIN REACTION

1.1 Abstract

DNA sequences similar to those in the organellar genomes are also found in the nucleus. These non-coding sequences may be co-amplified by PCR with the authentic organellar DNA sequences, leading to erroneous conclusions. To avoid this problem, we describe an experimental procedure to prevent amplification of this "promiscuous" DNA when total tissue DNA is used with PCR. First, primers are designed for organelle-specific sequences using a bioinformatics method. These primers are then tested using methylation-sensitive PCR. The method is demonstrated for both end-point and real-time PCR with *Zea mays*, where most of the DNA sequences in the organellar genomes are also present in the nucleus. We use this procedure to quantify those nuclear DNA sequences that are near-perfect replicas of organellar DNA. This method should be useful for applications including phylogenetic analysis, organellar DNA quantification and clinical testing.

1.2 Introduction

Although it came as a great surprise when organellar-like DNA sequences were first discovered in the nucleus (du Buy and Riley, 1967; Timmis and Scott, 1983), such "promiscuous" DNA is now commonly found among eukaryotes (Bensasson *et al.*, 2001; Hazkani-Covo *et al.*, 2010; Timmis *et al.*, 2004). These non-coding sequences are known as nuclear mitochondrial DNA sequences (NUMTs) and nuclear plastid DNA sequences (NUPTs).

NUMTs and NUPTs might be co-amplified with authentic mitochondrial DNA (mtDNA) and plastid DNA (ptDNA) using the polymerase chain reaction (PCR) and total DNA extracted from tissue samples. Thus, inferences concerning functional organellar DNA drawn from PCR-based analysis of total tissue DNA may be erroneous. Our goal was to devise a method that can distinguish between authentic organellar DNA and NUPTs/NUMTs, so that changes in organellar DNA during development could be quantified. Other applications for such a method include phylogenetic analysis and clinical testing.

Here, we report a new experimental procedure to avoid the confusing influence of NUMTs and NUPTs when DNA from whole tissue samples is used with PCR. We first describe a bioinformatics method to find organelle-specific sequences for designing primers. Then we describe a method to test the primers using methylation-sensitive PCR (MeS-PCR). We demonstrate the use of this procedure with *Zea mays* var. B73, where >99% of ptDNA and ~95% of mtDNA sequences are also represented in the nucleus. Finally, we use real-time quantitative PCR (qPCR) to quantify the minor fraction of NUPTs and NUMTs that are nearly perfect replicas of authentic organellar DNA.

1.3 Materials and methods

1.3.1 *Plant material and DNA preparation*

Zea mays (inbred line B73) seeds were imbibed overnight and grown in a soil: vermiculite (1:1) mixture for 10 days under 16 h light/8 h dark photoperiods. Entire seedlings were harvested, soaked for three min in 0.5% (v/v) sarkosyl to reduce surface microbial contamination, rinsed with tap water and then with distilled water. Sections (0.5 cm) from the middle of the first leaf blade from several plants were combined and frozen in liquid nitrogen before extracting total tissue DNA using a Nucleon PhytoPure genomic DNA extraction kit (GE

healthcare).

1.3.2 *Finding organelle-specific sequences*

The maize nuclear genome sequence was downloaded from http://www2.genome.arizona.edu/genomes/maize. Then, the Blastn program (word size=11, match reward=2, mismatch penalty=-3, gap open/extension=5/2) was run using the ptDNA (NC_001666) as query and the maize nuclear genome (B73 RefGen_v2, AGI) as subject. This provided alignments between nuclear and ptDNA sequences present as NUPTs. The Blastn program was again run with ptDNA as query and mtDNA (NC_007982) as subject to identify alignments between plastid and mitochondrial DNA sequences: MIPTs (mitochondrial plastid DNA sequences). Combined NUPTs and MIPTs were then subtracted from the plastid genome sequence to give the sequences specific to the plastid genome. A computer program was developed to perform this process. An analogous procedure was used to identify the sequences specific to mitochondria, except that mtDNA was used as query with the maize nuclear genome and ptDNA as subjects.

1.3.3 *Designing primers*

Two approaches were used to design primers to amplify organelle-located DNA but not NUPTs or NUMTs. In the first, many primers were designed using Primer3 for maize ptDNA. These primers were then tested using the Blastn program for near-exact matches (Oligos) at http://www.maizesequence.org/blast. The program finds matches for the primers in the maize nuclear genome database. The primers having neither hits nor complete alignment with the nuclear sequence were selected for further testing. In the second approach, organelle-specific sequences were used to design the primers. This procedure was suitable for mtDNA because

some of these sequences are located only in the mitochondria. For ptDNA, however, the nucleus contains NUPTs with sequences similar (but not necessarily identical) to >99% of the sequences in the plastids. Thus, for designing primers specific to plastid-located ptDNA, we relied mostly on the first approach. Finally, only those primers that span restriction sites for methylation-sensitive restriction enzymes (*Hpa*II, for example) were selected.

1.3.4 *Testing the specificity of the primers*

To test the specificity of the primers, we employed MeS-PCR. In this assay, 0.8 µg of total tissue DNA was digested with the methylation-sensitive enzyme, *Hpa*II, for 2 h at 37°C, while 0.8 µg of the same DNA was left undigested. *Hpa*II is a frequent cutter, having 226 recognition sites (5'-CCGG-3') in the plastid genome and 1445 sites in mitochondrial genome. *Hpa*II cleaves both organellar DNAs because they are unmethylated, but does not cleave NUPTs or NUMTs containing 5-methylcytosine in the recognition site. PCR was carried out on digested and undigested total tissue DNA using the primers to be tested for their specificity in amplifying only organellar DNA. The annealing temperature for each primer set was determined using gradient PCR, and the maximum (and optimum) annealing temperature was selected for doing MeS-PCR. The gel bands found with digested total tissue DNA represented amplification products of NUPTs or NUMTs. Hence, primers that amplify NUPTs or NUMTs cannot distinguish genuine organellar DNA from nucleus-located organellar DNA, whereas primers that do not produce a gel band are specific to the organellar DNAs. It was important to optimize PCR conditions, especially the cycle number and annealing temperature, to identify primers that amplified only genuine organellar DNAs. A typical PCR reaction mix included 1X PCR buffer, 1.5 mM $MgCl_2$, 0.2 mM dNTP, 0.4 µM each primer, 2.5 U Taq DNA polymerase (Fermentas) and 40 ng of template.

1.3.5 *Quantifying nucleus-located organellar DNA using qPCR*

To quantify NUPTs and NUMTs, we used real-time qPCR with both *Hpa*II-digested DNA and undigested DNA. We designed primers spanning *Hpa*II or *Cla*I restriction sites. Like *Hpa*II, *Cla*I is a methylation-sensitive restriction enzyme. It has 67 recognition sites (5'-ATCGAT-3') in the plastid genome. The *ClaI*-digested DNA was used as a template only with the petA_F1 and petA_R1 primer set, whereas *Hpa*II-digested DNA was used with all of the other qPCR primer sets. Three replicates of each primer set were included in each experiment, and each experiment was repeated twice: six replicates per primer set. For real-time qPCR, iQ^{TM} SYBR Green Supermix (Bio-Rad Laboratories, Inc., Hercules, CA) was used in a 25 µl reaction containing 0.4 µM primer sets and template DNA. The qPCR program included an initial denaturation step at 94^{o}C, followed by 50 cycles of 15s denaturation at 94^{o}C, 15s annealing at 57^{o}C and a 20s extension step at 72^{o}C. A melting curve analysis was performed from 65^{o}C to 95^{o}C to confirm the amplification of a single product. Fluorescence during qPCR was monitored using the Chromo4 real time detection system (Bio-Rad Laboratories, Inc., Hercules, CA). The qPCR data were analyzed using the Opticon Monitor 3 program (Bio-Rad Laboratories, Inc., Hercules, CA), and organellar DNA copy number per nuclear genome was computed using the $2^{-\Delta ct}$ method (Pfaffl, 2001). The percentage of NUPTs/NUMTs was calculated by comparing the organellar DNA copy number obtained with the digested and undigested DNA.

1.4 Results

Our objective was to use PCR to assess the copy number of organellar genomes during development in maize. To do this we had to design primers that would amplify organellar DNA without also amplifying NUPTs or NUMTs. Our analysis using the Blastn program, however, shows that for the B73 inbred line of maize, >99% of the plastid genomic sequences are present

as NUPTs, whereas ~95% of mtDNA sequences are present as NUMTs. The size of the inserted NUPTs and NUMTs is highly variable, and their total length (2048 kb and 2913 kb, respectively) represents 15 and 5 genome equivalents, respectively, per haploid nuclear genome (Figure 1.1). A two-step experimental design was employed to overcome these potential difficulties and obtain organelle-specific PCR (Figure 1.1). We used two approaches to obtain primers that specifically amplify organellar DNA and tested them using MeS-PCR.

For ptDNA, we designed primers using Primer3 and then used the Blastn program to determine whether these primer sequences aligned with the nuclear DNA (Approach 1 in Figure 1.1). The design of mtDNA primers was less tedious because organelle-specific regions of mtDNA were more extensive (Approach 2 in Figure 1.1). The regions useful for primer design that are present only in the plastids and only in the mitochondria are shown in Table 1.2. Table 1.3 shows one pair of primers that did not distinguish sequences in the organelles from those in the nucleus, as well as 3 (for mitochondria) and 4 (for plastids) pairs of the primers that did achieve this distinction.

Primers were first tested using a temperature gradient to determine the optimum annealing temperature for PCR amplification. We sought a temperature at which a perfectly base-paired duplex between primer and authentic organellar template would be stable, but a mismatched duplex (primer and NUPT/NUMT) would not be stable. The basis for this reasoning is that NUPTs, NUMTs and MIPTs accumulate mutations when compared with their respective organellar DNAs (Table 1.6).

Table 1.1 Analysis of inserted organellar DNA sequences.

Parameter	NUPTs	NUMTs	MIPTs
No. of insertions	6799	10386	81
Largest insert (kb)	34.5	106.6	12.6
Shortest insert (bp)	34	35	35
No. of inserts >100 bp	4491	5596	26
No. of inserts >1 kb	282	293	11
Total size of insertions (kb)	2048	2913	52.2

NUPTs, NUMTs, and MIPTs represent 15, 5, and 0.1 genome equivalents, respectively, per nuclear or mitochondrial genome. For B73 maize, the genome sizes are 2.3 Gb for nucleus (Schnable *et al.*, 2009), 140 kb for plastid (Maier *et al.*, 1995), and 570 kb for mitochondrion (Lonsdale *et al.*, 1984).

Table 1.2 Blastn data analysis showing organellar DNA-specific sequences.

Accession[a]	Coordinates on the genome	Size (bp)
ptDNA NC_001666	11580-11674	95
	14326-14369	44
mtDNA NC_007982	8611-10088	1478
	78966-80560	1595
	95850-96848	999
	252700-253529	830
	516459-517631	1173

[a] All the ptDNA-specific sequences are shown, whereas only selected mtDNA-snpecific sequences are shown. A complete list of the mtDNA-specific sequences is given in Table 1.7.

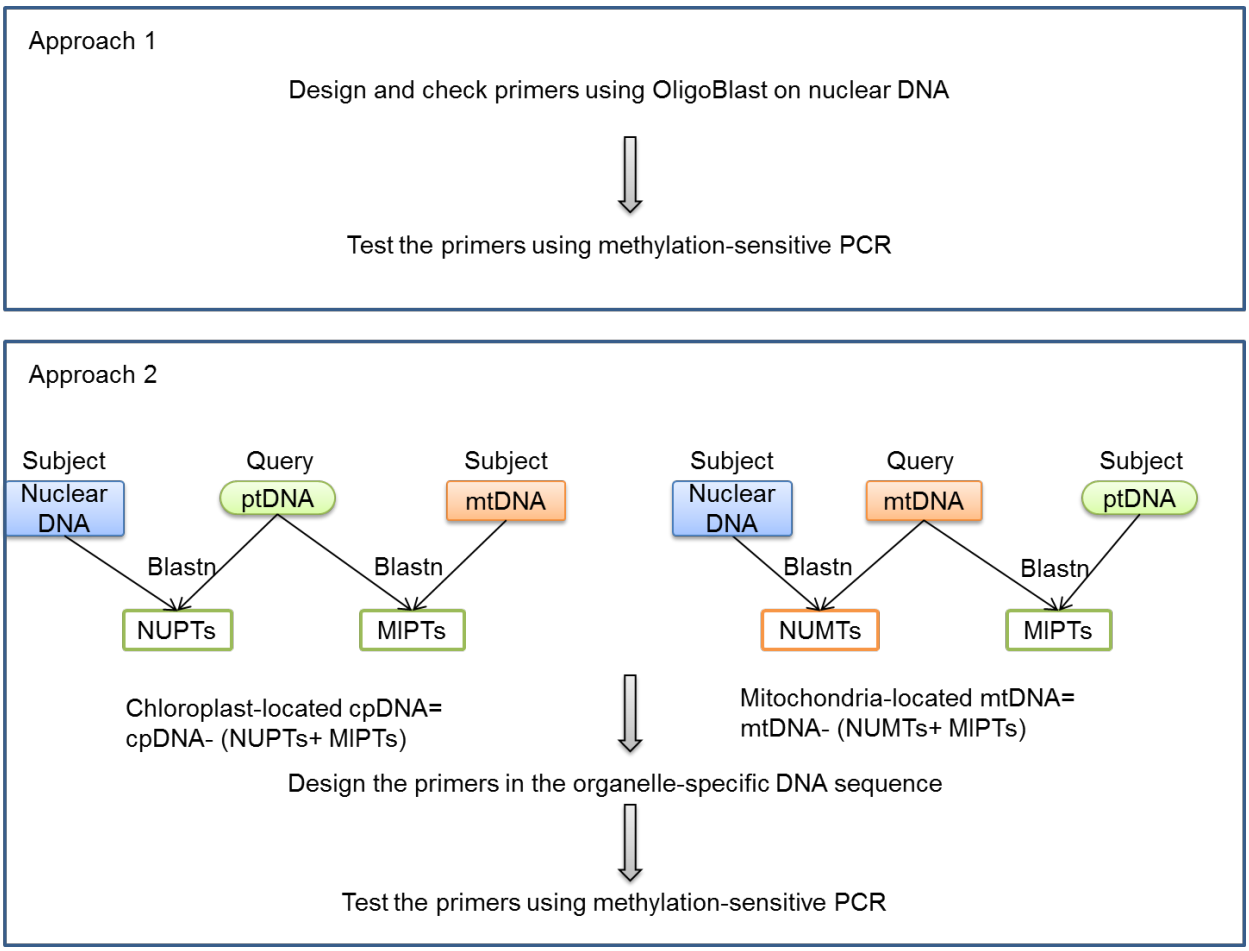

Figure 1.1 Two-step design for primers

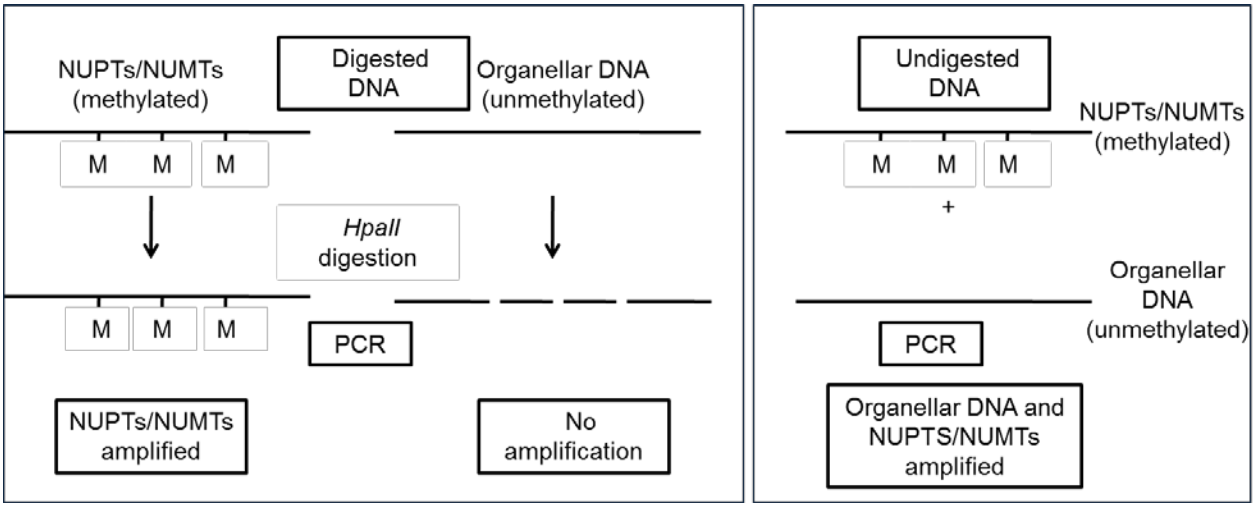

Figure 1.2 Rationale for methylation-sensitive PCR

Table 1.3 Primers, annealing temperatures, and number of amplification cycles used for end-point PCR.

Primer name[a]	Sequence (5' to 3')	Amplicon size (bp)	Amplicon coordinates on NC_007982	Ta (°C)	Number of cycles
mtDNA primers					
cox2_F1	ACGCAGCAACACCTATGATG	984	542042-543025	56	25
cox2_R1	CCCCTCTTGAGTCACCCTTA				
nad4_F1	GAAAAAGGGCTGAAGAAACCAGTC	900	79263-80162	61	25
nad4_R1	AGCAAGCGTAGGCAACCAAAC				
matr_F1	CCTGGGTCTTCTTCGGCTAATG	1126	268093-269218	56	25
matr_R1	AGACAACAGAGCCCTCATAGTGG				
ccmfc_F1	GCGTTGCGAACACTTTCAT	754	95704-96457	58	25
ccmfc_R1	GTAGTAGTCGTGACCAACAGC				
Primer name[a]	Sequence (5' to 3')	Amplicon size (bp)	Amplicon coordinates on NC_001666	Ta (°C)	Number of cycles
ptDNA primers					
rpoC1_F1	TCCTACCTAATGGGGAAGT	830	24812-25641	58	25
rpoC1_R1	GTTCCGACGGATAACTCTC				
psbC_F2	CATTCTTTGGTTATGTATGGCAAG	1136	10525-11660	58	23
psbC_R2	TTGAATACATTTGCTTCTTTCTATCT				
psbC_F3	CAAGGCTCTTTATTTTGGCG	1023	10622-11644	62	23
psbC_R3	CTTTCTATCTATGTTTTTCTTTGTGC				
atpA_F1	AATTCTCCGCGAACGTATTG	1085	36605-37691	62	22
atpA_R1	TTTGAGCTGCGGATCCTACT				
rps14_F1	ATCTTGTTGCACCCGGTAAC	960	38674-39635	62	25
rps14_R1	GCGGCGGTACTTGTGATATT				

[a] The *cox2* and *rpoC1* primers did not distinguish organellar sequences from those in the nucleus (NUMTs and NUPTs); all others primers did distinguish sequences located in mitochondria or plastids from NUMTs and NUPTs.

In the second design step, the primers were tested to determine whether they amplify NUPTs/NUMTs by MeS-PCR (Figure 1.2). For plants in general, both organellar genomes are nearly unmethylated, whereas most of the NUPTs/NUMTs are extensively methylated (Kleine *et al.*, 2009). Methylation in maize NUPTs/NUMTs was investigated by comparing the frequencies of 12 types of nucleotide substitutions, as described previously (Huang *et al.*, 2005; Noutsos *et al.*, 2005). From the high prevalence of C→T and G→A transitions (Figure 1.6), we infer that the NUPTs/NUMTs in maize are extensively methylated, as inferred previously for *Arabidopsis* and rice (Huang *et al.*, 2005; Noutsos *et al.*, 2005). Hence, when the total tissue DNA is digested with *Hpa*II, only the organellar genomes are cleaved, leaving the NUPTs/NUMTs intact. The primers are designed to span *Hpa*II restriction sites, so that any amplified product with *Hpa*II-digested DNA represents NUPTs/NUMTs. On the other hand, when the primers do not produce a gel band amplification product with *Hpa*II-resistant DNA, it can be concluded that the primers are specific for genuine organellar DNA.

Under optimized PCR conditions of annealing temperature and number of amplification cycles (Table 1.3), primers can distinguish between the NUPTs and authentic ptDNA. No band of amplified DNA is found for *Hpa*II-digested DNA (lanes 4, 6, 8 and 10 of Figure 1.3), whereas a band of amplified DNA of the expected size is found for the undigested DNA (lanes 5, 7, 9 and 11 of Figure 1.3). On the other hand, the primer that was intentionally designed for a ptDNA region that is also present in the nucleus did produce a band of NUPT for the *Hpa*II-digested DNA (lane 2, Figure 1.3), as well as the product from the undigested DNA (lane 3, Figure 1.3).

Using the same procedures, primers designed to amplify only mtDNA were able to distinguish between the NUMTs and DNA located within mitochondria (lanes 4, 6 and 8 of Figure 1.4). The primer set intentionally designed to be unable to distinguish between NUMTs

and mtDNA amplified both types of sequences (lane 2, Figure 1.4). In summary, the results show that our two-step experimental design allows genuine organellar DNA to be distinguished from NUPTs and NUMTs using the PCR.

Finally, we quantified the nucleus-located organellar DNA using qPCR and total tissue DNA digested or not digested with methylation-sensitive restriction enzymes. The primers spanned *Hpa*II or *Cla*I (used only for *petA*) restriction sites (Table 1.4). The amount of organellar-like DNA obtained using undigested DNA represents both NUPTs/NUMTs and true organellar DNA, whereas digested DNA yields PCR products only from NUPTs/NUMTs that are methylated. Any recognition sites that might not be methylated, so as to prevent cleavage by *Hpa*II or *Cla*I would lead to an underestimation of NUPT/NUMT copy number, and any methylation in true organellar DNA would lead to overestimation. Using four different primers for ptDNA, the NUPT copy number per haploid nuclear genome was 5 to 23 (Table 1.5), representing 0.3 to 1.4% of the total copy number obtained with undigested DNA. Using three mtDNA primers, the copy number was 0.5 to 9, representing 1.4 to 15% of the copy number from undigested DNA.

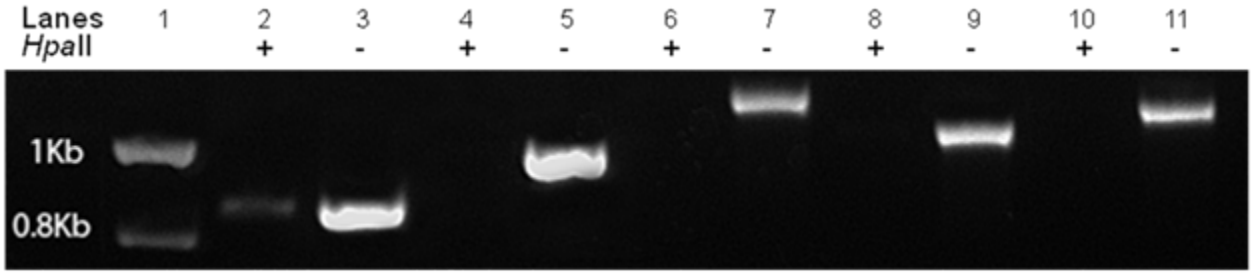

Figure 1.3 Methylation-sensitive PCR results for ptDNA primers

Lane 1: DNA size markers. Lanes 2, 4, 6, 8 and 10: HpaII-digested DNA amplified with rpoC1_F1+R1, rps14_F1+R1, psbC_F2+R2, psbC_F3+R3 and atpA_F1+R1 primer sets, respectively. Lanes 3,5,7,9 and 11: undigested DNA amplified with rpoC1_F1+R1, rps14_F1+R1, psbC_F2+R2, psbC_F3+R3 and atpA_F1+R1 primer sets, respectively.

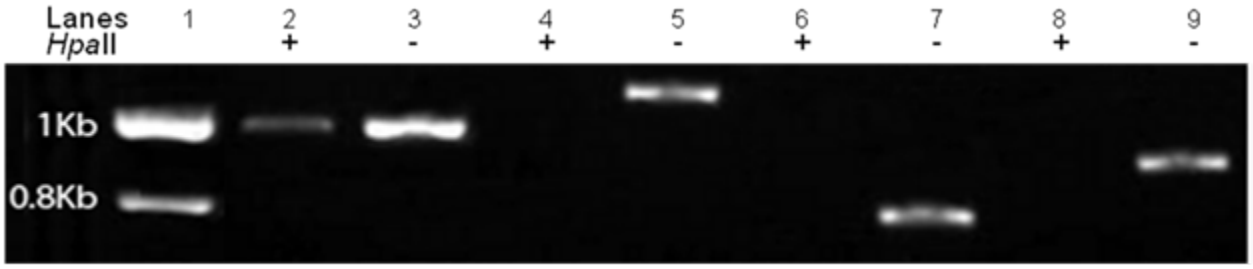

Figure 1.4 Methylation-sensitive PCR results for mtDNA primers

Lane 1: DNA size markers. Lanes 2, 4, 6 and 8: *Hpa*II-digested DNA amplified with cox2_F1+R1, matr_ F1+R1, ccmfc_F1+R1 and nad4_F1+R1, respectively. Lanes 3, 5, 7 and 9: undigested DNA amplified with cox2_F1+R1, matr_ F1+R1, ccmfc_F1+R1 and nad4_F1+R1, respectively.

Table 1.4 Primers used for qPCR.

Primer name	Sequence (5’ to 3’)	Amplicon size (bp)	Amplicon coordinates on NC_007982
mtDNA primers			
cox2_F2	ACAGCAGTGGCATACAACTTTGG	141	542658-542798
cox2_R2	AAGGAGGAGCAGGAACAACAGG		
ccmfc_F2	TCAGCGAAGCGTGAGCGG	172	96200-96371
ccmfc_R2	AACAAGCACCACTCGACGAGG		
nad4_F2	GCAAAAGTCCTTCCACGGCA	187	79976-80162
nad4_R1	AGCAAGCGTAGGCAACCAAAC		
Primer name	Sequence (5’ to 3’)	Amplicon size (bp)	Amplicon coordinates on NC_001666
ptDNA primers			
psbA_F1	CAATGTCAACCAAGCCAGC	156	1263-1418
psbA_R2	GACTAGTTCCGGGTTCGAG		
petA_F1	TGGTTAAAGGAACAGATGATTCG	157	61512-61668
petA_R1	AATGGCAATTGGCACATACA		
psbC_F1	CTACCACGTGGAAACGCTCT	155	10121-10275
psbC_R1	ATACGATTAATCCGGCATGG		
rps14_F1	ATCTTGTTGCACCCGGTAAC	127	38674-38800
rps14_R2	CCTACACGCCTTCATCGACGTT		
Primer name	Sequence (5’ to 3’)	Amplicon size (bp)	
Nuclear DNA primers			
Zmadh1_F3	GGAGGCGTTTCTTTCTTTGA	115	
Zmadh1_R3	GCCCTTGCTAAACACGGTAA		

Table 1.5 Quantification of nucleus-located organellar DNA using qPCR.

Primer pair used	NUPTs or NUMTs per haploid nuclear genome[a]	% NUPTs or NUMTs[a]
mtDNA primers		
cox2_F2 and cox2_R2	9.1 +/-2.2	14.7 +/-1.5
ccmfc_F2 andccmfc_R2	0.5 +/-0.2	1.4 +/-0.1
nad4_F2 and nad4_R1	0.9 +/-0.3	2 +/-0.4
ptDNA primers		
petA_F1 and petA_R1[b]	21.1 +/-1.7	1.6 +/-0.5
psbC_F1 and psbC_R1	4.6 +/-0.8	0.3 +/-0.1
psbA_F1 and psbA_R2	23.1 +/-2.6	1.4 +/-0.2
rps14_F1 and rps14_R2	10.9 +/-0.5	0.7 +/-0.3

[a] Averages of six determinations, with standard errors. These values may greatly underestimate the true values because of alignment discontinuity (Figure 1.5) and possible tandem repeats, as discussed in the text. The percentage of organellar-like DNA in the nucleus (% NUPTs or NUMTs) was determined as described in Materials and methods. Note that the % value for *cox2* is much larger than for the other primer pairs and that the degree of alignment discontinuity for *cox2* is the smallest of all seven amplicons analyzed (Figure 1.5).

[b] *Cla*I-digested DNA was used. *Hpa*II-digested DNA was used for all other primer pairs.

1.5 Discussion

The presence of NUPTs and NUMTs in the nuclear genome can confound the interpretation of DNA sequence data when investigating species relatedness and phylogeny, as well as organellar DNA function. The rise of PCR has permitted facile data acquisition from many tissues and individuals using total DNA quickly extracted from small amounts of material, thus avoiding the lengthy procedures of organelle purification. The assumption, of course, is that potentially troublesome effects could be ignored because NUPTs and NUMTs are far outnumbered by authentic organellar sequences or because amplification from NUPTs and NUMTs could be avoided (Arthofer *et al.*, 2010; Bensasson *et al.*, 2001; Sorenson and Quinn,

1998) by enrichment of organellar DNA (Sorenson and Quinn, 1998), judicious sequence analysis (Song *et al.*, 2008; Zheng *et al.*, 2011), or performing long or reverse transcriptase PCR (Collura *et al.*, 1996). These procedures do not assure complete avoidance of NUPTs/NUMTs, however, and they require extensive post-amplification analysis. Furthermore, these procedures are not effective for organellar DNA quantification, small tissue samples, and when "organellar DNA" is located mainly in the nucleus (Zheng *et al.*, 2011) or present as long runs of NUPT/NUMT sequence.

We have devised a novel procedure for designing primers specific for DNA within plastids and mitochondria. We used maize, a species for which our Blastn analysis shows that >99% of the plastid genome sequences are also found in the nucleus, including long stretches (>3 kb) of continuous NUPTs previously identified by fluorescence *in situ* hybridization (Roark *et al.*, 2010). We employed MeS-PCR, previously used in epigenetics research (Hashimoto *et al.*, 2007; Singersam *et al.*, 1990), to test the specificity of the primers because authentic organellar DNAs are nearly unmethylated, whereas NUPTs and NUMTs are extensively methylated (Huang *et al.*, 2005; Kleine *et al.*, 2009; Noutsos *et al.*, 2005). Our data indicate hypermethylation of NUPTs and NUMTs in the nuclear genome of maize (see Figure 1.6). The primers in Tables 3 and 4 may or may not be specific with other maize inbreds because of the variation in NUPT/NUMT frequency and chromosomal location among inbreds (Lough *et al.*, 2008; Roark *et al.*, 2010). Nonetheless, primer specificity can be tested even with species for which the nuclear genome has not been sequenced because the regions between the primer-binding sites can be subjected to MeS-PCR. We have also created a computer program to identify the organellar DNA-specific sequences, as well as sequence changes ("mutations") in NUPTs/NUMTs when compared with the respective organellar DNA.

The fraction of organellar-like DNA present as NUPTs/NUMTs can, in principle, be determined by either methylation-sensitive blot hybridization or by the quantitative MeS-PCR method described here. For *psbA*, we found 80-95% as NUPTs using blot hybridization with a 664-bp probe (Zheng *et al.*, 2011), but only 1.4% using MeS-PCR (Table 1.5). This large discrepancy can be attributed to two factors. First, most of the many NUPT sequences representing *psbA* are discontinuous and do not include regions that would be amplified with our primer pair (Figure 1.5), whereas this feature would have little effect in the blot hybridization method. Second, any tandemly repeating fragments of the *psbA* gene in the nuclear genome would probably not have been recorded in the presentation of the maize nuclear genome sequence. Any such tandem repeats that do not include the 156-bp sequence between our PCR primers would still contribute to the blot hybridization signal, but would not appear as high-copy DNA with qPCR. Thus, we conclude that MeS-PCR is far more sensitive to the fragmented nature of non-functional NUPTs than is blot hybridization and that the copy numbers derived from MeS-PCR data in Table 1.5 are greatly underestimated and probably differentially affected by the particular segment of the particular gene. A more realistic estimate of NUPT/NUMT copy number using MeS-PCR would be rather difficult, since it would require primer pairs that cover all sequences in the gene of interest and account for the fragmented nature of NUPTs/NUMTs. The abilility of MeS-PCR to amplify only the minor fraction of NUPTs and NUMTs that are nearly perfect replicas of true organellar DNA should facilitate functional and evolutionary investigations of interorganellar sequence transfer: for example, the selection of functional (among degenerate) versions of a gene to direct the protein back to its organelle of origin.

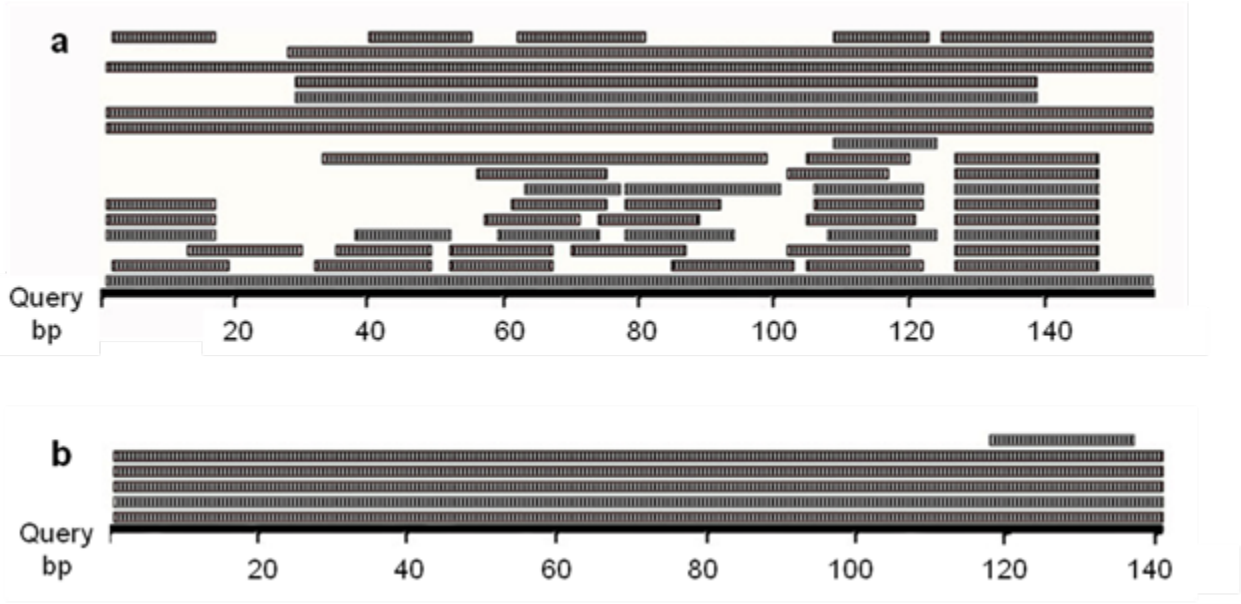

Figure 1.5 Alignment of NUPTs and NUMTs with qPCR primers

Amplicon (Query) was "blasted" against the maize genomic sequence using the near-exact matches setting (http://www.maizesequence.org/blast). Solid lines represent the amplicons. Lines with stripes represent sequences that align with the amplicon. Alignment of maize nuclear genome sequences with the amplicon spanned by psbA_F1 and psbA_R2 primers (a) and the amplicon spanned by cox2_F2 and cox2_R2 primers (b). The smallest degree of alignment discontinuity among the seven amplicons listed in Table 1.5 is shown in (b), whereas the large degree of discontinuity in (a) is typical of the other five amplicons (diagrams not shown).

Our procedures should facilitate the study of organellar DNA copy number. For example, the quantification of organellar genome copy changes during plant development has been controversial (Li *et al.*, 2006; Rowan and Bendich, 2009; Zoschke *et al.*, 2007). In our Blastn search, we found that the blot hybridization probe used by Li *et al*. (2006) to quantify mtDNA in *Arabidopsis* was identical to a NUMT sequence, whereas the target sequence used by Rowan and Bendich (2009) to quantify *Arabidopsis* ptDNA has no NUPT counterpart. Organelle-specific primers should also be useful for analyzing organellar genome copy number changes in mutants. For example, the ptDNA copy number was assessed in one photosynthetic mutant using probes that had >98% sequence similarity with the NUPT sequences (Prikryl *et al.*, 2008).

Species relatedness is another area in which primer specificity is important. Although there

are databases of PCR primers for plastid genomes of higher plants (Heinze, 2007), these primers may not have been tested for their specificity and thus may lead to erroneous phylogenetic inferences. Song *et al*. (2008) showed that the use of non-specific primers for DNA barcoding can result in overestimation of the number of species in two groups of arthropods. In one of the groups, the NUMT sequences were preferentially amplified when using universal primers. Another study reported a similar problem with NUPTs in the phylogeographic analysis of *Eryngium alpinum* (Naciri and Manen, 2009). Lastly, MeS-PCR should be useful in a clinical setting to distinguish between mutations in mtDNA and NUMTs (Wallace *et al.*, 1997; Yao *et al.*, 2008).

In conclusion, the procedure described here facilitates PCR-based methods for various applications. The advantages of small amounts of tissue and total tissue DNA extraction are clear, as long as primer specificity can be demonstrated.

1.6 Acknowledgements

We thank Ajay Kumar for assistance in developing a computer program and Delene Oldenburg for comments on the manuscript. This work was supported by the Department of Biology, University of Washington.

1.7 Supplemental Materials

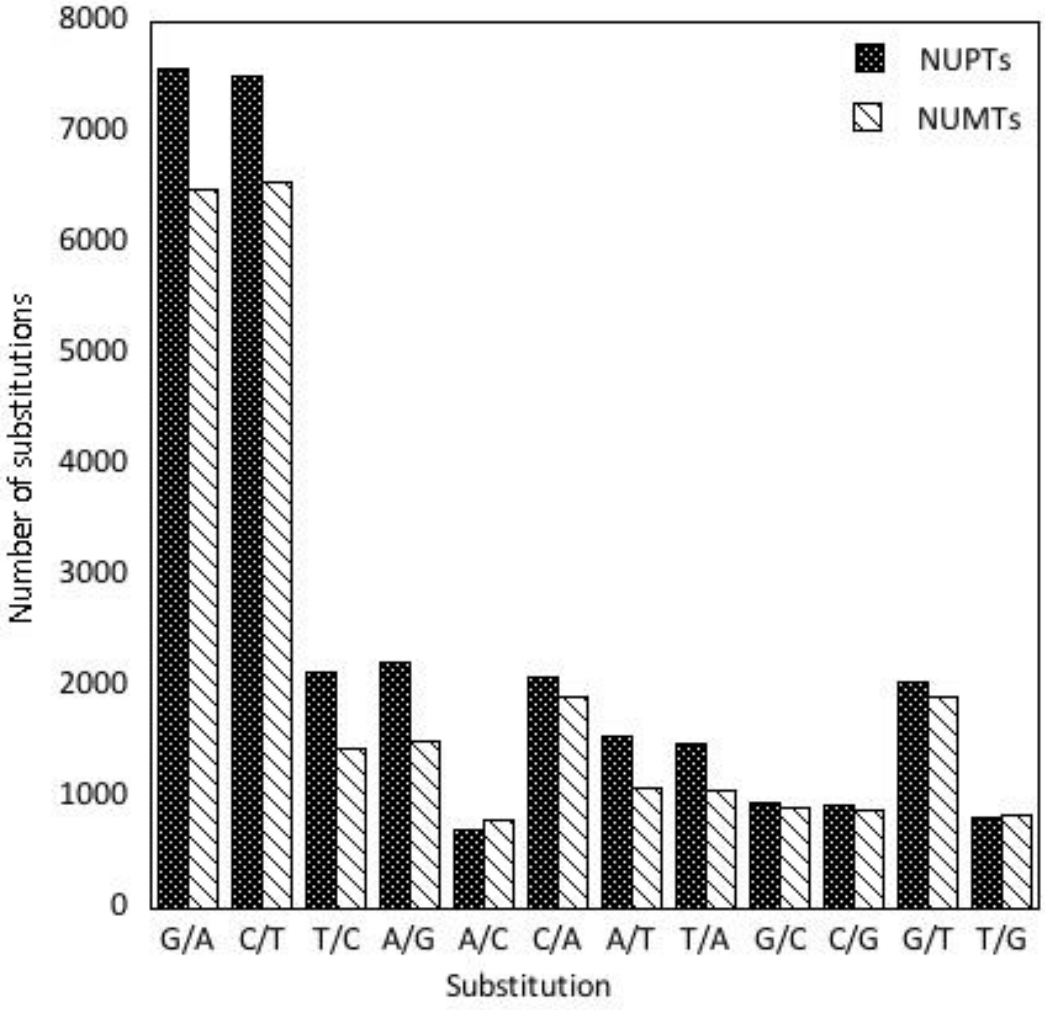

Figure 1.6 Nucleotide substitution frequencies in the NUPTs and NUMTs relative to the organellar genomes of maize

G/A indicates that G is present in the plastid or mitochondrial genome, where A is present in the nuclear genome. The substitution frequencies were determined by analyzing the total size of NUPT/NUMT sequences derived from alignments using MegaBlast. The total of all the substitutions in NUPTs/NUMTs for maize (from about 1000 to 7500) is much higher than for rice NUPT and *Arabidopsis* NUMT sequences (from about 10 to 90; Huang et al. 2005). This difference could be attributed to the total size of the NUPT/NUMT sequences analyzed. A total of 1550 kb and 2058 kb of NUPT and NUMT sequences, respectively, were analyzed for maize, whereas a 131 kb NUPT on rice chromosome 10 and a 262 kb NUMT on *Arabidopsis* chromosome 2 were analyzed (Huang et al. 2005).

Table 1.6 Mutations in NUPTs, NUMTs and MIPTs

	Insertion/kb	Deletion/kb	Transition/kb	Tranversion/kb
NUPTs	3.9	6.9	12.5	6.9
NUMTs	4.5	4.5	7.8	4.6
MIPTs	8.4	8.1	5.1	7

Table 1.7 Complete list of mtDNA-specific sequences

coordinates on NC_007982	**bp**
6825-6993	169
7135-7606	472
7810-8114	305
8220-8419	200
8611-10088	1478
10433-10523	91
10884-11224	341
13316-13380	65
36479-36557	79
36912-36916	5
36975-37052	78
37093-37115	23
77400-77602	203
77946-78281	336
78445-78739	295
78966-80560	1595
80703-80877	175
81066-81942	877
82035-82701	667
82814-82970	157
84309-84629	321
85118-85202	85
85358-85472	115
85560-86050	491
91465-91959	495

coordinates on NC_007982	bp
92279-92550	272
92592-92831	240
93051-93208	158
93413-93442	30
93626-93743	118
93779-94068	290
94157-94259	103
94331-94342	12
94761-94770	10
94806-94813	8
95546-95572	27
95634-95699	66
95850-96848	999
97928-97958	31
98177-98247	71
133126-133185	60
251366-252080	715
252239-252387	149
252700-253529	830
253718-253905	188
254491-254868	378
256896-256930	35
257246-257532	287
257616-258007	392
258056-258599	544
258692-258721	30
258768-259146	379
259362-259513	152
259588-260363	776
260546-260575	30
260638-260863	226
261285-261649	365
262380-262486	107

coordinates on NC_007982	bp
262874-263023	150
263236-263426	191
263521-263750	230
263826-264069	244
265798-266036	239
266105-266168	64
266236-266456	221
267638-267684	47
267854-268476	623
268820-269039	220
269103-269212	110
484805-485603	799
485786-485850	65
487195-487282	88
487594-487971	378
488340-488767	428
488909-489006	98
489060-489210	151
489350-489393	44
513449-513643	195
514008-514185	178
515124-515774	651
515944-516078	135
516459-517631	1173
518434-519038	605
520031-520787	757
520962-521166	205
521228-521702	475
521787-522571	785

Chapter 2

CHANGES IN DNA DAMAGE, MOLECULAR INTEGRITY, AND COPY NUMBER FOR PLASTID DNA AND MITOCHONDRIAL DNA DURING MAIZE DEVELOPMENT

2.1 Abstract

The amount and structural integrity of organellar DNAs change during plant development, although the mechanisms of change are poorly understood. Using PCR-based methods, we quantified DNA damage, molecular integrity, and genome copy number for plastid and mitochondrial DNAs of maize seedlings. A DNA repair assay was also used to assess DNA impediments. During development, DNA damage increased and molecules with impediments that prevent amplification by *Taq* polymerase increased, with light causing the greatest change. DNA copy number values depended on the assay method, with standard real-time qPCR values exceeding those determined by long PCR by a hundred- to a thousand-fold. As the organelles develop, their DNAs may be damaged in oxidative environments created by photo-oxidative reactions and photosynthetic/respiratory electron transfer. Some molecules may be repaired while molecules with unrepaired damage may be degraded to non-functional fragments measured by standard qPCR, but not by long PCR.

2.2 Introduction

The number of copies of the genome in the nucleus is two for most somatic cells in diploid plants and animals, regardless of developmental or environmental changes. For mitochondria and plastids, however, there are multiple copies of the genome and copy number changes greatly during development. For example, human mitochondrial DNA (mtDNA) copy number varies

from about 1000 to 10,000 among tissues, with large differences among individual persons (Frahm *et al.*, 2005). Furthermore, whereas nuclear DNA is stable during development, mtDNA is degraded and turns over in animals and plants (Bendich, 2010). Plant cells contain both mtDNA and plastid DNA (ptDNA), and copy numbers can change independently (Kuroiwa, 1991; Woloszynska, 2010). During development in maize, for example, organellar DNA (orgDNA) copy numbers can change 20-fold, with light differentially affecting both increases and decreases among different tissues (Oldenburg *et al.*, 2013; Oldenburg *et al.*, 2006; Zheng *et al.*, 2011). Even in the single-celled alga *Euglena* under constant growth conditions, both ptDNA and mtDNA are extremely unstable (half-lives of 1.6 and 1.8 cell doublings, respectively), whereas nuclear DNA turnover could not be detected (Manning and Richards, 1972; Richards and Ryan, 1974).

Why does orgDNA copy number vary so greatly? In an early proposal, high copy number reflects an increased demand for organellar ribosomes that can only be satisfied by the increased ribosomal RNA gene number that results from genome amplification (Bendich, 1987). More recently, an additional reason for copy number change emerged that also explained the turnover of mtDNA. If human mtDNA was damaged but not repaired, those damaged molecules were degraded to avoid mutation (Liu and Demple, 2010; Shokolenko *et al.*, 2009).

The frequency and repair of damage in mtDNA have been studied in animals and yeast by treatment with genotoxic agents (such as H_2O_2) or using mutants in repair functions and then measuring the resulting additional DNA lesions per 10 kb of DNA (Hunter *et al.*, 2010). These assays showed increases in DNA lesions following treatment but did not evaluate differences in mtDNA damage among tissues. Similarly, more damage to ptDNA in Arabidopsis was reported for a mutant in the DNA polymerase protein PolI compared to the wild type (Parent *et al.*, 2011).

DNA sustains damage mainly by oxidative and hydrolytic processes *in vivo* due to the presence of ROS and water. Lesions due to oxidative processes include 8-oxo-G, ring-saturated pyrimidines (e.g. thymine glycol, cytosine hydrates), and lipid peroxidation adducts (pyrimido[1,2-*a*]purin-10(*3H*)-one, etheno-DNA adducts). Hydrolytic lesions include depurination, depyrimidination and cytosine deamination (Table 2.1). In addition to these endogenous lesions, others may be caused by environmental factors like ultraviolet (UV) light (pyrimidine dimers). Although the DNA repair mechanisms operating in plant organelles are still poorly understood, it is likely that some lesions may be rectified. For example, in Arabidopsis the base excision repair pathway may remove oxidative lesions, such as thymine glycol (Gutman and Niyogi, 2009). In addition, proteomic analysis of maize plastids revealed developmental changes in DNA-associated proteins, including repair enzymes, likely to affect orgDNA copy number (Majeran *et al.*, 2012).

Various procedures have been used to assess changes in DNA copy number during development: (1) measuring the increase in the rate of probe DNA strand reassociation caused by the addition of a large amount of DNA extracted from total tissue (Lamppa and Bendich, 1984; Lamppa and Bendich, 1979); (2) blot-hybridization of a probe to restriction-digested total tissue DNA (ttDNA) (Li *et al.*, 2006; Oldenburg *et al.*, 2013; Udy *et al.*, 2012; Zheng *et al.*, 2011); (3) fractionation of orgDNA by pulsed-field gel electrophoresis (PFGE) (Oldenburg *et al.*, 2013; Oldenburg *et al.*, 2006; Shaver *et al.*, 2006); (4) quantitative fluorescence using a DNA-specific fluorophore and either intact cells or organelles isolated from cells (Oldenburg and Bendich, 2004a; Oldenburg *et al.*, 2013; Rowan *et al.*, 2004; Shaver *et al.*, 2006); and (5) real-time quantitative PCR (qPCR) (Preuten *et al.*, 2010; Rowan *et al.*, 2009; Udy *et al.*, 2012; Zoschke *et al.*, 2007). These procedures should yield equivalent results providing that the size and molecular

integrity of the DNA molecules are maintained, as is the case for chromosomal DNA in the nucleus. For orgDNAs, however, molecular integrity declines sharply during leaf development, so these procedures can yield conflicting results (Day and Madesis, 2007; Oldenburg *et al.*, 2014; Rowan and Bendich, 2009).

Here, we used qPCR and long-PCR assays to assess orgDNA damage and genome copy number as maize seedlings develop under light, dark-to-light and dark growth conditions. We also developed a new method, "molecular integrity PCR" (miPCR), to quantify long orgDNA molecules without DNA impediments that would (presumably) interfere with the coding and inheritance functions of the DNA. In addition, an *in vitro* DNA repair assay was used that confirmed the presence of DNA impediments, including those associated with oxidative processes. As seedlings develop, damage to orgDNA increases in dark-grown and dark-to-light-transferred plants, whereas high damage levels are found in light-grown plants. In addition, the level of "functional" orgDNA (as measured by miPCR) decreases in dark and dark-to-light plants and remains at a low level for light-grown plants. Remarkably, the levels of such functional orgDNA are greatly reduced compared to total copies as measured by standard qPCR. This finding can be attributed to the inability of qPCR to distinguish between intact and fragmented forms of orgDNA, thus inflating estimates of genome copy number. Overall, light affects both damage and levels of functional DNA in both plastids and mitochondria, even though mitochondria have no known photoreceptors. We surmise that functional ptDNA is maintained as required for chloroplast development, but soon after greening the DNA may be damaged by reactive oxygen species (ROS) and subsequently degraded. Functional mtDNA is also preserved prior to photosynthesis, but may no longer be needed in mature green cells of maize.

2.3 Materials and methods

2.3.1 *Plant tissue and DNA isolation*

Zea mays (inbred line B73) seeds were imbibed overnight and sown in sunshine soil mix #4. The seedlings were grown for 13 days with a 16h light/8h dark photoperiod or in continuous dark or 12 days in dark followed by one day in light. The light intensity was ~500 µmol per sec per m^2. Seedlings were washed with 0.5% sarkosyl for ~3 min and then rinsed with distilled water. Tissue was harvested from 20–25 plants: base of stalk, S1 (5 mm above the node), top of stalk, S2 (5 mm below the ligule of the first leaf), entire first and second leaf blades (leaf 1 or L1 and leaf 2 or L2, respectively). Stalk tissue was composed of several concentric rings of leaves, the outermost being the first leaf sheath. L1 was the fully-expanded blade whereas L2 was still developing, and for L2 tissue the unexpanded leaf blade above the L1 ligule was harvested. Five independent sets of plants were grown under the three growth conditions and the tissues were harvested, representing five biological replicates. Each biological replicate was comprised of twelve samples (4 tissues x 3 growth conditions) and a total of sixty samples were analyzed (12 tissues x 5 biological replicates). Total tissue DNA (ttDNA) was extracted using CTAB as described by Rogers and Bendich (1988). Tissue was frozen in liquid nitrogen and ground to a powder with dry ice. An equal volume of 2X cetyltrimethylammonium bromide (CTAB) buffer [2% CTAB (w/v), 100 mM Tris (pH 8.0), 20 mM EDTA, 1.4 M NaCl, 1% polyvinylpyrrolidone (Mr 40,000) (w/v); preheated to 65°C] was added to the frozen powder and incubated at 65°C for 30 min. Phenol was not used in the procedure. After chloroform extraction and isopropanol precipitation, the DNA was suspended in 10 mM Tris pH 8, 1 mM EDTA (TE), and DNA integrity was assessed by agarose gel electrophoresis. The ttDNA was quantified using Quant-it kit (Life Technologies, NY), diluted to 3 ng/µl, and 6 ng and 15 ng DNA was used for real-time

qPCR and longPCR assays, respectively.

For in-gel preparation of ptDNA, plastids from entire stalk and L1 from light-grown 14-day-old plants were isolated using high salt buffer and purified using Percoll (Oldenburg *et al.*, 2006). Isolated plastids were embedded in low-melting-point agarose (Oldenburg and Bendich, 2004a). In-gel plastids were soaked in lysis buffer (40 mM EDTA pH 8, 1% sarkosyl, 200 µg/mL proteinase K) overnight at 48°C. Proteinase K was inactivated with phenylmethylsulfonyl fluoride, and plugs were washed four times with TE. ptDNA in the lysis buffer and first TE wash (eluates) was extracted using Geneclean II (Qbiogene Inc.). Using qPCR and the standards described below, absolute quantification of ptDNA copies was determined for the lysis buffer, eluates, and fraction retained in-gel (after melting gel plugs at 75°C).

2.3.2 *DNA damage assay, miPCR, and determination of orgDNA without structural impediments*

Fragments of 11,207 bp and 11,164 bp were amplified using LongAmp *Taq* (New England Biolabs, MA) from ptDNA and mtDNA, respectively. The assay was optimized for cycle number to be in the exponential phase, primer efficiencies to be ~100%, and for orgDNA-specific primers for accurate quantification of long orgDNA copies (Figures 2.7-2.13).

The primers used for long PCR amplification were:

nad4, 11164 bp mtDNA-specific

nad4_F3, 5’-GTTGGACCACAGGCAAAAGT-3’

trnk_R1, 5’-GCGAGGAATGGAAGCAGTAG-3’

rps14, 11207 bp ptDNA-specific

rps14_F1, 5’-ATCTTGTTGCACCCGGTAAC-3’

rps14_R5, 5’-TATCCTGACCCTTTCTTGTGC-3’

The reaction mix contained 1X NEB LongAmp buffer, 1.9 mM (for ptDNA) or 1.6 mM (for

mtDNA) $MgSO_4$, 200 nM dNTP, 400 nM each primer, 2.5 U of NEB LongAmp enzyme and 15 ng ttDNA in 50 µL. For long PCR, this cycling program was used: 94°C 30 s, 20 (for ptDNA) or 22 (for mtDNA) cycles of 94°C 30 s, 65°C (for ptDNA) or 61°C (for mtDNA) 1 min, 65°C 7.2 min followed by a final extension at 65°C 10 min. Long-PCR products were fractionated by agarose gel electrophoresis along with 0.75–37.5 ng of DNA standards (MassRuler DNA, Fermentas, USA) that formed a "standard curve" for the absolute quantification of orgDNA (Figure 2.13). The band intensity was determined using NIH ImageJ (Schneider *et al.*, 2012).The ng of DNA in each long-PCR band was converted to end-point PCR copy number. The number of initial template DNA copies was then determined from end-point PCR (for example, at the end of 20 cycles) and the amplification factor: end-point copies / $2^{\text{number of PCR cycles}}$.

Template copies thus calculated were normalized to the orgDNA copy number as determined by qPCR (see below): long-PCR orgDNA copies/qPCR orgDNA copies. The sample with the highest value was considered the least damaged, set at 1, and used to determine the relative amplification for the other samples. For example, if the highest normalized value among samples was 0.5, this was set at 1, and the relative amplification would be 0.5 for another sample that had a normalized value of 0.25. Finally, orgDNA impediments/10 kb was determined using the formula: (-ln [relative amplification]) × 10000 bp / amplicon size bp. Four to six technical replicates per sample were used for DNA damage assays. Template copies for orgDNA without impediments (unimpeded orgDNA) were then normalized to qPCR-determined orgDNA copies and multiplied by 100 to give a percentage (Table 2.3). Template orgDNA copies were also normalized to a single copy nuclear DNA gene (*adh1* copies determined by qPCR, described below) to obtain miPCR copies (Table 2.3).

2.3.3 *Real-time qPCR*

Primers to amplify orgDNA and not NUPTs/NUMTs were designed (Kumar and Bendich, 2011).

The primers used for qPCR amplification were:

adh1, 156 bp nucDNA-specific

adh1_left, 5'-GCTCCTCACAGGCTCATCTC-3'

adh1_right, 5'-AGGCGGACCTTTGCACTT-3'

rps14, 127 bp ptDNA-specific

rps14_F1, 5'-ATCTTGTTGCACCCGGTAAC-3'

rps14_R2, 5'-CCTACACGCCTTCATCGACGTT-3'

nad4, 187 bp mtDNA-specific

nad4_F2, 5'-GCAAAAGTCCTTCCACGGCA-3'

nad4_R1, 5'-AGCAAGCGTAGGCAACCAAAC-3'

The qPCR reactions contained 1X iQ™ SYBR Green Supermix®, 400 nM of each primer and 6 ng ttDNA in 25 µL. A Chromo4™ thermal cycler (Bio-Rad, CA) was used for real-time qPCR using the cycling program: 94°C for 3.3 min, 40 cycles of 94°C for 15 s, 59°C for 15 s and 72°C for 20 s. qPCR data from six technical replicates were analyzed using Opticon Monitor™ software. Melting curves from 65°C to 95°C were analyzed to confirm the presence of a single product. qPCR efficiencies for the primer sets were between 1.9 to 2.1. The ptDNA and mtDNA copies per haploid nuclear genome were determined using absolute quantification with DNA standards produced using maize ttDNA template and the three primer sets. The concentration of the DNA standards was determined using the Quant-it assay. The range of copies was 100 and 10,000/µL for *adh1*, 10,000 and 1,000,000 copies/µL for *rps14*, and 1,000 and 100,000

copies/µL for *nad4*. We followed MIQE guidelines for qPCR (Bustin *et al.*, 2009).

2.3.4 *DNA repair*

In order to assess DNA damage and repairable lesions, orgDNAs were treated with repair enzymes, followed by long PCR. PreCR Repair mix (New England Biolabs, MA) contains seven enzymes that can repair most DNA lesions, including abasic sites, nicks, thymidine dimers, blocked 3'–ends, oxidized guanine, oxidized pyrimidines, and deaminated cytosine. Specifically, the mix contains enzymes for repair of oxidative damage (Endonuclease IV, Endonuclease VIII, formamidopyrimidine [fapy]-DNA glycosylase), UV damage (T4 pyrimidine dimer glycosylase), and hydrolytic damage (uracil-DNA glycosylase). It also contains DNA ligase and polymerase to complete the repair process. However, the repair mix will not mend protein-DNA crosslinks or join double-strand breaks (Figure 2.16). First, 200 ng ttDNA was combined with 1X ThermoPol Buffer, 100 µM dNTPs, 1X NAD^+ in a 98-µl reaction volume. This mixture was divided into two equal volumes. Then 1 µl PreCR repair mix was added to one tube (+Repair) and 1 µl water to the other tube (–Repair). The +Repair tube was incubated at 37 °C for 15 min. The +/–Repair mixtures then served as template for the long-PCR reaction, as described above, and the products were fractionated by agarose gel electrophoresis. ImageJ software was used to compare the pixel levels of the ethidium-DNA fluorescence between +Repair and –Repair PCR products and the fold change was calculated (Figure 2.5).

2.3.5 *Statistical Analysis*

Statistical analyses were performed on the data obtained by qPCR, long PCR (% unimpeded long orgDNA copies), and miPCR for five biological replicates (Tables 2.4-2.8). The ANOVA model was applied to assess differences among tissues during development, entire seedlings

under three growth conditions, and the combination of both (interaction). If ANOVA revealed a significant p value, then the Tukey HSD test for multiple comparisons was used to identify each pair of samples exhibiting a significant difference (Tables 2.5-2.8). Statistical analyses were not performed on the data obtained for impediments/10 kb because these are relative values that were determined independently for each biological replicate. Thus the values for all the replicates cannot be combined. Instead, normalized values (long-PCR orgDNA copies/qPCR orgDNA copies) for the replicates were averaged, and a single value of impediments/10 kb was determined for each tissue.

The relationship between ptDNA and mtDNA was evaluated for these parameters: 1) copy number from qPCR; 2) copy number from miPCR; 3) percentage of unimpeded orgDNA; and 4) orgDNA impediments/10 kb (Figures 2.17-2.24). The linear or logarithmic regression model was employed to obtain R^2 (coefficient of determination) and p values (Figures 2.17-2.24). A strong correlation between ptDNA and mtDNA would be indicated for a given parameter with R^2 close to 1 and p value <0.05.

2.4 Results

2.4.1 *DNA damage*

We previously reported a decline in both the structural integrity and copy number of orgDNA molecules during development of maize and proposed that unrepaired damage led to the degradation of the orgDNAs (Oldenburg and Bendich, 2004a; Oldenburg *et al.*, 2013; Oldenburg *et al.*, 2006). To test this hypothesis, we employed a long-PCR procedure previously developed to assess orgDNA damage caused by genotoxic agents and/or mutations (Parent *et al.*, 2011; Yakes and Van Houten, 1997). We quantified orgDNA damage during seedling development in wild-type maize without the addition of DNA-damaging agents.

The long-PCR assay was originally used to assess DNA damage caused by a specific stressor, such as H_2O_2 or UV light, and reported as DNA lesions per 10 kb. This method is based on the amplification of a long DNA fragment (3-20 kb) and the inability of *Taq* DNA polymerase to proceed past DNA lesions, such as pyrimidine dimers and oxidized pyrimidines. However, other structural features, such as single-strand gaps and double-strand breaks, would also prevent amplification of long DNA segments. Thus the orgDNA "damage" evaluated in this study may be more accurately termed as DNA impediments, meaning any feature that prevents PCR amplification. We define two categories of impediments, lesions (base alterations) and discontinuities (sugar-phosphate alterations), and provide examples in Table 2.1. We show here that the abundance of orgDNA impediments varies during development and among growth conditions. For maize, like other grasses, there is a developmental gradient from the base to the leaf tip (Stern *et al.*, 2004; Sylvester *et al.*, 1990). Thus, we evaluated orgDNA from four stages of development: the base of the stalk (S1), top of the stalk (S2), leaf 1 (L1), and leaf 2 (L2). The leaf number indicates the order in which maize leaves emerge; L1 emerges before L2, and thus is older. In addition, orgDNA was assessed from seedlings grown under three conditions: light-grown, dark-to-light and dark-grown seedlings. Plants grown under these conditions permit the analysis of proplastid-to-chloroplast, etioplast-to-chloroplast and proplastid-to-etioplast transitions, as well as the effect of light on mtDNA.

We performed long-PCR using total tissue DNA (ttDNA) and primers to amplify a 11207-bp region of ptDNA and a 11164-bp region of mtDNA (Materials and methods; Figures 2.7-2.15). The long-PCR reaction conditions were optimized to achieve ~100% efficiency, a requirement for accurate quantification (Figure 2.7-2.13). A representative gel image of the long-PCR assay is shown in Figure 2.15 for mtDNA. The sensitivity of our long-PCR assay to DNA

damage was confirmed by a control experiment showing that UV-light treatment of DNA inhibits amplification, leading to a faint band on the agarose gel (Figure 2.14).

The probability of *Taq* DNA polymerase encountering a DNA impediment is greater for long DNA (~11 kb) than for shorter sections (~150 bp). Thus to measure orgDNA damage, the amount of long-PCR product was normalized to orgDNA copies measured by qPCR (see below; Materials and methods). The tissue with the largest amount of amplified long-PCR product (thus least damaged orgDNA) was used as the baseline for comparison to other tissues. This was the base of the stalk from dark-grown maize seedlings, and the values for impediments in both ptDNA and mtDNA from other tissues are given relative to this tissue (Figure 2.1).

For light-grown seedlings, similar amounts of ptDNA damage (2-3 impediments/10 kb) were found in all tissues from the S1 to L1 blade, except for S2 (1/10 kb) (Figure 2.1A). In contrast, the ptDNA impediments/10 kb increased in dark and dark-to-light tissues during development (0-3/10 kb), with the highest levels of damage in L1. Since L1 is the oldest tissue, the high level of damage for this tissue in dark-grown seedlings may reflect the fragmentation of ptDNA associated with proplastid-to-etioplast differentiation. The difference in number of impediments between dark and dark-to-light for the developing tissues (stalk tissues and leaf 2), indicates light-induced ptDNA damage following etioplast-to-chloroplast differentiation. Overall, there is less damage in dark-grown (5.4 impediments/10 kb) than dark-to-light (8/10 kb) and light-grown (9.2/10 kb) seedlings.

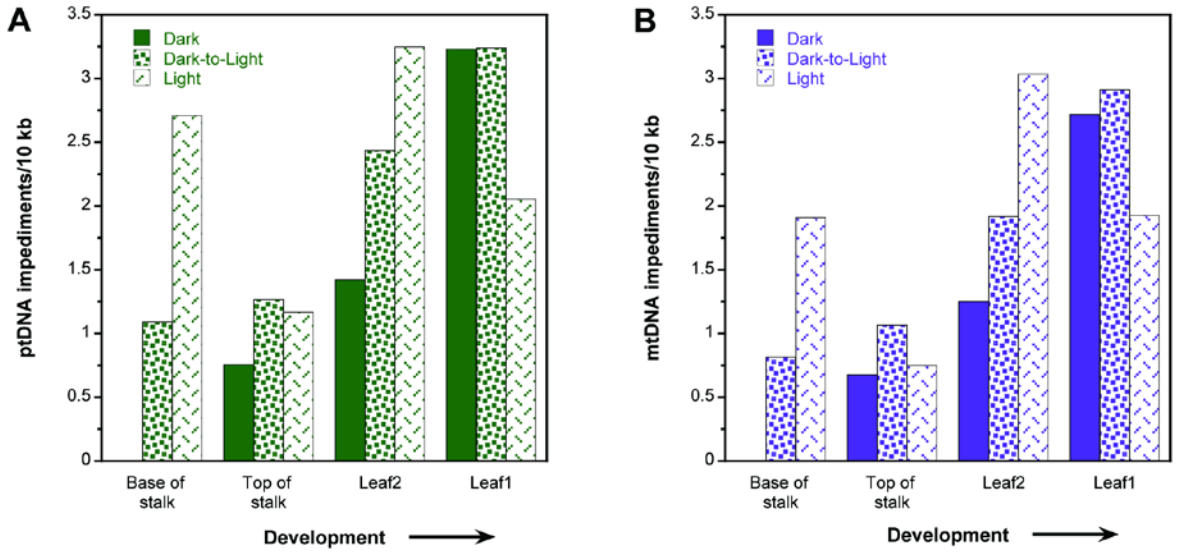

Figure 2.1 Organellar DNA damage during development of maize seedlings

Seedlings were grown under dark, dark-to-light, and light conditions and total tissue DNA was prepared from the base of stalk, top of stalk, leaf 2 and leaf 1. Organellar DNA impediments per 10 kb for ptDNA (A) and for mtDNA (B) was determined by amplifying ~11 kb organellar DNA using long PCR. The relative amplification values for five biological replicates were averaged and number of impediments determined (Materials and methods). Impediments/10 kb are relative to the tissue with the largest amount of long PCR amplification and is set at zero, in this case it is the base of stalk grown in dark for both organellar DNAs.

We found a similar trend for impediments/10 kb in mtDNA as was observed for ptDNA. As with ptDNA, there was a similar amount of mtDNA damage among tissues for light-grown seedlings (2/10 kb), except for S2 (1/10 kb). A substantial increase was observed in mtDNA damage during development for dark and dark-to-light conditions (Figure 2.1B). The highest level of mtDNA damage in the dark was in L1, as was found for ptDNA. Similar to ptDNA, more mtDNA damage was found upon transfer from dark-to-light for stalk and L2, suggesting that mtDNA damage is affected by light. In addition, dark-grown and dark-to-light L1 had more mtDNA impediments than light-grown L1, probably due to higher mtDNA-damaging respiratory activity in dark-grown tissue. Even though oxidative damage may occur in developing tissues (S2 and L2), the damage may be repaired, whereas in older tissue (L1) damage may persist. As

with ptDNA, overall there is less damage in dark-grown (~4.7 impediments/10 kb) than in dark-to-light (~6.7/10 kb) and light-grown (~7.6/10 kb) seedlings.

Since similar trends in DNA damage were observed for ptDNA and mtDNA, we evaluated the relationships for impediments/10 kb between the orgDNAs using regression analysis (Materials and methods). We found a strong correlation for the amount of damage as measured by impediments/10 kb between ptDNA and mtDNA (R^2=0.97 and p=1.3 X 10^{-8}; Figure 2.17). Specifically, samples with fewer impediments in ptDNA also had fewer mtDNA impediments, and those samples with higher amounts of damage in ptDNA also had more damage in mtDNA. This may indicate a common mechanism regulating DNA maintenance and repair for both the organelles.

Except for leaf 1, ptDNA and mtDNA damage overall was lower in dark-grown maize seedlings than in light and dark-to-light tissues. The higher damage levels in light-grown tissues and increase upon transfer from dark-to-light suggest that orgDNA maintenance is influenced by responses to light signals.

2.4.2 *orgDNA without structural impediments*

The DNA damage assay measures the relative amount of DNA impediments that inhibit *Taq* DNA polymerase amplification of long DNA sections. We also quantified ptDNA and mtDNA copies without impediments by determining the amount of DNA amplified by long PCR. We term the DNA amplified by long PCR as “unimpeded” DNA. The amount of unimpeded orgDNA relative to total orgDNA copies (as determined by qPCR) indicates the fraction of orgDNA without any structural impediment, including DNA lesions and discontinuities (Figure 2.2, Table 2.1). Remarkably, we found that unimpeded DNA accounts for only ~0.1–1% of all ptDNA (Figure 2.2A) and mtDNA (Figure 2.2B).

For ptDNA, there were significantly more unimpeded copies in dark-grown entire seedlings compared to light (Figure 2.2A, Table 2.5). The differences in amount of unimpeded ptDNA between growth conditions may be attributed to increased oxidative damage caused by increased ROS production during photosynthesis in light and may indicate less DNA damage or more *in vivo* repair of damaged DNA in dark compared to light-exposed tissues (repair is addressed below). The light-grown seedlings contained a low amount of unimpeded ptDNA throughout development (Figure 2.2A). There was, however, a 6-fold increase from S1 to S2, followed by a decline in L2 and L1 (10- and 3-fold, respectively). There were more copies in the stalk tissues (S1 and S2) than in leaf tissues (L1 and L2), and L2 had more copies than L1 (Figure 2.2A and Tables 2.6, 2.8). We also found a decline during development in unimpeded ptDNA (10–37-fold) for dark and dark-to-light tissues. At the base of the stalk, we found 3- and 21-fold more unimpeded ptDNA in dark compared to dark-to-light and light, respectively (Figure 2.2A). For leaf 1 of dark-grown seedlings, the amount of unimpeded ptDNA decreased with development to the amount found in leaf 1 of dark-to-light tissue. This result and the large amount of damaged ptDNA reported above suggest degradation of ptDNA during proplastid-to-etioplast differentiation in the oldest dark-grown leaf, whereas light-induced damage to ptDNA was evidenced by the decrease in unimpeded ptDNA of S1 upon transfer from dark to light.

A similar trend was found for mtDNA as for ptDNA: higher amounts of unimpeded mtDNA for dark-grown seedlings than for light (Figure 2.2B and Table 2.5). In addition, the percentage of unimpeded mtDNA decreased during development for all growth conditions, with stalk (S1 and S2) containing more copies than L1 and L2 (Figure 2.2B, Tables 2.6, 2.8). For light-grown tissues, we observed a 4-fold increase from base to top of stalk, followed by a 13-fold decline from S2 to L2, similar to ptDNA. We found a decline from S1 to L1 for dark-to-light (10-fold)

and dark-grown (21-fold) tissues during development (Figure 2.2B). Dark-grown S1 contained significantly higher copies compared to dark-to-light and light (Figure 2.2B and Table 2.7); however there were similarly low levels in L1 for all three light regimes (Figure 2.2B). Interestingly, light signaling appears to influence the amount of unimpeded mtDNA as indicated by the substantially more copies in dark. Light might prompt the abandonment of repair of oxidative damage in mtDNA, as ATP generation from photophosphorylation replaces that from respiration. Finally, the decline in unimpeded mtDNA for dark-grown L1 may be attributed to the lack of repair of mtDNA damaged by ROS during respiration. As with ptDNA, changes in structure/integrity likely affect the level of unimpeded mtDNA.

The developmental changes we observed were similar for ptDNA and mtDNA: a decrease in unimpeded DNA accompanied by increasing DNA impediments. Regression analysis revealed a strong correlation for percentage of unimpeded DNA in plastids and mitochondria (Figure 2.18), suggesting that common mechanisms influence the molecular integrity of these two orgDNAs.

In summary, dark-grown seedlings contain more orgDNA without impediments than do light-grown seedlings. During development, the amount of orgDNA damage increases and unimpeded orgDNA decreases.

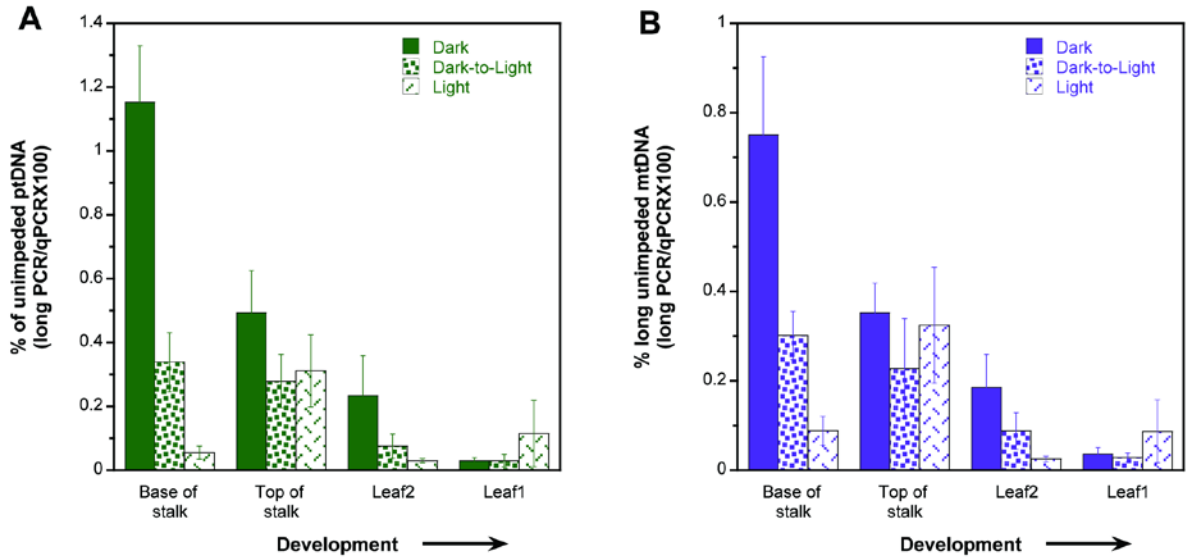

Figure 2.2 ptDNA and mtDNA without structural impediment

Seedlings were grown under dark, dark-to-light, and light conditions and total tissue DNA was prepared from the base of stalk, top of stalk, leaf 2 and leaf 1 (four stages of development). DNA without impediments was determined for ptDNA (A) and mtDNA (B). Total unimpeded orgDNA copies were determined as long-PCR copies, and the percentage is given relative to orgDNA copies as determined by qPCR (Materials and methods). Statistical analyses (ANOVA and Tukey HSD) were performed to compare differences between growth conditions and between developmental stages (tissues). In addition, individual sample comparisons were performed between growth conditions for each tissue and between the tissues for each growth condition. For growth conditions, dark compared to light was $p<0.05$ for both orgDNAs. For developmental stages, S1:L2, S1:L1, S2:L2, and S2:L1 was $p<0.05$ for both orgDNAs; L2:L1 was $p<0.5$ for ptDNA only. For individual sample comparisons and growth conditions, $p<0.05$ was determined for: S1 grown in dark and dark-to-light; S1 grown in dark and light; L2 grown in dark and light (ptDNA only) for both orgDNAs. For individual sample comparisons and developmental stages, $p<0.05$ was determined for: dark-grown S1:S2, S1:L2, S1:L1, S2:L1, L2:L1 (mtDNA only); dark-to-light-grown S1:L2, S1:L1, S2:L2 (ptDNA only), S2:L1 (ptDNA only); light-grown S1:L2 (ptDNA only), S2:L2, S2:L1 for both orgDNAs. All significant comparisons are also provided in Tables 2.4-2.8. Error bars represent standard errors determined for five biological replicates.

2.4.3 *qPCR and miPCR*

qPCR is a standard method used to determine genome copy number. We previously used qPCR to assess changes in copy number for ptDNA and mtDNA during development and in response to light for maize and other plants (Oldenburg *et al.*, 2013; Oldenburg *et al.*, 2006; Rowan *et al.*, 2009; Shaver *et al.*, 2008; Zheng *et al.*, 2011). In some, but not all cases, there were discrepancies between qPCR and other methods used to assess orgDNA levels, such as a decline in ptDNA with development. We suggested that one factor contributing to the observed differences could be amplification of nuclear plastid DNA sequences (NUPTs) and nuclear mitochondrial DNA sequences (NUMTs) by orgDNA primers (Kumar and Bendich, 2011; Oldenburg *et al.*, 2013; Zheng *et al.*, 2011). Thus, we designed a method to identify qPCR primer sets that would only amplify authentic orgDNA (Kumar and Bendich, 2011) and used these primers in the present study to assess changes in maize orgDNAs. We also developed the miPCR technique, which is based on long PCR, to assess the molecular integrity of orgDNA.

The dark-, dark-to-light-, and light-grown ttDNA samples were used for qPCR, and the amount of orgDNA per haploid nuclear genome (nucDNA) was quantified. For both ptDNA/nucDNA and mtDNA/nucDNA, there was no difference in copy number among the three growth conditions (Figure 2.3A, Figure 2.3C and Table 2.5). For ptDNA/nucDNA, copy number increased ~5-fold during development from S1 to L1 for dark, dark-to-light, and light tissues (Figure 2.3A and Table 2.8). In contrast, mtDNA/nucDNA decreased ~3-fold during development for all three growth conditions (Figure 2.3C, Tables 2.6 and 2.8). Overall, we found an increase in ptDNA/nucDNA during development, whereas mtDNA/nucDNA decreased during development.

Since we observed opposite trends between ptDNA/nucDNA and mtDNA/nucDNA, a linear

regression analysis was performed. Indeed, we found a strong correlation between the orgDNAs, which is reflected by R^2 of 0.8 and p=0.00014 (Figure 2.19). This result suggests a common mechanism for sensing (measuring) and altering orgDNA copies but leading to different responses in plastids and mitochondria. For example, during development we find an increase in ptDNA but a reduction of mtDNA copies.

The qPCR assay measures all orgDNA amplified by the primers (usually a 100-200 bp region of DNA) regardless of functional potential. For example, a *psbA* gene fragment of 150 bp can be scored by qPCR even though it cannot produce a functional gene product. Moreover, molecular integrity is important not only for transcription of a single gene, but multiple genes given the polycistronic nature of transcripts in organelles. Thus, we developed the miPCR assay to assess the molecular integrity of orgDNA. For miPCR, the unimpeded orgDNA copies generated by long PCR were normalized to a single-copy nuclear gene (Materials and methods, Table 2.3). The most remarkable result from the miPCR assay was the very low number of unimpeded orgDNA/nucDNA copies compared to the standard qPCR assay (Figure 2.3). Another interesting observation was that the general trends (increase, decrease, or no change) with development and/or light conditions, as assessed by qPCR and miPCR, were similar for mtDNA but not for ptDNA.

Using miPCR, we found that dark-grown seedlings contained significantly more unimpeded ptDNA copies (average of 8.3) than dark-to-light and light-grown seedlings (average of 3.7 and 3.1 copies, respectively) (Figure 2.3B; Table 2.5). For example, dark-grown S1 tissue contained 5-fold and 16-fold more unimpeded ptDNA than dark-to-light and light-grown stalk tissues, respectively, probably due to more DNA damage in the light. During development, the copy number of ptDNA first increased from the base to the top of the stalk (S1 to S2) and then

decreased in L1 for all growth conditions (Figure 2.3B, Table 2.6). Even though the trend was similar for all the growth conditions, there were differences in the magnitude of increase and decrease in unimpeded ptDNA/nucDNA. For example, a small increase (1.4- and 4-fold for S1 to S2) was followed by a larger decline (10- and 10-fold for S2 to L1) in dark-grown and dark-to-light tissues, respectively (Figure 2.3B). For the same developmental stages in light-grown tissues, however, a large increase (~12-fold) was followed by a small decrease (~2-fold).

Using miPCR, we found that dark-grown seedlings contained significantly more unimpeded mtDNA copies than light-grown seedlings (Figure 2.3D and Table 2.5). Furthermore, the amount of unimpeded mtDNA declined continuously from S1 to L1 (Figure 2.3D and Table 2.6). This same trend was also found using qPCR (Figure 2.3C and Table 2.6). The magnitude of decline in unimpeded mtDNA was strongly dependent on light. For example, the transition from S1 to L1 was accompanied by a decline of 50-fold for dark-grown, 29-fold for dark-to-light, and only 3-fold for light (Figure 2.3D).

Since the patterns of change during development differed between ptDNA and mtDNA using miPCR-determined orgDNA copies, we did not expect to find a relationship when comparison was performed with linear regression analysis. This was indeed the case as indicated by a low R^2 value of 0.2 and a p=0.14 (Figure 2.20). There were, however, enormous differences between the orgDNA/nucDNA copy number when measured by miPCR and by qPCR. We found 0.2-4 copies of unimpeded ptDNA/nucDNA using miPCR, whereas qPCR showed 200-1200 copies of ptDNA/nucDNA. The paucity of unimpeded ptDNA copies may be puzzling, especially for stalk tissue where high DNA levels would be needed for chloroplast biogenesis. This conundrum may be resolved, however, by considering the structure of replicating orgDNA and examining in-gel-prepared ptDNA with qPCR.

Plastids were isolated from the entire stalk and leaf 1 of 14-day-old light-grown seedlings and embedded in low-melting-point agarose (Materials and methods). The gel plugs were soaked in lysis solution and washed to yield a “retained in-gel” fraction of ptDNA. The ptDNA released into the lysis solution and the wash buffer represents the diffusible fraction not retained in the gel: the eluate. The in-gel and eluate fractions of ptDNA were then quantified by qPCR. For the stalk, about 99% of the ptDNA was retained in the agarose plugs, with only ~1% diffusing into the eluate (Figure 2.4). Thus most ptDNA in stalk tissue is too large to diffuse out of the gel. In contrast, nearly 35% of DNA in the green chloroplasts of leaf 1 was present as small, diffusible fragments. These results indicate that the molecular integrity of ptDNA molecules declines greatly during maize leaf development. Our previous studies showed that ~70-90% of in-gel ptDNA from the stalk was comprised of complex, branched molecules (Oldenburg and Bendich, 2004a). Thus, amplification of ptDNA (and mtDNA) by long PCR may be inhibited by discontinuities such as recombination branch points and replication forks, as well as by lesions in damaged DNA.

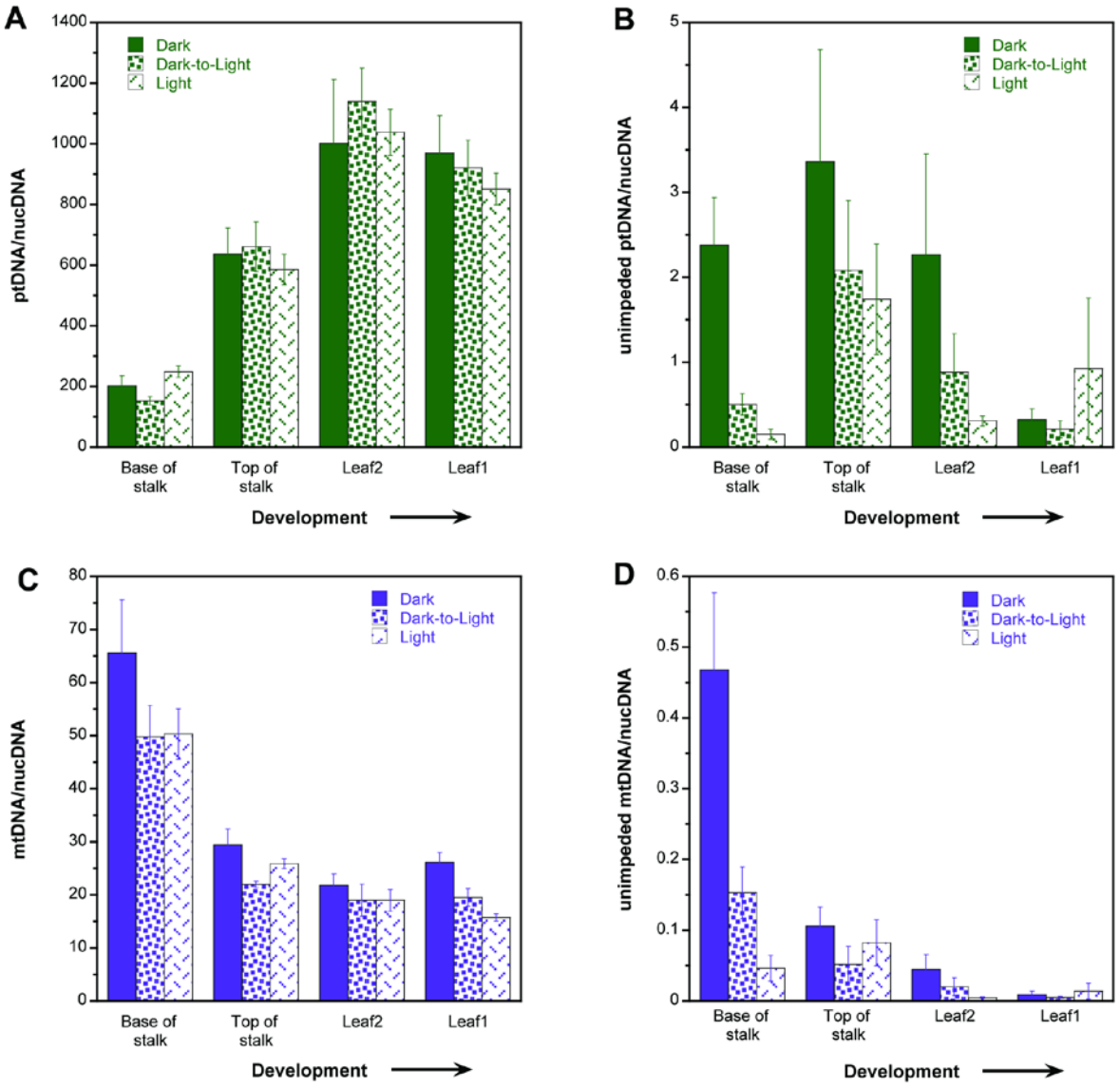
A
ptDNA/nucDNA
1400
1200
1000
800
600
400
200
0
Dark
Dark-to-Light
Light
Base of stalk
Top of stalk
Leaf2
Leaf1
Development
B
unimpeded ptDNA/nucDNA
5
4
3
2
1
0
Dark
Dark-to-Light
Light
Base of stalk
Top of stalk
Leaf2
Leaf1
Development
C
mtDNA/nucDNA
80
70
60
50
40
30
20
10
0
Dark
Dark-to-Light
Light
Base of stalk
Top of stalk
Leaf2
Leaf1
Development
D
unimpeded mtDNA/nucDNA
0.6
0.5
0.4
0.3
0.2
0.1
0
Dark
Dark-to-Light
Light
Base of stalk
Top of stalk
Leaf2
Leaf1
Development

Figure 2.3 Plastid and mitochondrial genome copy number determined by qPCR and miPCR

Seedlings were grown under dark, dark-to-light, and light conditions and total tissue DNA was prepared from the base of stalk, top of stalk, leaf 2 and leaf 1 (four stages of development). Organellar genome copies per haploid nuclear genome were determined for ptDNA (A and B) and mtDNA (C and D). Real-time qPCR copies (A and C) were determined by normalizing short orgDNA copies with nuclear DNA copies. miPCR copies (B and D) were determined by normalizing long PCR orgDNA copies with qPCR-determined nuclear DNA copies (Materials and methods, Table 2.3). The nuclear ploidy level is essentially constant at 2.8 during these stages of seedling development (Oldenburg *et al.*, 2006). qPCR scores most of the orgDNA copies, while miPCR scores only orgDNA copies without discontinuities or DNA lesions. Statistical analyses (ANOVA and Tukey HSD) were performed to compare differences between growth conditions and between developmental stages (tissues). In addition, individual sample comparisons were performed between growth conditions for each tissue and between the tissues for each growth condition. qPCR-determined copy differences were not significant for growth conditions for both orgDNAs. For developmental stages, S1:S2, S1:L2, S1:L1, S2:L2, and S2: L1 had $p<0.05$ for both orgDNAs. qPCR-determined copy differences were not significant for individual sample comparisons and growth conditions for ptDNA; for mtDNA, S2 grown in dark and dark-to-light, L1 grown in dark and dark-to-light, and L1 grown in dark and light conditions had $p<0.05$. For individual sample comparisons and developmental stage, dark-grown S1:S2, S1:L2, S1:L1, dark-to-light-grown S1:S2, S1:L2, S1:L1 and light-grown S1:S2, S1:L2, S1:L1, S2:L2 (ptDNA only) and S2:L1 (mtDNA only) had $p<0.05$ for both orgDNAs. miPCR-determined copy differences were significant between dark and dark-to-light (not for mtDNA) and dark and light for both orgDNAs, when growth conditions were compared. For developmental stages S1:S2 (ptDNA only), S1:L2 (mtDNA only), S1:L1(mtDNA only), S2:L2 (mtDNA only), S2:L1. L2:L1(ptDNA only) had $p<0.05$ for both orgDNAs. For individual sample comparisons and growth conditions, only S1 grown in dark and light had $p<0.05$ for both orgDNAs. For individual sample comparisons and developmental stages, dark-grown S2:L1, dark-light grown S2:L1, and light-grown S1:S2 had $p<0.05$ for ptDNA and for mtDNA, dark-grown S1:S2, S1:L2, S1:L1, S2:L1; dark-to-light grown S1:L2, S1:L1; light-grown S2:L2, S2:L1 had $p<0.05$. All significant comparisons are also provided in Tables 2.4-2.8. Error bars represent standard errors determined for five biological replicates.

2.4.4 *DNA repair*

The results from the DNA damage assay indicate that damage accumulates in both ptDNA and mtDNA during development and that the amount of damage depends on the light conditions. The basis for measuring damage is the inability of the DNA polymerase to amplify long PCR segments. The lack of amplification may be due to impediments including DNA lesions that block *Taq* polymerase progression and discontinuities such as branching in complex forms or breakage of the DNA into fragments lacking both primer sites (Table 2.1). The level of damage due to lesions may be assessed using an *in vitro* assay with DNA repair enzymes.

We performed an orgDNA repair assay on the ttDNA using a PreCR repair kit (Materials and methods) and long PCR. The enzymes in this repair mix can rectify most types of DNA lesions but will not affect discontinuities except to seal a nick or fill in a short single-strand gap (Table 2.1). Treatment with repair enzymes resulted in an increase in the amount of long-PCR product for both ptDNA and mtDNA (Figure 2.5). The magnitude of the increase was generally greater for seedlings exposed to light than grown in dark, indicating that light may lead to orgDNA lesions. Furthermore, repair was much greater for leaf than stalk tissues in all growth conditions, suggesting that orgDNA damage accumulates during development. The results are also consistent with the results from the damage assay: the amount of repair was directly proportional to orgDNA damage (impediments/10 kb) (Figure 2.21 and 2.22) and inversely proportional to the percentage of unimpeded orgDNA (Figure 2.23 and 2.24) using regression analysis.

The orgDNA may or may not be repaired with the PreCR kit depending on the type of damage. For example, DNA fragmented by double-strand breaks would not be repaired, whereas oxidized bases may be repaired (Table 2.1). Thus, the degree of repair may be correlated with the

amount of oxidatively-damaged orgDNA. For example, more repair was found for ptDNA in light-grown L2 and L1 (19- to 47-fold) than S1 and S2 (4- to-12-fold) or dark-grown L2 and L1 (12- to 23-fold). These results suggest that light causes oxidative damage to orgDNA and a decline in *in vivo* repair.

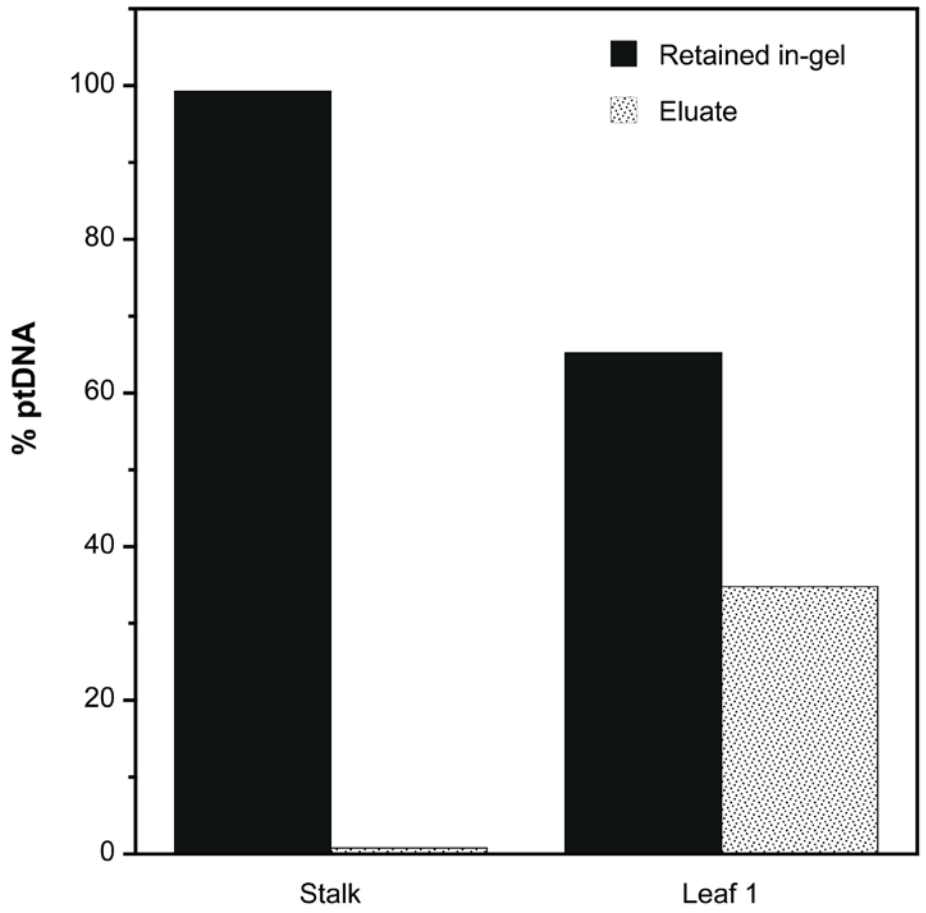

Figure 2.4 Amount of ptDNA retained in-gel and eluted from the gel

Plastids were isolated from the entire stalk and leaf 1 of 14-day-old light-grown plants, then embedded in agarose, treated with lysis solution, and washed with TE (Materials and methods). The ptDNA that diffused out of the agarose was recovered from the lysis and wash solutions (eluate). The ptDNA copy number for the in-gel and eluate fractions was determined using qPCR and given as percentage of total cpDNA from both fractions. Three technical replicates were used per sample.

Table 2.1 DNA impediments and their impact on long-PCR and repair assays

Impediment[1]			Repair by PreCR[2]
Lesions	Examples	Causes	
Pyrimidine dimer	Thymine dimer Cytosine dimer	UV light	Yes[3]
Abasic site	Depurination Depyrimidination	Hydrolysis	Yes Yes
Oxidized bases	8-oxo-G[4] 8-oxo-A Thymine glycol	Oxidation	Yes No Yes
Deaminated cytosine		Hydrolysis	Yes
Bulky adduct	Benzo[a]pyrene diol epoxide-dG M1dG	Lipid peroxidation	ND ND
Discontinuity			
SSB	Nick	Hydrolysis Endonuclease Topoisomerase	Yes
	Single-strand gap	Replication Transcription	Yes; 5-10 nucleotides
DSB	Fragmentation	Hydrolysis Endonuclease Topoisomerase	No[3]
Branch point	Replication fork Recombination junction		ND
Protein-DNA crosslinks		Topoisomerase Formaldehyde	No

[1] Types, examples, and causes of impediments are from (Friedberg *et al.*, 2006)

[2] NEB product website (https://www.neb.com/tools-and-resources/usage-guidelines/dna-damage-and-precr) and/or Tom Evans (product scientist for NEB)

[3] Figure 2.16

SSB = single-strand break; DSB = double-strand break; 8-oxo-G = 8-oxo-7,8-dihydro-2'-deoxyguanine; 8-oxo-A = 8-oxo-7,8-dihydro-2'-deoxyadenine; M1dG :pyrimido[1,2-*a*]purin-10(3*H*)-one; ND = Not determined

[4]Except for 8-oxo-G, all other impediments may inhibit LongAmp polymerase

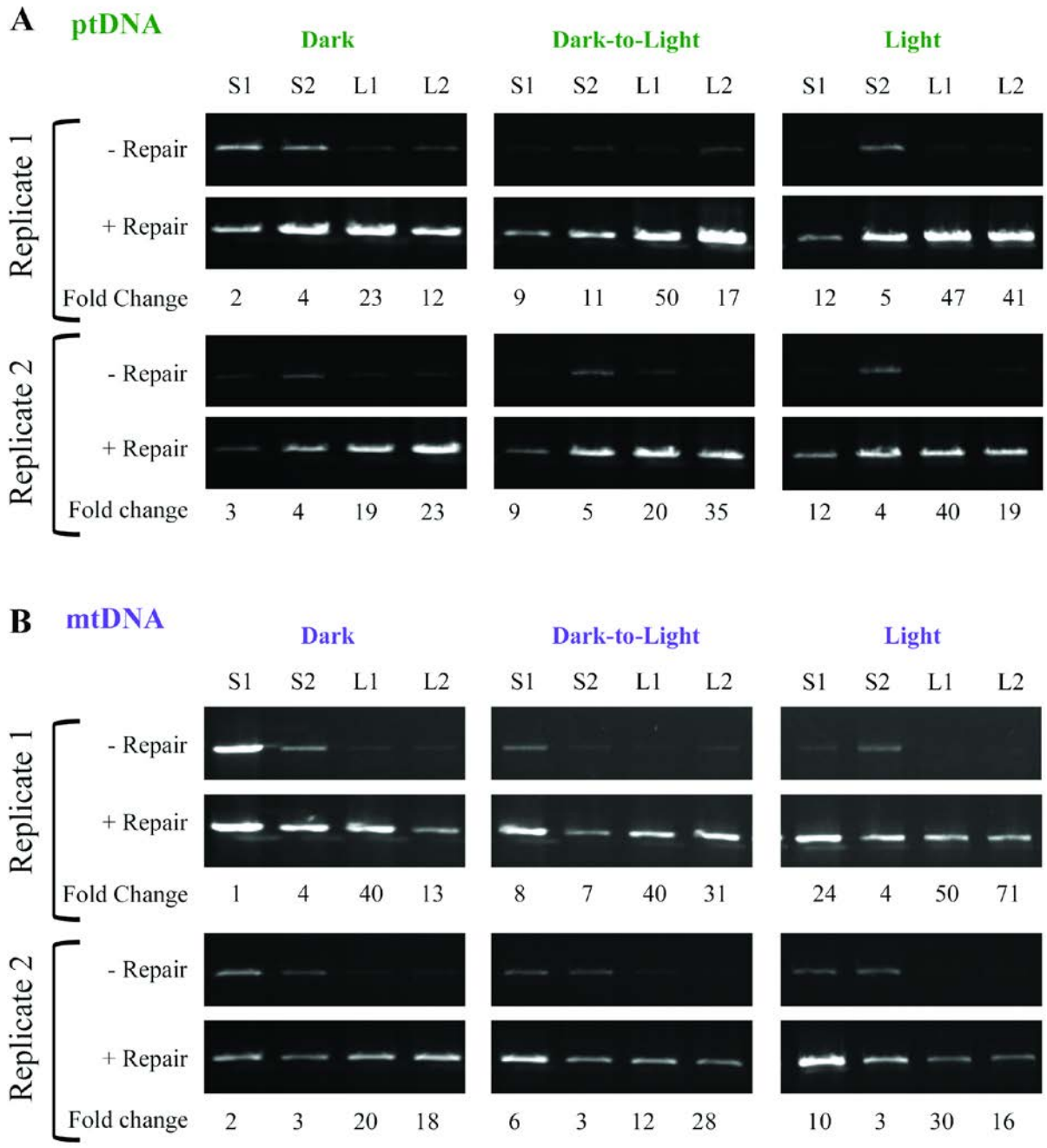

Figure 2.5 Repair of organellar DNA

Maize seedlings were grown in dark, dark-to-light and light conditions and total tissue DNA was prepared from base of stalk (S1), top of stalk (S2), leaf 1 (L1), and leaf 2 (L2). The amount of ~11 kb long-PCR product was assessed before and after treatment with DNA repair enzymes for two biological replicates (Materials and methods). The fold change in long PCR product as determined by ethidium-DNA intensity before and after repair treatment was determined and is given below the gel images. In general, there is an increase in repair from dark to dark-to-light to light and during development from S1 to L1.

2.5 Discussion

We previously found a dramatic decrease during maize development in genome copy number for plastids and mitochondria accompanied by a change in orgDNA structure from multi-genomic branched forms to linear molecules of sub-genomic size (Oldenburg and Bendich, 2004a; Oldenburg *et al.*, 2013; Oldenburg *et al.*, 2006). We proposed that the orgDNA was damaged because of the ROS produced in these organelles and that unrepaired orgDNA was degraded. Here, we quantify orgDNA damage, copy number and *in vitro* repair under dark, dark-to-light, and light growth conditions during seedling development.

Our results are summarized in Table 1.2 and reveal a strong effect of light on orgDNA damage and molecular integrity. OrgDNA from light-grown seedlings is highly damaged, with fewer unimpeded copies and more DNA repair *in vitro* than orgDNA from dark-grown seedlings, consistent with organelle-generated ROS determining the retention or degradation of orgDNA. In addition, for both ptDNA and mtDNA, we find a developmental increase in DNA impediments and a decrease in unimpeded orgDNA in both dark and dark-to-light (but not light) conditions. For ptDNA, qPCR-determined copy number increases, whereas miPCR-determined copy number first increases and then decreases. For mtDNA, copies determined by both qPCR and miPCR decrease, but the magnitude of decline is much greater with miPCR. For both orgDNAs, the number of copies per haploid nuclear genome determined by qPCR is much greater than that determined by miPCR. In order to understand the functional significance of orgDNA changes indicated by these analytical methods, we need to consider how DNA structure and integrity may affect the methods. Most of our findings apply to both ptDNA and mtDNA. For simplicity, however, the discussion below is focused on ptDNA.

Table 2.2 Summary of orgDNA properties for seedlings grown in light, dark-to-light, and dark conditions

		Light	Dark-to-light	Dark
damage		+++	++	+
		+++	++	+
% unimpeded		+	++	+++
		+	++	+++
in vitro repair		+++	+++	+
		+++	+++	+
copies	qPCR	+++	+++	+++
		+	+	+++
	miPCR	+	+	+++
		+	+	+++

Dark-grown seedlings contain orgDNA with less damage and greater integrity (fewer impediments) than seedlings grown in dark-to-light and light. Using the *in vitro* repair assay, orgDNA shows less repair when obtained from seedlings grown in dark than in dark-to-light and light. Using the qPCR assay, ptDNA copy number is similar among grown conditions, whereas there are more mtDNA copies in dark than in dark-to-light and light. However, no difference between ptDNA and mtDNA is found when copy number of long DNA molecules is measured using the miPRC assay. Relative levels are indicated by +, ++, and +++; green: ptDNA and purple: mtDNA.

2.5.1 *Structure and molecular integrity of orgDNA*

We employed a long-PCR assay that relies on the probability of *Taq* DNA polymerase encountering an impediment in a long DNA fragment (~11 kb) during amplification. The results from ptDNA damage assays under the three growth conditions (Table 2.2) indicate that the major cause of impediments is oxidative damage resulting from ROS produced during photosynthesis. This conclusion is supported by our finding of more *in vitro* repair, using enzymes that mend oxidative-type lesions, for light growth conditions than dark, as well as following transfer from dark to light. Some damage is evident even for dark-grown seedlings, however, that may be attributed to impediments accumulated during development. In addition to oxidative lesions, discontinuities in structure may prevent amplification of a long orgDNA fragment, as described below.

Our most remarkable result is the extremely low orgDNA/nucDNA copy number values obtained with the miPCR assay. It is difficult to reconcile such low miPCR copy number with the amount of functional orgDNA required for chloroplast or mitochondrial biogenesis. Besides DNA lesions, discontinuities such as recombination junctions, replication forks, and single-strand gaps could impede long-PCR amplification by *Taq* DNA polymerase (Table 2.1). In addition, some orgDNA molecules may not be long enough to serve as a template for long PCR. Thus discontinuities in orgDNA molecules may account for low amplification levels of long-PCR products, consistent with previous studies showing changes in orgDNA structure and integrity during development (Oldenburg and Bendich, 2004a; Rowan *et al.*, 2009; Shaver *et al.*, 2008).

The structure of orgDNA molecules has been assessed for maize and other plants using PFGE and DNA movies (ethidium-stained orgDNA) (Backert *et al.*, 1995; Bendich, 1996; Deng *et al.*, 1989; Shaver *et al.*, 2006). In maize, stalk tissue contains replicative forms of ptDNA comprised of branched multi-genomic molecules. The low copy number of unimpeded orgDNA we now find for stalk may be attributed mainly to DNA discontinuities in such molecules, including forks and gaps previously documented for ptDNA and mtDNA (Backert *et al.*, 1997; Oldenburg and Bendich, 1996; Rowan *et al.*, 2010). We proposed that during development the replicative forms may be resolved to unit-genome-sized linear molecules and then degraded until only sub-genomic linear fragments remain (Oldenburg and Bendich, 2004a). Here, evidence for replicative ptDNA in stalk tissue is indicated by ~99% DNA retention in-gel. In contrast, the ptDNA in the green leaf blade consists mostly of linear molecules fragmented to less than genome size, as indicated by the large fraction (35%) of in-gel diffusible DNA (Figure 2.4). Fragments shorter than 11 kb would not be amplified in our long-PCR assay, contributing to the

extremely low levels of unimpeded orgDNA in leaves. In some tissues, such as light-grown top of stalk, higher levels of unimpeded ptDNA may be attributed to long-PCR amplification from unit-genome-sized molecules. In addition, we find very low levels of *in vitro* repair for the stalk (Figure 2.5), suggesting little oxidative damage, as expected for non-photosynthetic tissue. Although light-grown stalk contains replicative ptDNA, PFGE shows more fragmentation to less than-genome-sized molecules than dark-grown stalk (Oldenburg *et al.*, 2013; Oldenburg *et al.*, 2006), and our present data show more impediments that require more *in vitro* repair in light-grown than dark-grown stalk for both orgDNAs. In general, dark-grown tissues also have more unit-genome-sized molecules that can be amplified by long-PCR than do light-grown tissues. Thus, our results using long-PCR assays are consistent with structural information revealed by PFGE and DNA movies for maize ptDNA and mtDNA.

In summary, although miPCR should report functional orgDNA, the amount will be underestimated because of developmental changes in DNA replication, molecular integrity, and damage. The underestimate would be large for meristematic cells at the base of the stalk, where long-PCR would be disrupted by the branch points associated with the recombination-dependent mode of orgDNA replication (Bendich, 2010; Oldenburg and Bendich, 2004a), decreasing as forks run out and replication ceases in the expanding leaf blade. Superimposed on this developmental program is the influence of growth conditions. Photosynthesis generates ROS leading to oxidatively-induced lesions and double-strand breaks. In developing chloroplasts of the stalk, ptDNA lesions may be due to ROS from the photo-oxidation of protochlorophyllide (Pchlide), a precursor of chlorophyll in proplastids and etioplasts (Erdei *et al.*, 2005; Solymosi and Schoefs, 2010). Development and growth conditions would also influence the levels of DNA-maintenance proteins. For example, proteomic analysis of maize proplastids revealed high

levels of antioxidant proteins, such as superoxide dismutase (Majeran *et al.*, 2012) that protect the ptDNA in meristematic tissues, minimizing the need for repair (Figure 2.5). In addition, ROS-generating photosynthesis does not occur in proplastids, further reducing ptDNA damage and the need for repair.

Mitochondria produce most of the ROS in non-green tissues (Moller, 2001). Hence, in the dark and in meristematic tissues, one might expect more DNA damage from ROS than in light. Surprisingly, we find more unimpeded mtDNA copies in dark than light and in stalk than leaves. This may be due to DNA repair that maintains "good" DNA to support respiration in dark; whereas meristematic cells at the base of the stalk probably utilize glycolysis rather than respiration (Bendich, 2010; Kelliher and Walbot, 2014) in hypoxic conditions. Similar trends for ptDNA and mtDNA concerning damage, unimpeded copies and *in vitro* repair suggest retrograde and inter-organellar signaling (Foyer and Noctor, 2003; Wright *et al.*, 2009). Signaling from plastids to mitochondria is also suggested by more damage when dark-grown plants are transferred to light. The effect of light on mtDNA damage may also be associated with a change in mitochondrial function as photophosphorylation replaces respiration.

A strong relationship between ptDNA and mtDNA for orgDNA damage (impediments/10 kb), long PCR (% unimpeded orgDNA), and copies determined by qPCR (Figure 2.17, 2.18 and 2.19) also indicates a common mechanism governing DNA maintenance and repair. Common repair pathways may include DNA repair enzymes targeted to both organelles, such as RECA2 in Arabidopsis (Shedge *et al.*, 2007). Thus, we may expect similar dual-targeted proteins maintaining copy numbers in both organelles (Carrie and Small, 2013).

The changes in DNA that accompany maize seedling development seem complex. Those changes are summarized in Figure 2.6.

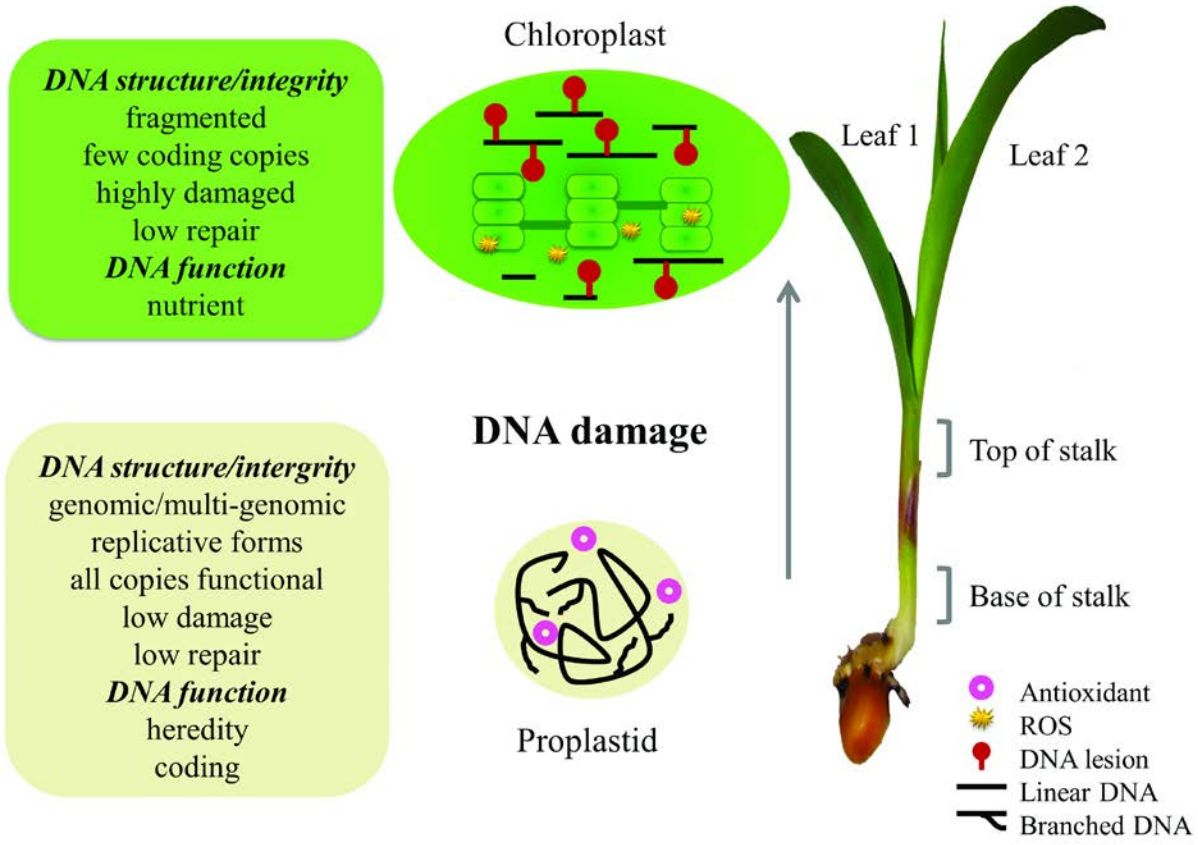

Figure 2.6 Changes in orgDNA during maize development

Recombination-dependent replication of orgDNA in the basal meristem produces branched, multi-genomic chromosomes in proplastids and mitochondria (not depicted). DNA-damaging oxidative stress is minimized, requiring little repair, by maintaining hypoxia, antioxidants, and no ROS-generating photosynthesis or respiration. Early in leaf development, orgDNA damage occurs due to ROS generated in photosynthesis, respiration, and oxidation of pigments and lipids. Later, when the damage level exceeds the repair capacity, orgDNA is fragmented and no longer functions in coding or heredity, mitochondria switch from respiration to photorespiration, and DNA copy number declines faster for mitochondria than chloroplasts.

2.5.2 *Functional organellar DNA and methods for orgDNA quantification*

How can PCR-based methods designed for copy number and damage analysis of long DNA molecules be used to evaluate the functional significance of highly fragmented molecules? What, if any, function is served by orgDNA fragments less than the size of a gene?

Various methods have been used to assess copy number of orgDNA in isolated organelles

(PFGE, DAPI-DNA, and DNA movies) and total tissue DNA (DNA reassociation kinetics, qPCR, and restriction/blot-hybridization). The former methods uniformly indicate a decline in orgDNA during development in the light, whereas the latter methods frequently show little or no change (Li *et al.*, 2006; Oldenburg *et al.*, 2014; Rowan and Bendich, 2009; Zoschke *et al.*, 2007). Previously, we proposed three factors that contribute to the discrepancy: (1) ignoring the fact that leaf tissue is comprised of different cell types and not all cells would contain equal amounts of orgDNA (Rowan and Bendich, 2009; Zheng *et al.*, 2011); (2) the age of plant tissues used for comparison (Rowan and Bendich, 2009); and (3) interference due to NUPTs/NUMTs (Kumar and Bendich, 2011). Here, although we used orgDNA-specific primers to avoid NUPTs/NUMTs, we still find the same disagreement between qPCR and other methods. With qPCR, the copy number of ptDNA/nucDNA actually increases during development for light-grown seedlings (Figure 2.3A), in contrast to other methods that indicate a decrease. Our miPCR results also show a decrease and provide an explanation for the discrepancy among methods: the potential to overestimate orgDNA copy number by qPCR and restriction/blot-hybridization.

Standard qPCR measures essentially all orgDNA in ttDNA regardless of size and molecular integrity since only a short DNA segment (100-200 bp) is amplified. Thus, for tissues with highly-fragmented orgDNAs, such as light-grown leaf 1, qPCR and restriction/blot-hybridization could lead to an overestimate of *functional* genome copies. For tissues with multi-genomic forms, however, qPCR should give an accurate estimate of functional orgDNA. In contrast, miPCR measures only orgDNA >11 kb, which would include both multi-genomic complexes and genomic linear molecules. All of the long-PCR-determined copies (from miPCR) are free of impediments and are, therefore, functional; such copies decline with development and in response to light, reflecting the decline revealed by DAPI-DNA, PFGE, and DNA movies. Much

of the orgDNA from maize stalk (and cultured tobacco and liverwort cells) remains immobile after PFGE, and low-resolution DNA movies revealed large blobs of ethidium staining from which long and branched fibers emanate (Oldenburg and Bendich, 1996, 1998, 2004b). These complex structures were interpreted as branched replicating orgDNA. High-resolution electron microscopy of analogous mtDNA structures from cultured *Chenopodium album* cells revealed a high density of multiply-branched DNA, also interpreted as replicating mtDNA (Backert and Börner, 2000). Such replicating forms would contain closely-spaced impediments, leading to an underestimate of functional orgDNA in the miPCR assay.

The qPCR assay is suitable to quantify DNA where all the templates are uniform. But for maize orgDNA extracted from green leaf 1, a 300-bp fragment that could not encode a typical protein would nevertheless be scored by qPCR. Given the polycistronic nature of organellar transcripts (Liere *et al.*, 2011; Zhelyazkova *et al.*, 2012), what function could be served by the transcription of (presumably highly-fragmented) ptDNA reported for green leaf 1 tissue of barley (Emanuel *et al.*, 2004)? Non-coding RNAs involved in post-transcriptional gene regulation is one possibility (Hotto *et al.*, 2012). Another involves the monitoring of DNA damage. Transcription-coupled repair (TCR) is one of many processes by which DNA damage is repaired in bacteria and the nucleus (Deaconescu *et al.*, 2012), and transcription has been proposed as a global surveyor of DNA damage (Epshtein *et al.*, 2014). TCR may be expected to operate in plastids and mitochondria early in development of these organelles. As the damage load accumulates in developing leaves, transcription may continue even though orgDNA has been "abandoned" because repair proteins are no longer supplied from nucleus-encoded genes (RecA, for example). In this scenario, the residual transcription of highly-fragmented orgDNA superficially suggests a coding function for such fragments. Instead, we suggest that such

transcripts do not benefit the cell because of their coding or structural potential and inaccurately inflate the copy number estimate of functional organellar genomes.

Whereas quantification of mitochondrial RNA and DNA (by qPCR) has been reported in other plants (Li *et al.*, 2006; Preuten *et al.*, 2010), parallel data for mtDNA molecular integrity have not been reported. Nonetheless, Liere et al. (2011) state that "No correlation between gene copy numbers and transcript levels were found during leaf development in Arabidopsis (Preuten et al., 2010) and *Phaseolus vulgaris* (Woloszynska and Trojanowski, 2009)", consistent with an overestimation of functional mtDNA copy number by qPCR in mature leaf tissue.

2.6 Concluding remarks

At early stages of organellar development, fully-functional orgDNA is needed for subsequent respiration and photosynthesis, just as fully-functional nuclear DNA is needed, but copy number changes only for orgDNA. As leaves develop and the physiological roles of the organelles change, the maintenance of high-copy orgDNA (but not nuclear DNA) lessens, damage persists, and orgDNA is degraded. This abandonment of orgDNA is abrupt for maize and gradual for ptDNA in some dicot plants (Oldenburg *et al.*, 2014; Rowan and Bendich, 2009; Shaver *et al.*, 2006). Energy metabolism poses a much greater threat to the genomes in mitochondria and chloroplasts than the nucleus. Whereas DNA repair suffices for the nucleus, orgDNA turnover, copy number change, and abandonment are also needed to maintain cellular homeostasis during development.

2.7 Supplemental Materials

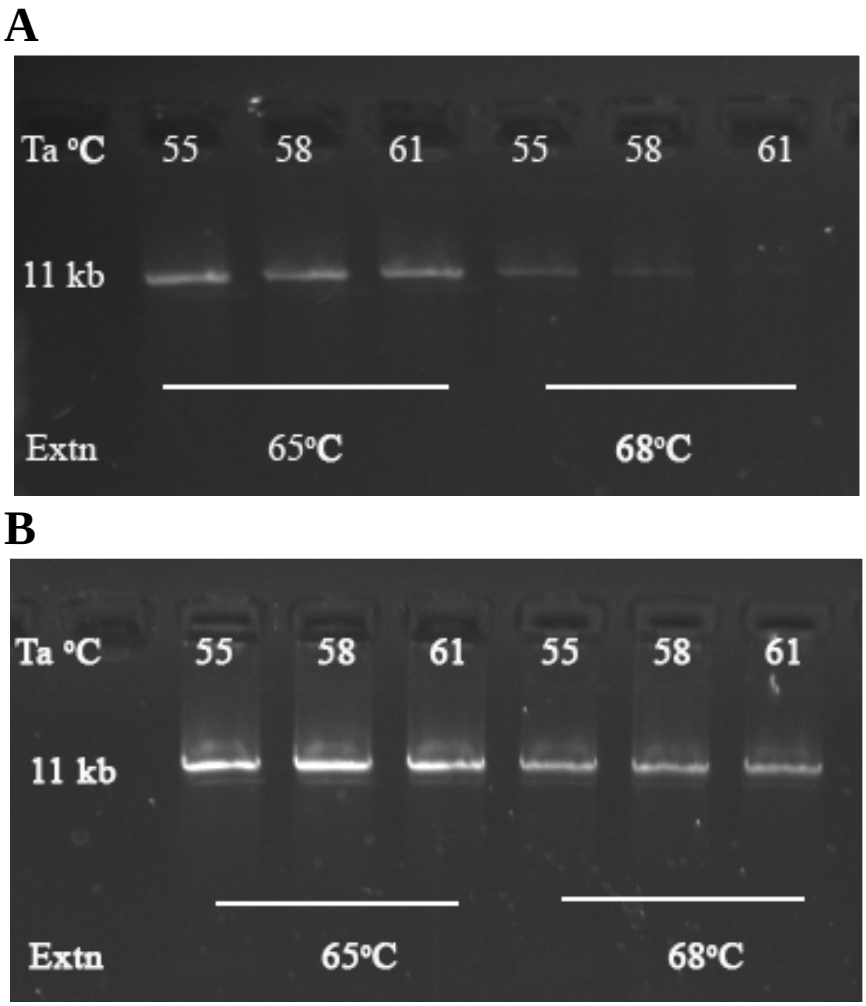

Figure 2.7 Optimization of extension time and temperature

Using a typical extension temperature of about 70°C, we obtained very little product. We then tested 65°C and 68°C, and the amount of product increased. We also found that the duration of extension step of 39 s/kb gave the best results for both ptDNA and mtDNA (data not shown). An extension temperature of 65°C was chosen for further use for both ptDNA (Figure 2.7A) and mtDNA (Figure 2.7B).

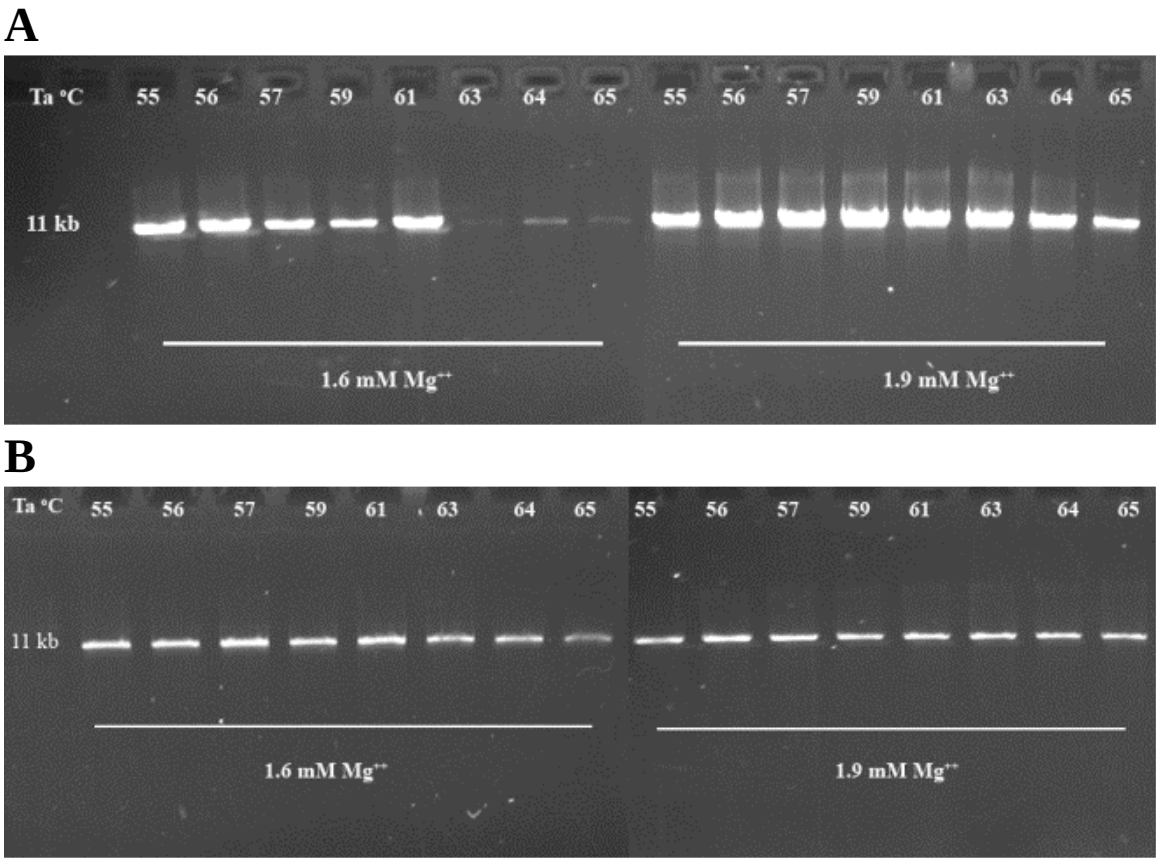

Figure 2.8 Optimization of anneal temperature and Mg^{++} concentration

We performed PCR using a range of annealing temperature (Ta) values from 55 to 65°C. We also tested Mg^{++} concentrations from 1 to 2.2 mM at these Ta values. We chose a high Ta that did not result in decreased PCR product and a low Mg^{++} concentration that did not yield non-specific products (DNA sizes other than 11 kb). We determined that the optimal Ta was 65°C and 61°C and Mg^{++} concentration was 1.9 mM and 1.6 mM for ptDNA (Figure 2.8A) and mtDNA (Figure 2.8B) primers, respectively.

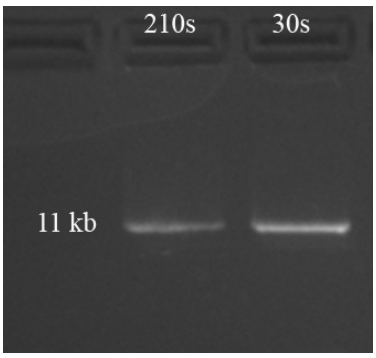

Figure 2.9 Optimization of initial denaturation time

Figure 2.9 shows that the duration of the initial denaturation (at 94°C) affected the PCR product. There was about two-fold less PCR product at 210 s then at 30s, most likely due to greater thermal scission of the DNA strands with the longer time. Thus we adopted 30 s as the initial denaturation time. We optimized the Ta and chose 61° and 65°C for ptDNA and mtDNA, respectively. We also found the optimal Mg^{++} concentration to be 1.9 mM and 1.6 mM for ptDNA and mtDNA, respectively. Finally, the extension temperature of 65°C at 39s/kb and denaturation time of 30 s was found to be optimal for both ptDNA and mtDNA.

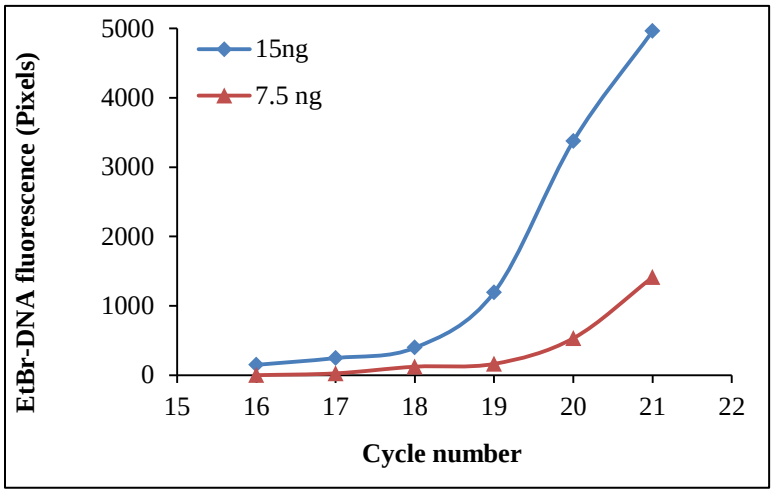

Figure 2.10 Cycle number optimization and efficiency

PCR product band intensities determined with ImageJ (Schneider *et al.*, 2012) over 16 to 21 cycles for ptDNA with 7.5 ng and 15 ng total tissue DNA. We performed long PCR over a range of cycles for both ptDNA and mtDNA and determined the cycle number for the approximate mid-point in the exponential phase. For example, 20 cycles was used for ptDNA (Figure 2.10 and Figure 2.11A) and 22 cycles for mtDNA (Figure 2.11B).For both ptDNA and mtDNA, the EtBr-DNA fluorescence intensity was about two times greater using 15 ng of total tissue DNA compared to using 7.5 ng and only one PCR product was produced with a size of ~11 kb, the interval between primers (Figure 2.11). Thus, the long PCR procedures appear to be quantitative and in the exponential range for these amounts of input DNA. Furthermore, these two DNA amounts were included as controls (see Figure 2.14) in all long-PCR experiments to validate the assay (see item 10, below) and to verify that the cycle number was in the exponential range for tissues with different levels of long unobstructed orgDNA.

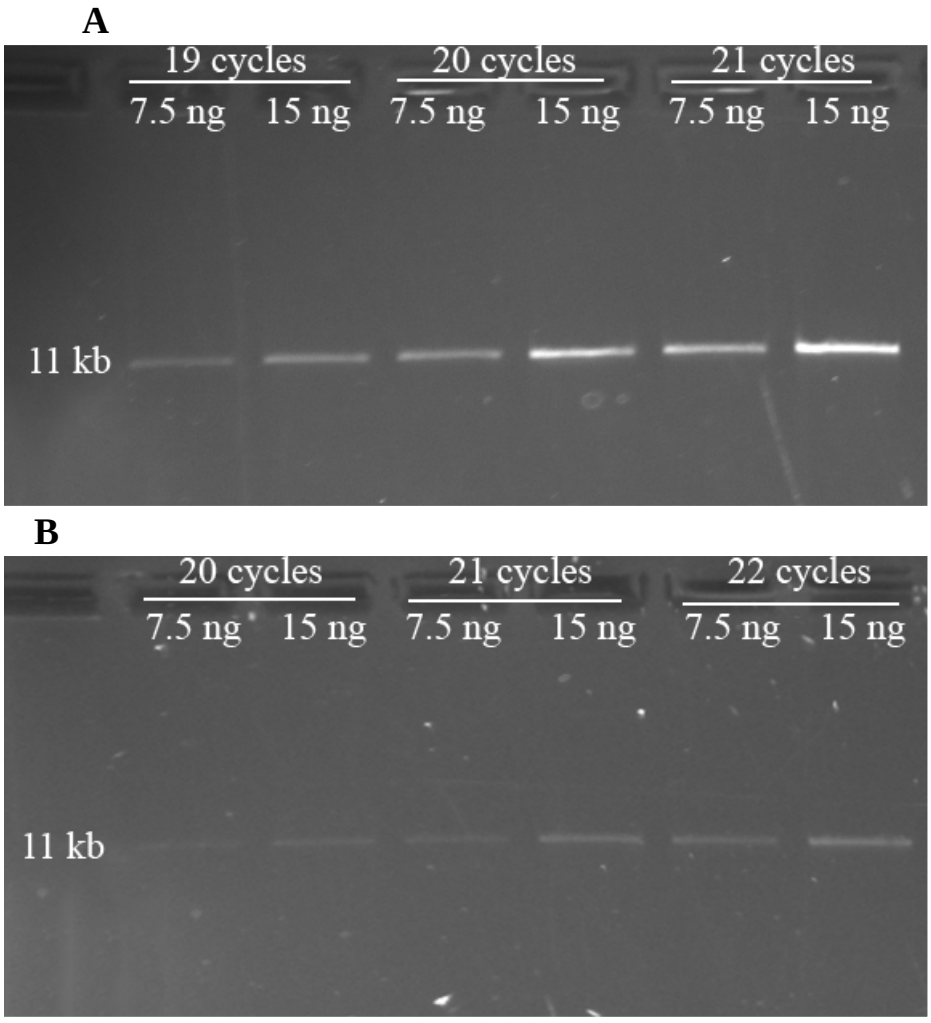

Figure 2.11 PCR products fractionated on agarose gels for ptDNA (A) and for mtDNA (B).

To determine the efficiency of long PCR, we modified a method commonly used for calculating qPCR efficiency (Pfaffl, 2001). We selected three points from the exponential curve and plotted the log of product-band intensity at a given cycle number. The slope of the line was then used to calculate the efficiency using the equation $10^{-(1/slope)}$ and determined as 2.1 or 110% for ptDNA and 2.0 or 100% for mtDNA (Figure 2.12). Generally acceptable efficiencies for qPCR are between 90-110%.

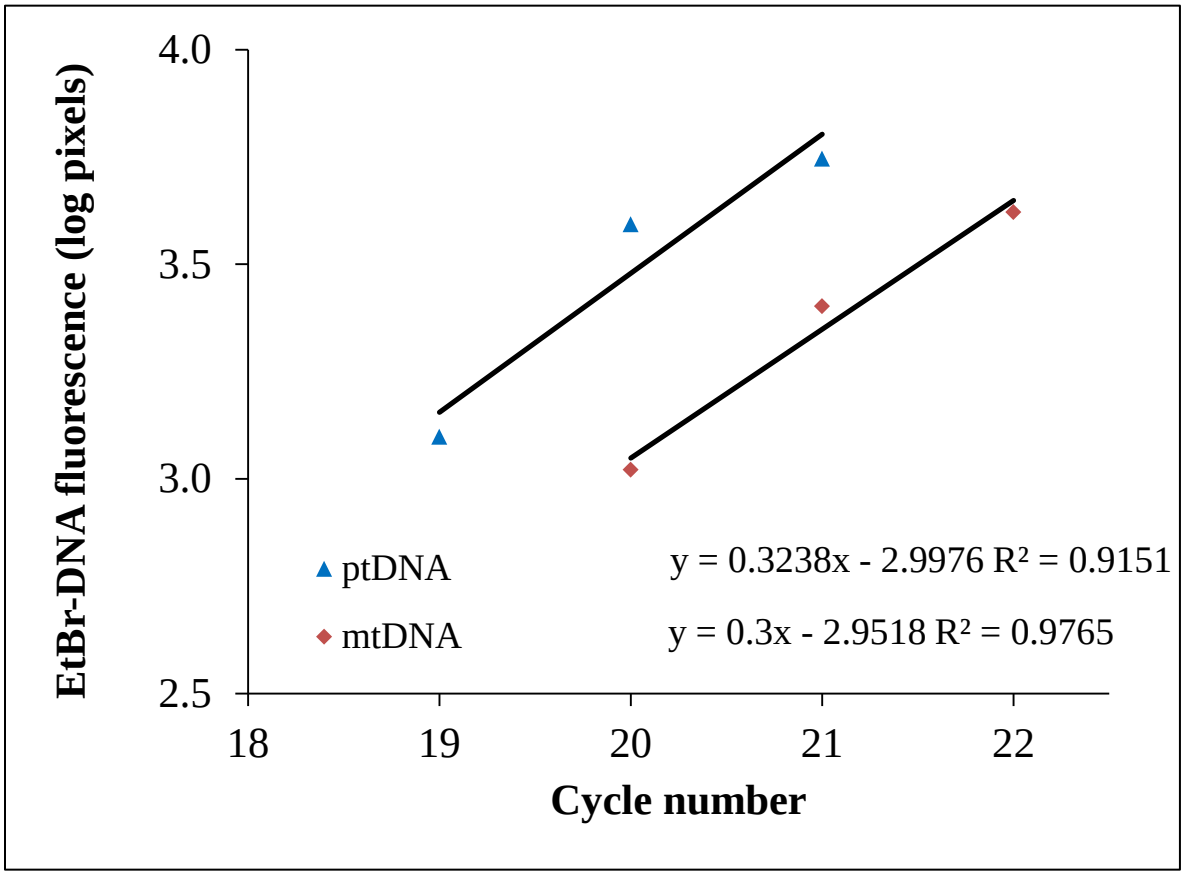

Figure 2.12 PCR products over three PCR cycles in the exponential phase for ptDNA

PCR products were quantified by measuring band intensities (in pixels) on agarose gels using ImageJ for ptDNA (blue) and mtDNA (red).

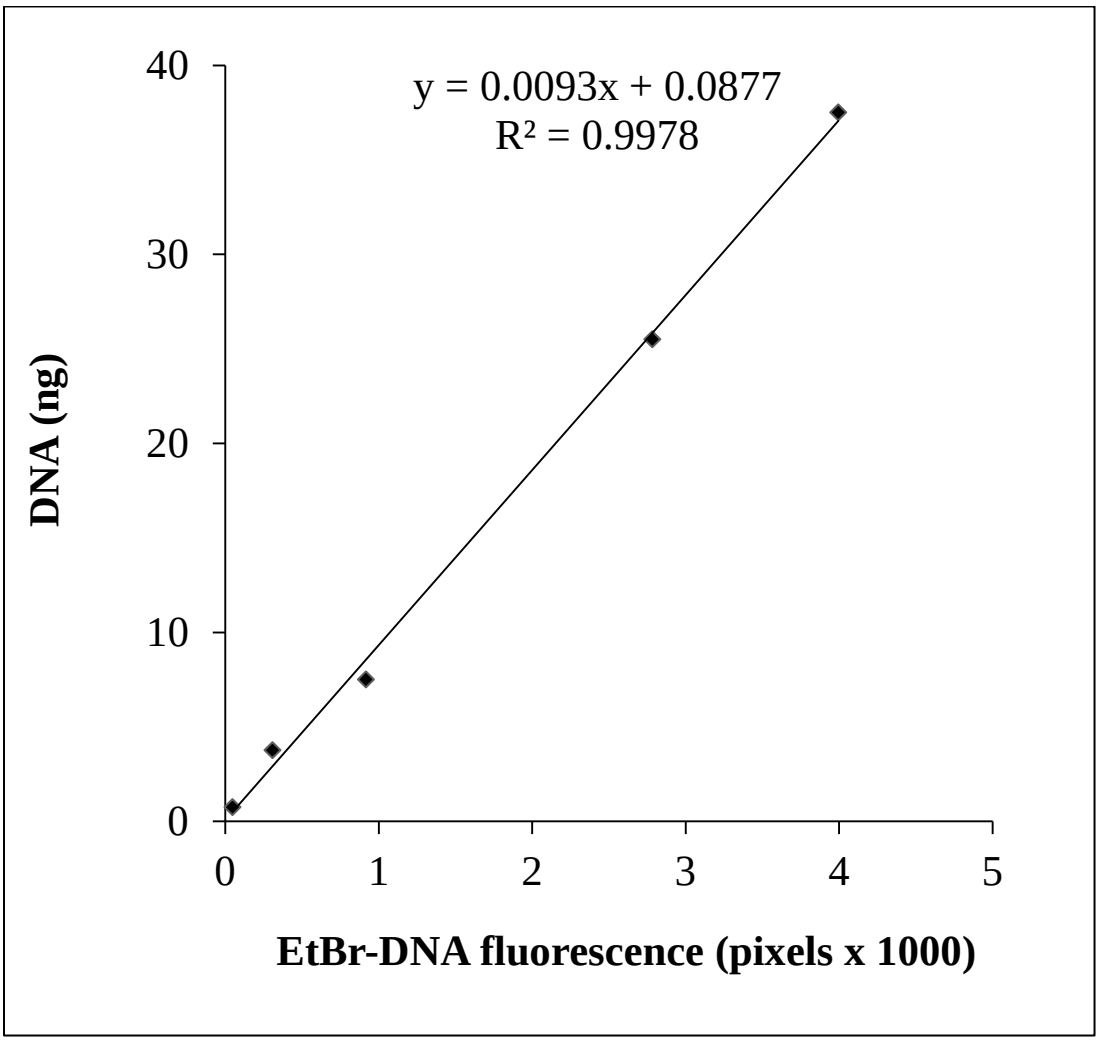

Figure 2.13 Gel quantification of long-PCR products using DNA mass standards

A DNA MassRuler (Fermentas) was used to quantify long-PCR products. A MassRuler standard curve (Figure 2.13) was produced using a dilution series (0.8 to 38 ng load) (see Figure 2.15), fractionation on an agarose gel, and measurement of the EtBr-DNA fluorescence (pixels) of the 10 kb standard (using ImageJ). DNA copy number at the end of the PCR was then calculated using the following equation:
(Amount of DNA in ng$\times 6.022\times 10^{23}$) ÷ (size of PCR product in bp$\times 10^{9}\times 650$).
Where, 6.022×10^{23} is Avogadro's number, the size of long PCR product for ptDNA is 11207 bp and 11164 bp for mtDNA, average weight of a base pair (bp) is 650 daltons, and multiplication by 10^{9} for ng conversion.
Finally, copies of orgDNA in template DNA was determined by
Number of copies at the end of PCR ÷ $2^{\text{number of cycles}}$.
A standard curve generated by fractionating MassRuler ladders with different concentrations (in ng) and band intensities (in pixels) for a 10 kb band.

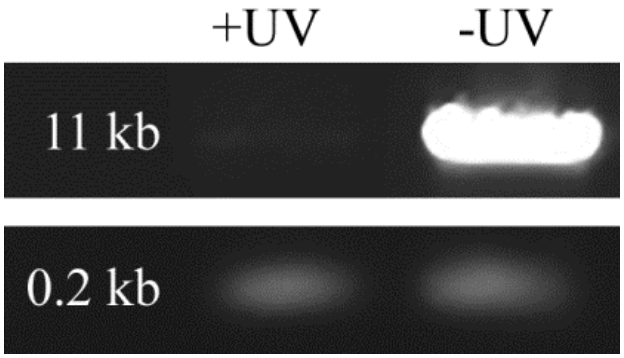

Figure 2.14 Validation of long PCR

PCR products of ttDNA treated with or without UV fractionated by agarose gel electrophoresis. ttDNA from light-grown top of stalk tissue (S2) was either treated with UV (~240 J/m^2) using Stratalink (+UV) or left untreated (-UV). A long PCR was performed to amplify an ~11 kb region of ptDNA and a short PCR was performed to amplify a 207 bp region of ptDNA. Short PCR served as a control for the amount of input DNA, which is evident by the presence of equal intensity bands in +/- UV samples. The presence of a very faint 11-kb band in +UV, compared with –UV, indicates that impediments due to UV treatment (pyrimidine dimers) can block the polymerase and decrease amplification, showing the sensitivity of the long-PCR procedure in detecting DNA lesions.

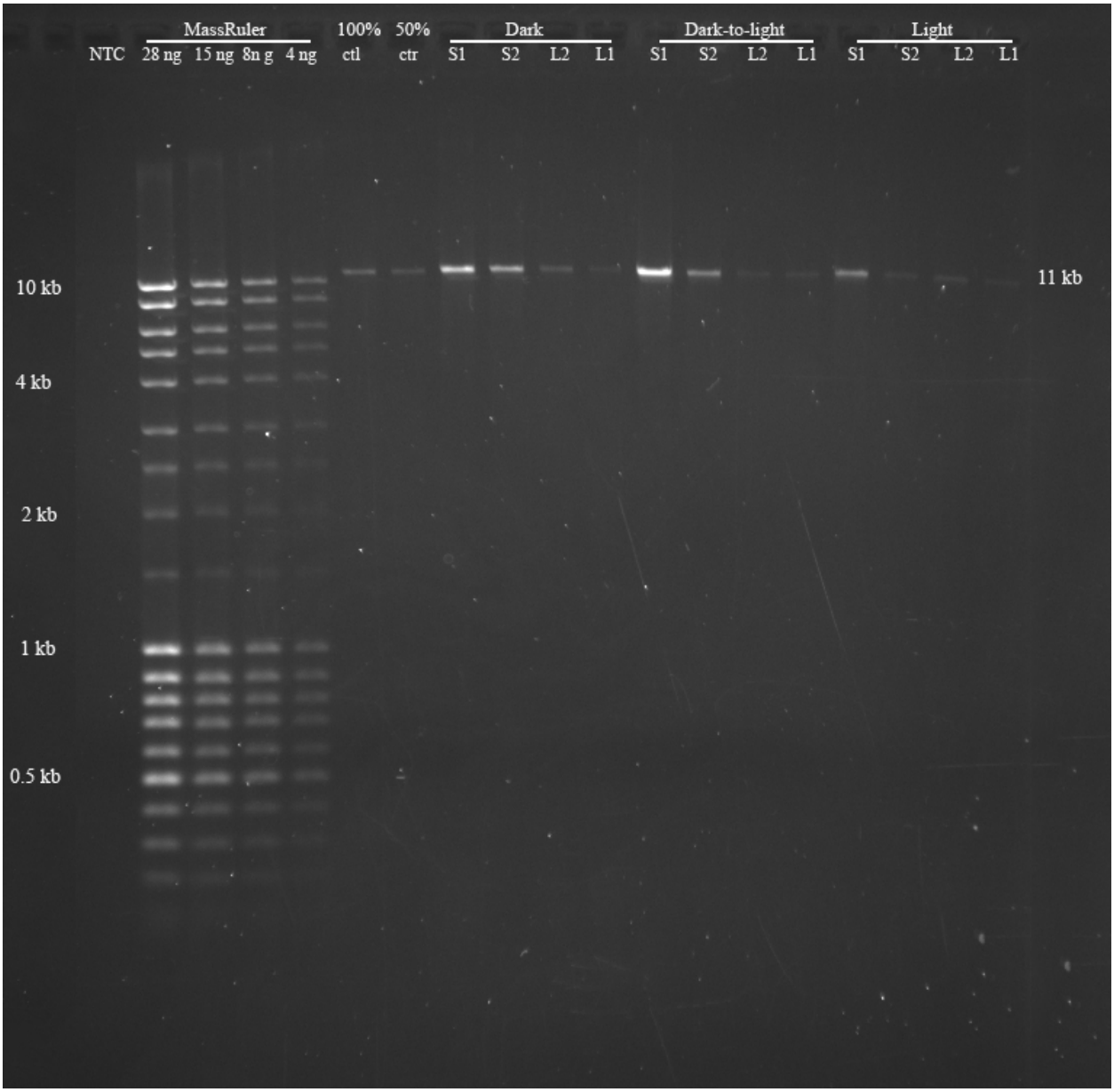
MassRuler
100%
50%
Dark
Dark-to-light
Light
NTC
28 ng
15 ng
8n g
4 ng
ctl
ctr
S1
S2
L2
L1
S1
S2
L2
L1
S1
S2
L2
L1
10 kb
4 kb
2 kb
1 kb
0.5 kb
11 kb

Figure 2.15 Performing long PCR on tissue samples

Controls and long PCR products fractionated by agarose gel electrophoresis. S1 is the base of the stalk, S2 is the top of the stalk and L2 and L1 are leaf 1 and leaf 2, respectively. The 11-kb mtDNA fragment is the only PCR product for each tissue, and the copy number varies among tissues. The 100% and 50% controls were used for every long PCR reaction, and this control was prepared from light-grown stalk tissue. Figure 2.15 shows the agarose gel-fractionation of the products from a typical long PCR experiment, using the optimized conditions described above. We include several controls in every long-PCR experiment: no DNA template control (NTC), template control (ctl) with 15 ng (100%) and 7.5 ng (50%) total tissue DNA, and MassRuler DNA standards. The assay is validated only if the EtBr-DNA fluorescence intensity of the 50% ctl is between 40-60% of the 100% ctl. For example, in Figure 2.15, the 50% ctl is 54% of the 100% ctl, validating the assay.To assess orgDNA lesions/10 kb, the sample band intensities are normalized to qPCR-determined orgDNA copies, as described in Materials and methods. The sample with highest normalized intensity is set at 1 and used to determine the relative amplification for the other samples.Using a standard curve generated by MassRuler (as shown in Figure 2.13), we determined the long-template copies for the samples as described above. These copies were then normalized to a single copy nuclear gene, *adh1*, for miPCR quantification.

Table 2.3 DNA copies determined using real-time qPCR, long PCR, and miPCR

Growth Condition	Tissues	**A** nucDNA copies (qPCR)[a]	**B** ptDNA copies (qPCR)[b]	**C** ptDNA copies (long PCR)[c]	**C/B×100** % unimpeded ptDNA[d]	**B/A** ptDNA/ nucDNA (qPCR)[e]	**C/A** unimpeded ptDNA/nucDNA (miPCR)[f]
Dark	Base of stalk	10316	3156667	30453	0.96	306	2.95
	Top of stalk	12028	9096667	13952	0.15	756	1.16
	Leaf 2	22020	15995833	33458	0.21	726	1.52
	Leaf 1	22742	19361667	2080	0.01	851	0.09
Dark-to-light	Base of stalk	17563	3427500	12703	0.37	195	0.72
	Top of stalk	9033	7330833	30657	0.42	812	3.39
	Leaf 2	11601	13617500	30715	0.23	1174	2.65
	Leaf 1	16809	17706667	1899	0.01	1053	0.11
Light	Base of stalk	20816	5715000	5572	0.10	275	0.27
	Top of stalk	15252	8848333	53449	0.60	580	3.50
	Leaf 2	15618	16776667	5528	0.03	1074	0.35
	Leaf 1	21373	16005000	3122	0.02	749	0.15

Growth Condition	Tissues	**A** nucDNA copies (qPCR)[a]	**D** mtDNA copies (qPCR)[b]	**E** mtDNA copies (long PCR)[c]	**E/D×100** % unimpeded mtDNA[d]	**D/A** mtDNA/ nucDNA (qPCR)[e]	**E/A** unimpeded mtDNA/nucDNA (miPCR)[f]
Dark	Base of stalk	10316	1009667	5636	0.56	98	0.546
	Top of stalk	12028	365000	623	0.17	30	0.052
	Leaf 2	22020	532083	891	0.17	24	0.040
	Leaf 1	22742	580667	78	0.01	26	0.003
Dark-to-light	Base of stalk	17563	1167667	4136	0.35	66	0.235
	Top of stalk	9033	194600	959	0.49	22	0.106
	Leaf 2	11601	355833	826	0.23	31	0.071
	Leaf 1	16809	367833	84	0.02	22	0.005
Light	Base of stalk	20816	1051333	1574	0.15	51	0.076
	Top of stalk	15252	401833	2643	0.66	26	0.173
	Leaf 2	15618	358333	105	0.03	23	0.007
	Leaf 1	21373	372417	103	0.03	17	0.005

Data are shown for one of the five biological replicates for qPCR and long-PCR assays and used to calculate org DNA copy number. Absolute values from qPCR and long-PCR assays were determined using DNA standards (Materials and methods)

[a] Genome copy number of nucDNA per ng of ttDNA was determined by qPCR based on the standard curve for a single copy gene, *adh1*.

[b] Genome copy number of ptDNA or mtDNA per ng of ttDNA was determined by qPCR based on the standard curve for a single copy gene, *rps14* or *nad4*, respectively.

[c] Genome copy number of ptDNA or mtDNA per ng of ttDNA was determined by long PCR and based on a standard curve using DNA ladder standards (MassRuler).

[d] The percentage of unimpeded orgDNA was determined by dividing long orgDNA copies by qPCR-determined orgDNA copies and multiplying by 100.

[e] orgDNA copies per haploid nucDNA was determined by dividing qPCR-determined orgDNA copies by nucDNA copies.

[f] orgDNA copies per haploid nucDNA using miPCR was determined by dividing long orgDNA copies by nucDNA.

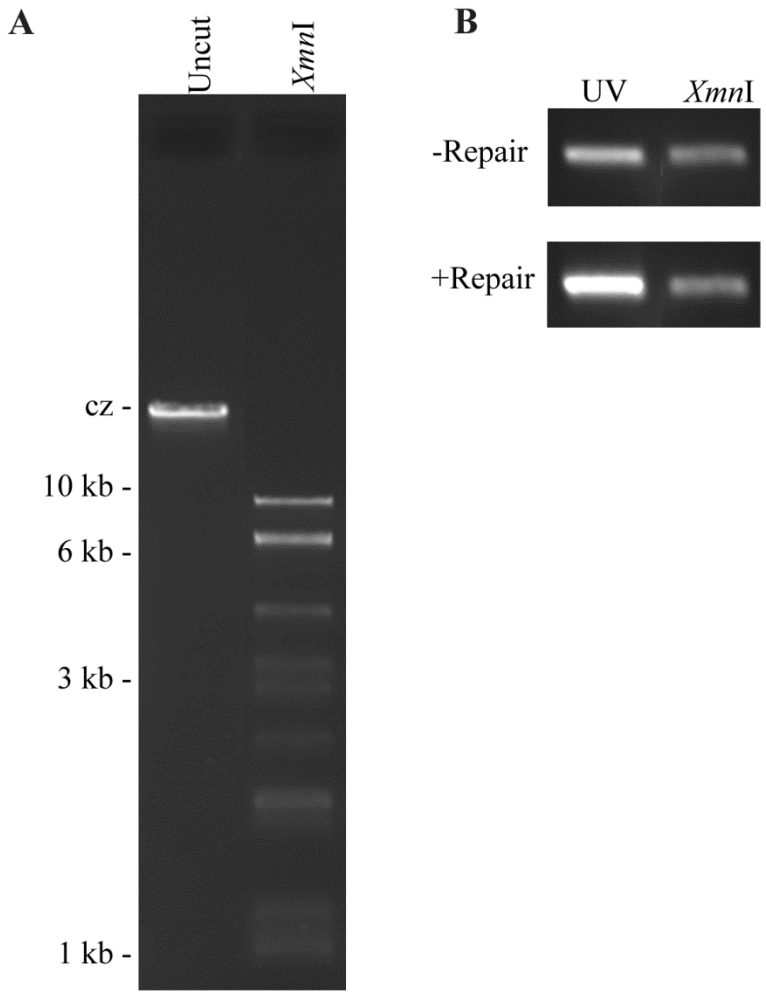

Figure 2.16 Validation of PreCR repair kit

Agarose gel electrophoresis of lambda DNA either not digested or digested with *Xmn*I (A).PCR products fractionated on agarose gels of UV-treated or *Xmn*I digested DNA (B). The PreCR repair kit (New England Biolabs, MA) was validated using the UV-treated control lambda DNA, provided by the manufacturer, as well as with the fragmented lambda DNA prepared by digesting with *Xmn*I. A complete digestion was confirmed by fractionating the products on agarose gel (Figure 2.15A). UV-treated and fragmented lambda DNA was either incubated with enzyme mix (+Repair) or left unrepaired (-Repair). PCR was performed to amplify a 1-kb product using L1 primers and UV-treated and fragmented lambda DNA. The PCR products were fractionated to compare band intensities for +Repair and –Repair (Figure 2.15B). The PreCR repair enzyme mix successfully repaired the UV-treated DNA but not the fragmented DNA.

Table 2.4 Abbreviations

Tissues	Abbreviation
Base of stalk	S1
Top of stalk	S2
Leaf2	L2
Leaf1	L1

Table 2.5 Tukey comparisons of growth conditions

Tissues compared	% unimpeded orgDNA	qPCR	miPCR	% unimpeded orgDNA	qPCR	miPCR
S1:S2	ns	***	**	ns	***	ns
S1:L2	*	***	ns	**	***	***
S1:L1	***	***	ns	***	***	***
S2:L2	*	***	ns	**	***	***
S2:L1	***	***	***	***	**	***
L2:L1	*	ns	**	ns	ns	ns

Maize seedlings were grown in three light conditions (dark, dark-to-light and light) and tissues representing four developmental stages (base of stalk; top of stalk; leaf1; and leaf2, see abbreviations in Table 2.4) were analyzed. Seedlings for five sets of independent biological replicates were grown and tissues harvested. A total of sixty ttDNA samples were produced (4 tissues x 3 growth conditions x 5 biological replicates). Statistical analyses were performed to compare the growth conditions. Color code: green for ptDNA; purple for mtDNA. ns: not significant. Significance codes: *** $p \leq 0.001$; ** $p \leq 0.01$; * $p \leq 0.05$.

Table 2.6 Tukey comparisons of developmental stages

Growth conditions compared	% unimpeded orgDNA	qPCR	miPCR	% unimpeded orgDNA	qPCR	miPCR
Dark and Dark-to-light	ns	ns	*	ns	ns	ns
Dark and Light	**	ns	**	*	ns	*
Dark-to-light and Light	ns	ns	ns	ns	ns	ns

Maize seedlings were grown in three light conditions (dark, dark-to-light and light) and tissues representing four developmental stages (base of stalk; top of stalk; leaf1; and leaf2, see abbreviations in Table 2.4) were analyzed. Seedlings for five sets of independent biological replicates were grown and tissues harvested. A total of sixty ttDNA samples were produced (4 tissues x 3 growth conditions x 5 biological replicates). Statistical analyses were performed to compare the developmental stages. Color code: green for ptDNA; purple for mtDNA. ns: not significant. Significance codes: *** $p \leq 0.001$; ** $p \leq 0.01$; * $p \leq 0.05$.

Table 2.7 Tukey multiple comparisons of growth conditions for each tissue

	% unimpeded orgDNA	qPCR	miPCR	% unimpeded orgDNA	qPCR	miPCR
Dark and Dark-to-light						
S1	**	ns	ns	*	ns	ns
S2	ns	ns	ns	ns	*	ns
L2	ns	ns	ns	ns	ns	ns
L1	ns	ns	ns	ns	*	ns
Dark and Light						
S1	***	ns	***	*	ns	**
S2	ns	ns	ns	ns	ns	ns
L2	*	ns	ns	ns	ns	ns
L1	ns	ns	ns	ns	***	ns
Light and Dark-to-light						
S1	ns	ns	ns	ns	ns	ns
S2	ns	ns	ns	ns	ns	ns
L2	ns	ns	ns	ns	ns	ns
L1	ns	ns	ns	ns	ns	ns

Maize seedlings were grown in three light conditions (dark, dark-to-light and light) and tissues representing four developmental stages (base of stalk; top of stalk; leaf1; and leaf2, see abbreviations in Table 2.4) were analyzed. Seedlings for five sets of independent biological replicates were grown and tissues harvested. A total of sixty ttDNA samples were produced (4 tissues x 3 growth conditions x 5 biological replicates). Statistical analyses were performed to compare growth conditions for each tissue. Color code: green for ptDNA; purple for mtDNA. ns: not significant. Significance codes: *** $p \leq 0.001$; ** $p \leq 0.01$; * $p \leq 0.05$.

Table 2.8 Tukey multiple comparisons of tissues for each growth condition

	% unimpeded orgDNA	qPCR	miPCR	% unimpeded orgDNA	qPCR	miPCR
Dark						
S1:S2	*	***	ns	*	***	**
S1:L2	**	***	ns	**	***	*
S1:L1	***	***	ns	***	***	***
S2:L2	ns	ns	ns	ns	ns	ns
S2:L1	**	ns	*	*	ns	*
L2:L1	ns	ns	ns	*	ns	ns
Dark-to-light						
S1:S2	ns	***	ns	ns	***	ns
S1:L2	**	***	ns	*	***	*
S1:L1	**	***	ns	*	***	***
S2:L2	*	ns	ns	ns	ns	ns
S2:L1	**	ns	*	ns	ns	ns
L2:L1	ns	ns	ns	ns	ns	ns
Light						
S1:S2	ns	***	**	ns	**	ns
S1:L2	*	***	ns	ns	***	ns
S1:L1	ns	***	ns	ns	***	ns
S2:L2	**	*	ns	*	ns	*
S2:L1	*	ns	ns	*	*	*
L2:L1	ns	ns	ns	ns	ns	ns

Maize seedlings were grown in three light conditions (dark, dark-to-light and light) and tissues representing four developmental stages (base of stalk; top of stalk; leaf1; and leaf2, see abbreviations in Table 2.4) were analyzed. Seedlings for five sets of independent biological replicates were grown and tissues harvested. A total of sixty ttDNA samples were produced (4 tissues x 3 growth conditions x 5 biological replicates). Statistical analyses were performed to compare the the tissues for each growth condition. Color code: green for ptDNA; purple for mtDNA. ns: not significant. Significance codes: *** $p \leq 0.001$; ** $p \leq 0.01$; * $p \leq 0.05$.

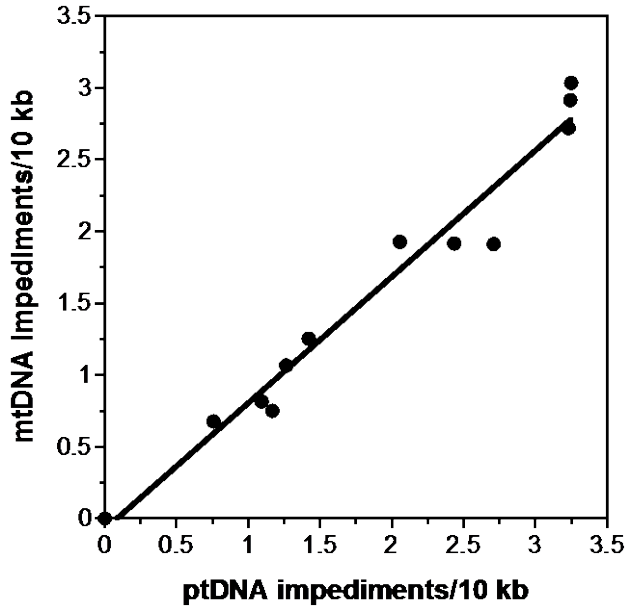

Figure 2.17 Correlation between ptDNA and mtDNA for impediments/10 kb

The relationship between ptDNA and mtDNA was analyzed by the linear regression model. The average values for all the tissues and growth conditions were used to plot the graph. Analysis showed a strong correlation between ptDNA and mtDNA, with $R^2 = 0.97$ and $p = 1.3 \times 10^{-8}$.

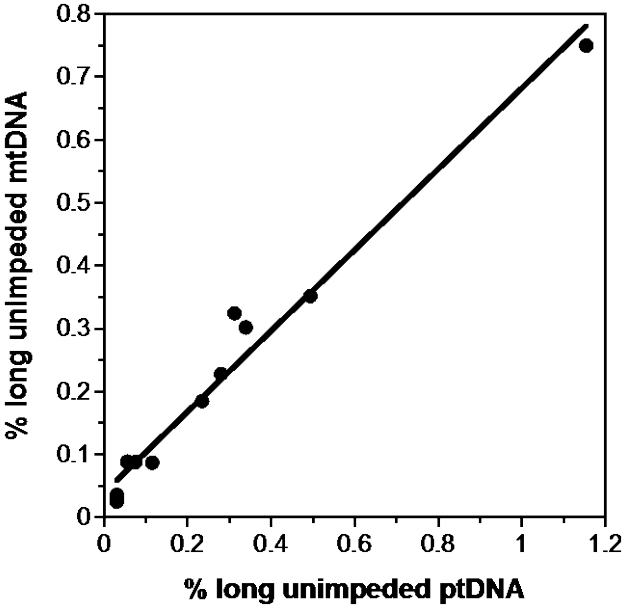

Figure 2.18 Correlation between ptDNA and mtDNA for percentage of unimpeded long orgDNA copies

The relationship between ptDNA and mtDNA was analyzed by the linear regression model. The average values for all the tissues and growth conditions were used to plot the graph. Analysis showed a strong correlation between ptDNA and mtDNA, with $R^2 = 0.97$ and $= 4.8 \times 10^{-9}$.

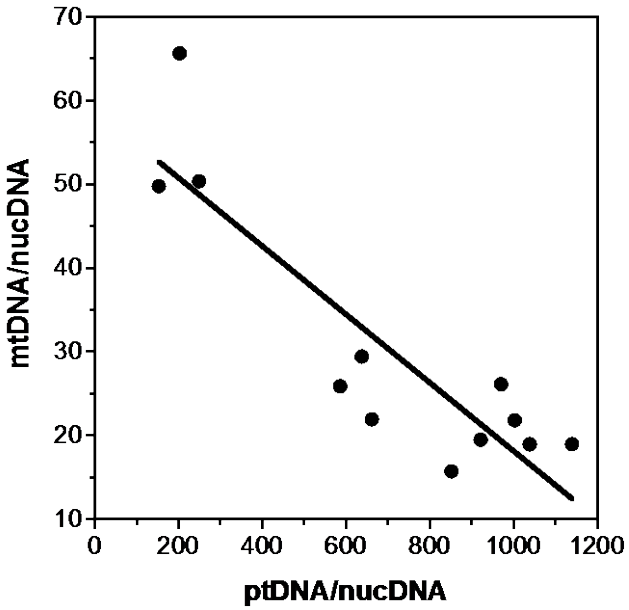

Figure 2.19 Correlation between ptDNA/nucDNA and mtDNA/nucDNA determined by qPCR

The relationship between ptDNA and mtDNA was analyzed by the linear regression model. The average values for all the tissues and growth conditions were used. There is a strong correlation between ptDNA and mtDNA, with $R^2 = 0.8$ and $p = 1.4 \times 10^{-4}$.

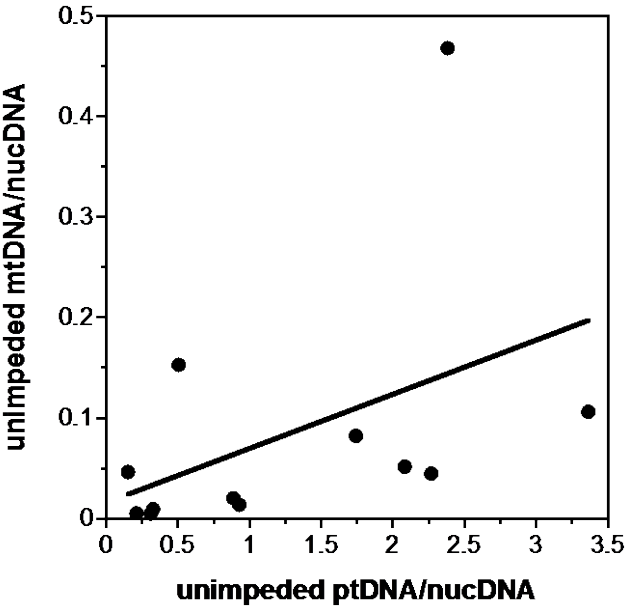

Figure 2.20 Correlation between ptDNA and mtDNA for unimpeded orgDNA/nucDNA

The relationship between ptDNA and mtDNA was analyzed by the linear regression model. The average values for all the tissues and growth conditions were used to plot the graph. Analysis showed no correlation between ptDNA and mtDNA, with $R^2 = 0.2$ and $p = 0.14$.

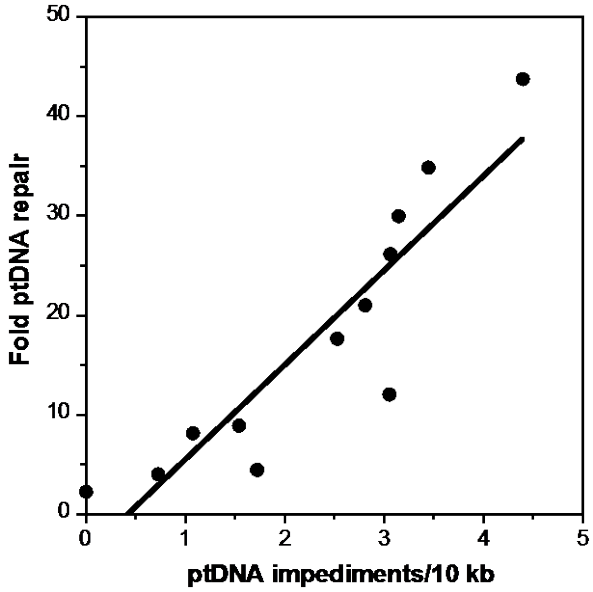

Figure 2.21 Correlation between fold ptDNA repair and ptDNA impediments/10 kb

The relationship between amount of ptDNA damage and repair was analyzed by the linear regression model. The average values for all the tissues and growth conditions were used to plot the graph. Analysis showed a strong correlation between ptDNA damage and repair, with $R^2 = 0.8$ and $p = 6.3 \text{ X } 10^{-5}$.

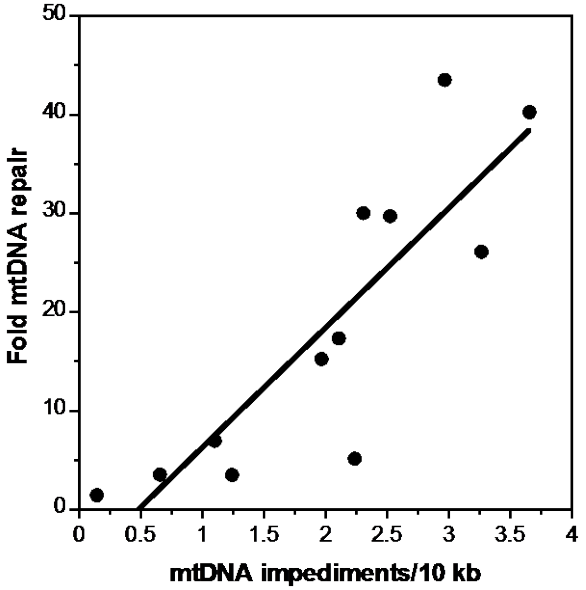

Figure 2.22 Correlation between fold mtDNA repair and mtDNA impediments/10 kb

The relationship between amount of mtDNA damage and repair was analyzed by the linear regression model. The average values for all the tissues and growth conditions were used to plot the graph. Analysis showed a strong correlation between mtDNA damage and repair, with $R^2 = 0.7$ and $p = 3.9,X,10^{-4}$.

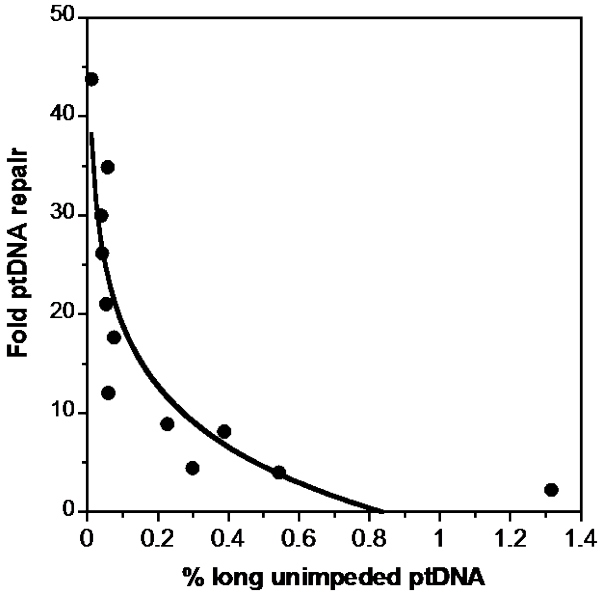

Figure 2.23 Correlation between fold ptDNA repair and % unimpeded ptDNA

The relationship between amount of ptDNA repair and % unimpeded ptDNA was analyzed by the logarithmic regression model. The average values for all the tissues and growth conditions were used to plot the graph. Analysis showed an inverse correlation between ptDNA repair and % unimpeded ptDNA, with $R^2 = 0.81$ and $p = 0.02$.

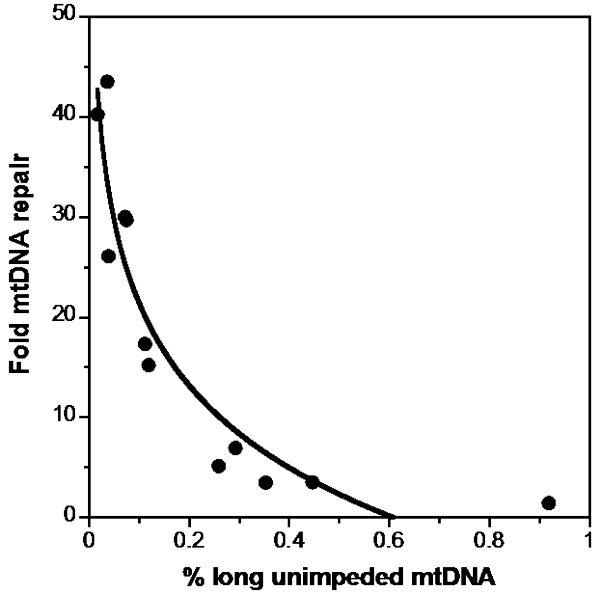

Figure 2.24 Correlation between fold mtDNA repair and % unimpeded mtDNA

The relationship between amount of mtDNA repair and % unimpeded mtDNA was analyzed by the logarithmic regression model. The average values for all the tissues and growth conditions were used to plot the graph. Analysis showed an inverse correlation between mtDNA repair and % unimpeded mtDNA, with $R^2 = 0.88$ and $p = 5 \text{ X } 10^{-3}$.

Chapter 3

MOLECULAR INTEGRITY OF CHLOROPLAST DNA AND MITOCHONDRIAL DNA IN MESOPHYLL AND BUNDLE SHEATH CELLS OF MAIZE

3.1 Abstract

Plants that conduct C_4 photosynthesis differ from those that employ C_3 photosynthesis with respect to leaf anatomy, biochemical pathways, and the proteins and RNA transcripts present in the leaf mesophyll (M) and bundle sheath (BS) cells. Here, we investigate the organellar DNA (orgDNA) from plastids and mitochondria in these two cell types. We use standard qPCR, long PCR, and DNA damage analysis to quantify the amount and quality of orgDNA in isolated M and BS cells of maize. When compared to M cells, BS cells have less orgDNA damage and a higher percentage of unimpeded orgDNA. In addition, the orgDNA is more fragmented in M than BS cells, although orgDNA in BS is subject to more *in vitro* repair. We suggest that the differences in molecular integrity of orgDNA in these two cells are due to higher levels of reactive oxygen species in M than BS cells.

3.2 Introduction

C_4 photosynthesis is partitioned into mesophyll (M) and bundle sheath (BS) cells, with light-dependent oxygenic reactions occurring in M and light-independent carbon reduction occurring in BS cells (Langdale, 2011). C_4 plants, such as maize, can use energy, nitrogen and water more efficiently than C_3 plants (Hibberd *et al.*, 2008). Maize exhibits a typical Kranz leaf anatomy, with a ring of BS cells surrounding the vascular bundle. The ratio of BS to M cells is high in a maize leaf, which increases the vein density compared to a leaf without Kranz anatomy. In

maize, the M cells have thin cell walls, whereas the walls in BS cells are thick and suberized, thus impeding the flow of gases (Langdale, 2011). In BS cells, chloroplasts are located centrifugally relative to the vein and adjacent to M cells, whereas mitochondria are located centripetally (Sage *et al.*, 2014). In M cells, however, both chloroplasts and mitochondria are distributed randomly and chloroplasts exhibit a strong photoavoidance response (Yamada *et al.*, 2009).

The anatomical differences between M and BS cells augment the biochemical differences revealed by physiological, proteomic, and transcriptomic analyses. The stacked grana in M cells contain photosystem I (PSI) and photosystem II (PSII), whereas the grana are unstacked in BS cells and contain mostly PSI with little PSII (Majeran and van Wijk, 2009). Kranz anatomy and increased vein density lead to physical associations between M and BS cells that facilitate the flow of metabolites (Nelson, 2011). Carbon is assimilated in M and transferred to BS cells, where it is reduced. M cells perform the energy-demanding synthesis of lipids, tetrapyrrole, and isoprenoids and contain antioxidant systems to minimize the effects of reactive oxygen species (ROS) generated during photosynthetic electron transport (Majeran *et al.*, 2005). M cells perform glycolysis, have low respiratory activity, and generate oxygen in the light-dependent splitting of water (Ku *et al.*, 1974; Li *et al.*, 2010). By contrast, BS cells perform the light-independent and oxygen-consuming reactions of respiration and photorespiration and may be hypoxic relative to M cells in maize.

Despite extensive studies comparing M and BS cells, little is known about the properties of organellar DNA (orgDNA) in chloroplasts and mitochondria for these two cell types. Lindbeck *et al.* (1989) reported similar amounts of DNA in chloroplasts of M and BS cells of maize using fluorochrome-based fluorescence of nucleoids, but also found that the nucleoids in BS were

smaller and more numerous than in M cells. Here, we compare orgDNA from M and BS cells using a recently-developed procedure for quantifying long DNA segments by PCR (Kumar *et al.*, 2014). In maize, we find more orgDNA damage, more fragmentation, and a lower percentage of orgDNA molecules with impediments that prevent amplification by *Taq* DNA polymerase in M than BS cells. An *in vitro* repair assay reveals more repairable lesions in orgDNA from BS than M cells. The decline during leaf development in orgDNA copies, structure, and integrity was attributed to accumulation of ROS causing DNA damage (Oldenburg *et al.*, 2013; Zheng *et al.*, 2011), and the differences between M and BS cells may be attributed to different levels of DNA-damaging ROS.

3.3 Materials and methods

3.3.1 *Isolation of mesophyll cells and bundle sheath strands*

Zea mays (inbred line B73) seeds were imbibed overnight and sown in Sunshine #4 soil. Plants were grown at 24°C with 16/8 hr photoperiods for 14 days (Figure 3.1A). Seedlings were washed with 0.5% sarkosyl for ~3 min and rinsed with distilled water to minimize microbial contamination. The leaf blades (above the ligule) from first (Leaf1), second (Leaf2) and third (Leaf3) leaves from 10-15 plants were harvested and used for the preparation of mesophyll (M) protoplasts and bundle sheath (BS) strands. Five independent sets of seedlings were grown, representing five biological replicates. Each biological replicate was comprised of six samples (3 leaves X 2 cell types) and a total of thirty samples were analyzed.

The procedure for preparation of mesophyll protoplasts was optimized by testing several parameters: concentration of osmoticum (0.4-0.8% mannitol), enzymes (1-2% cellulase and 0.1-0.5% macerase), time (1-3 hr) and temperature (4°C and room temperature) for protoplasting and Percoll concentration (25-40%) for purification of protoplasts (Figure 3.7-3.9). The best process

for preparation of M protoplasts was to cut the leaf blades into strips and vacuum-infiltrate with protoplasting buffer (PrB; 0.6 M mannitol, 10 mM MES pH 5.7, 1 mM $CaCl_2$, 5 mM β-mercaptoethanol and 0.1% BSA [w/v]) containing 1.5% cellulase [w/v] and 0.3% macerase [w/v] for 30 min, followed by incubation at room temperature with shaking (80 rpm) for 2 hr. The digested tissue was filtered through a 50-µm sieve and centrifuged at 150 x g for 2 min to pellet the protoplasts. Intact protoplasts were obtained by centrifugation using 25% Percoll (v/v) in PrB buffer and washed twice with PrB buffer. An aliquot of the purified M protoplasts was used to assess the purity (described below) and the remaining samples were frozen in liquid nitrogen for subsequent DNA extraction.

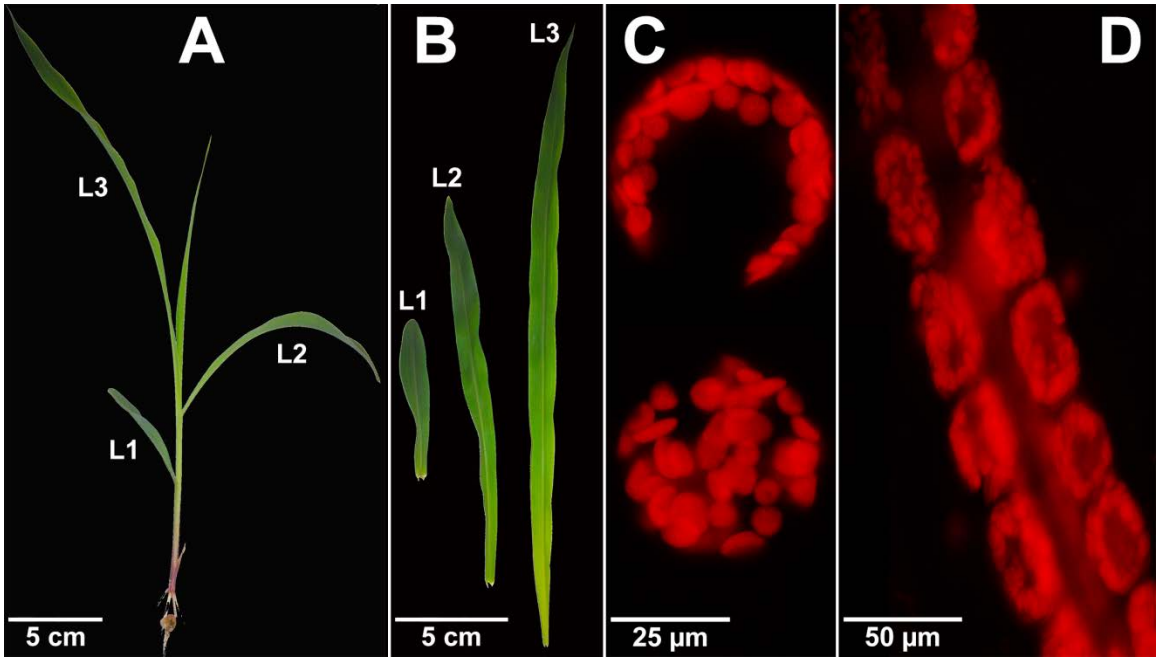

Figure 3.1 (A) maize seedling grown in light; (B) Leaf1 (L1), Leaf2 (L2) and Leaf3 (L3); (C) mesophyll protoplasts; (D) bundle sheath strand.

To isolate BS strands, leaf blades were cut into strips and the tissue was homogenized using a Polytron PT 3000 homogenizer (Kinematica Inc, NY) in high salt buffer (HSB; 1.25 M NaCl, 40 mM HEPES pH 7.6, 2 mM EDTA, 0.1% BSA [w/v] and 14.2 mM β-mercaptoethanol).We

assessed the type of homogenizer blades, the number and duration of pulses, and the speed for homogenization. The best results were obtained with small, sharp blades (PT DA 3020 generator) affixed to the Polytron PT 3000 homogenizer and using four-10 s pulses at 17,000 rpm. The homogenate was filtered through a 1200-µm sieve to remove large pieces of leaf tissue. The BS strands were then collected on a 100-µm sieve and washed with HSB until the filtrate was clear. An aliquot of the BS strands was used to assess purity and the remaining samples were frozen in liquid nitrogen for subsequent DNA extraction.

The purity of M protoplasts and BS strands was assessed in three ways. First, microscopic examination was performed. Then, the enzymatic activities of PEP carboxylase and NADP-malic enzyme were determined as indicators for M and BS, respectively (Kanai and Edwards, 1973). Oxidation of NADH and reduction of NADP was measured at 340 nm to determine the activity of PEP carboxylase and NADP-malic enzyme respectively (Table 3.2). Lastly, the chlorophyll a/b ratio was determined since M and BS have characteristic chlorophyll a/b ratios (Kanai and Edwards, 1973; Woo *et al.*, 1971). Chlorophyll was extracted using ethanol and absorbance was measured at 649 nm, 665 nm, and 700 nm to determine chlorophyll a/b (Table 3.2).

3.3.2 *DNA extraction*

Total tissue DNA (ttDNA) was extracted directly from frozen M protoplasts, whereas BS strands were powdered with dry ice before ttDNA extraction. The ttDNA was extracted using the CTAB procedure (Rogers and Bendich, 1988b), and DNA quality was assessed by agarose gel electrophoresis (Figure 3.7 and 3.9). The DNA concentration was determined using Quant-it kit (Life Technologies, NY) and then diluted to 3 ng/µl. A total of 6 ng and 15 ng DNA was used for qPCR and long PCR, respectively.

3.3.3 *Assays of real-time qPCR, DNA damage, unimpeded orgDNA copies, miPCR, and in vitro repair*

OrgDNA properties were assessed using procedures previously described (Kumar *et al.*, 2014). Briefly, qPCR was performed to determine orgDNA copy number using plastid-specific and mitochondrial-specific primers. Long PCR was used to assess DNA damage (impediments per 10 kb) and orgDNA copy number relative to the haploid nuclear genome (miPCR) or relative to orgDNA copies determined by qPCR (% unimpeded). The ptDNA and mtDNA copies per haploid nuclear genome were determined using absolute quantification with DNA standards produced using maize ttDNA as template and the three primer sets. At least three technical replicates were used for each sample. We followed MIQE guidelines for qPCR (Bustin *et al.*, 2009).

DNA fragments of 11,207 bp and 11,164 bp were amplified using LongAmp *Taq* (New England Biolabs, MA) from ptDNA and mtDNA, respectively. The assay was optimized for cycle number to be in the exponential phase, primer efficiencies to be ~100%, and for orgDNA-specific primers (Supplemental Material 1 in Kumar *et al*., 2014). The template copies obtained by long-PCR were used for determining damage (impediments/10 kb) and unimpeded orgDNA (percentage of unimpeded orgDNA and unimpeded orgDNA per haploid genome). For determining percentage of long unimpeded orgDNA copies, long-PCR template copies (unimpeded orgDNA) were normalized to qPCR-determined orgDNA copies and multiplied by 100 to give a percentage (Table S1 in Kumar *et al*., 2014). To obtain miPCR copies, long-PCR template orgDNA copies were normalized to a single copy nuclear DNA gene (*adh1* copies determined by qPCR, described below) (Table S1 in Kumar *et al*., 2014). In order to assess the amount of DNA damage attributed to repairable lesions, orgDNA was evaluated using long PCR with and without treatment with DNA repair enzymes (PreCR repair kit, New England Biolabs,

MS).

The primers used for qPCR amplification were:

adh1, 156 bp nucDNA-specific

adh1_left, 5’-GCTCCTCACAGGCTCATCTC-3’

adh1_right, 5’-AGGCGGACCTTTGCACTT-3’

rps14, 127 bp ptDNA-specific

rps14_F1, 5’-ATCTTGTTGCACCCGGTAAC-3’

rps14_R2, 5’-CCTACACGCCTTCATCGACGTT-3’

nad4, 187 bp mtDNA-specific

nad4_F2, 5’-GCAAAAGTCCTTCCACGGCA-3’

nad4_R1, 5’-AGCAAGCGTAGGCAACCAAAC-3’

The primers used for long PCR amplification were:

rps14, 11207 bp ptDNA-specific

rps14_F1, 5’-ATCTTGTTGCACCCGGTAAC-3’

rps14_R5, 5’-TATCCTGACCCTTTCTTGTGC-3’

nad4, 11164 bp mtDNA-specific

nad4_F3, 5’-GTTGGACCACAGGCAAAAGT-3’

trnk_R1, 5’-GCGAGGAATGGAAGCAGTAG-3’

3.3.4 *Statistical Analysis*

Statistical analyses were performed on the data obtained by qPCR, long PCR (% unimpeded long orgDNA copies), and miPCR for five independent biological replicates. The ANOVA model was applied to assess differences between M and BS from three leaves. If ANOVA revealed a significant p value, then the Tukey HSD test for multiple comparisons was used to

identify each pair of samples exhibiting a significant difference. Statistical analyses were not performed on the data obtained for impediments/10 kb because these are relative values that were determined independently for each biological replicate. Thus the values for all the replicates cannot be combined. Instead, normalized values (long-PCR orgDNA copies/qPCR orgDNA copies) for the replicates were averaged, and a single value of impediments/10 kb was determined for each tissue. The relationship between ptDNA and mtDNA was evaluated for these parameters: 1) copy number from qPCR; 2) orgDNA impediments/10 kb; 3) percentage of unimpeded orgDNA; and 4) copy number from miPCR. The linear regression model was employed to obtain R^2 (coefficient of determination) and p values. A strong correlation between ptDNA and mtDNA would be indicated for a given parameter with R^2 close to 1 and p value <0.05.

3.4 Results

Photosynthesis in maize is of the C_4 NADP-ME type and occurs in two cell types: light-dependent reactions in M cells and light-independent reactions in BS cells, leading to the differential accumulation of transcripts (Chang *et al.*, 2012) and proteins (Majeran *et al.*, 2005). The partitioning of photosynthesis may also lead to different redox conditions and levels of DNA-damaging ROS in these two cell types. Here, we investigate genome copy number and DNA damage within plastids and mitochondria of M and BS cells.

3.4.1 *Preparation of maize mesophyll cells and bundle sheath strands*

We optimized the isolation procedures for M protoplasts and BS strands to yield high-purity preparations, as well to obtain high-integrity DNA. The quality and purity of the M and BS preparations were evaluated by visual inspection, enzymatic analysis, and chlorophyll a/b ratios.

Intact M protoplasts and a BS strand are shown in Figure 3.1C and 1D, respectively. Microscopy showed neither BS strands in M preparations nor M protoplasts in BS preparations. Enzymatic activities for the M-specific PEP carboxylase and BS-specific NADP-malic enzyme revealed ~5% contamination of M with BS and ~6% contamination of BS with M (Table 3.2). The chlorophyll a/b ratio for maize was previously reported as ~3 for M and ~6 for BS (Kanai and Edwards, 1973; Woo *et al.*, 1971). The ratios we find are 3.2 ± 0.4 for M and 6.7 ± 0.3 for BS (Table 3.2). We conclude that cross-contamination is minimal for our preparations of M protoplasts and BS strands.

Total tissue DNA (ttDNA) was extracted from M protoplasts and BS strands obtained from the leaf blade of Leaf1, Leaf2, and Leaf3 of 14-day old maize seedlings (Figure 3.1). Both Leaf1 and Leaf2 were fully expanded, with the leaf blade separated from the sheath by the fully-developed ligule. Leaf3, however, had not yet reached full expansion and was partially curled within the stalk. After agarose gel electrophoresis, all of the ttDNA preparations showed a single band of high molecular weight DNA and no DNA-laddering, indicating DNA of high quality (Figure 3.7 and 3.9).

We previously employed qPCR to assess changes in ptDNA and mtDNA copy number during maize seedling development (Kumar *et al.*, 2014; Oldenburg *et al.*, 2013; Oldenburg *et al.*, 2006). We now use qPCR to evaluate orgDNA per haploid nuclear genome (nucDNA) in M and BS and find significantly higher ptDNA/nucDNA levels in M (average of ~2000-3300 copies) than BS (average of ~1100-1300 copies) ($p=0.002$, Figure 3.2A). Similar levels of ptDNA/nucDNA are found in all three leaves (Tables 3.5-3.7). ptDNA/nucDNA is less variable among biological replicates in BS (~900-1800) than in M (~800-7700) (Figure 3.10). For mtDNA/nucDNA, we find a significant difference between M and BS only for Leaf1 ($p=0.04$)

(Figure 3.2B, Table 3.6).

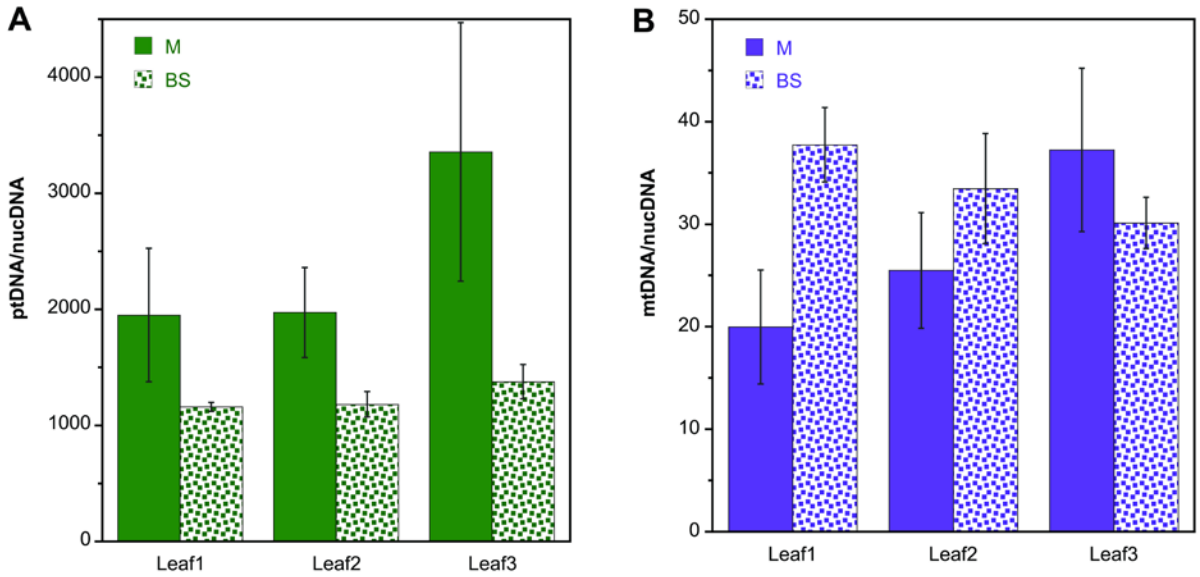

Figure 3.2 Plastid and mitochondrial genome copy number determined by qPCR

Total tissue DNA was prepared from mesophyll cells and bundle sheath strands isolated from Leaf1, Leaf2, and Leaf3 of seedlings grown in light for 14-days. Organellar genome copies were determined by real-time qPCR for ptDNA (A) and mtDNA (B) and normalized to the haploid nuclear genome. The ptDNA copies/nucDNA in M is significantly higher than in BS (p=0.002) when data from all three leaves were combined, using ANOVA model. For mtDNA/nucDNA, the difference between M and BS is significant for Leaf1 (p=0.04) using Tuckey HSD test.There are no significant differences between Leaf1, Leaf2, and Leaf3 for either organellar DNA, when M and BS data were combined. Error bars represent standard error determined for five biological replicates.

3.4.2 *Real-time qPCR*

Linear regression analysis reveals a strong positive correlation between ptDNA/nucDNA and mtDNA/nucDNA from M for each of the three leaves analyzed either separately or combined as a single data set (Figure 3.10). In all cases, R^2 is ≥0.95 and the p values are ≤0.015 (Figure 3.10A). For BS, we find no such correlation with the combined three-leaf data set. When each leaf is analyzed independently, however, we find a significant correlation for Leaf2 (R^2=0.89, p = 0.04) and Leaf3 (R^2=0.89, p = 0.045), but not for Leaf1 (Figure 3.10B). These correlations may indicate a common pathway for maintaining ptDNA and mtDNA levels in M

and probably also in BS.

3.4.3 *orgDNA damage, unimpeded orgDNA, and miPCR*

We previously employed long PCR to study DNA damage and molecular integrity for ptDNA and mtDNA during maize seedling development (Kumar *et al.*, 2014) and now use long PCR with orgDNA from M protoplasts and BS strands. The assay is based on the inability of *Taq* DNA polymerase to proceed beyond DNA impediments such as lesions and discontinuities. DNA damage is assessed by the amount of long-PCR-amplified product (~11 kb in size) relative to short-qPCR-amplified product (~150 bp). The amount of damage is expressed as impediments/10 kb and is relative to the tissue showing the largest amount of 11-kb product, in this case Leaf2 from BS for both ptDNA and mtDNA. The amount of damage is greater in M than BS for both ptDNA (Figure 3.3A) and mtDNA (Figure 3.3B). Damage levels in M are similar for all three leaves: ~ 0.7 impediments/10 kb for ptDNA and 0.7-1.1/10 kb for mtDNA. For BS, there are more orgDNA impediments in the older Leaf1 than the younger leaves. In addition, linear regression analysis shows a strong positive correlation between damage levels for ptDNA and mtDNA (R^2=0.9, p=0.007), suggesting a common pathway for maintaining both orgDNAs (Figure 3.11).

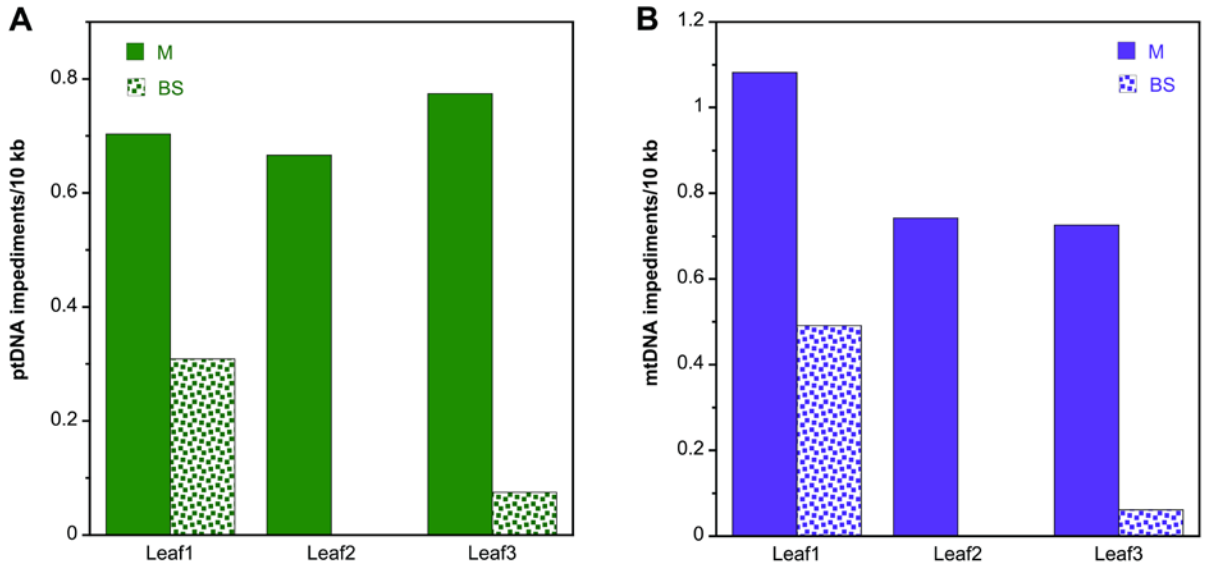

Figure 3.3 Organellar DNA damage

Total tissue DNA was prepared from mesophyll cells and bundle sheath strands isolated from Leaf1, Leaf2, and Leaf3 of seedlings grown in light for 14-days. Organellar DNA impediments per 10 kb for ptDNA (A) and for mtDNA (B) determined by amplifying ~11 kb organellar DNA using long PCR. The values for relative amplication from five biological replicates were averaged and number of impediments determined (Materials and methods). Impediments/10 kb are relative to Leaf2 of M for both ptDNA and mtDNA, which is set at zero.

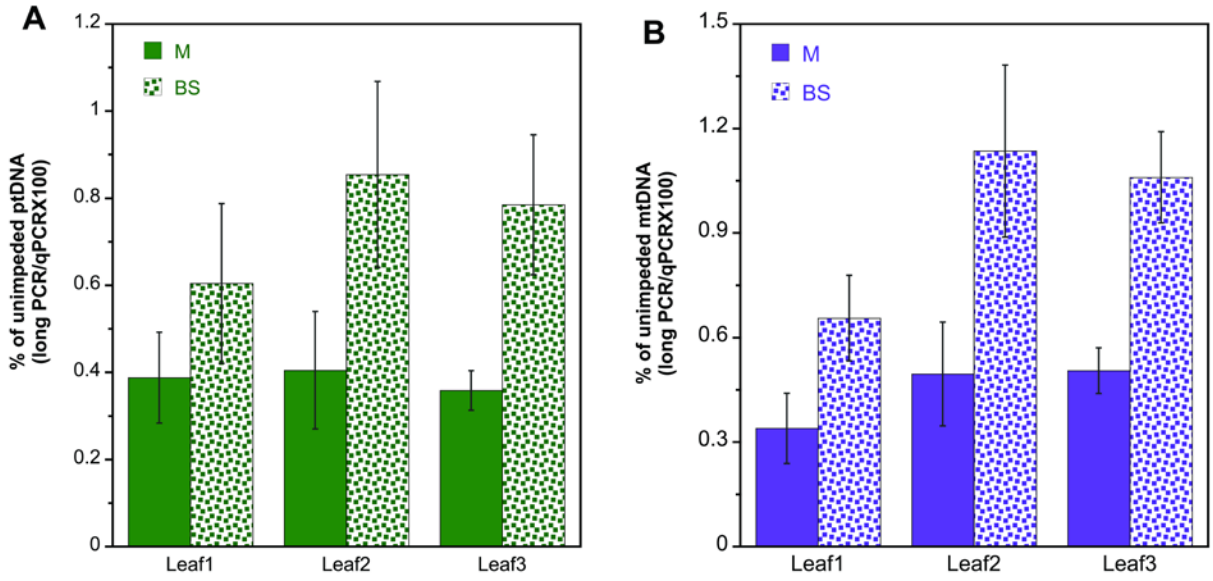

Figure 3.4 ptDNA and mtDNA without impediments

Total tissue DNA was prepared from mesophyll cells and bundle sheath strands isolated from Leaf1, Leaf2, and Leaf3 of seedlings grown in light for 14-days. DNA copies without structural impediments was determined for ptDNA (A) and mtDNA (B). Total unimpeded orgDNA copies were determined as long-PCR and the percentage is given relative to orgDNA copies as determined by real-time qPCR (Materials and methods). There is a significantly higher percentage in BS than M for both ptDNA ($p=0.008$) and mtDNA ($p=0.0003$), using ANOVA model. Significant differences are not evident between leaves for ptDNA or mtDNA, when BS and M data were combined for ptDNA and mtDNA. BS of Leaf1 contains less mtDNA copies than BS of Leaf3 ($p=0.05$),using Tuckey HSD test. Error bars represent standard error determined for five biological replicates. Two technical replicates for each biological replicate were used.

The long-PCR assay can also be used to assess the amount of "unimpeded" orgDNA, a measure of DNA without damage or structural impediments (Kumar *et al.*, 2014). We report the amount of unimpeded ptDNA (Figure 3.4A) and mtDNA (Figure 3.4B) as the percentage of long-PCR-orgDNA copies relative to qPCR-orgDNA copies. BS has significantly more unimpeded orgDNA than M for both ptDNA ($p=0.008$) and mtDNA ($p=0.0003$). The amount of unimpeded ptDNA is similar for each of the three leaves for M (~0.4) and BS (0.6-0.9) (Tables 3.5-3.7). For mtDNA, Leaf2 and Leaf3 of BS contains more unimpeded copies than Leaf1 BS, but this difference is only significant between Leaf3 and Leaf1 (Table 3.7). For M, however, there are no significant differences among the three leaves. For both ptDNA and mtDNA, the percentage of unimpeded orgDNA copies is very low (<1.5%) in M and BS, indicating very few molecules >11 kb without polymerase-blocking impediments. Linear regression analysis reveals a positive correlation between unimpeded ptDNA and mtDNA for both M ($R^2=0.7$, $p=0.0002$) and BS ($R^2=0.6$, $p=0.0009$) (Figure 3.12), suggesting a common regulatory mechanism for maintaining ptDNA and mtDNA.

In the "molecular integrity PCR" (miPCR) procedure, the amount of unimpeded orgDNA amplified by long PCR is determined relative to the amount of nucDNA amplified by qPCR (Kumar *et al.*, 2014)). The miPCR-determined copy number represents potentially functional orgDNA, whereas orgDNA fragments (150 bp, e.g.) too small to encode functional genes would nonetheless be included among the amplified products in standard qPCR. With miPCR, we report unimpeded ptDNA/nucDNA (Figure 3.5A) and mtDNA/nucDNA (Figure 3.5B) in both M and BS cells. We find no difference between M and BS for ptDNA, although there are significantly more mtDNA copies in BS (~0.3) than M (~0.1) ($p=0.002$). In general, no difference is found among the three leaves for either ptDNA or mtDNA, except that Leaf1 M

contains less mtDNA/nucDNA than Leaf3 (p=0.04), suggesting a decrease in mtDNA with leaf development. Note that the average copy number of unimpeded mtDNA is <1 per cell, suggesting that the gene-coding function of mtDNA is not required in most cells of mature maize leaves. Linear regression analysis shows a strong positive correlation between unimpeded ptDNA and mtDNA in M (R^2=0.8, p=1 X 10^{-5}) and BS (R^2=0.7, p= 8 X 10^{-5}), suggesting a common pathway for maintaining both orgDNAs (Figure 3.13).

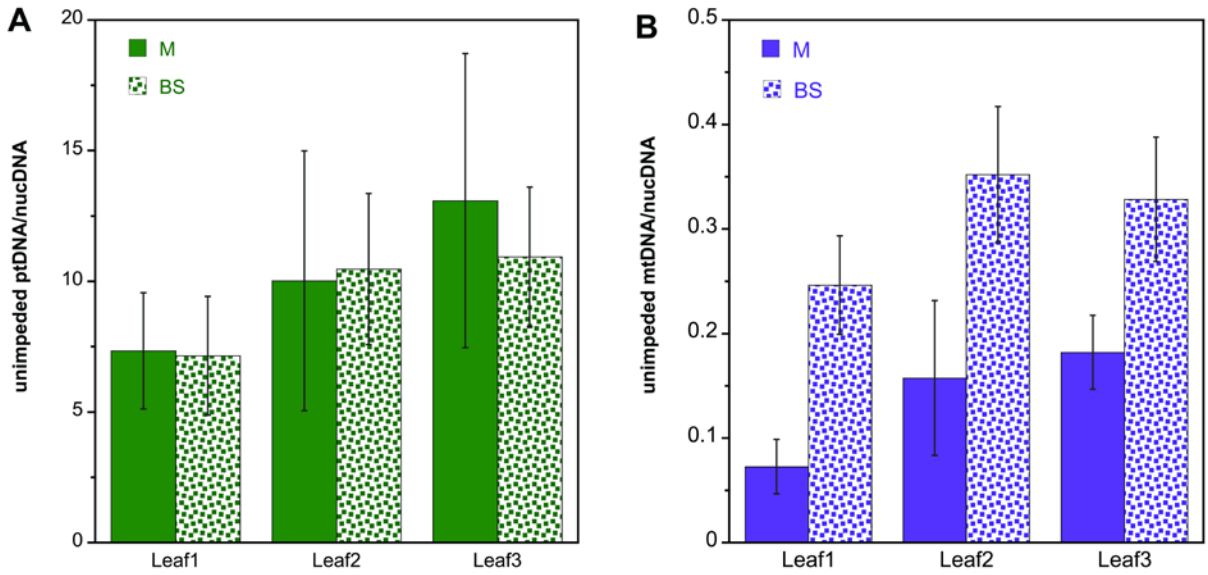

Figure 3.5 Plastid and mitochondrial genome DNA copy number determined by miPCR

Total tissue DNA was prepared from mesophyll cells and bundle sheath strands isolated from Leaf1, Leaf2, and Leaf3 of seedlings grown in light for 14-days. Unimpeded organellar DNA copies per haploid nuclear were determined as long-PCR relative to qPCR for ptDNA (A) and mtDNA (B). Using ANOVA model, we find no significant difference between M and BS for ptDNA. In contrast, for mtDNA the miPCR assay indicates significantly lower molecular integrity in M than BS (p=0.002). Leaf1 in M contains significantly fewer mtDNA copies than Leaf3 M (p=0.04). Error bars represent standard error determined for five biological replicates. Two technical replicates for each biological replicate were used.

3.4.4 *DNA repair*

The orgDNA damage assays reveal more damage in M than BS and in older than young leaves. This assay is based on the inability of DNA polymerase to amplify long DNA segments,

which may be due to impediments including DNA lesions that block *Taq* polymerase progression, discontinuities at branch points, and breakage of DNA into fragments lacking both primer sites (Kumar *et al.*, 2014). The level of damage due to polymerase-blocking lesions may be assessed *in vitro* using DNA repair enzymes. Repair was performed by quantifying long-PCR products either before or after treatment of ttDNA with a PreCR repair kit. We find more *in vitro* repair of ptDNA and mtDNA for BS than M (Figure 3.6). In addition, repair is slightly greater for Leaf3 than Leaf1 or Leaf2 for both orgDNAs in M. These results suggest more repairable lesions and less fragmented orgDNA in BS than M.

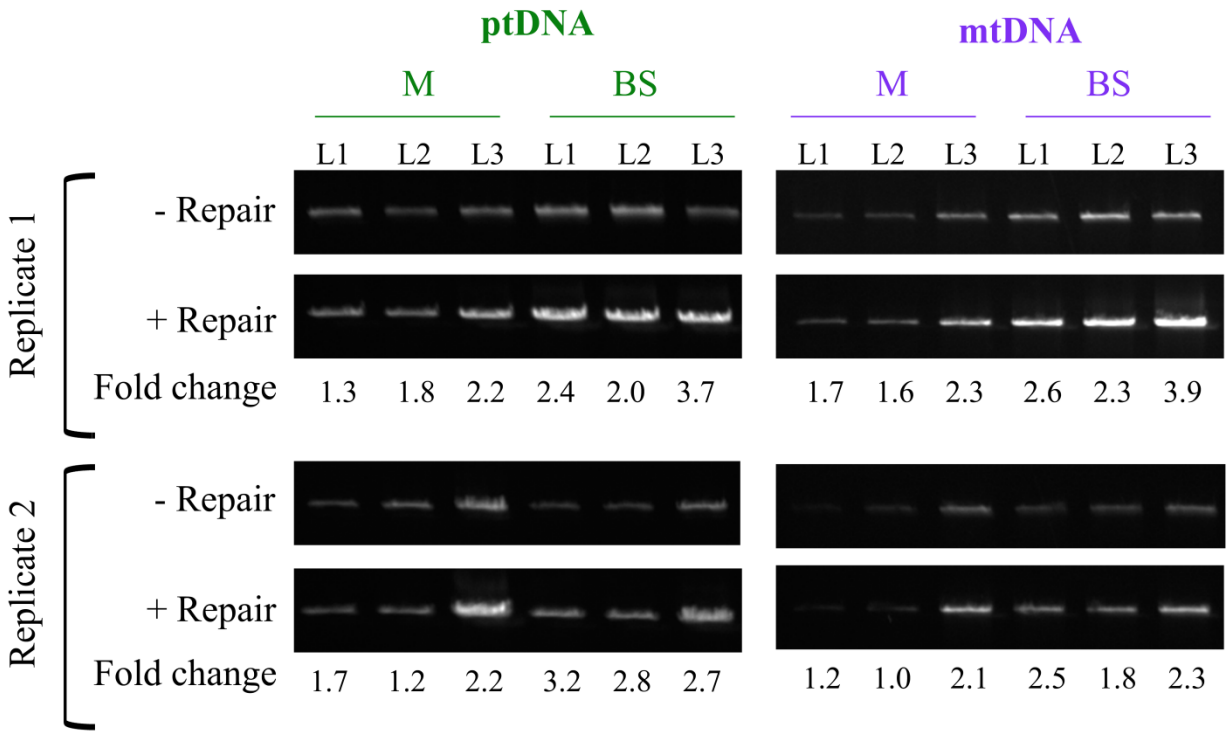

Figure 3.6 *In vitro* repair of organellar DNA

Total tissue DNA was prepared from mesophyll cells and bundle sheath strands isolated from Leaf1 (L1) Leaf2 (L2), and Leaf3 (L3) of seedlings grown in light for 14-days. The amount of ~11 kb long PCR product was assessed before and after treatment with DNA repair enzymes for two biological replicates (Materials and methods). The fold change in long PCR product as determined by ethidium-DNA intensity before and after repair treatment was determined and is given below the gel images. On average, BS contained more copies of orgDNA that could be repaired, compared to M.

3.5 Discussion

Here, we examine orgDNA from two photosynthetic cell types (mesophyll and bundle sheath) of wild-type maize seedlings without imposing stressful conditions or genotoxic agents. We find less orgDNA damage, a higher percentage of unimpeded orgDNA, and more *in vitro* repair of orgDNA in BS than M (Table 3.1). The orgDNA differences between these two types of photosynthetic cells may be attributed to different levels of DNA-damaging ROS. In M cells, oxygenic photosystem II may raise ROS levels, whereas in BS the absence of photosystem II and suberization of cell walls may lead to hypoxia and reduced ROS levels (Langdale, 2011). High orgDNA damage and low *in vitro* repair suggests greater fragmentation of orgDNA in M.

Table 3.1 Summary of orgDNA properties for M and BS cells.

		ptDNA	**mtDNA**
damage		M>BS	M>BS
% unimpeded		M<BS	M<BS
in vitro repair		M<BS	M<BS
copies	qPCR	M>BS	M=BS[1]
	miPCR	M=BS	M<BS

[1] Leaf1 contains significantly more mtDNA copies in BS than in M.

3.5.1 *Organellar DNA in M and BS cells*

C_4 photosynthesis in maize is partitioned between M and BS cells, with carbon assimilation in M and carbon reduction in BS plastids. ROS levels are higher in M than BS cells (Majeran and van Wijk, 2009), leading to the expectation of lower levels of orgDNA damage in BS cells. The higher levels of antioxidant systems in M also suggest higher ROS levels in M than BS cells (Friso *et al.*, 2010; Majeran *et al.*, 2005; Majeran *et al.*, 2008). Maize BS cells may even be

hypoxic because oxygenic photosystem II is restricted to M cells, the highly suberized BS cell walls should impede entry of oxygen, and respiration and photorespiration consume oxygen (Langdale, 2011). Furthermore, the accumulation of CHL 27 protein (Majeran *et al.*, 2008) and nodulin-family transcripts (Chang *et al.*, 2012) may indicate hypoxia. CHL 27 is an aerobic cyclase in chlorophyll synthesis that requires oxygen and NADPH for its activity. Nodulin-family transcripts encode transmembrane proteins in plant cells that maintain impermeability to specific substances, including oxygen. The number of orgDNA "copies" per haploid nuclear genome using qPCR greatly outnumbers that using miPCR. A DNA fragment of 150 bp (shorter than a typical gene) is scored as a copy in our qPCR assay, whereas miPCR scores only copies that are >11 kb and likely represent functional DNA. With qPCR, M contains ~2-fold more ptDNA copies than BS (2400 and 1200 copies, respectively), whereas miPCR reveals no M/BS difference, 10 copies for both cell types. For mtDNA, similar copy numbers were found between M and BS using qPCR, whereas miPCR gives twice as many copies in BS than M. However, the number of copies per cell (haploid nucDNA) basis determined by qPCR (~30) was much higher than determined by miPCR (<1). Thus, qPCR greatly overestimates the number of functional orgDNA copies. The lower copy values measured by miPCR are likely due to fragmentation resulting from double-strand breaks and blocking of amplification by nucleotide lesions. We conclude that DNA is more highly fragmented in M than BS, although the *in vitro* assay indicates more repairable lesions in BS than M cells.

3.5.2 *Similarities between ptDNA and mtDNA*

The ptDNA properties (damage, unimpeded DNA, and *in vitro* repair) we find to differ between M and BS cells might be an expected consequence of altered redox conditions attending the partition of photosynthesis into M and BS cells. But what accounts for the similarity we

observe between ptDNA and mtDNA when these properties are compared? For example, M cells have more impediments/10 kb in both ptDNA and mtDNA than do BS cells, suggesting common processes that maintain molecular integrity of orgDNA. Possibilities include organellar signaling and dual targeting of antioxidants and repair proteins.

Signaling between organelles maintains redox homeostasis in a plant cell, so that perturbing one organelle may affect another. For example, ROS (superoxides) can be released from mitochondria in cultured tobacco cells and isolated rat mitochondria (Rhoads *et al.*, 2006). Released ROS can then move to chloroplasts and/or the nucleus to either increase ROS or modify gene expression to modulate ROS levels. The alternative oxidase component of the mitochondrial respiratory chain can reduce ROS levels in mitochondria and also affect chloroplast signaling to the nucleus (Schwarzlander and Finkemeier, 2013). In addition, orgDNA damage can increase ROS levels by leading to defective proteins that further elevate ROS levels, causing even more damage to orgDNA. Dual targeting of nuclear-encoded, plastid-targeted proteins may regulate ROS levels in both organelles jointly. For example, RecA proteins are associated with DNA recombination/repair processes (Cox, 2007) and are implicated in orgDNA maintenance (Jeon *et al.*, 2013; Miller-Messmer *et al.*, 2012). In Arabidopsis, three RecA proteins have been identified: plastid-targeted RecA1, mitochondrial-targeted RecA3, and dual-organelle-targeted RecA2. Maize also has organelle-specific RecA1 and RecA3, but in addition has dual-targeted proteins RecA2a and RecA2b (Miller-Messmer *et al.*, 2012). If the expression of RECA2a and RECA2b were also M and BS cell-specific, this could result in coordinate repair of ptDNA and mtDNA. Indeed, we find similar damage levels (impediments/10 kb) and amount of *in vitro* repair.

3.5.3 *Comparing orgDNA from entire leaf and M/BS cells*

We previously reported changes in orgDNA during maize seedling development (Kumar *et al.*, 2014). The fully-expanded leaf blade is comprised of photosynthetic (M and BS) and non-photosynthetic (epidermis, E) cells, raising the question — what is the distribution of orgDNA among cell types? We determined the proportion of each cell type to be 44% M, 23% BS, and 33% E by analyzing maize leaf cross sections. In contrast to the mature chloroplasts in M and BS cells, however, most E cells (except guard cells) only have small, undifferentiated plastids (Pyke, 2009). We compare orgDNA copy number from the entire leaf tissue with M and BS (Leaf1 = 0.44 x M + 0.23 x BS + 0.33 x E; Table 3.3). Given that qPCR gives total orgDNA copies, we find that copy number in Leaf1 equals that of the averaged value for the photosynthetic cells (M and BS), indicating that E cells contain little or no orgDNA (Table 3.3). Thus, this comparison probably leads to an underestimate of orgDNA copy values per haploid nuclear genome for photosynthetic cells. Furthermore, a higher proportion of unimpeded orgDNA copies are preferentially retained in M and BS, as seen by the differences between M and BS/Leaf1 for % unimpeded orgDNA (4- and 6-fold for ptDNA and mtDNA, respectively) and unimpeded orgDNA/n (8- and 12-fold; Table 3.3). This retention of unimpeded orgDNA probably reflects functional needs in M and BS cells not shared by epidermal cells.

3.5.4 *Converting C_3 to C_4*

The plan to introduce maize-type C_4 photosynthesis (the NADP-ME type) into C_3 plants such as rice considers modifying cellular anatomy, physiology, and nuclear DNA (Karki *et al.*, 2013; Sawers *et al.*, 2007), but does not address the orgDNA differences we find. Based on results given above, we infer that non-photosynthetic epidermal cells contain little, if any, functional orgDNA. Non-photosynthetic cells of wheat (C_3) including epidermal and bundle

sheath cells, contain very low levels of ptDNA compared to photosynthetic mesophyll cells (Miyamura *et al.*, 1990). Non-photosynthetic bundle sheath cells in C_3 rice may also contain little functional orgDNA. In order to convert C_3 rice to C_4, the provision of a maize-like level of orgDNA function in BS cells may be critical. Merely increasing the number and size of organelles in BS cells may be insufficient to achieve the maize-type efficiency of photosynthesis.

3.6 Supplemental Materials

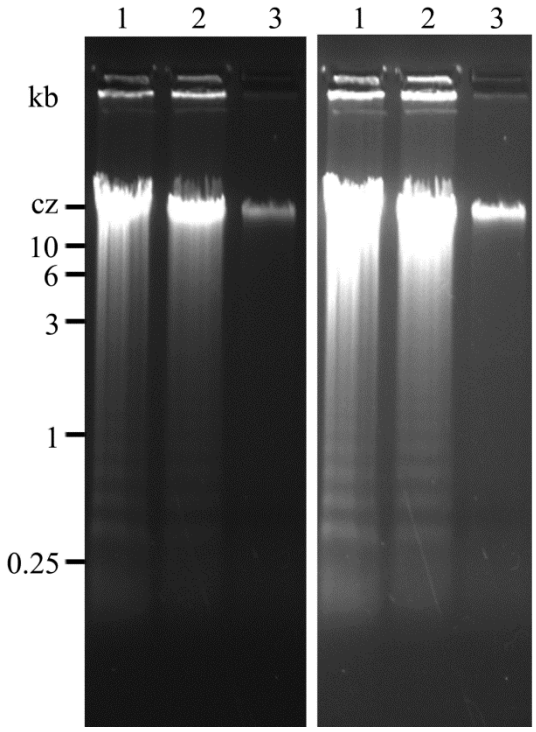

Figure 3.7 Total tissue DNA from preparations of mesophyll cells

Mesophyll (M) cells were islolated from leaves of 14-day seedlings and total tissue DNA (ttDNA) was prepared without (lane 1) and with (lanes 2 and 3) Percoll purification and separated on an agarose gel. The ttDNA from the pellet and suspended fractions from 30% Percoll are shown in lanes 2 and 3, respectively. The pellet from Percoll purification contained broken M, as seen by microscopic examination while the suspended fraction contained intact M. Lanes 1 and 2 show DNA laddering, indicating nuclease activity. High quality ttDNA was obtained from the intact M cells, as indicated by the absence of DNA laddering in lane 3. The two gel images were taken at different exposures.

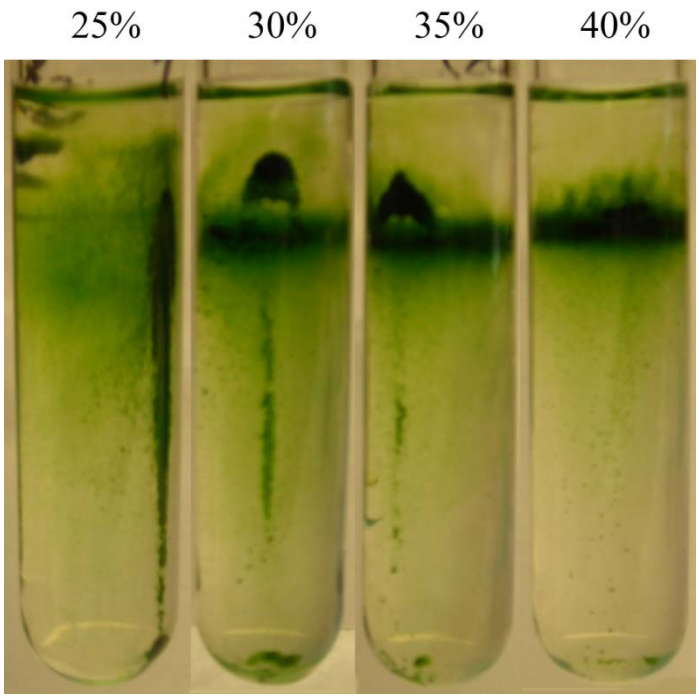

Figure 3.8 Purification of mesophyll cells using different Percoll concentrations

Four different Percoll concentrations were tested for separation of intact mesophyll (M) cells from broken M. The 25% and 30% Percoll were better than the higher concentrations for isolating intact M. At lower Percoll concentration, two distinct fractions were formed; a suspended fraction containing intact M and the pellet against the wall and at the bottom of the test tube containing broken M. At higher Percoll concentrations, 35% and 40%, both intact and broken fractions aggregate in a single band.

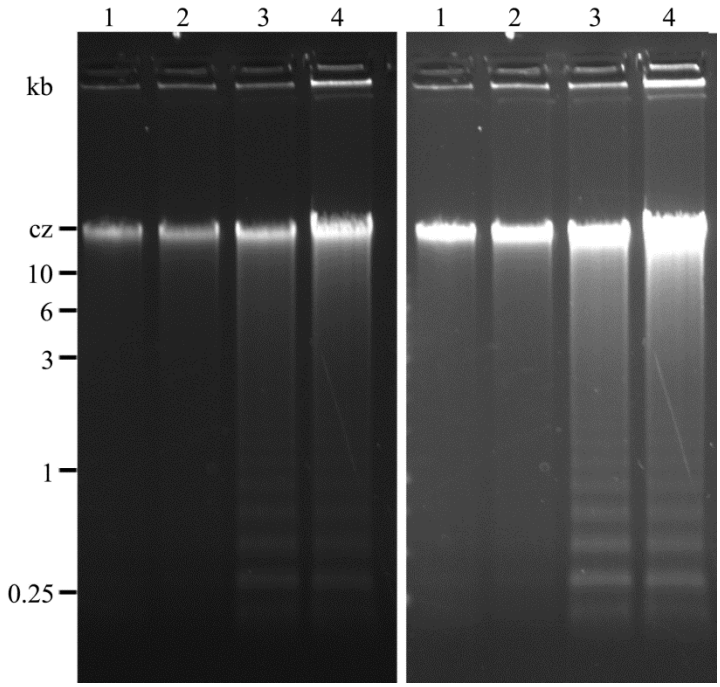

Figure 3.9 Assessment of high molecular weight total tissue DNA from Percoll-purified mesophyll cells

Mesophyll (M) cells were islolated from leaves of 14-day seedlings, purified using 25% (lane 1), 30% (lane2), 35% (lane 3) and 40% Percoll (lane 4) (Figure 3.8), then total tissue DNA (ttDNA) was extracted and fractionated on agarose gel. The ttDNA recovered from 35% and 40% Percoll showed laddering on the gel, indicating nuclease activity. Concentrations of 25% and 30% Percoll yielded high molecular weight ttDNA from the M preparations. The higher concentrations of Percoll were inefficient at separating intact from broken M (see Figure 3.7).

Table 3.2 Assays to assess of the purity of mesophyll and bundle sheath cell preparations.

Assay	M	BS
Enzyme assay % cross contamination	4.9 ± 1.0	5.9 ± 1.1
PEPC	8.0 ± 0.1	0.5 ± 0.1
NADP-ME	0.3 ± 0.1	6.6 ± 0.2
Chlorophyll a/b	3.2 ± 0.4	6.7 ± 0.3
Chlorophyll a^+	8.9 ± 1.2	6.4 ± 1.1
Chlorophyll b^+	2.8 ± 0.2	1.0 ± 0.2

The amount of M-specific PEPC and BS-specific NADP-ME enzyme activity was measured for both M and BS preparations. The units of enzyme activity are µmoles per hr per mg chlorophyll. One unit of PEPCase will form 1 µmole of oxalacetate from phospho(enol)pyruvate and CO_2 per minute at pH 8.5 at 25°C. One unit of NADP-ME will convert 1 µmole of L-malate and NADP to pyruvate, CO2 and NADPH per minute at pH 7.4 at 25°C. The % cross contamination was determined: units BS/units M x 100 for PEPC and units M/units BS x 100 for NADP-ME.

The chlorophyll a and b content was measured as µg using the equations:

Chlorophyll a = 13.7 (A665-A700)-5.76 (A649-A700)

Chlorophyll b = 25.8 (A649-A700)-7.6 (A665-A700)

Averages of three replicates with standard errors for enzyme activity and chlorophyll content are given.

Table 3.3 Comparisons of orgDNA from entire leaf, mesophyll, and bundle sheath cells

	ptDNA/n	% unimpeded ptDNA	unimpeded ptDNA/n	mtDNA/n	% unimpeded mtDNA	unimpeded mtDNA/n
Leaf1_M	1951 ± 575	0.4 ± 0.1	7 ± 2	20 ± 6	0.3 ± 0.1	0.1 ± 0.03
Leaf1_BS	1160 ± 39	0.6 ± 0.2	7 ± 2	38 ± 4	0.7 ± 0.1	0.2 ± 0.05
Leaf1_M & BS[1]	1555 ± 302	0.5 ± 0.1	7 ± 1	29 ± 4	0.5 ± 0.1	0.16 ± 0.04
Leaf1[2]	851 ± 52	0.12 ± 0.1	0.9 ± 0.8	16 ± 1	0.09 ± 0.07	0.014 ± 0.01
M&BS/Leaf1[3]	**2***	**4**	**8**	**2***	**6**	**12**

[1]The values determined after averaging of M and BS cells are shown.
[2]The values for Leaf1 are from Kumar *et al*., 2014.
[3]The fold differences between averaged M & BS and Leaf1 are shown.

OrgDNA/n copies determined by qPCR are not statistically significant between entire leaf and M&BS ($p>0.05$; *). The differences are significant for unimpeded orgDNA between entire leaf and M &BS ($p<0.05$). Averages for five biological replicates along with standard errors are given.

We determined the proportion of each cell type to be 44% M, 23% BS, and 33% E by analyzing maize leaf cross sections. Given that qPCR gives total orgDNA copies, we find similar levels of orgDNA copies between entire leaf (M+BS+E) and averaged copies M and BS[1] (M & BS), indicating that E cells contain little or no orgDNA.

For example,

Assuming orgDNA copies are ~1000 for Leaf1, ~2000 for M, and ~1000 for BS, then

Leaf1 = 0.44 x M + 0.23 x BS + 0.33 x E

1000 = (0.44 x 2000) + (0.23 x 1000) + (0.33 x E)

1000 = 880 + 230 + 0.33 x E

1000 = 1110 + 0.33 x E

Leaf1 copies = M + BS and E=0

Therefore the M + BS copies account for all of the Leaf1 copies measured by qPCR and E cells have essentially no orgDNA.

Table 3.4 Comparing M and BS after combining data from Leaf1, Leaf2 and Leaf3

	qPCR	% unobstructed orgDNA	miPCR	qPCR	% unobstructed orgDNA	miPCR
	0.002	0.008	ns	ns	0.003	0.002

Maize seedlings were grown at 24°C with 16/8 hr photoperiods for 14 days and leaf blades (above the ligule) from first (Leaf1, L1), second (Leaf2, L2) and third (Leaf3, L3) leaves from 10-15 plants were harvested and used for the preparation of mesophyll (M) protoplasts and bundle sheath (BS) strands. Five independent sets of seedlings were grown, representing five biological replicates. Each biological replicate was comprised of six samples (3 leaves X 2 cell types) and a total of thirty samples were analyzed. Statistical analyses were performed to compare M and BS after data from all three leaves were combined. Color code is green for ptDNA and purple for mtDNA; ns for not significant.

Table 3.5 Comparing leaves (Leaf1, Leaf2 and Leaf3) after combining data from BS and M

	qPCR	% unobstructed orgDNA	miPCR	qPCR	% unobstructed orgDNA	miPCR
L1and L2	ns	ns	ns	ns	ns	ns
L1and L3	ns	ns	ns	ns	ns	ns
L2and L3	ns	ns	ns	ns	ns	ns

Maize seedlings were grown at 24°C with 16/8 hr photoperiods for 14 days and leaf blades (above the ligule) from first (Leaf1, L1), second (Leaf2, L2) and third (Leaf3, L3) leaves from 10-15 plants were harvested and used for the preparation of mesophyll (M) protoplasts and bundle sheath (BS) strands. Five independent sets of seedlings were grown, representing five biological replicates. Each biological replicate was comprised of six samples (3 leaves X 2 cell types) and a total of thirty samples were analyzed. Statistical analyses were performed to after combining data from BS and M. Color code is green for ptDNA and purple for mtDNA; ns for not significant.

Table 3.6 Comparing M and BS within each leaf

	qPCR	% unobstructed orgDNA	miPCR	qPCR	% unobstructed orgDNA	miPCR
L1	ns	ns	ns	0.04	ns	0.01
L2	ns	ns	ns	ns	ns	ns
L3	ns	ns	ns	ns	ns	ns

Maize seedlings were grown at 24°C with 16/8 hr photoperiods for 14 days and leaf blades (above the ligule) from first (Leaf1, L1), second (Leaf2, L2) and third (Leaf3, L3) leaves from 10-15 plants were harvested and used for the preparation of mesophyll (M) protoplasts and bundle sheath (BS) strands. Five independent sets of seedlings were grown, representing five biological replicates. Each biological replicate was comprised of six samples (3 leaves X 2 cell types) and a total of thirty samples were analyzed. Statistical analyses were performed to compare M and BS within each leaf. Color code is green for ptDNA and purple for mtDNA; ns for not significant.

Table 3.7 Comparing each leaf for M and BS

	qPCR	% unobstructed orgDNA	miPCR	qPCR	% unobstructed orgDNA	miPCR
M						
L1and L2	ns	ns	ns	ns	ns	ns
L1and L3	ns	ns	ns	ns	ns	0.04
L2and L3	ns	ns	ns	ns	ns	ns
BS						
L1and L2	ns	ns	ns	ns	ns	ns
L1and L3	ns	ns	ns	ns	0.05	ns
L2and L3	ns	ns	ns	ns	ns	ns

Maize seedlings were grown at 24°C with 16/8 hr photoperiods for 14 days and leaf blades (above the ligule) from first (Leaf1, L1), second (Leaf2, L2) and third (Leaf3, L3) leaves from 10-15 plants were harvested and used for the preparation of mesophyll (M) protoplasts and bundle sheath (BS) strands. Five independent sets of seedlings were grown, representing five biological replicates. Each biological replicate was comprised of six samples (3 leaves X 2 cell types) and a total of thirty samples were analyzed. Statistical analyses were performed to compare each leaf for M and BS. Color code is green for ptDNA and purple for mtDNA; ns for not significant.

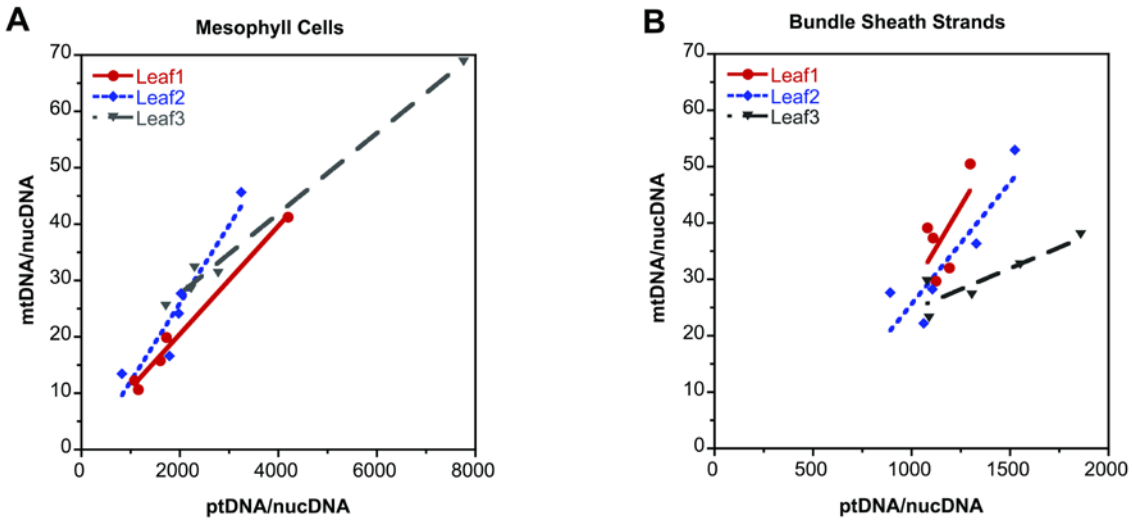

Figure 3.10 Correlation between ptDNA/nucDNA and mtDNA/nucDNA in M and BS

The relationships between ptDNA/nucDNA and mtDNA/nucDNA in M and BS were analyzed by linear regression. The results shown here suggest a common DNA regulatory mechanism for both the organelles. All three leaves in M exhibited a very strong correlation between ptDNA and mtDNA with R^2 value close to 1 and $p < 0.05$. (Leaf1, $R^2 = 0.99$, $p = 0.0007$; Leaf2, $R^2 = 0.9$, $p = 0.015$; Leaf3, $R^2 = 0.99$, $p = 0.0003$). No correlation was observed for Leaf1 ($R^2 = 0.4$, $p = 0.25$) in BS, whereas Leaf2 and Leaf3 exhibited a significant correlation between ptDNA and mtDNA. (Leaf2, $R^2 = 0.79$, $p = 0.04$; Leaf3, $R^2 = 0.79$, $p = 0.045$). Each symbol (circles, squares and triangles) indicates a single biological replicate for each of the three leaves.

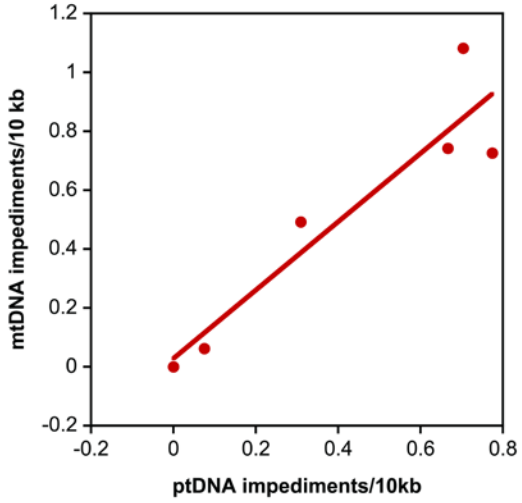

Figure 3.11 Correlation between impediments/10 kb for ptDNA and mtDNA

A correlation was observed between impediments/10 kb ptDNA and mtDNA when data from M and BS were combined (R^2=0.9, p=0.007) using linear regression model. This suggests a common regulatory pathway maintaining both orgDNA.

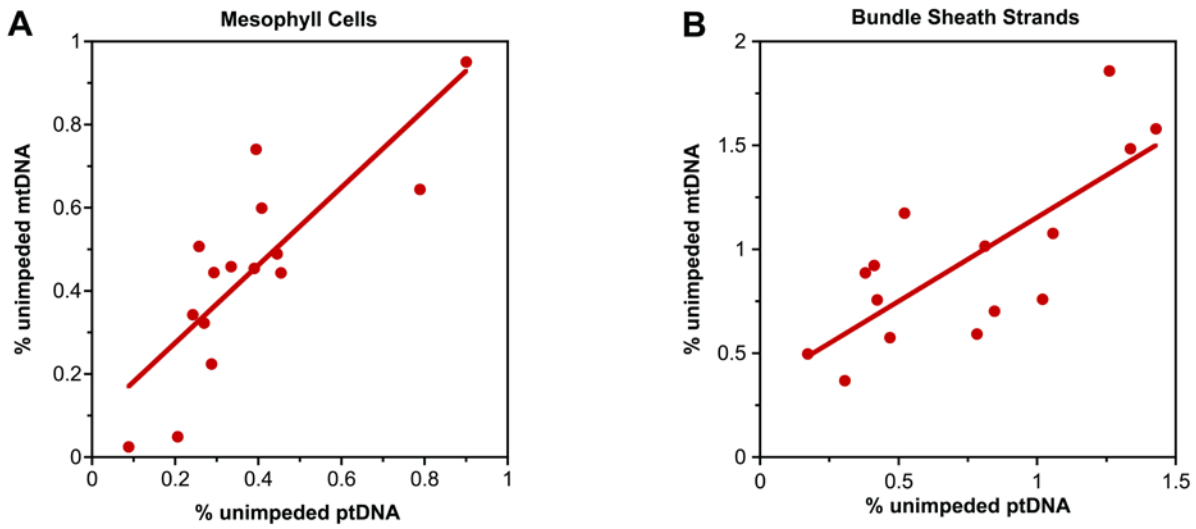

Figure 3.12 Correlation between % unimpeded ptDNA and mtDNA in M and BS

A correlation was observed between % unimpeded ptDNA and mtDNA in M (R^2=0.7, p=0.0002) and BS (R^2=0.6, p=0.0009), using linear regression model. This suggests a common regulatory pathway maintaining both orgDNA.

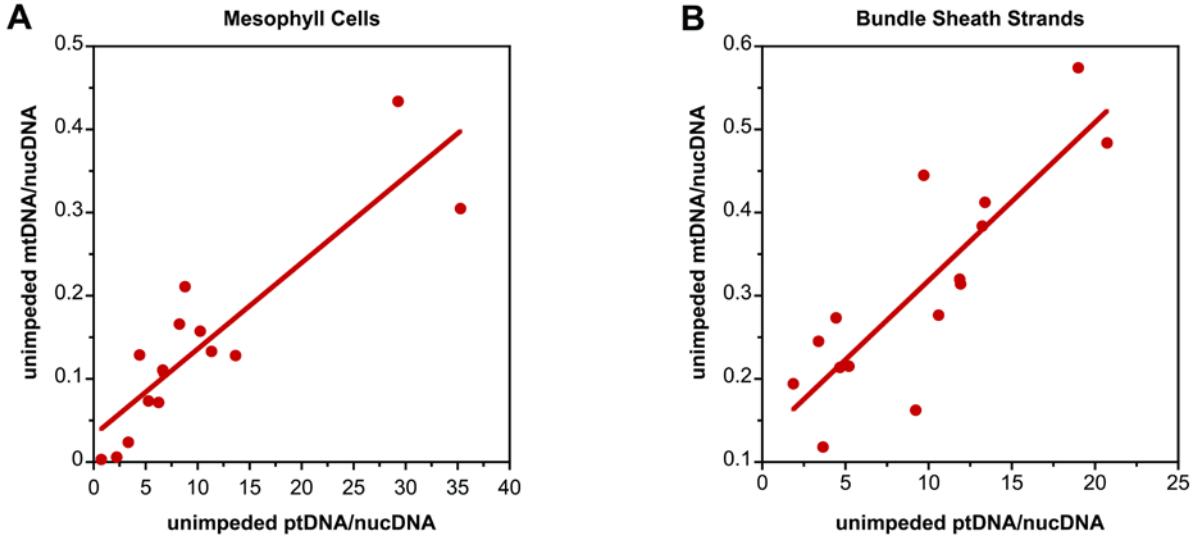

Figure 3.13 Correlation between unimpeded ptDNA/nucDNA and mtDNA/nucDNA in M and BS

A correlation was observed between unimpeded ptDNA and mtDNA per haploid nuclear gene in M (R^2=0.8, p=1 X 10^{-5}) and BS (R^2=0.7, p= 8 X 10^{-5}), using linear regression model. This suggests a common regulatory pathway maintaining both orgDNA.

Chapter 4 (Appendix)

THE AMOUNT AND INTEGRITY OF MTDNA IN MAIZE DECLINE WITH DEVELOPMENT

Delene J. Oldenburg, Rachana A. Kumar, and Arnold J. Bendich

4.1 Abstract

In maize and other grasses there is a developmental gradient from the meristematic cells at the base of the stalk to the differentiated cells at the leaf tip. This gradient presents an opportunity to investigate changes in mitochondrial DNA (mtDNA) that accompany growth under light and dark conditions, as done previously for plastid DNA. Maize mtDNA was analyzed by DAPI-DNA staining of individual mitochondria, gel electrophoresis/blot hybridization, and real-time qPCR. Both the amount and integrity of the mtDNA were found to decline with development. There was a ~25-fold decline in mtDNA copy number per cell from the embryo to the light-grown leaf blade. The amount of DNA per mitochondrial particle was greater in dark-grown leaf blade (~24 copies, on average) than in the light (~2 copies), with some mitochondria lacking any detectable DNA. Three factors that influence the demise of mtDNA during development are considered: (i) the decision to either repair or degrade mtDNA molecules that are damaged by the reactive oxygen species produced as byproducts of respiration; (ii) the generation of ATP by photophosphorylation in chloroplasts, reducing the need for respiratory-competent mitochondria; and (iii) the shift in mitochondrial function from energy-generating respiration to photorespiration during the transition from non-green to green tissue.

4.2 Introduction

The number of copies of the genome in the nucleus (the ploidy level) usually remains constant as the adult develops from the fertilized egg in plants and animals. Exceptions to this general rule include endopolyploidy in Arabidopsis leaf cells (Galbraith *et al.*, 1991; Jacqmard *et al.*, 1999; Rowan *et al.*, 2009) and polyteny in salivary glands of *Drosophila* (Lucchesi, 1973). For mitochondria and plastids, however, DNA copy number (per organelle and per cell) is highly variable: each cell contains several organelles and each organelle may contain multiple genome copies (Bendich, 1987, 1993; Braschi and McBride, 2010; Carling *et al.*, 2011; Falkenberg *et al.*, 2007; Poulton *et al.*, 2010; Ravi V, 2008; Sakamoto *et al.*, 2008; Takano *et al.*, 2010). Changes in mitochondrial DNA (mtDNA) content have been documented for Arabidopsis root and shoot (Fujie *et al.*, 1993; 1994) and *Pelargonium* root (Kuroiwa *et al.*, 1992), where mtDNA replication (and increasing copy number) is restricted to meristematic regions, followed by a decline in mtDNA as cells divide and tissues begin to differentiate.

In maize the plastid DNA (ptDNA) level increases and then declines, in some cases to undetectable levels in individual plastids, during plant development and in response to light (Oldenburg and Bendich, 2004a; Oldenburg *et al.*, 2006; Zheng *et al.*, 2011). High levels of ptDNA are maintained in dark-grown seedlings, but ptDNA declines rapidly upon exposure to light. Might light also affect mtDNA levels?

The size of the maize mitochondrial genome is ~570 kb (Clifton *et al.*, 2004). It had been proposed that mtDNA *in vivo* exists as a genome-sized circular “master chromosome” with subgenomic circular molecules produced by recombination between large repeated sequences (Fauron *et al.*, 1995; Lonsdale *et al.*, 1984; Palmer and Herbon, 1986; Stern and Palmer, 1986). No evidence, however, of a circular master chromosome has been found for any vascular plant

(Bendich, 1993; Preuten *et al.*, 2010). Genome-sized molecules in linear form were found for the liverwort, *Marchantia polymorpha* (Oldenburg and Bendich, 1998, 2001), and maize mtDNA molecules probably exist as a mixture of multigenomic, branched complex forms and subgenomic linear and circular forms, as found for tobacco (Oldenburg and Bendich, 1996) and *Chenopodium* (Backert *et al.*, 1996; 1997). The multigenomic complex forms likely represent the replicating form, with replication proceeding via a T4 phage-like recombination-dependent mechanism (Backert and Börner, 2000; Oldenburg and Bendich, 1998). The subgenomic linear and circular forms may arise as replication ceases, through recombination between repeats in the complex forms, as mitochondria divide and mtDNA is partitioned and/or during degradation of the mtDNA (Fujie *et al.*, 1993; Oldenburg and Bendich, 1996; Preuten *et al.*, 2010). Rapid turnover of mtDNA in mung bean seedlings has been reported (Dai *et al.*, 2005).

Genome copy number determination for ptDNA may be complicated by the presence of NUPTs (nuclear sequences of plastid origin) (Kumar and Bendich, 2011; Roark *et al.*, 2010; Zheng *et al.*, 2011), and the same difficulty may be faced in measuring mtDNA due to NUMTs (nuclear sequences of mitochondrial origin) (Hazkani-Covo *et al.*, 2010; Timmis *et al.*, 2004). Both organelles are derived from prokaryotic precursors (cyanobacteria and alpha-proteobacteria, respectively) (Gould *et al.*, 2008). During the evolution of these organelles, most of the original prokaryotic genes were transferred to the nuclear genome, with a subset retained in the organellar genomes (Kleine *et al.*, 2009; Timmis *et al.*, 2004). This process is ongoing and can lead to a large amount of NUPTs and NUMTs in the nuclear genome (Bergthorsson *et al.*, 2003; Gray, 2011; Huang *et al.*, 2005; Richardson and Palmer, 2007; Smith *et al.*, 2011), especially for maize (Kumar and Bendich, 2011; Lough *et al.*, 2008; Roark *et al.*, 2010).

We examined mtDNA from maize plants grown under either light or dark conditions and at

different stages of development. The amount of mtDNA and its molecular structure were assessed for embryo, root, stalk (including the basal meristem) and leaf blade from seedlings and from adult plants. We employed three methods of analysis: DAPI-DNA fluorescence of individual mitochondria stained with Mitotracker Green, ethidium bromide (EtBr) staining and blot hybridization after pulsed-field gel electrophoresis (PFGE), and real-time quantitative PCR (qPCR). We determined the amount of DNA per mitochondrial particle and per cell (or haploid nuclear genome) as genome equivalents, although we report the data as genome copy numbers or "copies". In addition, total tissue DNA (ttDNA) was analyzed using methylation-sensitive (MeS) and methylation-insensitive (MeI) restriction enzymes and hybridization to mitochondrial and nuclear gene probes. This methodology allows discrimination of authentic mtDNA from NUMTs.

For light-grown plants, we found substantial levels of mtDNA in roots and stalk, but mtDNA was barely detectable in leaves. For dark-grown plants, however, roots, stalk, and leaves showed comparable levels of mtDNA. Most or all of the mtDNA was seen as small linear molecules, but for stalk some was found in large complex forms that probably represent replicating mtDNA. Our results show that there is more mtDNA in non-green tissue (roots, meristem, and etiolated leaf tissue) than in green leaves. We conclude that the retention of DNA in mitochondria probably depends on the respiration requirement of the tissue and that mtDNA damaged by reactive oxygen species (ROS) is degraded rather than repaired.

4.3 Materials and methods

4.3.1 Plant tissue and growing conditions

Maize (*Zea mays* (L.), inbred line B73 [seeds originally obtained from Agricultural Research Service, Ames, IA, then propagated annually in our greenhouse] and commercial

hybrid Mycogen 2722 [provided by Arthur Oldenburg, Rutland, IL]) seedlings were grown in temperature-controlled rooms for 9-20 days under light (16 h light/8 h dark cycles), continuous dark, or in dark for 9 days followed by 3 days in light. Seed was soaked overnight and then sown in either vermiculite/soil mix for harvesting above-ground tissue or in Turface for harvesting of roots as well as above-ground tissue. Adult plants (63 and 89 days old) were grown in a greenhouse. Stalk refers to the region in the juvenile plants between the basal node and the ligule of the first leaf (L1) (Figure 4.6). Thus the stalk presumably includes both mature non-dividing cells of the L1 sheath and dividing cells of the basal meristem and younger immature leaves.

4.3.2 Preparation of mitochondria, mtDNA, nucDNA, and ttDNA

Maize tissue was washed 3-5 min in 0.5%, w/v sarkosyl, rinsed exhaustively in tap water, followed by distilled water, and blotted dry. Tissue sections were excised, weighed, wrapped in aluminum foil, frozen in liquid nitrogen, and stored at -80°C until used to isolate mitochondria or total tissue DNA (ttDNA). Embryo and endosperm tissues were obtained from maize seed soaked for 24 h in water at 4°C or room temp (RT), dissected with a scalpel, then ttDNA and nuclear DNA (nucDNA) prepared as described below from either frozen, powdered or fresh tissue. For mitochondria and ttDNA, frozen tissue was ground to a fine powder with dry ice in either a mortar and pestle or coffee grinder, mixed with high salt buffer (HSB: 1.25 M NaCl, 40 mM HEPES pH 7.6, 2 mM EDTA pH 8, 0.1% w/v, BSA, 0.1% -mercaptoethanol [ME], by vol), and filtered through 1-3 layers of Miracloth into centrifuge tubes. Washed mitochondria were prepared by 2-3 rounds of differential centrifugation: low speed to pellet and remove nuclei and plastids and high speed of the supernatant to pellet mitochondria (Oldenburg and Bendich, 1996, 1998). The mitochondrial pellet was washed in dilution buffer (DB: 0.4 M sorbitol, 1 mM EDTA, 0.1%, w/v BSA, 20 mM Hepes-KOH, pH 7.5) and the final pellet resuspended in the

same buffer. The mtDNA was prepared in-gel as described below. The ttDNA was prepared from the powdered frozen tissue using either the cetyltrimethylammonium bromide method (CTAB) (Rogers and Bendich, 1988b) or PhytoPure resin (GE Biosciences). The DNA concentration was determined using the QuantIT assay (Invitrogen).

For blot hybridization (Figure 4.4a and b), the nucDNA and ttDNA were prepared from fresh (not frozen) tissue (Bino *et al.*, 1993; Oldenburg *et al.*, 2006). Sarkosyl-washed plant tissue was chopped with a razor blade in chopping buffer (CB; 15 mM HEPES, 1 mM EDTA, 80 mM KCl, 20 mM NaCl, 300 mM sucrose, 0.5 mM spermine, 0.1%, w/v [illegible] 2-ME) and filtered through one layer of Miracloth on ice. The filtrate was divided into two tubes. For ttDNA, the filtrate was centrifuged for 15 min at 1200*g*. The pellet was washed twice in CB and ttDNA extracted with PhytoPure resin. For nucDNA, 0.2% Triton X-100, by vol was added to the filtrate to release nuclei followed by 7 min centrifugation at 500*g*. The nuclei were washed 2-3 times with CB + 0.2% Triton X-100 and nucDNA extracted with PhytoPure resin.

4.3.3 Fluorescence microscopy imaging of mitochondrial particles and their DNA

Mitochondria isolated as described above were fixed with FAA (3.7% formaldehyde, 5% acetic acid, 50% ethanol, by vol) in DB and stored at 4°C. Mitotracker Green FM (10 µM, 490ex, 516em) was used to visualize and identify mitochondrial particles and DAPI (1-2 µg/mL; 360ex, 450/50em) was used to stain *in organellar* DNA. Low melting point agarose (0.75%, w/v) was used to immobilize the mitochondria, 1% [illegible] 2-ME, by vol the fluorescent dyes, and the edges of the coverslip were sealed with clear nail polish. Images were recorded with a Retiga QImaging digital camera and OpenLab software. Quantification of the DAPI-DNA fluorescence was performed by first selecting the mitochondrial particle from the Mitotracker image and then measuring the DAPI fluorescence intensity (mtDAPI FI) of the same

area (mtArea). For each field of view, an area without mitochondria was assessed for background DAPI-fluorescence (bgFI). The total mtDAPI FI per mitochondrial particle was determined as (mtDAPI FI-bgFI) x mtArea. The genome copy number (genome equivalents) per mitochondrial particle was determined from the total mtDAPI FI relative to DAPI FI from vaccinia virus using a method analogous to that described in (Miyamura *et al.*, 1986) and used to determine ptDNA copy number (Oldenburg and Bendich, 2004a; Zheng *et al.*, 2011). The total DAPI FI per virus was determined as 25±11 pixels x μm^2 (Oldenburg and Bendich, 2004a). This value was then used to calculate the fluorescence intensity of a mitochondrial particle relative to that of a vaccinia particle in vaccinia virus equivalents or 'V' units (V=total DAPI FI per mitochondrial particle/total DAPI FI per virus particle). Using vaccinia as the standard, the genome copy number per mitochondrial particle was then calculated by the equation: copy number=0.41xV. The value 0.41 is a constant factor that accounts for the differences in DNA base composition and size between the vaccinia and the mitochondrial genomes, and was determined as (%A+T of vaccinia genome/%A+T of mitochondrial genome) x (bp vaccinia DNA/bp mtDNA), where %A+T is 66.6 for vaccinia (Copenhagen strain) and 56.1 for *Z. mays* (L.). The bp is 197,361 for vaccinia (strain vTF7.3) and 569,630 for *Z. mays* (L.) (accession NC_007982).

4.3.4 Gel electrophoresis, restriction digestion, and blot hybridization

For pulsed-field gel electrophoresis (PFGE), the isolated mitochondria were resuspended in an equal volume of DB, mixed with low melting point agarose, lysed overnight at 48°C in 40 mM EDTA pH 8, 1%, w/v sarkosyl, 200 µg/mL proteinase K, then washed extensively in TE (10 mM Tris, pH 8, 1 mM EDTA) and treated with PMSF to inactivate the proteinase K. The in-gel mtDNA was treated ±DNase in order to assess the amount of non-DNA EtBr-fluorescence in the well-bound fraction. The in-gel mtDNA was fractionated by PFGE as described previously

(Oldenburg and Bendich, 1996, 1998), stained with EtBr, and images recorded. The DNA was transferred under alkaline condition to a N+ nylon membrane and hybridized with a mitochondrial *cox*3 gene probe labeled with digoxigenin (DIG) and detected using anti-DIG antibody and chemiluminescence (Roche). The *cox3* gene was cloned from *Marchantia polymorpha* mtDNA, plasmids pLP201 provided by Kanji Ohyama (Oda *et al.*, 1992; Oldenburg and Bendich, 1998).

Equal amounts of uncut or restriction-digested ttDNA (0.5 or 1 µg) were fractionated using conventional agarose gel electrophoresis. Restriction enzymes used were methylation-insensitive (MeI; *Msp*I, *Eco*RI, *Hind*III) and methylation-sensitive (MeS; *Hpa*II, *Ava*I, *Sna*BI, *Sal*I). The expected size of the mtDNA fragments following restriction digestion was determined using the maize mitochondrial genome (accession NC-007982) and NEBcutter 2.0). The expected and actual size of the fragments was confirmed by aligning 1:1 images of the EtBr-DNA and blot hybridization. Partial digestion of nucDNA was observed with *Ava*I, however, even though it is considered by the supplier (NEB) as sensitive to cytosine CpG methylation (Figure 4.3). The *cox1* and *atp6* genes were PCR products amplified from maize mtDNA. The *adhI* gene was a PCR product amplified from maize ttDNA. The primers used for PCR amplification were:

cox1, 598 bp:

ZmcoxI-L2, 5’-CATAGGAGGGCTCACTGGAA-3’

ZmcoxI-R1, 5’-TTAAGGCAAAGCCCAAACAA-3’

atp6, 629 bp:

Zmatp6-L1, 5’-CCTTGCATCTCGGTCACTTT-3’

Zmatp6-R1, 5’-ACCGCTACATTTCTGGAACG-3’

adh1, 582 bp:

Zmadh1-L2, 5’-TCGAGGAGGTGGAGGTAGC-3’

Zmadh1-R2, 5’-TCCAAGCTGTACGTGCCTTT-3’

Quantification of EtBr-DNA and hybridization signal was performed using digitized images of gels and blots with NIH ImageJ. For well-bound mtDNA (Figure 4.2 c-e), in-gel mtDNA was treated with DNase prior to electrophoresis in order to determine and then subtract the amount of non-DNA signal from mtDNA samples not treated with DNase.

4.3.5 Real-time qPCR

Maize seedlings were grown for 13 days in either light or dark. The base of stalk (5 mm above node), top of stalk (5 mm below ligule of leaf 1) and entire blade of first and second leaves were harvested, frozen in liquid nitrogen, and stored at -80°C. Using the CTAB method, ttDNA was extracted from seedling tissues, as well as embryo and endosperm imbibed at either 4°C or room temperature for ~24 h. The integrity of extracted DNA was analyzed by agarose gel electrophoresis and the concentration was determined using QuantIT assay. The DNA was diluted to 3 ng/µl, and a total of 6 ng was used. Primers designed to amplify mtDNA but not NUMTs were designed as described previously (Kumar and Bendich, 2011).

The primers used for qPCR amplification were:

adh1, 156 bp nucDNA specific

adh1_left, 5’-GCTCCTCACAGGCTCATCTC-3’

adh1_right, 5’-AGGCGGACCTTTGCACTT-3’

nad4, 187 bp mtDNA specific

nad4_F2, 5’-GCAAAAGTCCTTCCACGGCA-3’

nad4_R1, 5’-AGCAAGCGTAGGCAACCAAAC-3’

qPCR was performed with a Chromo4™ thermal cycler (Bio-Rad) using this program: 94ºC

for 3 min and 15 s, 40 cycles of 94ºC for 15 s, 59ºC for 15 s and 72ºC for 20 s. qPCR data from six replicates was analyzed using Opticon Monitor™ software. Melting curves from 65ºC to 95ºC showed single products. qPCR efficiencies were determined to be 1.95 and 2.0 for *adh1* and *nad4* primers, respectively. The mtDNA copies per haploid nucDNA were determined using absolute quantification with DNA standards. The standards were produced by PCR with the primers listed above and maize ttDNA template. The concentration of PCR products for both genes was determined using the QuantIT assay. The range of copies for the *adh1* gene was between 100 and 10,000/µL and for the *nad4* gene was between 10,000 and 100,000 copies/µL. The qPCR experiments were performed following MIQE guidelines to the best of our ability (Bustin *et al.*, 2009).

4.4 Results

4.4.1 Fluorescence microscopy of maize mitochondria stained with MitoTracker and DAPI

Isolated mitochondria from 11-day maize seedlings and 63-day adult plants were stained with a mitochondrial-specific dye (MitoTracker Green), a DNA-specific dye (DAPI), and imaged by fluorescence microscopy (Figure 4.1). The seedlings were grown under either 16/8 h light/dark cycles or continuous dark. Mitochondria were isolated from the roots, base of the stalk, and first leaf (L1) blade and from the seventh leaf (L7) from adult plants grown in a greenhouse (Materials and methods).

The MitoTracker-stained mitochondrial particles were irregular in shape and variable in size. An individual mitochondrial particle may be comprised of a single mitochondrion or an aggregate composed of two or more mitochondria. The mtDNA was visualized as a diffuse DAPI fluorescence throughout the mitochondrial area and as discrete, bright nucleoids (mtDNA-

protein complexes). For light-grown seedlings, the mitochondria from the roots were slightly larger (mean of 8.6 μm^2) with more mtDNA (mean of 18 genome copies per mitochondrial particle) than in the stalk (4.1 and 6, respectively) (Figure 4.1j). For both tissues, however, the range in size and mtDNA content was similar (<1 to ~30 μm^2 and <1 to ~100 genome copies). In contrast, the mitochondria from the L1 blade were smaller overall (<1 to 11 μm^2) with much less mtDNA (maximum of 14 and mean of 2 copies per mitochondrial particle). Most of the mitochondria from the L7 blade of an adult plant contained <10 genome copies and were small in size (<15 μm^2) with a few larger ones (up to 50 μm^2).

For dark-grown seedlings, the size (mean of 18-25 μm^2) and mtDNA content (mean of 17-24 copies per mitochondrial particle) were similar in all three tissues (root, stalk and L1). In the roots, a few mitochondria were larger for dark-grown than light-grown seedlings. In the stalk and L1, the size and DNA content of mitochondria were higher for dark than light growth conditions. Most notable is the finding that in L1 of dark-grown seedlings the mtDNA was retained, whereas L1 mtDNA declined sharply in the light. Five of the 38 examined mitochondrial particles from light-grown L1 contained no detectable DAPI-DNA fluorescence, whereas DNA was detected in all mitochondria from all other tissues (legend to Figure 4.1). We also found that individual mitochondrial particles of similar size may contain different amounts of mtDNA, as we reported previously for individual maize plastids (Zheng *et al.*, 2011).

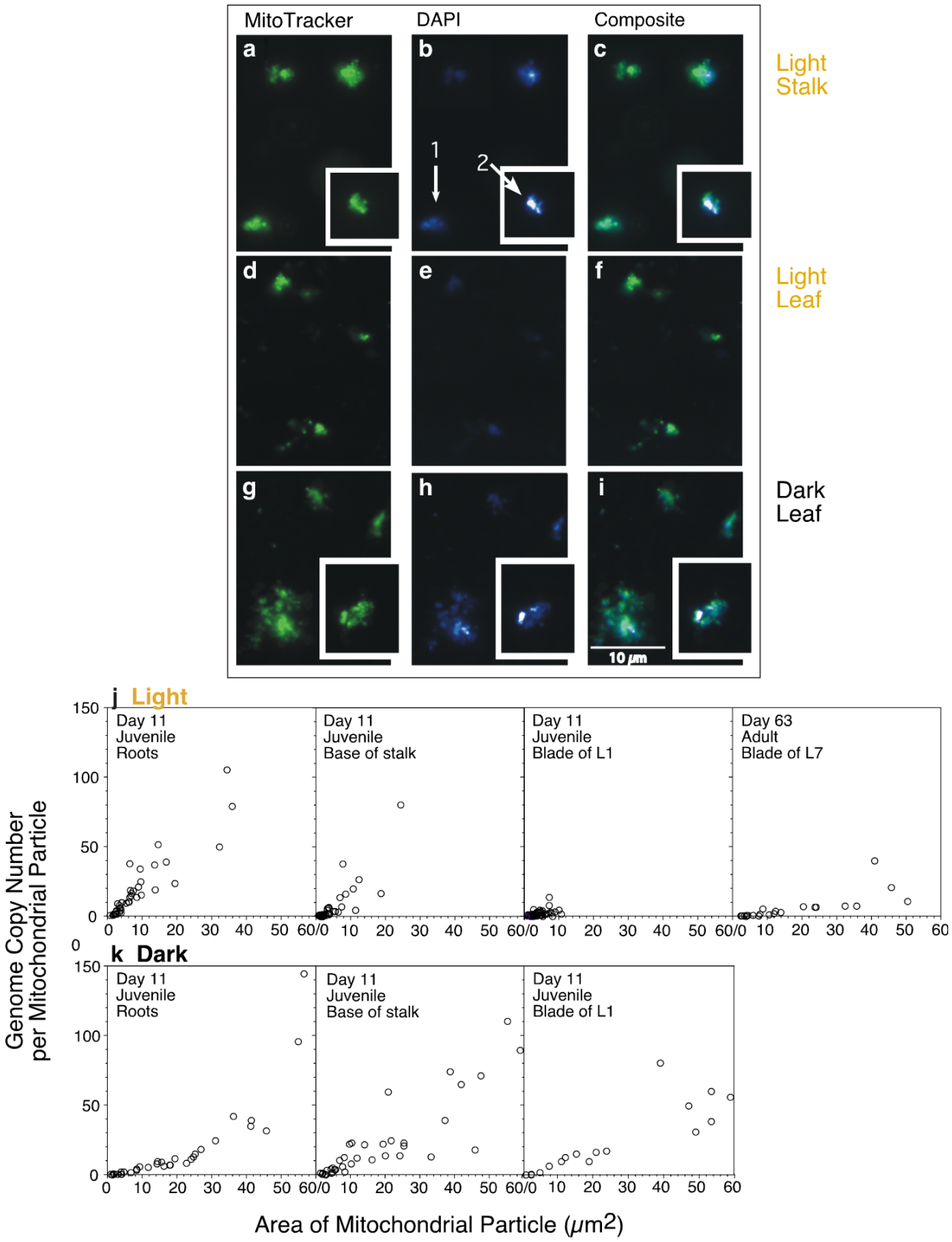
MitoTracker
DAPI
Composite
a
b
c
1
2
Light
Stalk
d
e
f
Light
Leaf
g
h
i
Dark
Leaf
10 µm
j Light
k Dark
Day 11
Juvenile
Roots
Day 11
Juvenile
Base of stalk
Day 11
Juvenile
Blade of L1
Day 63
Adult
Blade of L7
Genome Copy Number
per Mitochondrial Particle
Area of Mitochondrial Particle (µm2)

Figure 4.1 Fluorescence microscopic imaging of isolated mitochondria.

Individual mitochondrial particles were identified by staining with MitoTracker Green (a, d, g) and DNA content was determined by DAPI fluorescence (b, e, h). c, f, i Composite images of MitoTracker and DAPI-DNA fluorescence. Mitochondrial particles of similar size can have different DNA contents (arrows 1 and 2 in b). The mtDNA content was generally lower for light-grown leaves (d-f) than the base of the stalk (a-c) or dark-grown leaves (g-i). Scale bar in (i) applies to all images. j-k Mitochondrial particle area and genome copy number of isolated individual mitochondrial particles. Mitochondria from roots, base of stalk, mature L1 blade of light-grown 11-day seedlings and mature L7 blade of 63-day adult plant (j) and dark-grown juvenile 11-day seedlings (k). Number of mitochondrial particles measured, number with no detectable DNA, number with <1 genome copy, mean genome copy number, and mean area (μm^2) (n/n0/n<1/c/A) are: light-grown root (37/0/2/18/8.6); stalk (51/0/22/6/4.1); L1 (38/5/21/2/4.1); L7 (23/0/8/6/16.3); dark-grown root (34/0/7/17/18.2); stalk (37/0/3/22/17.9); L1 (17/0/3/24/24.7). Mitochondrial particle area was determined from MitoTracker staining. Genome copy number was determined from the DAPI-DNA fluorescence and using vaccinia virus as a standard (Materials and methods).

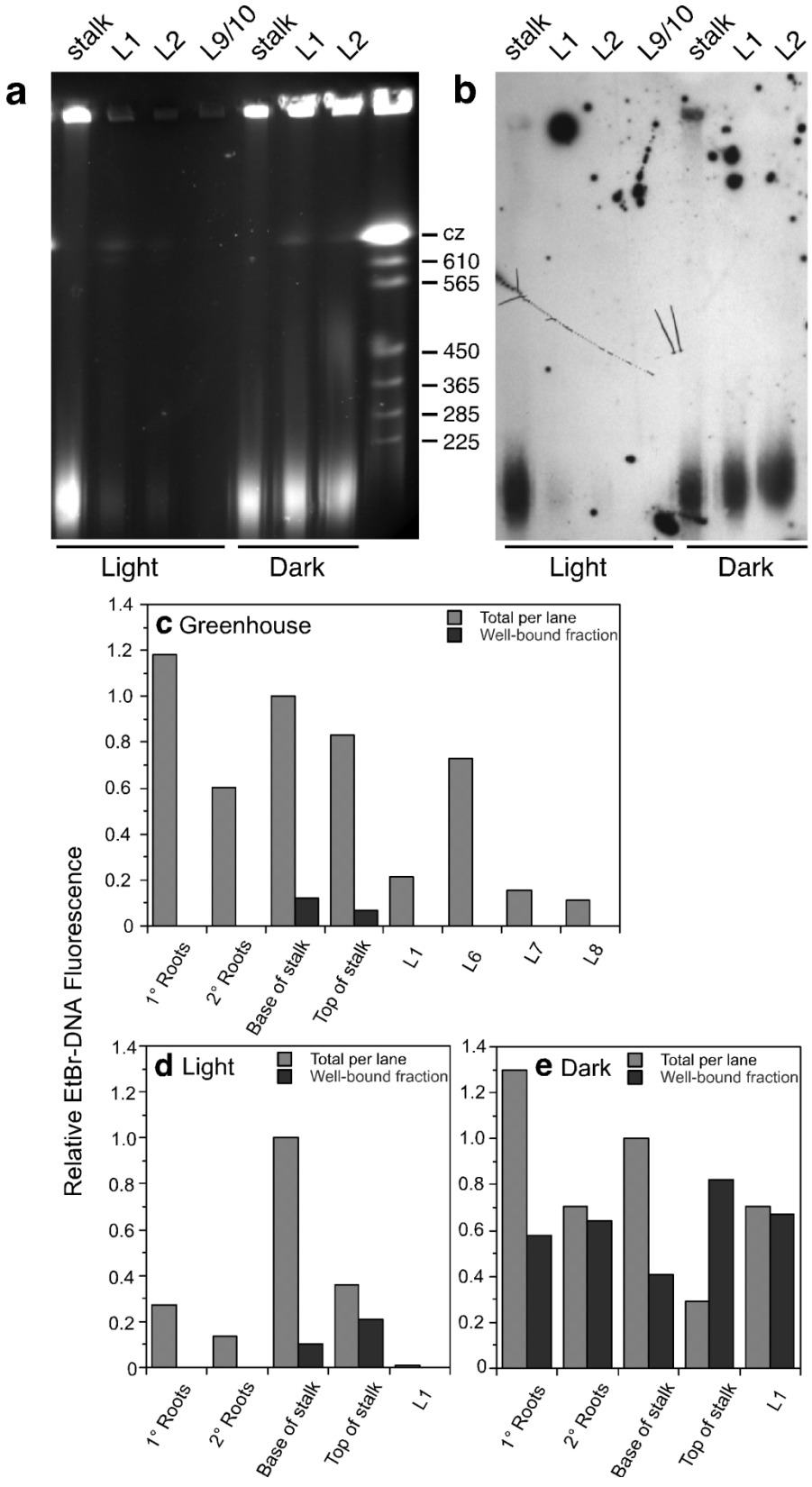
a
stalk
L1
L2
L9/10
stalk
L1
L2
cz
610
565
450
365
285
225
Light
Dark
b
stalk
L1
L2
L9/10
stalk
L1
L2
Light
Dark
c Greenhouse
Total per lane
Well-bound fraction
Relative EtBr-DNA Fluorescence
1° Roots
2° Roots
Base of stalk
Top of stalk
L1
L6
L7
L8
d Light
Total per lane
Well-bound fraction
1° Roots
2° Roots
Base of stalk
Top of stalk
L1
e Dark
Total per lane
Well-bound fraction
1° Roots
2° Roots
Base of stalk
Top of stalk
L1

Figure 4.2 Pulsed-field gel electrophoresis of maize mtDNA.

a and b The mtDNA from the entire stalk and blades of the first and second emerging leaves (L1 and L2, respectively) of 14-day juvenile seedlings and the blades of the 9th and 10th leaves (L9/10) of 89-day adult plants is shown. The plants were grown either in the light or dark as indicated. a EtBr-DNA fluorescence (some fluorescence in the well-bound fraction is due to auto-fluorescent material, not EtBr-DNA). DNA size markers (in kb) are yeast YNN295 chromosomes. The compression zone is indicated by cz. b Blot hybridization with a mitochondrial *cox*3 gene probe. The hybridization signal in each lane was determined relative to that for light-grown stalk (Materials and methods): for light, stalk is 1, L1 is 0.06, L2 is 0.03, L9/10 is 0; for dark, stalk is 1.31, L1 is 1.13, L2 is 1.23. c-e Maize mtDNA was analyzed by PFGE and EtBr-DNA fluorescence from 1° and 2° (seminal) roots, base of the stalk, top of stalk, and blade of the first leaf (L1) of 11-day juvenile seedlings and the blades of the 6th leaf (L6) of 34-day adult plants and the 7th and 8th leaves (L7 and L8, respectively) of 63-day adult plants. The L6 leaf was immature and unfurled, whereas L7 and L8 were mature, fully-expanded leaves (see Figure 4.6). The plants were grown in either (c) the greenhouse, (d) 16/8 h light/dark cycles or (e) continuous dark. The amount of mtDNA in each lane is given relative to the amount found in the base of the stalk. The percentage of mtDNA in the well-bound fraction is given relative to the total EtBr-DNA fluorescence in each sample and was determined by subtracting the total fluorescence (EtBr-DNA + auto-fluorescence; no DNase treatment) from the amount of auto-fluorescence (after DNase treatment) (Materials and methods)

4.4.2 Pulsed-field gel electrophoresis and blot hybridization of maize mtDNA

Mitochondria were isolated from seedlings and adult plants that were grown either in the greenhouse, under 16/8h light/dark cycles, or continuous dark (Figure 4.6). The DNA from the isolated mitochondria was analyzed by PFGE, EtBr-DNA fluorescence, and blot hybridization with a mitochondrial *cox3* gene probe (Figure 4.2). For mtDNA prepared by in-gel methods for PFGE, we sometimes find that the EtBr fluorescence in the well-bound fraction may be comprised of two components: EtBr-DNA and auto-fluorescent material. This auto-fluorescent material is not completely removed during the in-gel organellar lysis and washing steps and the amount can vary from among preparations and tissue types. Thus the mtDNA was treated with and without DNase before PFGE in order to quantify the well-bound EtBr-mtDNA fraction (Materials and methods).

When fractionated by PFGE, most of the mtDNA was found as a smear of linear molecules about 50 to 150 kb in size, with the remaining DNA immobile in the well-bound fraction of the gel (the replicating form; (Backert *et al.*, 1995; Bendich, 1996; Oldenburg and Bendich, 1996, 1998). The level of DNA per volume of isolated mitochondria declined dramatically during plant development. For 14-day seedlings grown under 16/8 h cycles, the amount of mtDNA determined by *cox3*-hybridization (Figure 4.2b) was highest in the stalk; it then decreased (to only 3-6% of stalk levels) in the L1 and L2 leaves and to an undetectable amount in the adult L9/10 leaves of 89-day greenhouse-grown plants. For the stalk, 3% of the mtDNA was found in the well-bound fraction, whereas no well-bound mtDNA was apparent from the mature leaves (L1, L2, and L9/10). In contrast, mtDNA was retained in dark-grown leaf tissue (L1 and L2) at a level similar to that found in the stalk. For the well-bound fraction, the largest amount of mtDNA was found in the dark-grown stalk (15%), and none was found for L1 or L2.

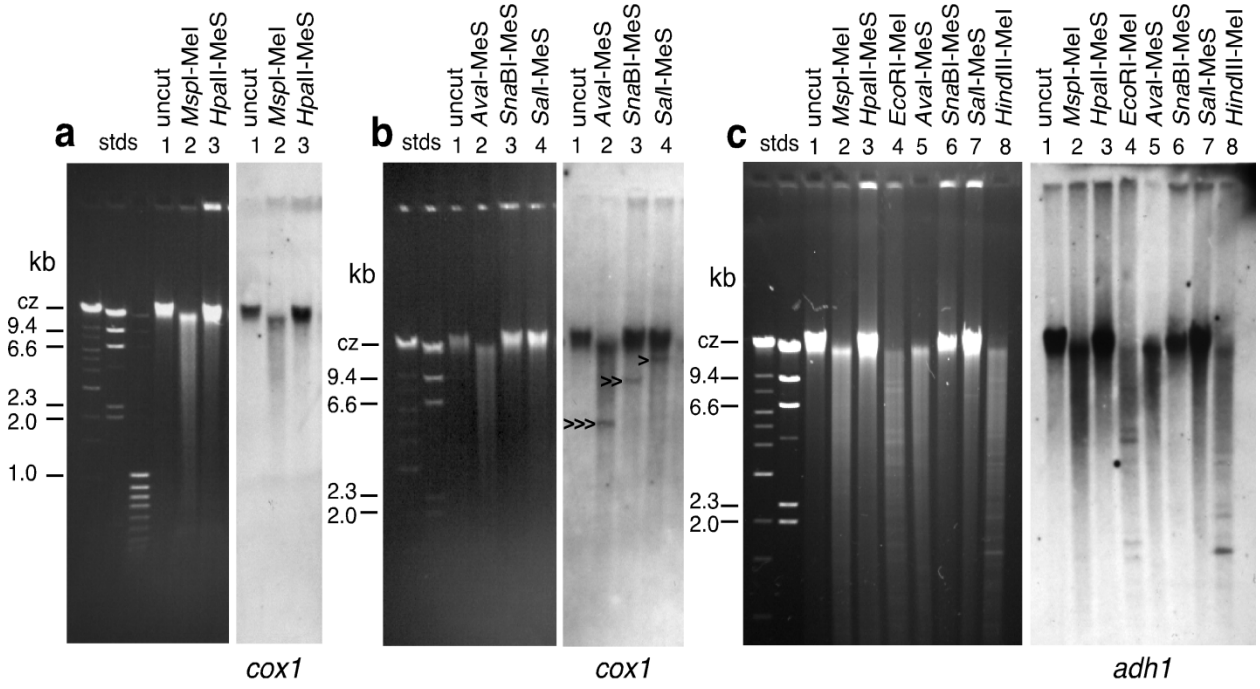

Figure 4.3 Blot hybridization of total tissue DNA with *cox1* and *adh1* gene probes.

Total tissue DNA was prepared from 17-day light-grown seedlings, digested with methylation-sensitive (MeS) and methylation-insensitive (MeI) restriction enzymes, fractionated by conventional gel electrophoresis, and hybridized to mitochondrial (*cox1*) or nuclear (*adh1*) gene probes. For (a-c) ethidium-stained DNA (with size standards) shown on left and hybridization on right. a *cox1* probe. Lanes 1 uncut DNA; lanes 2 *Msp*I (MeI); lanes 3 *Hpa*II (MeS). b *cox1* probe. Lanes 1 uncut DNA; lanes 2 *Ava*I ("MeS"); lanes 3 *Sna*BI (MeS); lanes 4 *Sal*I (MeS). c *adh1* probe. Lanes 1 uncut DNA; lanes 2 *Msp*I (MeI); lanes 3*Hpa*II (MeS); lanes 4 *Eco*RI (MeI); lanes 5 *Ava*I ("MeS"); lanes 6 *Sna*BI (MeS); lanes 7 *Sal*I (MeS); lanes 8 *Hind*III (MeI). The size of the mtDNA fragments are 0.55 and 0.4 kb for *Msp*I and *Hpa*II (these fragments are not visible), 4.8 kb for *Ava*I (triple arrowhead), 8.6 kb for *Sna*BI (double arrowhead), and 12.8 kb for *Sal*I (single arrowhead). Compression zone: cz

PFGE analysis was also performed with mtDNA from roots, stalk, and leaf blade of 11-day seedlings and leaves from 34-day and 63-day adult plants (Figure 4.2c-e). For these samples, mtDNA amount was determined by EtBr-DNA fluorescence before and after digestion with DNase (Figure 4.2c-e)(Materials and methods). In light-grown, 11-day seedlings, roots and stalk had similar amounts of mtDNA, but the linear molecules were smaller in the roots (<50 kb) than in the stalk (where the smear of linear molecules extended above 50 kb). The well-bound fraction was undetectable in all tissues except for the stalk. Both the roots and stalk contained about 5- to 10-fold more mtDNA than mature leaves. For the 34-day adult plant, the L6 blade was unfurled and thus not yet fully developed. The mtDNA was retained in L6 at a level similar to that found in the seedling stalk. In contrast, mtDNA from the fully-expanded L7 and L8 leaves of 89-day plants declined to levels similar to those found in the seedling L1 leaf blade. For the dark-grown, 11-day seedlings, all tissues (including the L1 blade) maintained a high level of mtDNA, and 40 to 80% of the mtDNA was found in the well-bound fraction.

These results indicate that in light-grown seedlings, mtDNA replication and/or repair occurs primarily in the stalk, followed by degradation in the fully-developed leaf blade. By contrast, in dark-grown seedlings, mtDNA is maintained by continued replication and/or repair in the roots and stalk and even in the L1 blade.

4.4.3 Discrimination of authentic mtDNA and NUMTs using MeS and MeI restriction enzymes

Dot-blot hybridization has been used to assess changes in DNA content during plant development (Baumgartner *et al.*, 1989; Cahoon *et al.*, 2003). We used this method to monitor mtDNA levels using total tissue DNA (ttDNA) from light-, dark-, and dark-to-light-grown maize. The amount of hybridization with *cox1* (a mitochondrial gene probe), however, was

similar in all tissues and the ratios of *cox1* to *adh1* (a nuclear gene probe) signals were comparable (data not shown). This result suggested that most of the *cox1* hybridization signal originated from the nuclear DNA (nucDNA) component of the ttDNA, not from DNA within mitochondria. NUMTs (mtDNA-like sequences within the nuclear genome) are especially prevalent in maize (Lough *et al.*, 2008). The presence of NUPTs (ptDNA-like sequences within the nuclear genome) in several plants was previously demonstrated by cytosine (CpG) methylation-sensitive (MeS) restriction enzyme digestion and blot hybridization (Ayliffe *et al.*, 1998). Thus, we applied this method of using MeS and MeI (methylation-insensitive) enzymes to differentiate authentic mtDNA and NUMTs in maize, as we have done previously to distinguish ptDNA and NUPTs (Zheng et al. 2011).

Total tissue DNA from light-grown, 17-day entire seedlings (stalk, L1, and L2) was digested with the isochizomers *Mpa*I (MeI) and *Hpa*II (MeS) and hybridized with a *cox1* gene probe (Figure 4.3a). A smear of *cox1*-hybridized fragments was found with *Msp*I (lane 2), but with *Hpa*II (lane 3) hybridization was found only at the position of undigested nucDNA. The two mtDNA *cox1*-fragments expected from *Msp*I or *Hpa*II digestion are only 0.28 and 0.43 kb and were not visible. Thus, all of the detectable *cox1* hybridization can be attributed to NUMTs. In order to better differentiate mtDNA and NUMTs, three other MeS enzymes were tested (Figure 4.3b). One of these, *Ava*I, is supposedly MeS, although partial digestion of the nucDNA was observed (lane 2). In addition, a mtDNA fragment of the expected size (4.8 kb) was found. For *Sna*B1 and *Sal*I, fragments of 8.6 and 12.8 kb, respectively, were found as expected for the mtDNA, and the nucDNA was undigested (lanes 3 and 4). With all three enzymes, the amount of *cox1* hybridization was greater for the NUMTs (75-85%) than for the authentic mtDNA (15-25%). Total tissue DNA was also hybridized with the nuclear-specific gene probe, *adh1*, after

digestion with MeS and MeI enzymes. As expected, nucDNA was not digested with the MeS-enzymes (lanes 3, 6, and 7 in Figure 4.3c).

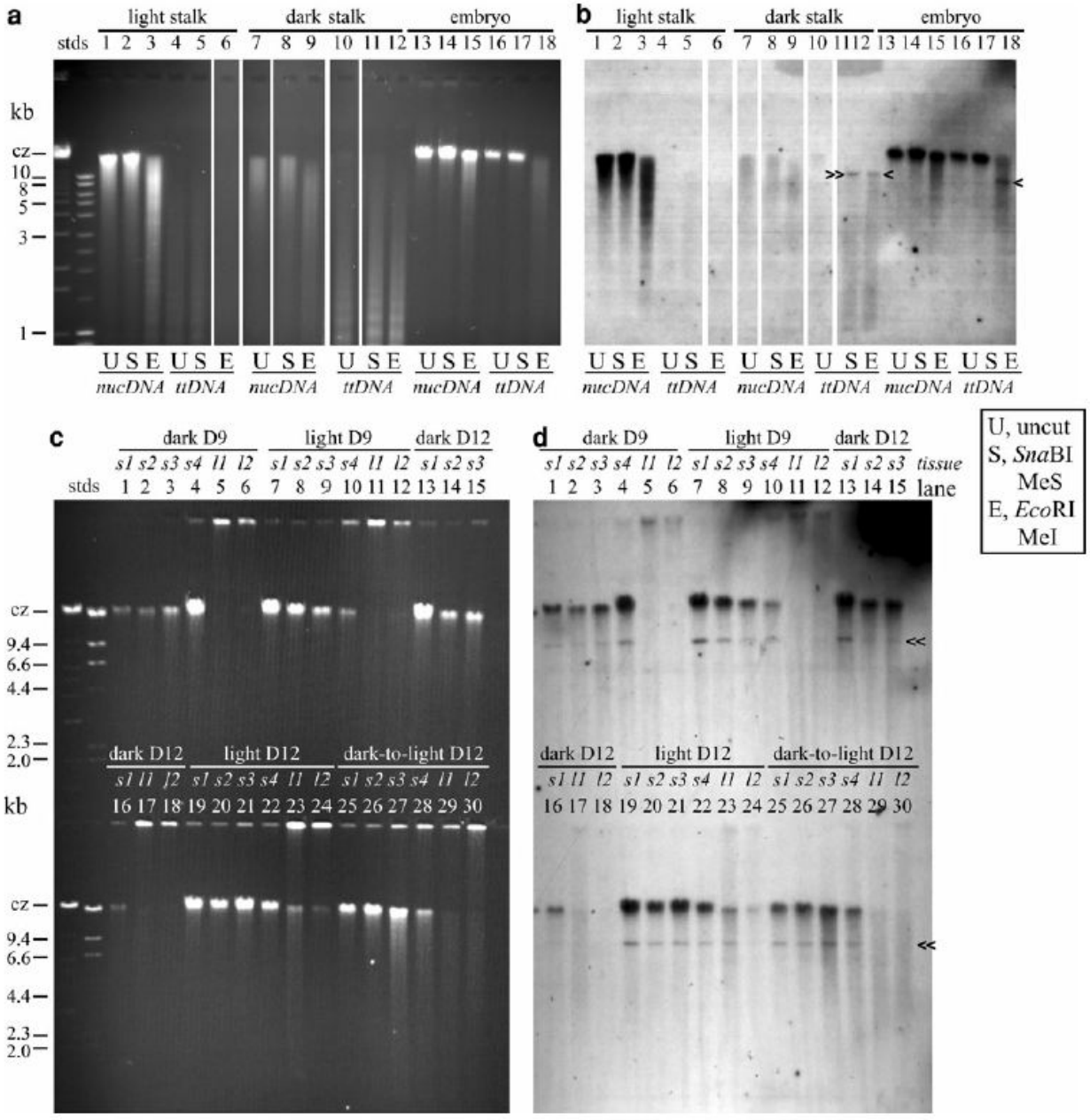

Figure 4.4 Total tissue and nuclear DNA hybridized with *cox1* gene probe and digested with *Sna*B1 (MeS) and *Eco*RI (MeI).

a, c Etidium-stained DNA. b, d *cox*1 hybridization. a and b Nuclear (*nucDNA*) and total tissuse (*ttDNA*) DNA from 9-day stalk of light-grown (lanes 1-6) and dark-grown (lanes 7-12) seedlings and embryo (lanes 13-18). For each sample, DNA is uncut (U) or digested with *Sna*BI (S; MeS) or *Eco*RI (E; MeI). c and d The ttDNA from 9- and 12-day (D9 and D12, respectively) light-grown, dark-grown, and 12-day (9 days dark, 3 days light) dark-to-light transferred seedling, digested with *Sna*BI, and hybrided with *cox1* gene probe. For each growth condition, the ttDNA was isolated from 6 seedling sections from the base of the stalk (*s1*-*s4*) to tip of leaf 1 (*l1*, *l2*). The relative *cox1* intensity for mtDNA/NUMTs is given in Table 4.1. The size of the mtDNA fragments are 8.6 kb for *Sna*BI (double arrowhead) and 8.8 kb for *Eco*RI (single arrowhead). Compression zone: cz

Table 4.1 Relative amount of authentic mtDNA to NUMTs.

	Figure 4.4d	Ratio mtDNA/NUMTs					
Growth conditions	**Lanes**	**s1**	**s2**	**s3**	**s4**	**l1**	**l2**
Dark 9-day	1-6	0.26; 0.13	0.37; 0.14	0.22; 0.14	0.22; 0.14		
Light 9-day	7-12	0.24; 0.23	0.17; 0.27	0.21; 0.24	0.43; 0.44		
Dark 12-day	13-18	0.20; 0.21	0.26; 0.29	0.16; 0.29	0.43; 0.32		
Light 12-day	19-24	0.21; 0.15	0.20; 0.17	0.19; 0.09	0.20; 0.13	0.18	0.22
Dark-to-light 12-day	25-30	0.29; 0.13	0.36; 0.22	0.39; 0.23	0.51; 0.21		

The *cox1* hybridization signal was measured for the NUMTs fraction (cz) and mtDNA *Sna*B1-fragment in each lane as shown in Figure 4.4d. For each growth condition, ttDNA was prepared from six sections along a developmental gradient from the base of the stalk (s1) to the tip of L1 blade (l2). The relative amount (ratio) of mtDNA to NUMTs was determined, as the mtDNA *cox1* signal/NUMT *cox1* signal (see Materials and methods). The first value in each pair was determined from Figure 4.4d (0.5 µg ttDNA per lane) and the second was from a gel loaded with 1.0 µg ttDNA per lane (data not shown). Only the data from Figure 4.4d were used for l1 and l2

The *cox1* hybridization was also assessed for nucDNA and ttDNA from the embryo and the stalk of light-grown and dark-grown seedlings (Figure 4.4b). For the embryo, both nucDNA and ttDNA were found in the compression zone (cz), where linear molecules longer than ~50 kb are not fractionated on the basis of size (Figure 4.4a lanes 13 and 16, respectively). Strong *cox1* hybridization in these uncut DNAs was found in the cz (Figure 4.4b lanes 13 and 16, respectively). As expected, strong hybridization of NUMTs was also found for nucDNA and ttDNA in the cz (lanes 14 and 17) after *Sna*BI digestion, but surprisingly no mtDNA fragment was detected in the ttDNA. In contrast, after digestion with *Eco*RI (MeI), a fragment of the expected size (8.8 kb) for mtDNA was found for ttDNA but not nucDNA (lanes 18 and 15, respectively). The absence of an *Eco*RI fragment in the nucDNA likely is due to incomplete digestion as indicated by the EtBr-DNA and *coxI* signals in the cz (lane 15). The *Eco*RI fragment, however, was found with embryo nucDNA, as well as ttDNA, when the restriction

digestion and blot hybridization was repeated (data not shown). The absence of a *Sna*BI/mtDNA fragment in the ttDNA from the embryo is somewhat surprising, given that a 598-bp *cox1* region is amplified using embryo ttDNA and the *cox1* PCR primers (Figure 4.8a). These results suggest that the 8.8-kb *Eco*RI fragment may be from NUMTs and not from mtDNA because the MeI-*Eco*RI fragment is found with both nucDNA and ttDNA, but the MeS-*Sna*BI fragment of authentic mtDNA is not found with the ttDNA. That mtDNA was not detected in ttDNA by blot hybridization could be due to several reasons. (i) A low amount of mtDNA relative to ttDNA in the embryo and the relative insensitivity of blot hybridization when compared with PCR. (ii) Preferential degradation of mtDNA in the ttDNA sample during preparation, leaving only nucDNA. (iii) The mtDNA structure in embryo cells. If the embryo cells in maize contain both a few large chromosomal mtDNA molecules and many small mtDNA molecules (subgenomic degradation products), then the amount of mtDNA *Sna*BI fragments may be too low to detect by blot hybridization, but sufficient for detection by PCR and qPCR, as shown in Figure 4.7a and Figure 4.5, respectively. (iv) In addition, the large chromosomal mtDNA may have been removed in the centrifugation step during the ttDNA isolation process. This is the most likely explanation as we found that large ptDNA molecules may also be removed during in-liquid DNA preparation and centrifugation (unpublished data). (v) The MeI-*Eco*RI fragment is from both NUMTs and mtDNA, but the *Sna*BI failed to digest the mtDNA. As shown in Figure 4.8, however, several NUMTs corresponding to *cox1* sequences are present in the maize nuclear genome, and a 598-bp cox1 fragment is amplified by PCR with both nucDNA and ttDNA from embryo tissue. Thus, most of the embryo *cox1* hybridization is due to NUMTs, and the MeI-*Eco*RI-NUMT fraction of ttDNA would be detectable as both a smear and a fragment of the expected size, as seen in Lane 18 of Figure 4.4b.

Most of the nucDNA from light-grown stalk tissue was undegraded (Figure 4.4a lane 1), but some degradation is indicated by the smear below the cz. In contrast, the light-grown ttDNA, as well as the dark-grown nucDNA and ttDNA (Figure 4.4a lanes 4, 7, and 10) were highly degraded, with a ladder pattern seen for the ttDNA but not the nucDNA. The *cox1* hybridization of NUMTs was found with the nucDNA from both light- and dark-grown tissue (Figure 4.4b lanes 1-3 and 7-9). For the ttDNA, no mtDNA restriction fragment was observed from light-grown tissue, although this may be due to extensive degradation of both nucDNA and mtDNA. On the other hand, even though the NUMT fraction of the ttDNA was degraded for dark-grown tissue, *cox1* fragments from both *Sna*BI and *Eco*RI digestion were found corresponding to the size expected for authentic mtDNA (Figure 4.4b lanes 11 and 12). In contrast to the embryo where the *Eco*RI fragment is most likely from NUMTs, in the dark-grown stalk the *Eco*RI fragment is probably from authentic mtDNA for two reasons. (i) The nucDNA fraction of ttDNA is highly degraded and <8.8 kb, the size of the fragment. (ii) There are similar amounts of *cox1* hybridization for both the MeS-*Sna*BI and MeI-*Eco*RI fragments.

The degraded nature of the ttDNA from the light- and dark-grown seedlings is probably due to the use of fresh tissue (as required for nuclei preparations). In order to obtain undegraded ttDNA from maize seedlings, we have found that it is necessary to keep the tissue frozen until DNA extraction buffer is added (unpublished data). Even then, ttDNA quality may suffer depending on the tissue (as demonstrated below) and method of preparation (Cankar *et al.*, 2006; Guo *et al.*, 2009; Jasbeer K, 2009); our data not shown). The degradation is likely due to nuclease(s) present in the seedling shoot tissue but not the embryo, given the lack of degradation of the ttDNA.

The amounts of mtDNA and NUMTs from light-grown, dark-grown, and dark-to-light-

transferred maize tissues were determined using *Sna*BI (since its 8.6 kb mtDNA fragment was well separated from the uncut NUMTs) and both *cox1* (Figure 4.4d, Table 4.1) and *atp6* (data not shown) gene probes. The tissue was kept frozen prior to extraction of the ttDNA for these samples. A *cox1* hybridization signal was found in the NUMT (undigested) fraction and in the 8.6-kb fragment of mtDNA. There was little difference in the relative amounts of mtDNA and NUMTs among the samples, with 3- to 10- fold more NUMT than mtDNA *cox1* hybridization in most samples. In all cases, the ttDNA from the stalk (lanes 1-4 Figure 4.4c, for example) was of high quality. The quality of the ttDNA from the L1 blade (lanes 5 and 6), however, was low as indicated by the faint smear and lack of nucDNA in the cz and some DNA remaining in the well (immobile fraction) even after *Sna*B1 digestion.

In summary, MeS and MeI restriction digestion of maize ttDNA showed that the amount of NUMTs is higher than the amount of authentic mtDNA, as determined by blot hybridization with mitochondrial gene probes. This result suggests that NUMTs may interfere with copy number measurements of authentic mtDNA by blot hybridization and qPCR unless mtDNA-specific primers that do not amplify NUMTs are employed. A difference in mtDNA content among embryo and seedling tissues was observed, in spite of nucDNA degradation for some tissues (Figure 4.4b). The amount of mtDNA was beneath the detection limit of our blot hybridization assay (only NUMT hybridization was found) for the embryo in the ungerminated seed. The mtDNA level increased in the dark-grown stalk, indicating mtDNA replication in this metabolically active tissue. The ratio of mtDNA/NUMTs did not change with development from the base of the stalk to the leaf tip in dark-grown, light-grown, and dark-to-light transferred seedlings, similar to our findings for maize ptDNA (Zheng *et al.*, 2011). Lastly, a method that yields high quality ttDNA is required for accurate quantification of NUMTs and mtDNA.

4.4.4 Determination of mtDNA copy number using real-time qPCR

Maize ttDNA extracted from seedling, embryo, and endosperm tissues was used for qPCR to determine mtDNA copy number. For this assay, we used mtDNA-specific primers to amplify authentic mtDNA sequences and not NUMTs (Materials and methods) (Kumar and Bendich, 2011).

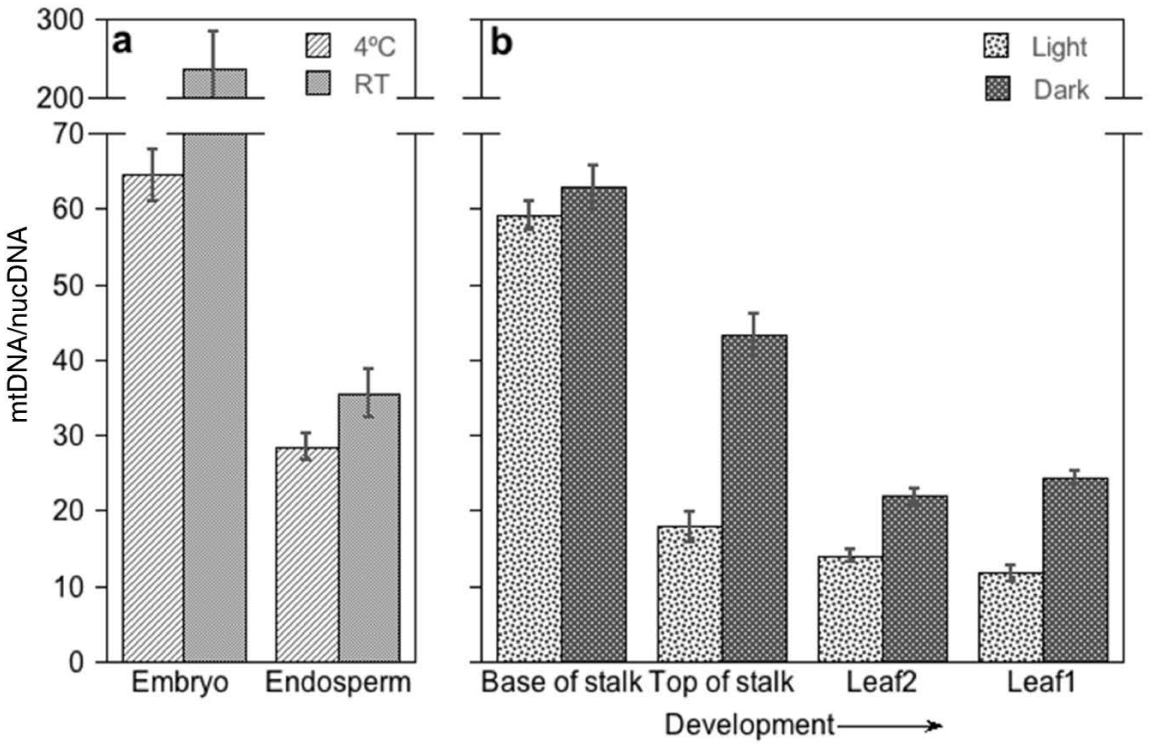

Figure 4.5 mtDNA copies per nucDNA as determined by qPCR. mtDNA/nucDNA was determined in embryo, endosperm, and light- and dark-grown seedlings during development.

a mtDNA/nucDNA for embryo and endosperm imbibed at 4ºC and room temperature (RT). b mtDNA/nucDNA for tissues grown in light and dark during development from base of stalk to leaf 1. Primers that amplify authentic mtDNA and not NUMTs were used and copy number was determined using absolute quantification of mtDNA and nucDNA standards (Materials and methods). The average mtDNA copy number/nucDNA is: 65 for embryo at 4°C and 236 at RT; 28 for endosperm at 4°C and 36 at RT; light, 59 for base of stalk, 18 top of the stalk, 14 leaf 2, and 12 leaf 1; dark, 63 for base of stalk, 43 top of the stalk, 22 leaf 2, and 24 leaf 1

The mtDNA copy number per haploid genome (mtDNA/nucDNA) was determined using

absolute quantification (Figure 4.5). Copy number increased by ~4-fold between embryos imbibed at 4°C and those imbibed at room temperature (RT). In contrast, mtDNA copies remained constant for endosperm from the same seeds imbibed at these temperatures (Figure 4.5a). Seeds imbibed at 4°C are metabolically quiescent, whereas seeds imbibed at RT are metabolically active. The copy numbers determined for embryo tissue likely are an underestimate because of qPCR-inhibitory components in the ttDNA extracts (Figure 4.7).

For the basal 5-mm stalk section, similar mtDNA copy numbers were found for both light- and dark-grown tissues, as well as the 4°C embryo tissue. Interestingly, there was a dramatic decline from the high levels of mtDNA in RT embryo to the much lower levels in the base of the stalk. For light-grown plants mtDNA/nucDNA declined by ~5 fold during development from base of the stalk to L1, while the decline was ~3-fold for dark-grown plants (Figure 4.5b). The decline from base to top of stalk was greater in light compared with dark-grown tissues.

4.5 Discussion

We previously reported a sharp decline in the quantity and molecular integrity of ptDNA when maize seedlings developed in the light but not under dark conditions (Oldenburg and Bendich, 2004a; Oldenburg *et al.*, 2006; Zheng *et al.*, 2011). The demise of ptDNA was attributed to the onset of photosynthetic electron transport and the degradation of ROS-damaged ptDNA molecules that were not repaired. Now we find that mtDNA, too, is rapidly degraded in light, although mtDNA is retained under dark growth conditions. The decline in ptDNA should come as no surprise for the light-mediated transition from proplastid to chloroplast and the onset of photophosphorylation. On the other hand, one might expect greatly reduced damage to mtDNA in photosynthetic tissue since mitochondrial respiration is no longer required as the sole source for ATP production. Why then would mtDNA also decline in response to light when

mitochondria do not use light for energy production?

4.5.1 Decline in mtDNA with development

We found a substantial difference in the size and DNA content of mitochondrial particles isolated from the below-ground and above-ground tissues of light-grown maize seedlings. The mitochondrial particles from roots were 2-fold larger with 3- to 9-fold more DNA than those from the stalk and L1 blade. The mtDNA per mitochondrial particle declined 3-fold from the stalk to L1 blade, although the particle size was similar. Mitochondrial particles from all of the tissues of the dark-grown seedling were similar in size and mtDNA copy number. The L1 blade of dark-grown seedlings had mitochondrial particles 6-fold larger with 12-fold more DNA than those from the L1 blade of light-grown seedlings. A few mitochondrial particles from all of the maize tissues had <1 copy, whereas others had >100 copies. Mitochondria continually fuse and fragment within living cells, leading to a wide variation in both organelle volume and mtDNA content (Arimura *et al.*, 2004; Segui-Simarro *et al.*, 2008; Sheahan *et al.*, 2005; Woloszynska, 2010). Furthermore, electron microscopy of fixed tissue sections reveals an enormous variation in the volume of individual mitochondria among and within individual plant cells (Bendich, 1984; Segui-Simarro *et al.*, 2008). Thus the variation we find in Figure 4.1 is not surprising, although it remains possible that aggregation of individual mitochondria during isolation may have contributed to the variation.

The largest amount of mtDNA on a per cell basis (mtDNA/nucDNA) was found for embryo tissue that had been imbibed for 24 h at RT: a ~4-fold increase compared to embryos imbibed at 4°C. Thus the transition from metabolically inactive to active tissue includes an increase in mtDNA replication. The values determined by qPCR in embryo tissue, however, are likely underestimates due to inhibitory substances in the ttDNA extracts. Nevertheless, the CTAB

method for ttDNA extraction generally yields high quality DNA for qPCR and other methods of analysis (Rogers and Bendich, 1988b; Vinod, 2004). As an example, we show here that endosperm ttDNA extracted by CTAB and other methods does not contain PCR-inhibitory components. Thus for the purpose of assessing changes in mtDNA/nucDNA with development, the CTAB method was employed for ttDNA extraction from light- and dark-grown maize seedlings, as well as embryo and endosperm tissues.

The mtDNA of highest amount and integrity was found in the base of stalk, and both of these qualities decreased during leaf development. For example, using 5-mm tissue sections for qPCR, there was a ~6-fold decrease in mtDNA per cell between the meristematic tissue at the base of stalk and the L1 leaf blade. The decrease was from 5- to 16-fold when the entire stalk was used for PFGE/blot hybridization, even though the meristem comprised a smaller fraction of the tissue analyzed. The difference in fold decrease may be attributed to 1) the parameter of measurement, mtDNA copies per haploid nuclear genome and relative EtBr/hybridization signal intensity, and 2) sensitivity with respect to the minimal size of mtDNA measured. For PFGE the size range for measurement is ~25-200 kb (smear of linear molecules), whereas a ~150 bp gene fragment amplified by qPCR would also measure mtDNA <25 kb in size. Regardless of these differences, our results show that mtDNA declines substantially during development in maize.

The decrease in mtDNA with development is greater for light-grown seedlings than for those grown in the dark. Higher levels of mtDNA in the dark may be due to continued replication and repair of mtDNA that is necessary for continued respiratory activity, whereas in the light, respiration is no longer needed to supply energy for growth as this function is now performed by photosynthesis. There is still a decline from the base to leaf in the dark that may be attributed in part to partitioning of DNA into dividing mitochondria as cells divide, expand, and differentiate

during development. Some decrease may also be due to degradation of damaged mtDNA since respiration and ROS production would continue in the dark fully-expanded leaf blade. In contrast, we found that ptDNA did not decline from base to leaf in dark-grown seedlings (Oldenburg *et al.*, 2006; Zheng *et al.*, 2011). This high level of ptDNA is probably maintained to provide for expression of photosynthetic proteins needed for light-dependent etioplast-to-chloroplast development, after which ptDNA levels decline.

4.5.2 Mitochondrial function and DNA retention

One essential function of mitochondria in plants and other eukaryotes is respiration and generation of ATP (Bowsher and Tobin, 2001; Fernie *et al.*, 2004; Millar *et al.*, 2011). These organelles, however, are also important for other metabolic functions such as biosynthesis of amino acids, fatty acids, and Fe-S clusters, as well as programmed cell death (Balk *et al.*, 2003; Balk and Pilon, 2011; Logan, 2006). Another important mitochondrial function in plants is participation, with peroxisomes and chloroplasts, in photorespiration (Maurino and Peterhansel, 2010). Although as a C4 plant maize can minimize photorespiration by conducting different photosynthetic activities in bundle sheath and mesophyll cells (Dai *et al.*, 1995; Williams, 2012), some photorespiration is necessary for avoiding glycolate toxicity (Zelitch *et al.*, 2009).

Mitochondrial proteins required for respiration are encoded by genes in both the mitochondrial and nuclear genomes, whereas those for other metabolic processes, including photorespiration and DNA synthesis, are found only in the nuclear genome (Burger *et al.*, 2003; Elo *et al.*, 2003; Logan, 2006). Respiratory activity is typically measured using whole plants or leaf tissue (Hunt, 2003; Ribas-Carbo M *et al.*, 2010) so that variation among cell types is not addressed. In wheat leaves, mesophyll cells contribute 55% of the volume of mitochondria, with 37% and 8% contributed by epidermis and vascular, respectively (for wheat leaves, Bowsher and

Tobin, 2001). In maize, photosynthesis and photorespiration are conducted by mesophyll (MS) and bundle sheath (BS) cells, considered below as “green cells”, whereas “non-green cells” are those from proto-MS and -BS (containing proplastids), partially developed MS and BS of dark-grown seedlings (containing etioplasts), epidermis, vasculature, and roots.

Plant cells may be divided into two groups: non-green cells with mitochondria performing an essential function of respiration; and green cells with mitochondria performing an essential function of photorespiration. This division of cell types may also represent those that maintain mtDNA and those that do not. In the first case, mtDNA is necessary for respiratory-competent mitochondria, although the ROS byproduct of respiration can lead to damage and degradation of mtDNA (Shokolenko *et al.*, 2009). Protective agents, however, can reduce damage (antioxidants and alternative oxidase) (Chew *et al.*, 2003; Cvetkovska and Vanlerberghe, 2012; Guo and Crawford, 2005; Yoshida *et al.*, 2011) or repair the damage (RecA, for example) (Griffiths *et al.*, 2009; Miller-Messmer *et al.*, 2012; Tahbaz *et al.*, 2012). Another way to maintain “good DNA” is turnover of (presumably damaged) mtDNA by continual replication and degradation, as reported for mitochondria of mung bean (Dai *et al.*, 2005; Lo *et al.*, 2011). Turnover is indicated by the substantial amounts of the replicative forms of mtDNA (well-bound fraction in PFGE) we find in roots and base of stalk of both light- and dark-grown maize plants. For dark-grown plants, we find less mtDNA in leaves than in the base of stalk, suggesting a decline in mtDNA protection, resulting in the loss of *some* mtDNA via ROS-induced damage and degradation. However, for photorespiratory function in non-respiratory, green cells, there is no apparent reason to maintain DNA in mitochondria. Thus upon the transition from respiratory to photorespiratory function during cellular differentiation, mtDNA protection is abandoned, and all mtDNA is damaged and degraded. Some mtDNA, however, is probably maintained in the

epidermal and vascular cells of green tissue.

4.5.3 Organellar crosstalk

The ultimate decision to retain or degrade mtDNA and ptDNA is made within the nucleus. Recent research has revealed elaborate communication networks between the nucleus, mitochondrion, and plastid (Butow and Avadhani, 2004; Pesaresi *et al.*, 2007; Woodson and Chory, 2008) and a connection between chloroplast biogenesis and mitochondrial function/mtDNA retention (Quesada *et al.*, 2011; Roussell *et al.*, 1991; Toshoji *et al.*, 2012). One outcome of organellar crosstalk is the adjustment of redox balance, which probably involves the assessment of energy production in both mitochondria and chloroplasts.

It may seem surprising that during maize development in the light, both mtDNA and ptDNA show a similar decline in amount and integrity. In the dark, however, ptDNA does not decrease from base of stalk to leaf blade, whereas mtDNA does decrease. A likely mechanistic feature for both organelles is a response to ROS-induced DNA damage and a decision by the nucleus as to whether the organellar DNA is maintained by replication/repair or degraded. Thus the light-induced decline in ptDNA and the dark-decline in mtDNA can be rationalized from the roles in energy metabolism of these organelles. But why does light trigger a decline in the DNA within mitochondria, organelles with no known photoreceptors?

Photomorphogenesis involves changes in nuclear gene expression leading to the proplastid-to-chloroplast transition and a profound alteration in the energy metabolism. Not only does light directly drive photophosphorylation, but it may indirectly cause a mitochondrial shift from ATP production by respiration to protection against glycolate toxicity by photorespiration. Since photorespiratory proteins are encoded by nuclear genes, mtDNA is no longer necessary and may be degraded. Thus, mitochondrial function may determine whether mtDNA is retained or

degraded in somatic cells.

4.5.4 Acknowledgements

This work was supported in part by the United States Department of Agriculture, awards 2002-35318-12384 and 2008-39211-19557. The authors thank Yunqi Lu, Jeffery Dines, and Kathryn Bofferding for their assistance on this project.

4.6 Supplemental Materials

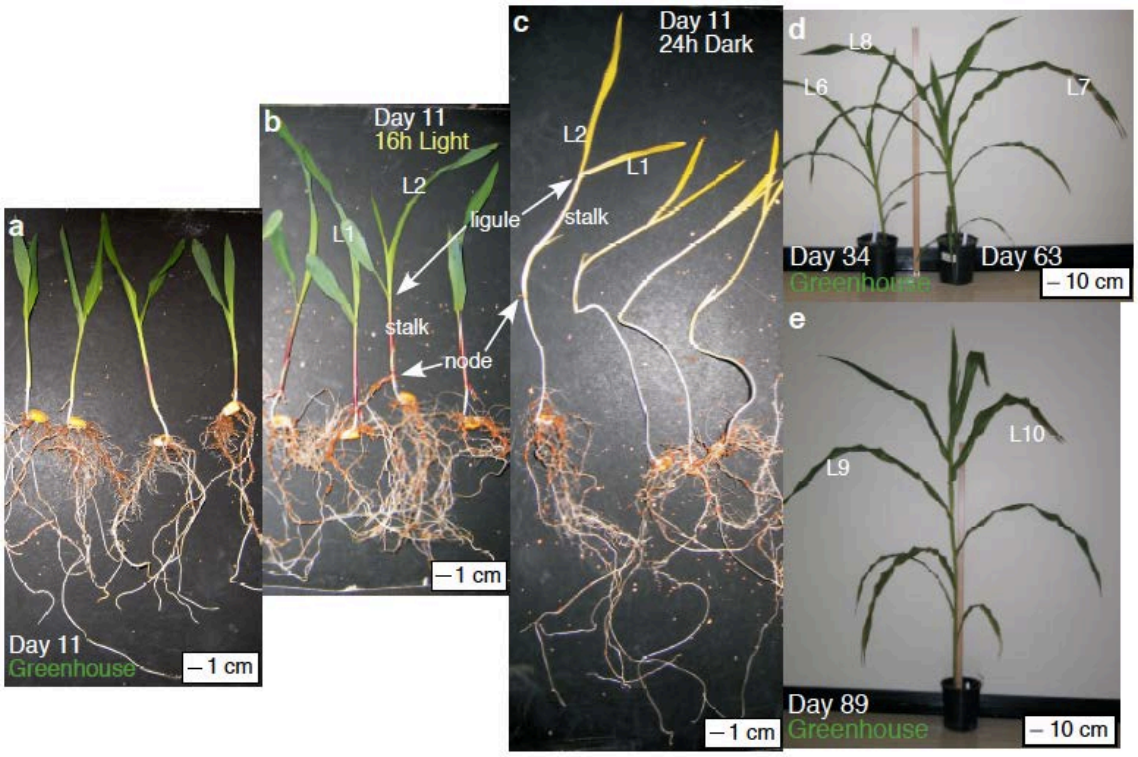

Figure 4.6 Maize seedlings and adult plants.

Juvenile plants (seedlings) were grown in **(a)** the greenhouse, **(b)** under 16 hr light/8 hr dark cycles or **(c)** continuous dark from seed sown in Turface. Mitochondria were isolated from the primary and seminal roots, the stalk (between basal node and L1 ligule) and the leaf blade. **d** and **e** Adult plants were grown in the greenhouse from seed sown directly in soil or transplanted seedlings. The entire leaf blade was used for mitochondrial isolation.

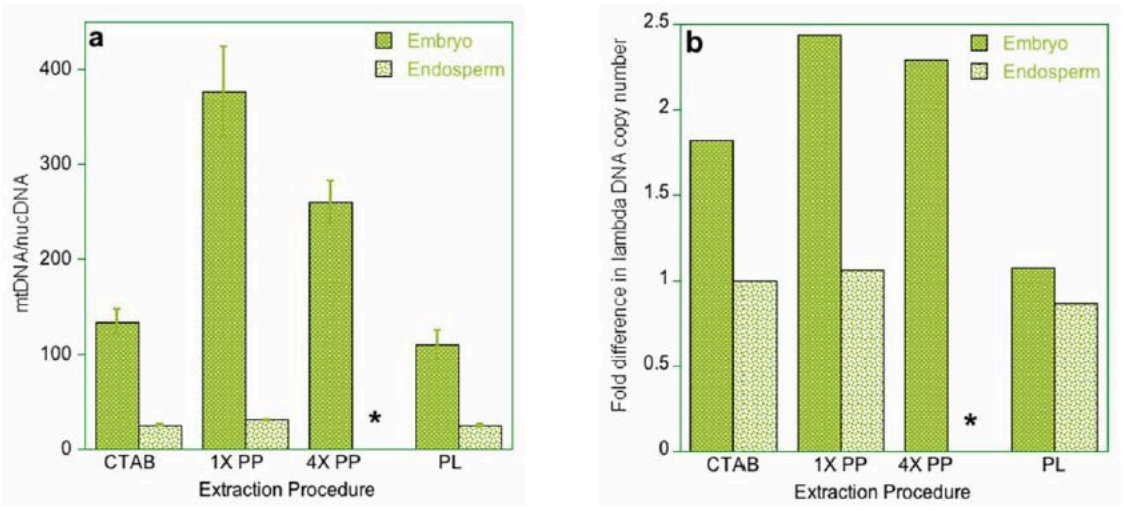

Figure 4.7 Effect of different DNA extraction procedures on qPCR.

Total tissue DNA (ttDNA) extracted from maize embryo, but not endosperm, contained PCR-inhibiting contaminants, possibly pectin-like substances. Four different ttDNA extraction procedures were tested for removing the inhibitory substances: CTAB procedure (Rogers and Bendich, 1988a), resin-based kit (Phytopure, GE Biosciences) with either the recommended concentration of resin (1x PP) or four times the recommended amount (4x PP), and column-based kit (PureLink, Life Technologies) (PL). **a** mtDNA/nucDNA quantification from embryo and endosperm tissues. Note that the different methods led to higher variability among embryo than endosperm samples. The variability among replicates, as indicated by standard errors, was also higher for embryo than endosperm. The ttDNA extraction procedures greatly influenced mtDNA copy numbers determined by qPCR for embryo, but not for endosperm tissue. Only the PL column-based kit showed no inhibition with the qPCR assay. Furthermore, the DNA size limit of column-based kits is only ~25-30 kb, so that larger forms of mtDNA and nucDNA would be excluded in the final ttDNA extracts. In addition to PCR inhibition, the ratio of mtDNA to nucDNA varied depending on ttDNA extraction procedure and contributed to the wide range (~100-375) in copy number of mtDNA/nucDNA for embryo tissue. For comparison of mtDNA copy number among embryo, endosperm, and seedling tissues from dark- and light-grown plants, the CTAB procedure was used (Figure 4.5). **b** qPCR inhibition assay. λ DNA copy number (template was 5×10^{5} copies or 8×10^{-5} ng) determined with or without the addition of ttDNA extracted by different procedures from embryo and endosperm. Relative quantification ($2^{-\Delta ct}$) (Livak and Schmittgen, 2001) was used to determine the fold difference in copy number with and without total ttDNA. Values above one indicate inhibition, and one indicates no inhibition of qPCR. Embryo DNA extracted with PL showed the least inhibition of the qPCR reaction. *Endosperm ttDNA extracted using 4x PP was not included in qPCR assays.

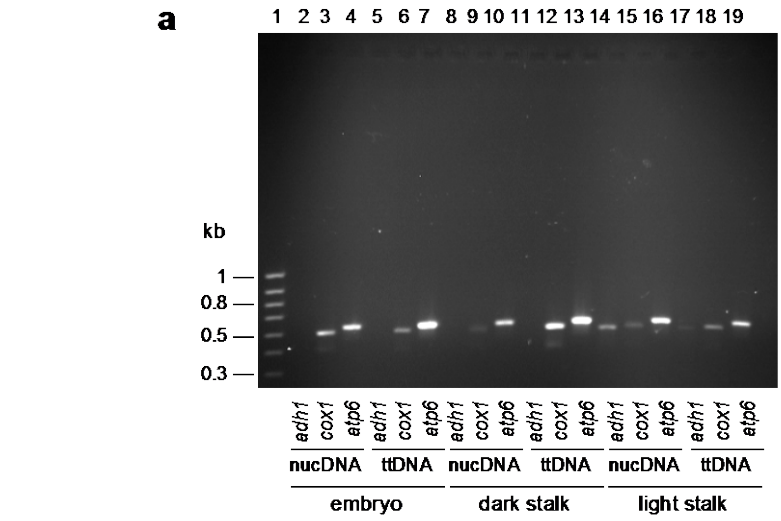
a
1 2 3 4 5 6 7 8 9 10 11 12 13 14 15 16 17 18 19
kb
1
0.8
0.5
0.3
adh1 cox1 atp6 adh1 cox1 atp6 adh1 cox1 atp6 adh1 cox1 atp6 adh1 cox1 atp6 adh1 cox1 atp6
nucDNA ttDNA nucDNA ttDNA nucDNA ttDNA
embryo
dark stalk
light stalk

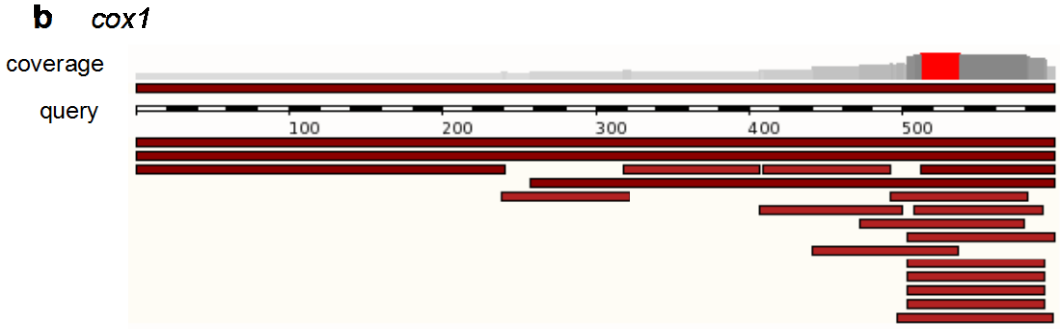
b cox1
coverage
query
100
200
300
400
500

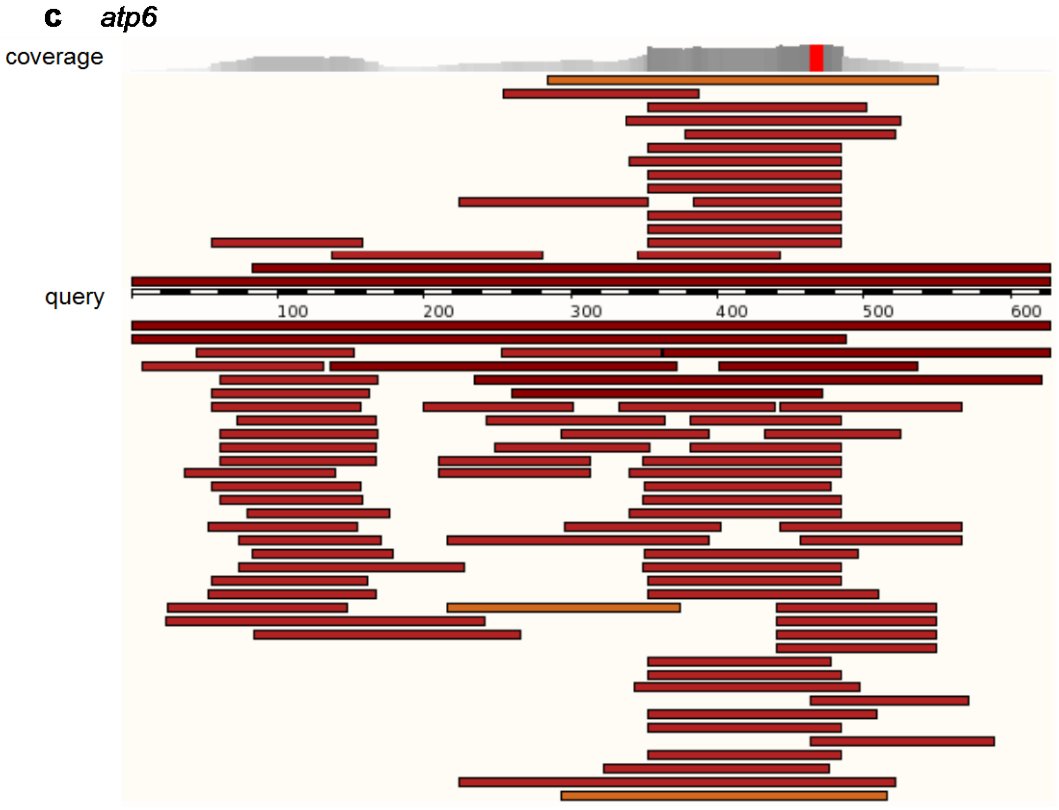
c atp6
coverage
query
100
200
300
400
500
600

Figure 4.8 PCR products amplified from nucDNA and ttDNA with *adh1*, *cox1*, and *atp6* primers, and alignment of NUMTs with mtDNA *cox1* and *atp6* sequences used as probes for blot hybridization.

a The 582-bp *adh1* nuclear gene region was amplified using primers Zmadh1-L2/Zmadh1-R2. This PCR product was only found using the nucDNA and ttDNA templates from the light-grown stalk. The 598-bp *cox1* and 582-bp *atp6* mitochondrial gene regions were amplified using primers Zmcox1-L2/Zmcox1-R2 and Zmatp6-L1/Zmatp6-R1 primers, respectively. These PCR products were found using the nucDNA and ttDNA from all three tissues: embryo, dark- and light-grown stalk. Comparisons of the amounts of PCR products among the DNA samples are not meaningful because different amounts of template DNAs were used. The lack of the single-copy *adh1* product in some samples may be due in part to low template concentration and/or non-optimum PCR conditions (such as Tm) for this primer set. The BlastN results (**b** and **c**) suggest there are NUMTs that could be amplified with the *cox1* and *atp6* primers, and the PCR products found using the nucDNA samples indicate these NUMTs are present. In addition, the brighter bands with the *atp6* primers suggest higher NUMT copy number for this gene that for the *cox1* gene. **b** Alignment of unmasked maize nuclear genome sequences (http://www.maizesequence.org/index.html) with the 598-bp *cox1* probe generated using primers Zmcox1-L2/Zmcox1-R1 and corresponding to mitochondrial genome sequence nucleotides 355,917 to 356,514, accession NC_007982. Nineteen NUMTs are shown with size range of 87 to 598 bp and % identity range of 63% to 100%. There are 8 NUMTs with size >100 bp. **c** Alignment of unmasked maize nuclear genome sequences (http://www.maizesequence.org/index.html) with the 629-bp *atp6* probe generated using primers Zmatp6-L1/Zmatp6-R1 and corresponding to mitochondrial genome sequence nucleotides 563,419 to 564,044, accession NC_007982. Eighty-eight NUMTs are shown with size range of 106 to 629 bp and % identity range of 58% to 100%. There are eleven NUMTs with size >300 bp.

Coverage indicates frequency at which a given region of the query sequence (*cox1* or *atp6*) is recognized within the nuclear genome; the highest frequency is in red, and dark-to-light gray indicates decreasing frequency. Solid bars above and below the query sequence (black and white striped bar) are the regions identified as high scoring pairs (HSPs; similar to the *cox1* or *atp6* query sequences). Color indicates % identity: dark red >80%, red >60%, and orange <60%. The maize genome includes nuclear, mitochondrial, and plastid sequences; thus one of the HSPs identified corresponds to the mitochondrial sequence. The unmasked maize genome was not run through the RepeatMasker program, so that all repeats of a given query region and located at more than one nuclear locus are shown. For example, there are five 138-bp repeat loci (one on chromosome 2 and four on chromosome 4) corresponding to an *atp6* query region. Alignments were performed with BlastN set at high sensitivity: E-value 10, Word size 9, Match score 1, Mismatch score -1, Gap 2/1.

The PCR amplification using nucDNA as template and the identification of many similar *cox1* (and *atp6*) NUMTs by BlastN analysis (and see below) indicate that in the compression zone (cz) of Figures. 4.3 and 4.4, NUMTs are the source of the hybridization signal found with the MeS restriction enzymes.

Using fluorescence *in situ* hybridization (FISH), Lough et al. (2004) showed the extent of NUMTs across maize inbred line B73 nuclear chromosomes. For cosmid clone 14 that contained the *cox1* probe sequence, hybridization was reported on two chromosomes (the *atp6* probe sequence was on cosmid clones 1 and 20 and FISH signal was reported on four and two chromosomes, respectively). Of interest is the finding that when FISH was performed with two other B73 seed sources, a total of six and eight

chromosomal loci were shown to hybridize to the *cox1*-cosmid 14 probe. Thus, the B73 used in our study may contain from two to ten chromosomal loci with a *cox1*-like sequence. Furthermore, this is a minimal estimate since only very large loci would be detectable by FISH (Lough et al. (2004) used cosmids of ~30-40 kb).

The number of NUMTs is estimated to be 19 loci (copies) for the 598-bp *cox1* probe sequence as determined by the BlastN analysis. The authentic mtDNA was determined to be ~12 and 24 copies/haploid nuclear genome by qPCR for light- and dark-grown seedlings, respectively. These results suggest that one may expect the NUMT and mtDNA *cox1*-hybridization signals to be approximately equal. On average, however, there is ~4-fold more NUMT *cox1* hybridization signal in the cz than in the authentic 8.6-kb mtDNA fragment (the range is 2- to 10-fold more NUMTs). The BlastN analysis, however, was performed such that there are no gaps between adjacent homologous regions. If gaps had been allowed, the number of *cox1*-NUMTs would surely be greater. Additionally differences in NUPT content have been reported among individual plants and tissues from the same plant (Ayliffe et al. 1998). It is likely that the same would apply to NUMTS, and our unpublished data indicate changes in NUMTs/NUPTs with maize development. Thus, it is not surprising that the blot hybridization signal indicates more NUMTs than authentic mtDNA using the *cox1* gene probe.

Chapter 5 (Appendix)

ON THE FATE OF PLASTID DNA MOLECULES DURING LEAF DEVELOPMENT

Delene J. Oldenburg, Beth A. Rowan, Rachana A. Kumar, and Arnold J. Bendich

In their commentary, Golczyk et al. (2014) state that the level of plastid DNA (ptDNA) remains approximately constant during mature, aging, and senescent stages of leaf development, in apparent contrast with our conclusion of ptDNA decline from previous studies. However, the ptDNA decline that we reported was found during proplastid-to-chloroplast development, before the mature-to-senescent leaf stages. We found little change in ptDNA after chloroplast maturation. Furthermore, we argue that their data fail to demonstrate constancy in ptDNA during development: most of their data are not quantitative and demonstrate neither constancy nor change in ptDNA content. We also show that our inability to detect DAPI-stainable DNA in some plastids is not due to "artefact-prone methods" as suggested by Golczyk et al. In our opinion, the fundamental issues concern whether ptDNA content declines during leaf development, the magnitude of that decline, and by extension, the functional relevance of such a decline. Our conclusions for three plant species with respect to changes in ptDNA content during leaf development are summarized in Figure 5.1, based on four methods that provide quantitative data on ptDNA mass per plastid and per cell and on molecular structure. The only quantitative data provided by Golczyk et al. (2014) are based on amounts of DNA between two closely-spaced qPCR primers and thus depend on the unvalidated assumption that such tiny DNA fragments represent genome-sized ptDNA molecules. We conclude that an accurate assessment of ptDNA must consider not only ptDNA quantity but also molecular quality, a parameter not

addressed by Golczyk et al. In our opinion, the manner of data presentation is the principal difference leading to our opposing conclusions.

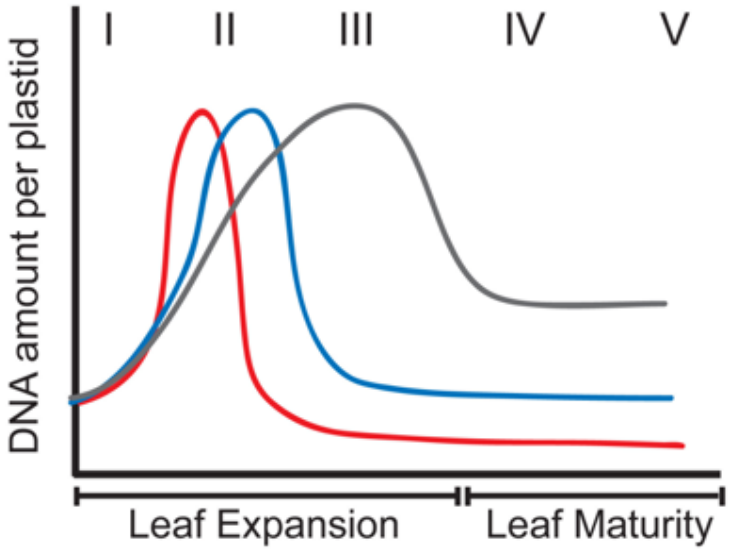

Figure 5.1 Schematic representation of changes in the amount of ptDNA per plastid during development in three plant species.

Increase in ptDNA amount due to ptDNA replication occurs very early in development in maize (red line), followed by a rapid decline. For Arabidopsis (blue line), the increase in ptDNA occurs slightly later and the decline in ptDNA amount is much later. For tobacco (grey line), ptDNA increases more gradually and the decline is less severe. The Roman numerals indicate stages of leaf development. I-III represent expanding leaves, and IV and V represent expanded leaves. Reprinted from Rowan and Bendich (2009), Figure 5.1.

5.1 Quantitative conclusions from non-quantitative data

Although Golczyk et al. (2014) used four methods for assessing the presence of ptDNA during the development of green leaves, three of these methods involved microscopic examination that did not provide quantitative information for either ptDNA per plastid, ptDNA per cell, or ptDNA per nuclear DNA (nucDNA) amount. DAPI-DNA fluorescence revealed DNA within chloroplast nucleoids that was characterized by “visual inspection…indicating unaltered DNA contents per organelle” in young and mature leaves. Furthermore, for none of the

four plant species examined (Arabidopsis, sugar beet, tobacco, maize) was statistical data provided concerning the number of cells or plastids chosen for analysis or the fraction of cells or plastids that exhibited DAPI-DNA fluorescence at different stages of leaf development. Using electron microscopy, fibrils were identified as DNA-containing areas, but no statistical analysis of the data was provided and no quantitative conclusion was drawn.

By contrast, the data presented in our previous papers for ptDNA of Arabidopsis, tobacco, *Medicago truncatula*, pea and maize were quantitative, revealing an increase followed by a decrease in ptDNA during the transition from proplastid to pale-green chloroplast to fully-green chloroplast (as well as the etioplast-to-chloroplast transition upon illumination of etiolated maize seedlings) (Oldenburg and Bendich, 2004a; Oldenburg *et al.*, 2006; Rowan and Bendich, 2009; Rowan *et al.*, 2004; Shaver *et al.*, 2006, 2008; Zheng *et al.*, 2011). Those data (summarized in Figure 5.1) show that after the decrease to the level in mature chloroplasts, ptDNA remains essentially constant as leaves reach maturity, in agreement with the conclusion of Golczyk et al. As for gerontoplasts in senescing leaves, although Golczyk et al. concluded that the ptDNA level remains unchanged, their description may, in fact, reflect a decline in ptDNA, as they noted that "DNA fluorescence became more and more diffuse and difficult to visualize". In our work, we analyzed leaves long before the onset of leaf senescence, except for Arabidopsis where we reported "a slight decline in cpDNA content as mature leaves senesce" (Rowan and Bendich, 2009) and concluded that "the demise of organellar DNA can be independent of its effect on senescence" (Oldenburg and Bendich, 2004a).

The only quantitative assay of ptDNA reported by Golczyk et al. (2014) was real-time quantitative PCR (qPCR). Using standard qPCR procedures, our group (Rowan and Bendich, 2009) and Thomas Boerner and colleagues (Zoschke *et al.*, 2007) reported constant values for

plastid genome equivalents per nuclear genome equivalent (ptDNA/nucDNA) during Arabidopsis leaf development. The qPCR data presented by Golczyk et al. include sugar beet (a plant we have not investigated), tobacco, and maize. Since maize is the plant we have studied most intensively, and the decline in ptDNA is greater for maize than tobacco (Figure 5.1), we focus on maize.

Golczyk et al. show that for maize, ptDNA/nucDNA increases from ~800 at stage I of leaf development to ~1200-1400 for stages III-VI. Unfortunately, they provide neither images of nor a definition of "stage" for maize leaves used in their experiments. Furthermore, the reference given for maize "grown in a greenhouse as previously described (Li *et al.*, 2006)" applies only to tobacco and Arabidopsis, not to maize. Thus, we cannot compare the leaf material used by Golczyk et al. directly with the plant tissue we used in our experiments, where both images and detailed descriptions of seedling development were provided (Oldenburg and Bendich, 2004a; Oldenburg *et al.*, 2006; Zheng *et al.*, 2011). Using standard qPCR procedures, the ptDNA/nucDNA values we reported ranged from 1200 to 1600 for the mature first leaf blade of 10- to 12-day-old seedlings (stage IV-V in Figure 5.1) (Zheng *et al.*, 2011). Thus, using the standard qPCR assay, there appears to be no conflict in ptDNA copy number between our data and those of Golczyk et al. The real conflict appears to be related to assumptions about the quality and functionality of the ptDNA present.

In the standard qPCR procedure, the short segment (~150 base pairs) of ptDNA that is amplified is usually taken to represent a genome-sized molecule of ptDNA assumed to exist *in vivo*, thus permitting the inference that "copy number" of the short segment represents the copy number of the plastid genome. This assumption is likely valid for nuclear DNA that (presumably) exists as intact chromosomal DNA molecules throughout the development of the

maize leaf prior to leaf senescence. The quality of ptDNA molecules declines rapidly as plastids mature (described below), so that the copy number of the short segments amplified by standard qPCR may not represent the copy number of the genome or of DNA segments long enough to encode functional products. This hypothesis can be tested using a qPCR procedure in which copy number of long DNA segments (11 kb, for example) is compared with copy number obtained with the standard 0.15-kb segments. We conclude that in addition to copy number data, the quality of ptDNA must be considered when assessing the contribution of ptDNA to plastid function during leaf development.

In addition to the dubious practice of drawing quantitative inferences from visual inspection of microscopic images of plastid nucleoids, the appearance of DAPI-fluorescent nucleoids reveals little of the quality (molecular integrity and molecular weight) of the ptDNA molecules in those nucleoids. Similarly, our quantitative DAPI-DNA data using plastids isolated from the cell reported DNA mass but not quality. DNA quality currently can be assessed only after the DNA is extracted from the cell. Using pulsed-field gel electrophoresis (PFGE) and/or moving pictures of ethidium-stained ptDNA, we found a decline in the size of DNA molecules that accompanied chloroplast maturation in all five plants examined (Oldenburg and Bendich, 2004a; Oldenburg *et al.*, 2006; Rowan and Bendich, 2009; Rowan *et al.*, 2004; Shaver *et al.*, 2006). We interpreted these data to indicate that ptDNA was damaged by reactive oxygen species (byproducts of photosynthesis) and progressively degraded during leaf development. In some plants, like tobacco, ptDNA repair maintains ptDNA integrity longer during leaf development than in others, like maize, resulting in the species differences shown in Figure 5.1. Thus, the amount of high-quality ptDNA may decline much faster during leaf development than does the amount of total ptDNA, as we reported (Shaver *et al.*, 2006). In addition, the capacity to encode

useful plastid gene products could decline before the microscopic appearance of the nucleoid *in situ* reveals the ptDNA degradation process. As the ptDNA becomes more highly fragmented, the appearance of the nucleoid would deteriorate until the nucleoid is no longer evident *in situ*. Inspection of the images (Figures 2 and Supplemental figures 1-4) presented by Golczyk et al. (2014) can be interpreted to indicate this progression. Highly fragmented ptDNA, either still aggregated to form a nucleoid or dissociated from the nucleoid, could also affect the interpretation of results from the qPCR assay.

5.2 Artefacts and methodology

Golczyk et al. (2014) suggest that methodological artefacts could account for our finding of a developmental decline in ptDNA. One example was "possible technical problems with insufficient DAPI dye penetration (Evans *et al.*, 2010; Sellden and Leech, 1981)". However, the data presented in the cited articles are not indicative of poor DAPI penetration of the plastid envelope. Sellden and Leech (1981) wrote that DAPI "did not penetrate either whole cells or isolated protoplasts", without reference to chloroplasts or whether fixed or unfixed tissue was used. Evans et al. (2010) suggested plastid impermeability as an explanation for why chloroplasts were not convincingly stained in mature tissues, but presented no data on permeability. In our opinion, these two citations mislead the reader as to the possibility that chloroplast impermeability to DAPI is a likely explanation for our inability to detect DNA-containing nucleoids in mature leaf tissue. Furthermore, DAPI-DNA nucleoids are clearly visible in plastids for ~60% of the cell regions in mature maize leaf blade sections (see below, Table 5.1; Figure 5.2; Figure 5.4) and although fainter than in younger leaves, visible in mature leaves of Arabidopsis (Figures 1E and 3H in Rowan et al. 2009), as well as in the images presented by Golczyk et al. (2014).

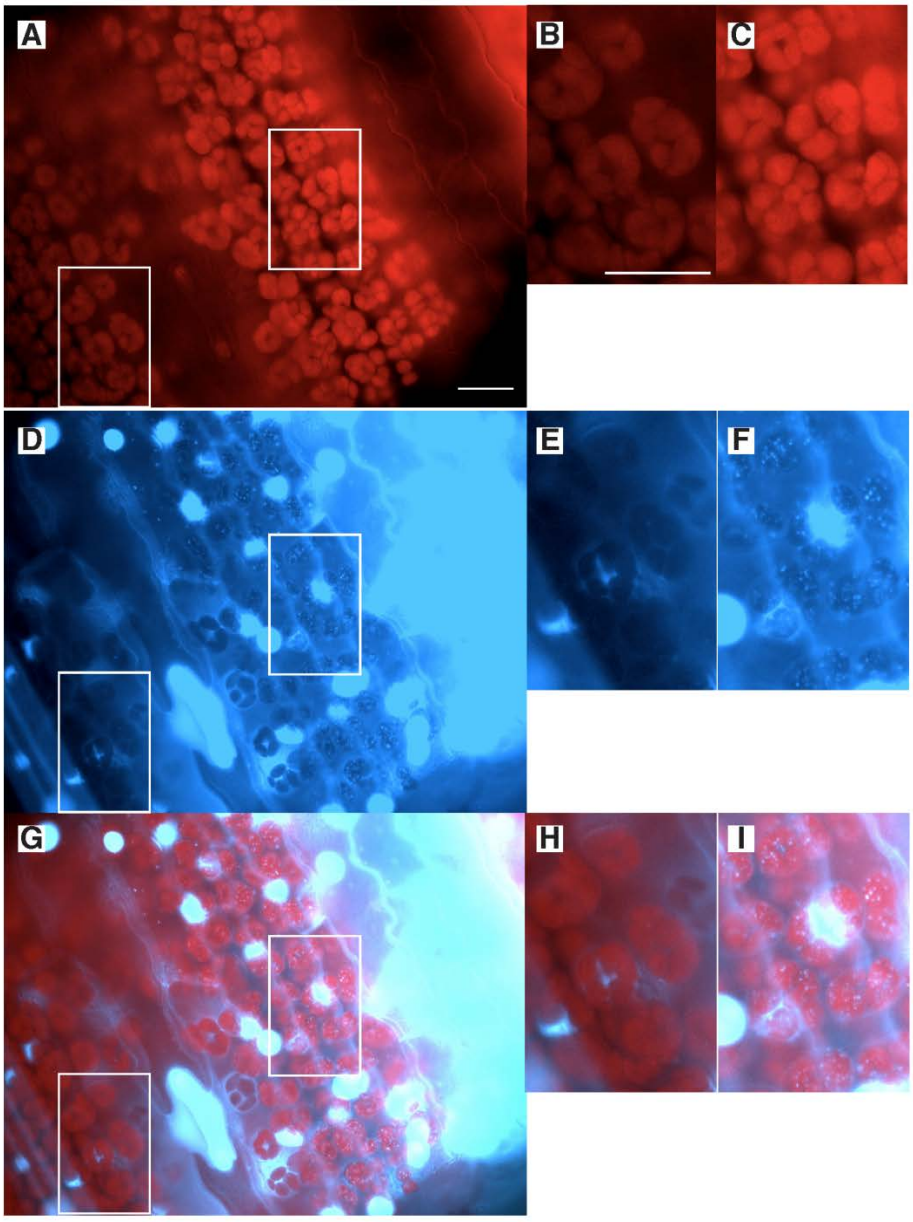

Figure 5.2 Fluorescent microscopy images of a tissue section from the mature first leaf blade of maize.

The tissue section is from the middle of the leaf blade from 11-day seedlings. The top panels show chlorophyll autofluorescence; middle panels show DAPI fluorescence; and bottom panels are merged images. B, E, H show plastids in Category 3 (undectable DAPI-DNA) and C, F, I in Category 1 (discrete DAPI-DNA nucleoids) and are enlargements of boxed regions in A, D, and G. Scale bar in A is 25 µm for B-C, E-F, and H-I. Images produced as described in Methods and shown in Figure S1.

Table 5.1 Maize plastids with and without discrete DAPI-DNA fluorescence.

	Category 1[a] discrete	**Category 2** diffuse pattern and discrete	**Category 3** undetectable
Cells in tissue sections[b]	69	NA	46
Protoplasts[c]	4	3	8
Isolated plastids[d]	51	42	38

[a]Three categories of DAPI-DNA patterns in plastids were scored by visual examination of fluorescence microscopic images: (1) plastids with many nucleoids as indicated by discrete DAPI-DNA spots, (2) plastids with a diffuse DAPI-DNA signal and a few nucleoids, and (3) plastids with neither a diffuse DAPI-DNA signal nor discrete nucleoids. Examples of categories 1 and 3 are shown in Figure 5.2 for tissue sections and for categories 1-3 in Figure 5.3 for mesophyll protoplasts and Figure 5.6 for isolated plastids.

[b]The number of cells with and without discrete DAPI-DNA nucleoids was determined for both fixed-then-sectioned and sectioned-then-fixed tissues from the first leaf blade of 11-day and 10-day seedlings, respectively (Methods and example shown in Figure 5.5H). Since only two categories (discrete and undetectable) were scored, the second category is not applicable (NA) for tissue sections. For fixed-then-sectioned tissue, four fields of view were examined with 45 cells in category 1 and 28 in category 3; these values for sectioned-then-fixed were three fields with 24 and 18 cells, respectively.

[c]Fifteen mesophyll protoplasts from the first leaf blade of 10-day seedlings were examined.

[d]A total of 131 isolated plastids from the first leaf blade of 9- and 11-day seedlings were examined.

At the opposite extreme, Golczyk et al. claim that the membranes of mature chloroplasts are "leaky", allowing the ptDNA to be degraded by endogenous DNase. Reference was made to Sellden and Leech (1981) showing loss of ptDNA only in damaged plastids when their plastid isolation buffers contained Mg^{++}. However, our sorbitol and high salt plastid isolation buffers contain EDTA, so that the leaky-membrane/DNase explanation is implausible. Experiments in which exogenous DNase is added to isolated plastid preparations indicate that mature chloroplasts may be more susceptible to membrane damage than proplastids and developing plastids (Sellden and Leech, 1981; Shaver *et al.*, 2006). One procedure for plastid isolation included DNase treatment to remove DNA/chromatin from the outside of plastid membranes (Oldenburg and Bendich, 2004a; Rowan *et al.*, 2004). For maize, we found undetectable DAPI-DNA in 85% and 82% of the plastids treated with and without DNase, respectively; for

Arabidopsis, the corresponding values were 7% and 7% (Oldenburg and Bendich, 2004a; Rowan *et al.*, 2004). In subsequent work we omitted the DNase and used a high-salt buffer to remove DNA/chromatin and still found plastids with no DAPI-DNA: 9% for pea; 11-34% for *M. truncatula*; 2-36% for maize from DAPI-DNA quantification and 80-87% for maize from visual scoring (Oldenburg *et al.*, 2006; Shaver *et al.*, 2006, 2008; Zheng *et al.*, 2011). These data indicate that the absence of detectable DAPI-DNA fluorescence in some plastids is not due to an artefact arising from DNA degradation by nucleases during plastid isolation. Leaky plastid membranes were also suggested by Golczyk et al. to be caused by polyvinyl pyrrolidone and by high salt, but neither data nor references were provided to support this speculation. In sum, Golczyk et al. alternately invoke both impermeable and extremely permeable membranes to conclude that the chloroplasts without DAPI-DNA staining resulted from artefacts in our experimental procedures. However, our voluminous data (and some of their own micrographs), a more accurate reading of the cited literature, and data presented below refute their conclusion.

Golczyk et al. also claim that a "lack of appropriate controls checking the biochemistry (was) used" for our DAPI-DNA imaging and quantification of ptDNA. The DNA-specificity of DAPI has been well documented (Coleman, 1979; Lawrence and Possingham, 1986; Miyamura *et al.*, 1986). Nonetheless, we have employed numerous controls for our fluorescence microscopic imaging of DAPI-stained ptDNA. These include measuring the levels of DAPI-fluorescence in unstained plastids and fixed plastids pretreated with DNase and then stained with DAPI. We also determined optimal exposure times, since DAPI-DNA signal intensity is generally higher for proplastids than mature chloroplasts (see Figure 5.6). We switched from using a broad-band DAPI filter to a narrow-band filter to reduce plastid autofluorescence from chlorophyll and accounted for any background fluorescence in our calculations of plastid DAPI-

DNA values. We also demonstrated that chlorophyll autofluorescence does not mask or quench the plastid DAPI-DNA signal (Zheng *et al.*, 2011). Thus, we conclude that DAPI-DNA quantification is reliable for determining ptDNA mass.

5.3 DAPI-DNA in maize tissue sections, protoplasts, and isolated plastids

The fluorescent microscopic images of plastid nucleoids presented by Golczyk et al. (2014) were obtained using tissues that were treated with fixative prior to protoplasting, squashing, and DAPI staining of the tissues, whereas analogous images we reported previously were obtained by sectioning leaves and immediately plunging the tissue into fixative (Rowan and Bendich, 2009; Shaver *et al.*, 2006). Thus it is possible that the lack of detectable DAPI-stained, punctate nucleoids we reported for mature tissues of Arabidopsis and maize could have been due to amounts of ptDNA below the detection limit, as was our interpretation, or nuclease activity in the mature (but not younger) tissue that degraded the ptDNA before the fixative inactivated the nuclease, as suggested by Golczyk et al.

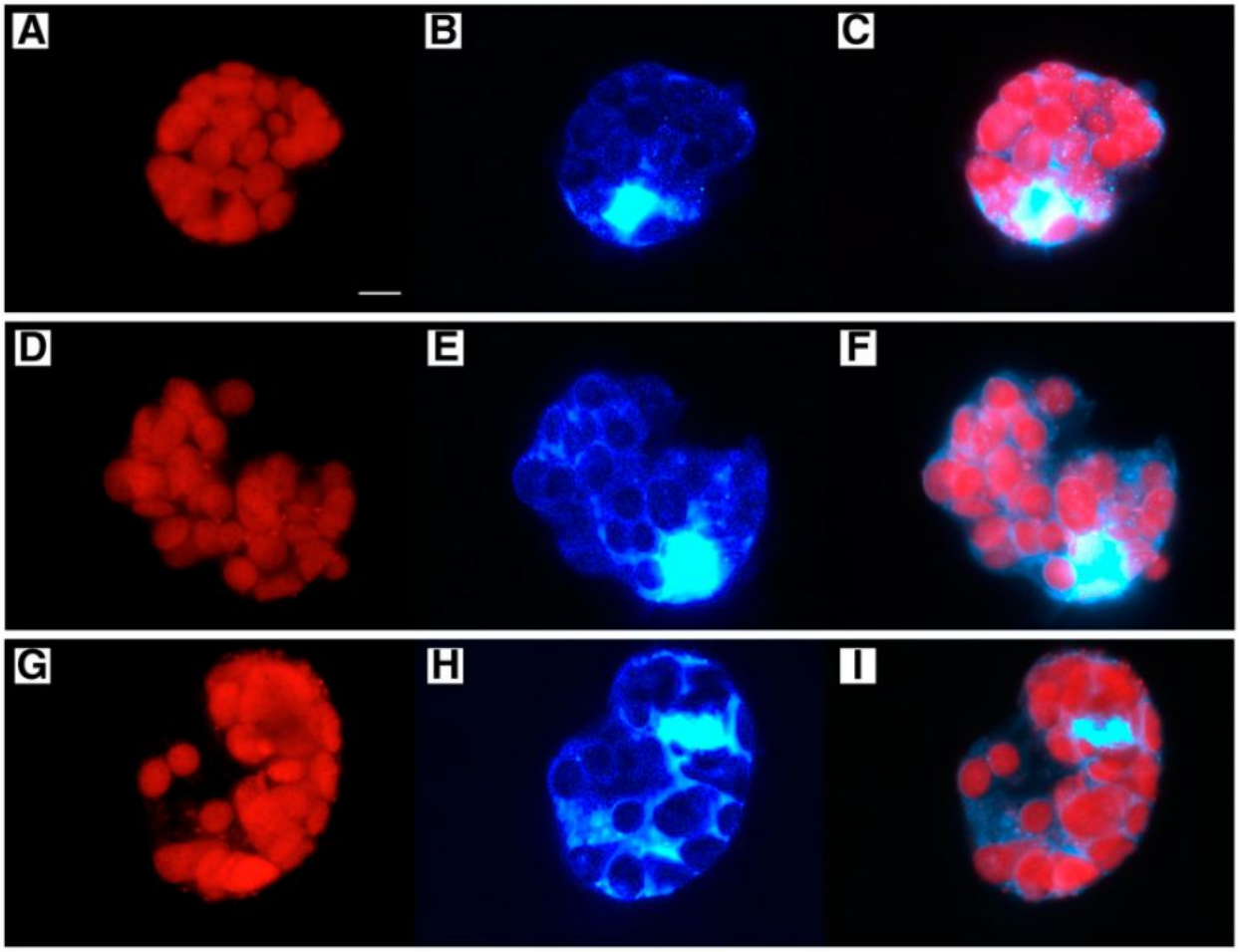

Figure 5.3 Fluorescence Microscopy Images of Protoplasts from the Mature First Leaf Blade of Maize 10-d-Old Seedlings.

The left panels show chlorophyll autofluorescence, middle panels show DAPI fluorescence, and right panels are merged images. The protoplasts in (A) to (C) contain plastids in Category 1 (discrete DAPIDNA nucleoids), (D) to (F) plastids in Category 2 (diffuse pattern and discrete DAPI-DNA nucleoids), and (G) to (I) plastids in Category 3 (undetectable DAPI-DNA). Bar in (A) is 10 μm for all panels.

Table 5.2 Size and genome copy number for individual maize plastids

		Size (μm^2)	Genome copy number
Base of stalk	pt1	6.7	209
	pt2	3.6	113
	pt3	7.1	307
	pt4	8.7	251
Middle of stalk	pt5	17.0	331
	pt6	13.1	302
	pt7	22.7	334
	pt8	20.9	387
Top of stalk	pt9	22.6	727
	pt10	30.1	652
	pt11	16.0	160
	pt12	26.7	650
Leaf 1 blade	pt13	24.3	0
	pt14	14.0	10
	pt15	83.5	241
	pt16	48.1	218

The plastid size and copy number are given for some of the plastids shown in Figure 5.6. The number of plastids measured, average copy numbers ± standard errors and (ranges) for the complete data set were 55, 113±9 (11-307) for base of stalk; 54, 252±23 (42-766) for middle of stalk; 43, 241±33 (0-1047) for top of stalk; and 52, 106±13 (0-351) for the first leaf blade (Zheng *et al.*, 2011).

We vacuum-infiltrated maize tissues with fixative, prepared tissue sections, and performed DAPI staining as described in Methods. A tissue section from the mature first leaf blade is shown in Figure 5.5 that contains both a region where DAPI-DNA nucleoids are clearly visible in the plastids and an adjacent region containing plastids with no detectable DAPI-DNA fluorescence (additional images are shown in Figure 5.4). Examples of protoplasts (Figure 5.3) and isolated chloroplasts (Figure 5.6G-G°) with and without detectable DAPI-DNA fluorescence

are also shown. We classified the chloroplasts into three types with respect to DAPI-DNA signal and then scored the number of cells (see Figure 5.5; Methods), protoplasts, and isolated chloroplasts in each category (Table 5.1). These results demonstrate that plastids without detectable DAPI-DNA are present in the mature leaf blade and indicate that our inability to detect punctate forms of ptDNA in some chloroplasts cytologically is not attributable to a DNase artefact, as suggested by Golczyk et al., but to a decrease in ptDNA content and/or molecular integrity as leaves develop, as we concluded previously (Oldenburg and Bendich, 2004a; Oldenburg *et al.*, 2006; Rowan and Bendich, 2009; Rowan *et al.*, 2004; Shaver *et al.*, 2006, 2008; Zheng *et al.*, 2011). This progression of proplastid-to-chloroplast development is shown in Figure 5.6, illustrating a visible reduction in DAPI-DNA intensity and decreased genome equivalents per plastid for the mature chloroplasts (Table 5.2). We report zero genome equivalents for one plastid (pt13 in Table 5.2; Figure 5.6G), although our interpretation of a plastid with "no detectable DAPI fluorescence…does not imply…absolutely no DNA within the plastid" (Oldenburg and Bendich, 2004a). For the images shown in Golczyk et al. (2014), it is important to ascertain the degree to which an image of a cell with punctate chloroplast nucleoids (e.g. Golczyk et al. Figure 2I) represents all cells at stage III/IV of maize leaf development and whether that degree changes as the leaf develops. To obtain this information, statistical data of the type we provide in Table 5.1 must be presented, but such data are lacking in the Golczyk et al. Commentary.

Golczk et al. state that "undetectability of stainable DNA…is *per se* not a valid criterion to postulate the absence of DNA or to assess nature and impact of changes of in-gel DNA structures remaining after lysis of embedded chloroplasts". We have employed assays that quantify ptDNA mass (DAPI-DNA per plastid, blot-hybridization, and qPCR) and monitor ptDNA molecular

size/structure (PFGE and in-gel DNA movies) during plastid development, in addition to the less informative (and qualitative) presence/absence assay for DAPI-stained nucleoids. Our data reveal a developmental decline in both ptDNA amount and quality, leading to the conclusion that the lack of visible DAPI-DNA nucleoids in mature plastids is due to ptDNA degradation and fragmentation to less-than-genome-sized molecules that occurs *in vivo*.

5.4 Photosynthesis without ptDNA?

Golczyk et al. (2014) make the argument that chloroplasts would not be able to conduct photosynthesis after leaf maturation without ptDNA and support their argument with "the maximum mRNA half-life reported for (barley) *psbA* are in the range of 40 h". In fact, the reported half-life was >40 h, the mRNA level did not change over a 30-hour period, and mRNA stability increased at least five-fold during chloroplast development (Kim *et al.*, 1993). Furthermore, Baumgartner et al. (1993) reported an increase in *psbA* mRNA stability of >100-fold during development of young barley seedlings. Unfortunately, no long-term studies of plastid mRNA and protein stability have been reported that could support or refute the possibility that photosynthesis can continue for months without the coding function of ptDNA. Nonetheless, it is generally accepted that the expression of photosynthetic genes in ptDNA is modulated primarily at the post-transcriptional, translational, and post-translational levels by nucleus-encoded factors (Barkan, 2011; Eberhard *et al.*, 2002; Mulo *et al.*, 2012).

5.5 Concluding remarks

Long molecules of ptDNA are found in immature, non-green plastids in stalk tissue of light-grown maize seedlings (Oldenburg and Bendich, 2004a), and the amount of ptDNA decreases 2- to 3-fold to ~100 genome equivalents per plastid in the green leaf blade (Zheng *et al.*, 2011).

Molecular integrity, however, declines to the point at which most ptDNA is present as less-than-genome-sized fragments or ptDNA is no longer recognized in DNA movies or PFGE (Oldenburg and Bendich, 2004a; Oldenburg *et al.*, 2006). Some ptDNA molecules may be fragmented to a size less than that required to encode the function served at an earlier stage of plastid development, even if those ptDNA fragments can be detected by standard qPCR and DAPI-DNA fluorescence. Thus, ptDNA "copy number" can appear similar at different stages of leaf development, even as the contribution of ptDNA to plastid coding function declines.

5.6 Methods

5.6.1 Preparation of maize tissue, cells, and plastids for fluorescence microscopy

Seedlings of maize (*Zea mays*, inbred line B73) were sown in Sunshine mix #4 and grown under 16 hr/8 hr light/dark cycles in a controlled growth room for 9-12 days. Whole seedlings were harvested, washed in 0.5% sarkosyl, and rinsed in distilled H_2O.

For the fixed-then-sectioned tissue shown in Figure 5.5 and Figure 5.4, whole seedlings (11-day) were immediately immersed and fixed in 0.8% glutaraldehyde (v/v) in 0.33 M sorbitol, 20 mM HEPES pH 7.6, 2 mM EDTA, 0.1% bovine serum albumin (BSA) (w/v). Fixation was performed by vacuum infiltration of the whole seedling for about 3 hr, by which time no more air bubbles were observed to surface from the seedling tissue. Fixed tissues not immediately used for imaging were stored at 4°C. Sectioned-then-fixed tissue (Table 5.1) from the first leaf blade of 10-day seedlings was prepared as described (Shaver *et al.*, 2006).

For the protoplasts shown in Figure 5.3, the first leaf blade (unfixed) was digested in PrB#5 (1% cellulysin (w/v), 0.1% macerase (w/v), 0.5 M sorbitol, 10 mM MES pH 5.7, 1 mM $CaCl_2$, 1 mM $MgCl_2$, 0.1% BSA [w/v], 1.4 mM β-mercaptoethanol (βME)) as follows. The leaf tissue was cut into small pieces using a razor blade, placed in PrB#5, vacuum infiltrated for 20 min,

incubated for 2 hr at room temperature with gentle shaking (40 rpm), and then at 80 rpm for 30 min to release protoplasts (all steps performed in the dark). The digestion solution containing the protoplasts was filtered through a 100 µm mesh, centrifuged at 150 x g to pellet the protoplasts, washed twice with PrB#5 (without enzymes), then resuspended, and glutaraldehyde was added to give a final concentration of 0.8% (v/v). The fixed protoplasts were directly prepared for imaging or stored at 4°C.

5.6.2 Fluorescence microscopy

Our general procedures for microscopic imaging have been described in detail previously (Oldenburg and Bendich, 2004a; Rowan and Bendich, 2011; Shaver *et al.*, 2006; Zheng *et al.*, 2011). Some specifics are as follows. For imaging, the samples were stained in 1 µg/mL DAPI with 1% βME (v/v) added to reduce fading. Multiple images were recorded at exposure times from 0.1 to 2 sec with a narrow-band DAPI filter (360ex, 450/50em) and at several focal planes (z-axis, z-stacks). Plastid autofluorescence images were recorded using a G1B filter (546ex, 590em). Although not shown, white light images were also recorded. A 20x or 40x objective was used for tissue sections and 40x or 60x oil emersion objective for protoplasts and isolated plastids.

Digital images were acquired using a QImaging Retiga 1300 camera and OpenLab software. The images shown in the figures were modified to optimize visualization of DAPI-DNA signal in the plastids. Openlab and Adobe Photoshop were used to refine the images by (1) merging multiple images from a z-stack into a single image, (2) subtracting the background fluorescence, and (3) adjusting the brightness and contrast. For the merged z-stack, deconvolution was tested, but did not improve the images produced using Photoshop. In fact, deconvolution created a color change that improved neither image quality nor detection of DAPI-DNA fluorescence (Figure

5.5). The original grayscale images were colorized to show plastids in red for chlorophyll autofluorescence, DAPI staining of DNA in blue-white for plastids and nuclei, and for merging of the two images to show overlap of ptDNA within plastids. An example of some original images and the subsequent steps used to produce the final image is presented in Figure 5.5.

5.6.3 Classification of DAPI-DNA fluorescence in maize plastids

Recorded images were examined visually to classify maize plastids with respect to their DAPI-DNA fluorescence. We report three types of DAPI-DNA signals in Table 5.1. Category 1: plastids with many discrete DAPI-DNA nucleoids; Category 2: a diffuse DAPI signal throughout the plastids and in some, but not all, cases a few discrete nucleoids were also visible; Category 3: plastids with no detectable DAPI-DNA fluorescence. The images of chlorophyll autofluorescence were used to identify plastids and to verify the co-localization of the DAPI-DNA signal. Multiple DAPI-stained images were examined that were recorded at different exposure times of the same field of view for tissue sections, protoplasts, and isolated plastids. For tissue sections and protoplasts, DAPI-stained nuclei were clearly evident, indicating that DAPI entered the fixed cells. For tissue sections, unambiguous identification of individual cells (even after merging of z-stacks) was generally not achieved because cell boundaries are not always visible and there were several layers of cells. A few bundle sheath cells, however, were clearly identifiable on both sides of the autofluorescent vascular tissue (Figure 5.4 L and R). Thus, for the purpose of quantification, a “cell” was assigned to a region containing one or more clusters of plastids and a DAPI-staining nucleus (a few regions without nuclei were also counted). An example is shown in Figure 5.5H, where each “cell region” has been circled. Both the original single focal planes and composite images were examined in order to estimate the number of cells within a tissue section, as well as the presence or absence of DAPI-DNA signal

in plastids. For isolated plastids, the same images used for determination of DNA copy number per plastid (Zheng *et al.*, 2011) were used here for assignment into Category 1, 2, or 3 (Table 5.1) and examples shown in Figure 5.6 with copy numbers given in Table 5.2. The procedures used to quantify genome copy number per plastid from DAPI-DNA fluorescence were described in Zheng et al. (2011).

5.7 Supplemental Materials

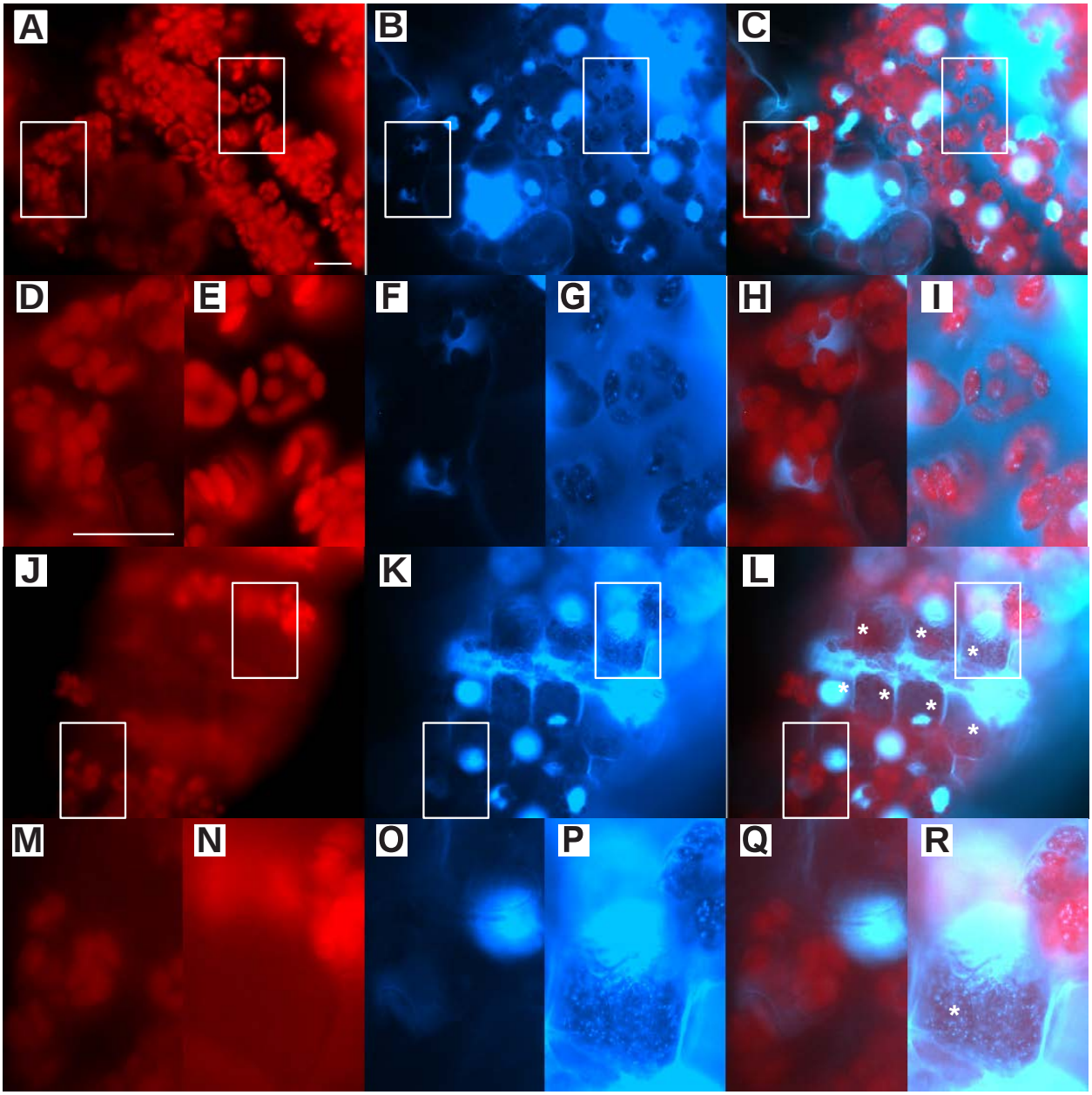

Figure 5.4 Fluorescent microscopy images of tissue sections from the middle of the mature first leaf blade of 11-day maize seedlings.

The left panels show chlorophyll autofluorescence; middle panels show DAPI fluorescence; and right panels are merged images. **D-I** and **M-R** are enlargements of boxed regions in **A-C** and **J-L**, respectively. **F, H, O, Q** show plastids in Category 3 (undetectable DAPI-DNA) and **G, I, P, R** in Category 1 (discrete DAPI-DNA nucleoids). Rectangular-shaped bundle sheath cells are indicated by stars (*) in **L** and **R** and display less chlorophyll auto- fluorescence than mesophyll cells. Scale bar in **A** is 25 µm for **A-C** and **J-L** and in **D** is 25 µm for **D-I** and **M-R**. Images produced as described in Methods.

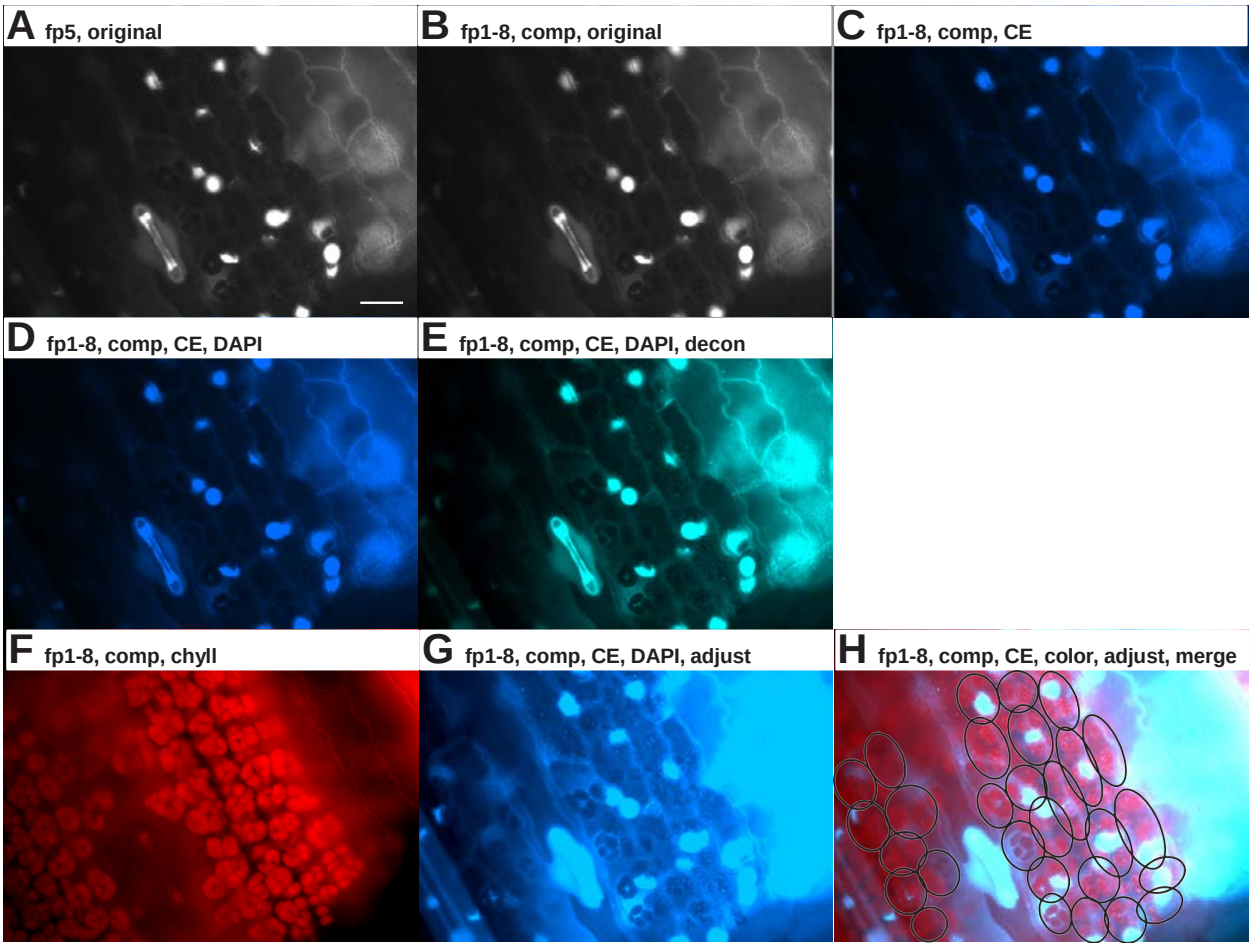

Figure 5.5 Process used to optimize visualization of DAPI-DNA signal in plastids.

A Original DAPI image of a single focal plane (fp5) from the middle of a z-stack consisting of eight focal planes through a tissue section from the first leaf blade of maize. **B** Composite (comp) of the original eight focal planes (fp1-8). **C** Contrast enhancement (CE) to increase visibility of DAPI-DNA in plastids. **D** Colorization to DAPI fluorescence. **E** Deconvolution of image **D**. **F** Composite of eight focal planes and colorization to chlorophyll autofluorescence. **G** Adjustment to enhance visualization of colorized image **D**. **H** Merging of images **F** and **G** to illustrate co-localization of DAPI-DNA and plastids. Each circle indicates one "cell" for the purpose of scoring as described in Methods and given in Table 5.1. Scale bar in **A** is 25 µm for **A-H**.

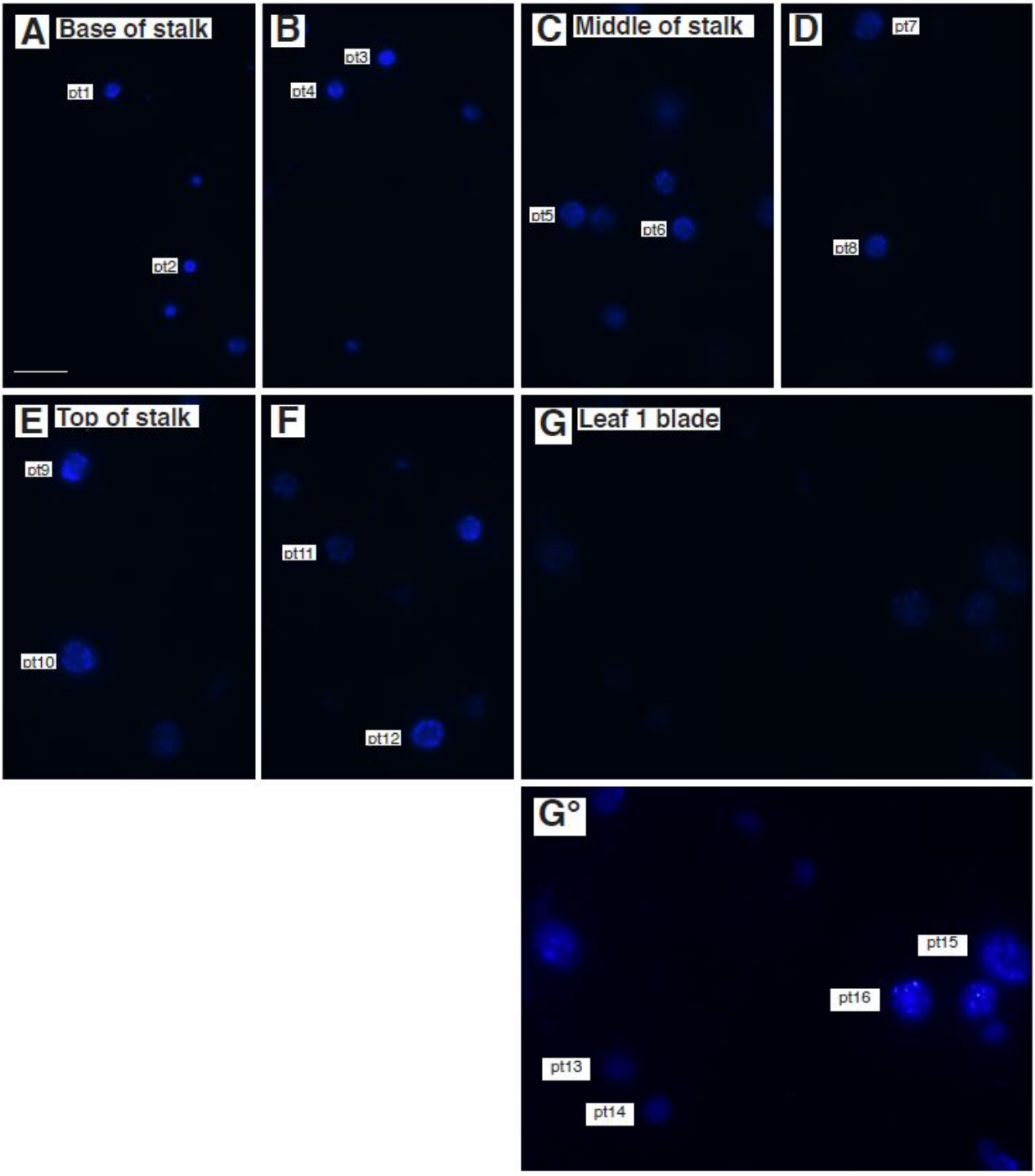
A Base of stalk
pt1
pt2
B
pt3
pt4
C Middle of stalk
pt5
pt6
D
pt7
pt8
E Top of stalk
pt9
pt10
F
pt11
pt12
G Leaf 1 blade
G°
pt15
pt16
pt13
pt14

Figure 5.6 Fluorescent microscopy images of isolated plastids from maize seedlings.

DAPI-DNA fluorescence is shown for individual plastids along the developmental progression from proplastid- to-chloroplast. Proplastids from base of stalk **A-B**; developing plastids from middle **C-D** and top **E-F** of stalk; and mature chloroplasts from the first leaf blade **G-G°**. **A-G** are original images, except that grayscale was changed to DAPI color at 460 nm. Image **G°** was adjusted to increase visibility of the DAPI staining in **G**. The genome copy number for individual plastids pt1-pt16 is given in Table 5.2. These images are examples of those used for the genome copy number determinations shown in Figure 5.1B of Zheng et al. (2011). All images were recorded using 0.5 sec exposure. Scale bar in **A** is 10 μm for **A-G°**.

Chapter 6 (Appendix)

VIRUS-INDUCED GENE SILENCING AS A TOOL FOR COMPARATIVE FUNCTIONAL STUDIES IN *THALICTRUM*

Verónica S. Di Stilio§, Rachana A. Kumar, Alessandra M. Oddone, Theadora R. Tolkin, Patricia Salles and Kacie McCarty.

6.1 Abstract

Perennial woodland herbs in the genus *Thalictrum* exhibit high diversity of floral morphology, including four breeding and two pollination systems. Their phylogenetic position, in the early-diverging eudicots, makes them especially suitable for exploring the evolution of floral traits and the fate of gene paralogs that may have shaped the radiation of the eudicots. A current limitation in evolution of plant development studies is the lack of genetic tools for conducting functional assays in key taxa spanning the angiosperm phylogeny.

We first show that virus-induced gene silencing (VIGS) of a *PHYTOENE DESATURASE* ortholog (*TdPDS*) can be achieved in *Thalictrum dioicum* with an efficiency of 42% and a survival rate of 97%, using tobacco rattle virus (TRV) vectors. The photobleached leaf phenotype of silenced plants significantly correlates with the down-regulation of endogenous *TdPDS* ($P<0.05$), as compared to controls.

Floral silencing of *PDS* was achieved in the faster flowering spring ephemeral *T. thalictroides*. In its close relative, *T. clavatum*, silencing of the floral MADS box gene *AGAMOUS* (*AG*) resulted in strong homeotic conversions of floral organs.

In conclusion, we set forth our optimized protocol for VIGS by vacuum-infiltration of *Thalictrum* seedlings or dormant tubers as a reference for the research community. The three

species reported here span the range of floral morphologies and pollination syndromes present in *Thalictrum*. The evidence presented on floral silencing of orthologs of the marker gene *PDS* and the floral homeotic gene *AG* will enable a comparative approach to the study of the evolution of flower development in this group.

6.2 Introduction

Thalictrum, in the buttercup family Ranunculaceae, comprises approximately 190 species globally distributed in temperate regions (M, 1995). The genus exhibits a range of floral morphologies including four breeding systems and two pollination syndromes (O, 1995). Commonly known as “meadow rues”, these perennial woodland herbs have been actively studied for the medicinal value of their secondary metabolites (Khamidullina *et al.*, 2006; Liscombe *et al.*, 2009; Lutskii *et al.*, 2005). This lineage is ideally suited for the study of the origins of core eudicot diversity because of: (1) Its basal phylogenetic position within the eudicots and (2) The presence of ancestral floral traits, such as free, uniovulate carpels with ascidiate (open) development and variable number of spirally arranged floral organs (Endress, 1995).

A major hurdle in obtaining functional data from emerging model systems like *Thalictrum*, is a lack of transgenic techniques and genomic tools that are readily available for established model plants such as *Arabidopsis thaliana.* A single report of stable transgenesis in *Thalictrum* involves cell culture, with a low efficiency of explant regeneration (Samanani *et al.*, 2002). The advent of virus-induced gene silencing (VIGS) by tobacco rattle virus (TRV) as a laboratory technique (Ratcliff *et al.*, 2001), offered a fast and effective solution to the need for functional data, and promises to bridge the gap between established and emerging model plant systems (Abzhanov *et al.*, 2008; Becker and Lange, 2010).

VIGS was developed as a way of harnessing the RNA-mediated post-transcriptional gene

silencing (PTGS) defense system naturally present in plants and other organisms to fight pathogens (reviewed in (Burch-Smith *et al.*, 2004; Dinesh-Kumar *et al.*, 2003; Robertson, 2004)). The technique relies on the use of viral vectors carrying a transgene that can trigger the PTGS system, causing the degradation of its homolog within the plant. One such viral vector is based on TRV and consists of a binary transformation system, pTRV1 and pTRV2, the latter carrying one or more transgene/s. TRV has been the virus of choice in a variety of plant species due to its minimal pathogenic effects, its wide host range and its ability to cause infection to meristematic tissues, including flowers (Ratcliff *et al.*, 2001).

Initially developed in members of the Solanaceae (Brigneti *et al.*, 2004; Fu *et al.*, 2005; Kumagai *et al.*, 1995, Liu, 2002 #36; Liu *et al.*, 2004; Liu *et al.*, 2002), VIGS has proved useful in several other plants species. For example, in *Petunia* it has been used to help elucidate mechanisms of floral scent production (Spitzer *et al.*, 2007), while in soybean it has facilitated the dissection of the flavonoid biosynthetic pathway (Nagamatsu *et al.*, 2007; Spitzer *et al.*, 2007). The application of such a convenient, fast and cost-effective tool is facilitating more comprehensive comparisons of gene function across diverse plant taxa, including monocots and basal eudicots (Gould and Kramer, 2007; Hileman *et al.*, 2005; Orashakova *et al.*, 2009; Renner *et al.*, 2009; Wang *et al.*, 2010; Wege *et al.*, 2007; Ye *et al.*, 2009).

PHYTOENE DESATURASE (*PDS)* encodes an enzyme that catalyzes an important step in the carotenoid biosynthesis pathway (Cunningham and Gantt, 1998). Silencing of this enzyme blocks the production of carotenoids (umbrella pigments for chlorophyll), causing the photodegradation of chlorophyll and consequently giving plants an easily recognizable photobleached appearance.

Our goal was to generate loss-of function phenotypes in the early-diverging eudicot

Thalictrum, in order to understand gene function and enable a comparative approach. To that end, we first show the successful implementation of VIGS in seedlings of *T. dioicum*, by silencing the ortholog of the *PDS* marker gene, *TdPDS*, in leaves. Subsequently we apply a modified protocol to tubers of two fast-flowering spring ephemeral species and show silencing of *PDS* and an *AG* ortholog in flowers. These three species span the range of floral morphologies present in *Thalictrum*: wind pollinated, inconspicuous flowers with green sepals (*T. dioicum*) and showy, insect pollinated flowers with petaloid sepals (*T. thalictroides*) or petaloid stamens (*T. clavatum*) (Di Stilio *et al.*, 2009).

This approach will be subsequently applied to unravel the functional significance of other genes in these and related species. For example, it will allow to extend the study of previously described gene duplications undergone by critical flower transcription factors, such as the B and C class MADS box genes, to this early-diverging eudicot (Kramer *et al.*, 2003; Kramer *et al.*, 2004).

6.3 Materials and Methods

6.3.1 Plant Materials

Thalictrum dioicum seeds (greenhouse-collected from wild accessions) were imbibed in distilled water for 2 days at 4^0 C, then sown on Turface soil medium (Buffalo Grove, IL) 288-cell trays or in Oasis Wedge system foam medium (Kent, OH) 102-cell trays. Trays with sown seed were stratified for six weeks at 4^0 C covered in plastic to avoid evaporation, then uncovered and transferred to the UW greenhouse (20^0C, 14-16 hr days), where germination was seen within approximately 2 weeks. Seedlings with 2-3 true leaves were used for further experiments. Flowering of *T. dioicum* seedlings typically occurred 6 months after sowing.

T. thalictroides bare root plants were purchased from nurseries and kept at 4^0C in peat moss until infiltration.

T. clavatum plants that had died back were vernalized in a 4^0C room for 8 weeks, the small tubers were then dug up and used in the experiments.

Voucher specimens for the three species in this study are: *T. dioicum,* V. Di Stilio 101 (A); *T. thalictroides* V. Di Stilio 124 (WTU) and *T. clavatum,* V. Di Stilio 127 (WTU).

6.3.2 Cloning of Thalictrum PDS

In order to clone the PDS ortholog, total RNA was isolated from *Thalictrum dioicum* and *T. thalictroides* leaves using TRIzol® Reagent (Invitrogen, Carlsbad, CA), following manufacturer's instructions. Samples were treated with amplification-grade DNaseI (Invitrogen, Carlsbad, CA), followed by First-Strand Synthesis with Oligo (dT) using the SuperScript III® System (Invitrogen, Carlsbad, CA). A 441bp fragment of the *Thalictrum dioicum* ortholog of *PDS (TdPDS)* was amplified by PCR using PDS-F2-XbaI and PDS-R3-BamH1 primers (Gould and Kramer, 2007) and cloned into pCR2.1 using the TA cloning kit (Invitrogen, Carlsbad, CA). Three positive clones were verified by sequencing (Biochemistry DNA Sequencing Facility, University of Washington) and BLAST search (NCBI). In order to design endogenous *TdPDS* specific primers, we cloned a longer fragment of *TdPDS* . To that end we used primers designed to *Aquilegia vulgaris PDS* (GenBank DQ923721, (22)): AqPDS specific F1 5'-AAT GCC AAG CAA GCC AGG AG -3' and AqPDS specific R1 5'-TCA GGG AAG AGT TTC GCA AGC -3', at 53^oC and 30 cycles. The resulting 830 bp partial coding sequence (*TdPDS*, deposited as GenBank FJ457899) was used to design primers outside of the region contained in the silencing construct.

The same approach was applied to isolate the orthologous *PDS* fragment from *T.*

thalictroides (*TtPDS*, deposited as GenBank HM48111), which was similarly used to design RT-PCR locus-specific primers outside of the region used in the silencing construct.

6.3.3 Preparation of the TRV2-TdPDS construct

The *TdPDS* clone was PCR amplified using the forward and reverse primers described above with added restriction sites for cloning: 5'-AGTGGATCCCAGCCGATTTGATTTCCCAGAT-3' (TdPDS_F_BamHI) and 5'-AAGCTCGAGGAGAATTGAGTGGGACTTCACCA-3' (TdPDS_R_XhoI). The resulting amplicon was gel purified using QIAquick Gel Extraction Kit (Qiagen, Valencia, CA). Dr. Dinesh Kumar kindly authorized us to use the TRV1 and TRV2 vector system developed in his laboratory. The TRV2 plasmid and *TdPDS* fragment were digested with BamH1 and Xho1 (New England Biolabs, Ipswich, MA), ligated using T4 DNA ligase (Invitrogen, Carlsbad, CA) and transformed into One Shot® TOP10 Chemically Competent *E. coli* (Invitrogen, Carlsbad, CA). Colonies were selected on LB plates containing 50µg/ml of Kanamycin and the presence of insert was confirmed by PCR with primers spanning the Multiple Cloning Site of pTRV2 (156 F: 5'- TTA CTC AAG GAA GCA CGA TGA GC -3' and 156 R: 5'- GAA CCG TAG TTT AAT GTC TTC GGG -3') (Gould and Kramer, 2007). In the absence of insert, the expected size of the PCR product is 160 bp; in the presence of *TdPDS*, the resulting amplicon size should be 585 bp. TRV2-*TdPDS* plasmid was purified from a single positive colony using FastPlasmid Mini kit (Eppendorf, Hauppauge, NY), then confirmed by sequencing.

6.3.4 Preparation of Thalictrum AG-1 construct:

Since the *TAG-1* locus is highly conserved within *Thalictrum* and even among genera of the Ranunculaceae (Di Stilio *et al.*, 2005), we used a *T. thalictroides* existing construct (TRV2-

TtAG-1) on *T. clavatum*, after checking for sufficient homology between the two to elicit silencing. The complete coding region of *TcAG-1* was cloned (deposited as GenBank HM488113). Since both species share 99% nucleotide identity in the region used for silencing, we will refer to this construct as TRV2-*TAG*-1 (for *Thalictrum AG-1*). To prepare the silencing construct, flower bud cDNA of *T. thalictroides* was used as template in PCR with *AG-1* specific primers and added XbaI and BamHI restriction sites: TthAG1_fwd_xba1 (5' AGG TCT AGA GCA ATG ATC GCT GCA AAC GAG 3') and TthAG1_rev_BamHI (5' AAT GGA TCC CAG ACA AAA TGC CAA GTC CCT C 3'). A PCR product of approximately 500 bp was excised from the agarose gel, and extracted using QiaQuick gel extraction kit (Qiagen, Valencia, CA). The resulting DNA was digested with XbaI/BamHI restriction enzymes (New England Biolabs, Ipswich, MA) to create sticky ends and ligated into a similarly digested TRV2 vector, yielding the TRV2-*TtAG-1* construct. The identity of the insert was confirmed by sequencing.

6.3.5 Transformation of Agrobacteria with TRV constructs

Electrocompetent Agrobacteria GV3101 were prepared as described elsewhere (Weigel, 2002) and transformed with 2 µl of pTRV2-*TdPDS*, pTRV2-*TAG*-1, pTRV2 (empty) or pTRV1. Electroporation was carried out at 2.4 Kv for 5 ms on a MicroPulser Electroporator (Bio-Rad Laboratories, Hercules, CA). Cells were selected on LB plates containing 50µg/ml Kanamycin, 25µg/ml Rifampicin and 50µg/ml Gentamycin. Colonies were confirmed by PCR as explained above, sequenced and stored as glycerol stocks at -80°C.

6.3.6 Infiltration of T. dioicum seedlings

In order to achieve suppression of expression of *TdPDS*, a total of 117 *T. dioicum* seedlings at the 2-3-leaf stage across 3 independent experiments were infiltrated with *Agrobacterium*

containing pTRV1 and pTRV2-*TdPDS*. A negative control (or mock treatment) consisted of infiltrating 50 seedlings with a mixture of pTRV1 and empty pTRV2 to test for background viral effects; another group of 5 seedlings was left untreated and grown under the same conditions.

Agrobacteria were prepared for infiltration following (Gould and Kramer, 2007), with modifications. Starter overnight LB cultures (5 ml) of pTRV1, pTRV2-*TdPDS* and empty pTRV2 were grown overnight with selective antibiotics and used subsequently to inoculate 50ml and 500ml cultures. 1M MES (2-(4-Morpholino)-Ethane Sulfonic Acid) and 0.1M Acetosyringone (3',5' -Dimethoxy-4'-hydroxyacetophenone) were added to the final cultures. These were grown to an OD_{600} of 2.0, then centrifuged at 4,000 g for 15 min at 4°C. Cells were resuspended in infiltration medium (10 mM MES, 20 μM acetosyringone, and 10 mM $MgCl_2$) to a final OD_{600} of 2.0 and incubated for 3 hrs at room temperature. Cultures of pTRV1 were mixed in a 1:1 ratio in a 2-liter plastic container with either pTRV2-*TdPDS* (silencing treatment) or empty TRV2 cultures (mock control), adding 100ul/l Silwet L-77 (Lehle Seeds, Round Rock, TX) as a surfactant. Seedlings were removed from Turface or foam medium, roots were rinsed in distilled water and whole seedlings were submerged in infiltration medium containing either pTRV1 mixed with pTRV2- *TdPDS* or TRV1 mixed with empty TRV2 (mock control). A -100 kPa vacuum was applied in a chamber for 2 minutes. Following infiltration, seedlings were potted in soil and grown in the greenhouse. Photobleaching of leaves, detectable two weeks after infiltration, was scored for up to 4 months following inoculation. Photobleached, variegated and green leaves were collected starting at 3 weeks post infiltration, flash-frozen in liquid nitrogen and stored at -80°C until processing.

In order to record photobleached phenotypes, plants were photographed using a hand held digital camera and a dissecting microscope (Nikon SMZ800, Nikon Instruments Inc.**,** Melville,

NY) equipped with a QImaging MicroPublisher 3.3 RTV digital camera (Surrey, BC, Canada). Images were processed in Adobe® Photoshop® CS2 v 9.0.2 and figures were assembled using Adobe® Illustrator®CS2 v. 12.0.1.

6.3.7 Infiltration of T. thalictroides and T. clavatum dormant plants

Dormant underground tubers of *T. thalictroides* and *T. clavatum* were cleaned of soil, then kept in the dark covered in wet paper towels until infiltration media were ready. The small tubers were wounded lightly before infiltration using a clean razor blade to facilitate the entrance of *Agrobacteria* carrying the TRV plasmids. Vacuum infiltration was carried out as above, except the infiltration time was longer: 10 min for *T. thalictroides* and 5 minutes for *T. clavatum* (smaller tubers).

Given the high conservation of the *PDS* locus, silencing constructs can be used successfully across species. Therefore, *T. thalictroides* plants were treated with the available *T. dioicum PDS* construct, TRV2-*TdPDS*, which is 99% identical at the nucleotide level over the silencing fragment. Similarly, *T. clavatum* was treated with a *T. thalictroides AG-1* construct (99 % identical, see details above). For simplicity, these constructs are referred to as TRV2-*TPDS* and TRV2-*TAG-1* throughout the text. Mock-treated controls were infiltrated identically, except the TRV2 vector did not contain an insert. Untreated plants were given identical treatment, but without infiltration.

After infiltration, tubers where potted in 2.5” Deepots™ (Stuewe & sons, Tangent, OR) using Sunshine Mix #4 soil (Sun Gro, Bellevue, WA) without watering and transferred to the UW greenhouses (20^0C, 14-16 hrs light), where they flowered in less than 2 weeks *(T. thalictroides*) to 3 weeks (*T. clavatum*). Pots were covered with plastic for 24 hours, then uncovered and watered twice a week for the duration of flowering.

Plants were monitored daily throughout the flowering period. Once flowers started to show homeotically converted organs, they were collected and flash frozen in liquid nitrogen for later analysis. Flowers from mock-treated and untreated plants were collected similarly to use as controls.

6.3.8 Semi-quantitative analyses by RT-PCR

Total RNA was extracted from frozen leaves as described above. First strand synthesis was carried out using the pTRV1 specific primer OYL 198 (5'- GTA AAA TCA TTG ATA ACA ACA CAG ACA AAC -3') (Hileman *et al.*, 2005), pTRV2 specific primer 156 R (Gould and Kramer, 2007), or Oligo (dT). A set of reactions without Reverse Transcriptase was used to control for presence of genomic DNA. Reverse transcriptase (RT)-PCR was performed for 25 cycles using pTRV1 specific primers OYL195 (5'- CTT GAA GAA GAA GAC TTT CGA AGT CTC -3') and OYL198 (Hileman *et al.*, 2005), 51^{o}C anneal ; TRV2 specific primers 156 F and 156 R (Gould and Kramer, 2007), 51^{o}C anneal; and *Thalictrum ACTIN* specific primers TthActin for 2 (5'-GCAGAACGGGAAATTGTCCGC-3' and TthActin rev 2 (5'-CCTGCAGCTTCCATTCCGATCA-3'), 58^{o}C anneal; or endogenous *TdPDS* specific primers TdPDS_F_RT (5'-TGA ATA ATG ATG GAA CCG TG-3') and TdPDS_R_RT (5'-GTC AGC ATA CAC ACT CAA AAG G-3'), 50^{o}C anneal.

RT-PCR products were run on a 1.2% agarose gel. For the *T. dioicum* experiment, *TdPDS* band intensity was quantified using ImageJ (NIH), normalized against *TdACTIN* controls. The statistical significance of the difference in normalized *TdPDS* expression among treatments was tested by one-tailed ANOVA followed by Tuckey test in JMP (statistical discovery software, Cary, NC).

Untreated, mock treated and photobleached leaf and floral tissue of *T. thalictroides* was

collected, processed for cDNA and assessed for gene expression as explained above, except the forward *PDS* primer used to detect expression in cDNA was adjusted to be species-specific: *TthPDS*_F_RT (5'- TGA ACA ACG ATG GAA CCG TG-3'), and 32 cycles (at 53^{o}C) were run on floral tissue due to lower levels of PDS compared to leaves.

Silenced flowers of TRV2-*TthAG-1* treated *T. clavatum* plants that showed homeotic conversions were similarly collected, processed and compared to controls (untreated and empty TRV2). *Thalictrum AG-1* specific primers TthAG1_fwd_qPCR (5'-AGTCTCTCAGCAATCTCAATATCAGGG-3') and TthAG1_rev_qPCR (5'-GCCCTGAGATACTTGTTATCAGRTCTGC-3') for 23 cycles at 53°C, were used to determine *TcAG-1* expression levels. Previously designed *PDS* and *ACTIN* primers for *T. thalictroides* were used on *T.clavatum*, due to high sequence similarity between the two closely related species.

6.4 Results

6.4.1 Silencing of PDS in leaves of T. dioicum

Our initial goal was to test whether the VIGS approach would be successful in our study system. To that end we set out to silence the ortholog of *PHYTOENE DESATURASE*, commonly used as a marker due to the easy-to-score resulting photobleached phenotype.

The overall survival rate of treated and mock-treated plants was 97%, indicating that *Thalictrum dioicum* seedlings are hardy and resilient to vacuum infiltration. Initiation of photobleaching in TRV2-*TdPDS* treated plants was observed approximately 2 weeks post-infiltration; after 2 months 42% of treated plants showed some degree of *TdPDS* silencing. Twelve percent of treated plants showed strong silencing, where a whole compound leaf, including the petiole, was photobleached, as compared to untreated plants (compare Figure 6.1A

to B-E). Intermediate phenotypes included scattered sectors of white throughout the plant (Figure 6.1F), and milder ones exhibited photobleaching restricted to the vasculature of leaflets (Figure 6.1G). Photobleached leaves often looked pink, due to the natural presence of anthocyanins, which were exposed by the photo-degradation of chlorophyll (Figure 6.1B, H and I, first two leaflets). Overall, there was a gradient of silencing phenotypes at the leaflet level (Figure 6.1I). The duration of silencing varied from six to eight weeks from onset, with a few outliers in which silencing continued for up to three months. Photobleached tissue was more vulnerable and typically died off over time, causing an overall apparent decline of silencing over time. Mock-treated plants were undistinguishable from untreated plants (not shown), suggesting no visible viral effects in this species at the vegetative level.

In order to confirm that the leaf photobleached phenotypes described above correlated with reduced endogenous levels of *TdPDS*, we performed Reverse Transcriptase (RT) PCR with locus-specific primers on leaf tissues from each of the three treatment groups (Figure 6.2). Amplification of the *ACTIN* ortholog, *TdACTIN* was used as a template concentration control (Figure 6.2A, top gel). To test if the phenotype observed in treated plants was due to the presence of the viral vectors, the presence of TRV1 and TRV2 transcripts in cDNA was also determined by RT-PCR (Figure 6.2A, bottom 2 gels). Samples from the untreated group did not show viral expression and had high expression of *TdPDS*, as expected. Half of the mock-treated plants shown in Figure 6.2 had both vectors, consistent with the 42% observed incidence of photobleaching in the TRV2-*TdPDS* treatment. RT-PCR performed with TRV2-specific primers spanning the multiple cloning site produced a smaller product size (160 bp) in two of the mock-treated plants, corresponding to the distance between primers in the absence of insert, therefore confirming the presence of TRV2 and the absence of the *TdPDS* transgene fragment (Figure

6.2A, smaller bands in TRV2 panel). The same two plants also amplified TRV1 transcript. Expression of *TdPDS* in this treatment group was similar to that of untreated plants, suggesting that the viral treatment does not interfere with *TdPDS* expression. We further subdivided the pTRV2-*TdPDS* treatment into three categories based on silencing phenotype intensity: green (from partially silenced plants), variegated (green leaflets with white silenced sectors) and completely photobleached tissues (white leaflets). All of the TRV2-*TdPDS* treated photobleached plants showed presence of transcript from both vectors. Detection of the *TdPDS* transgene in pTRV2 is indicated by the larger PCR product size (Figure 6.2A , 585 bp band in TRV2 panel).

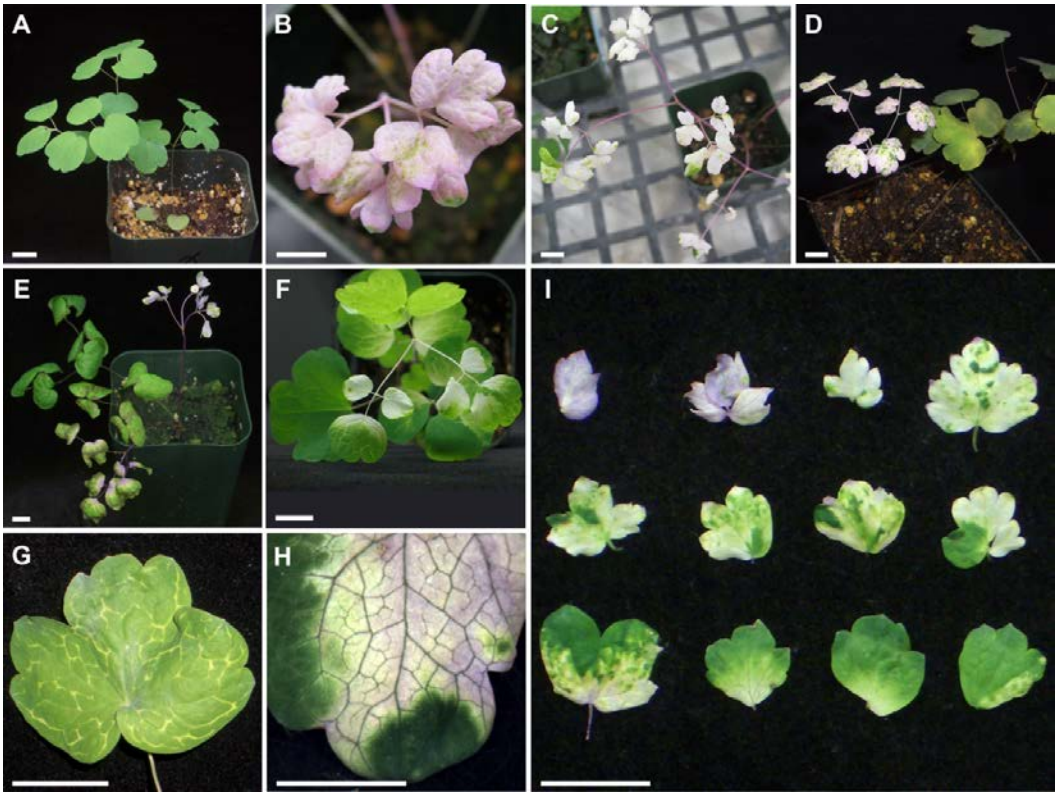

Figure 6.1 VIGS of *Thalictrum dioicum* PHYTOENE DESATURASE ortholog TdPDS results in varying degrees of leaf photobleaching.

A: Untreated *T. dioicum* plant. B-F: Distribution of photobleaching in TRV2-*TdPDS* treated plants. G: Leaflet showing signs of silencing along the vascular tissue. H: Detail of partially photobleached leaflet. I: Typical range of silencing in TRV2-*TdPDS* treated leaflets. Scale bar = 1cm.

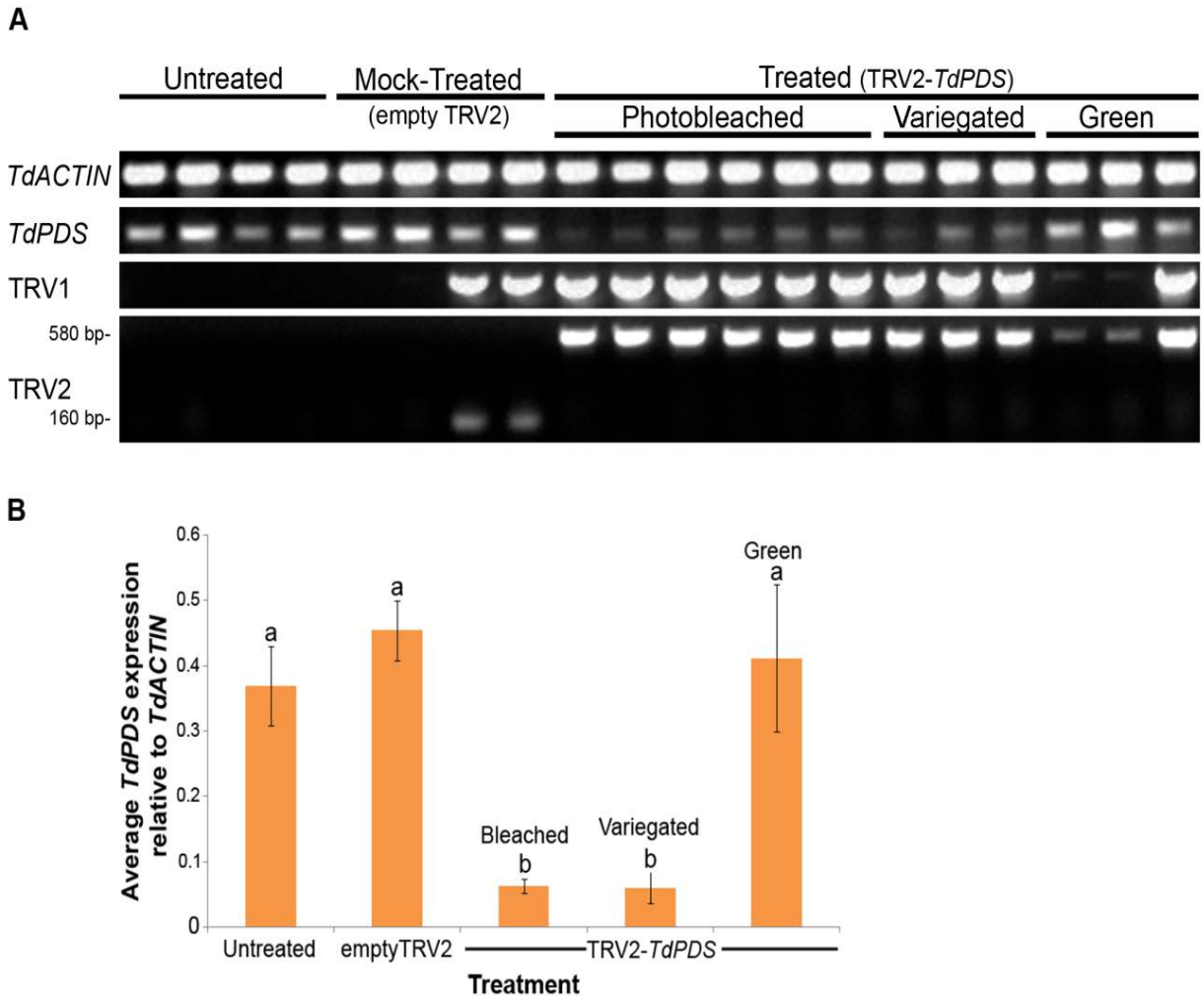

Figure 6.2 Downregulation of *TdPDS* and detection of TRV transcripts in VIGS photobleached leaves of *Thalictrum dioicum*.

A: Expression of TdACTIN control, native TdPDS and viral transcripts in leaves by Reverse Transcriptase (RT)-PCR.

Untreated and mock-treated (empty TRV2) T. dioicum plants are compared to TRV2-TdPDS treated plants showing photobleached (white), variegated (green/white) and green leaf tissue. RT-PCR was performed with locus-specific primers to the housekeeping gene ACTIN (loading control), to endogenous TdPDS and to the viral transcripts TRV1/TRV2. Approximate band size indicated for TRV2: larger band results from the presence of the TdPDS insert, smaller band from an empty TRV2 (mock control).

B: Comparative expression of TdPDS normalized with TdACTIN among treatments and resulting phenotypes of *Thalictrum dioicum*.

Values based on quantification of RT-PCR gel bands in part A using ImageJ (see text for details). Different letters indicate statistical significance in a one-way ANOVA followed by Tuckey test ($p<0.05$), same letters indicate no statistical difference. Average and standard error bars are shown. Sample sizes are n=4 for untreated and mock-treated, n=6 for treated bleached and n=3 for treated variegated or green.

Quantification of band intensity (from the RT-PCR gels in Figure 6.2A) confirmed a statistically significant down-regulation of *TdPDS* (relative to *ACTIN*) in fully photobleached and variegated leaf samples compared to untreated and mock-treated controls and treated-green leaves ($p<0.05$, denoted by different letters on top of the bars in Figure 6.2B). The decrease in levels of endogenous *TdPDS* in bleached and variegated leaves was not statistically significant at the resolution allowed by RT-PCR (equal letters above bars in Figure 6.2B), a more quantitative expression method may be needed to detect these more subtle differences. For our purposes, variegated leaves may be considered as silenced. Green leaves from plants that had shown silencing in other leaf tissue had endogenous *TdPDS* levels undistinguishable from the untreated or mock-treated plants, indicating that treated plants are chimeras of silenced and non-silenced tissue for *TdPDS*.

Since silencing lasts for 2-3 months, it became apparent that the time to flowering in seedlings of *T. dioicum* is typically greater (4-6 months) than the duration of our silencing phenotypes. To implement VIGS to the study of flower development we extended the silencing assays to include faster flowering species within the genus.

6.5 Floral silencing in fast-flowering spring ephemerals

6.5.1 PDS silencing in T. thalictroides:

In order to achieve floral silencing, we infiltrated dormant, bare-root plants of the spring ephemeral hermaphrodite *T. thalictroides* (Figure 6.3Ai). In this species, flowers develop from a fleshy root (a small tuber) simultaneously with leaves in the second year. Therefore, photobleaching due to *PDS* silencing can be rapidly detected (less than 2 weeks, and as little as 4 days) not only in leaves (Figure 6.3Aii, Aiii detail), but also in photosynthetic carpels and young

stamens (compare Figure 6.3Aiv-Av).

Survival in this experiment was only 25% (5 out of 20 treated plants), presumably due to the plants being young; the small tender tubers did not respond well to wounding and longer infiltration time. Age at infiltration was especially critical for bleached plants; in the absence of green photosynthetic leaves, the young tubers did not have enough stored metabolites to sustain them and the plants died. Only 2 bleached plants survived, and one flowered. Subsequently, we have experimented with older plants, with significantly increased survival rates. All mock-treated plants survived, and approximately two thirds flowered (10/15); of these, most (8/10) showed varying degrees of necrosis (black spots) and reduced sepal size (Figure 6.3Avi). These phenotypes were interpreted as background viral effect, and discounted from further analyses of floral silencing.

Detection of TRV1 and TRV2 transcripts in cDNA provided evidence that silencing was due to the viral treatment (Figure 6.3B). Downregulation of *TtPDS* was most marked in photobleached leaves, where expression was not even detectable by RT-PCR (Figure 6.3B left panels*). TtPDS* downregulation was less pronounced in flowers, where the bulk of the tissue (petaloid sepals) is white (Figure 6.3B, right panels).

6.5.2 Silencing of an ortholog of the floral MADS box gene AGAMOUS in Thalictrum clavatum

T. clavatum is a close relative of *T thalictroides* representing a different type of flower morphology, with smaller pink/white petaloid sepals that fall off in mature flowers and prominent stamens with flattened, petaloid filaments (compare Figs. 3Ai and 4Ai). This species was treated with a TRV2-*ThtAG-1* single construct, to silence the ortholog of the *Arabidopsis* floral MADS box gene *AGAMOUS*, described earlier (Kramer *et al.*, 2004). Silenced flowers

showed homeotic conversion of stamens and carpels to petaloid sepals (Figure 6.4A, the entire genus *Thalictrum* lacks petals), as described for *ag* loss of function mutants in *Arabidopsis* (Bowman *et al.*, 1991). Untreated flowers consist of 4-6 white sepals, 26-39 stamens with flattened petaloid filaments and 5-9 stalked carpels (flower counts based on 15 flowers from 5 plants) (Figure 6.4Ai, Aiv). No viral effects were detected in the TRV2 empty controls for this species. Two of the treated plants showed strong phenotypes (Figure 6.4Aii) in 9 and 15 flowers respectively, consisting of complete conversion of reproductive organs (stamens and carpels) into sterile organs (sepals) of different size and shape (different degrees of narrowing at the base); no effects were evident in sepals (Figure 6.4Av). Intermediate phenotypes were also observed in 3-4 flowers per plant (Figure 6.4Aiii), consisting of partially converted organs, including sepaloid organs with anther tissue (Figure 6.4Avi, arrows) and staminoid organs with unusually expanded filaments, becoming reduced in size towards the center of the flower (Figure 6.4Avi). While intermediate organs with staminoid features were common, none of the silenced flowers had carpels. Silenced flowers had immature organs that continued to develop in the center throughout the life of the flower; consistent with the role of *AG* in flower determinacy in *Arabidopsis* (Bowman *et al.*, 1991).

Phenotypes were validated at the molecular level: all untreated and mock-treated plants tested had higher expression of *TcAG-1* than treated plants, as shown by RT-PCR on individual flowers, relative to *ACTIN* (Figure 6.4B). TRV transcripts were present in treated-silenced and one of the two mock treated flowers shown (like in the other species, infiltration efficiency is not 100%) and absent from untreated flowers, as expected (Figure 6.4B). Larger bands in TRV2 (580 bp) correspond to the presence of the *TAG-1* insert in treated plants, whereas smaller bands (160 bp) correspond to an empty TRV2 in the mock controls (as explained for Figs. 2A and 3B;

all inserts are approximately 400 bp).

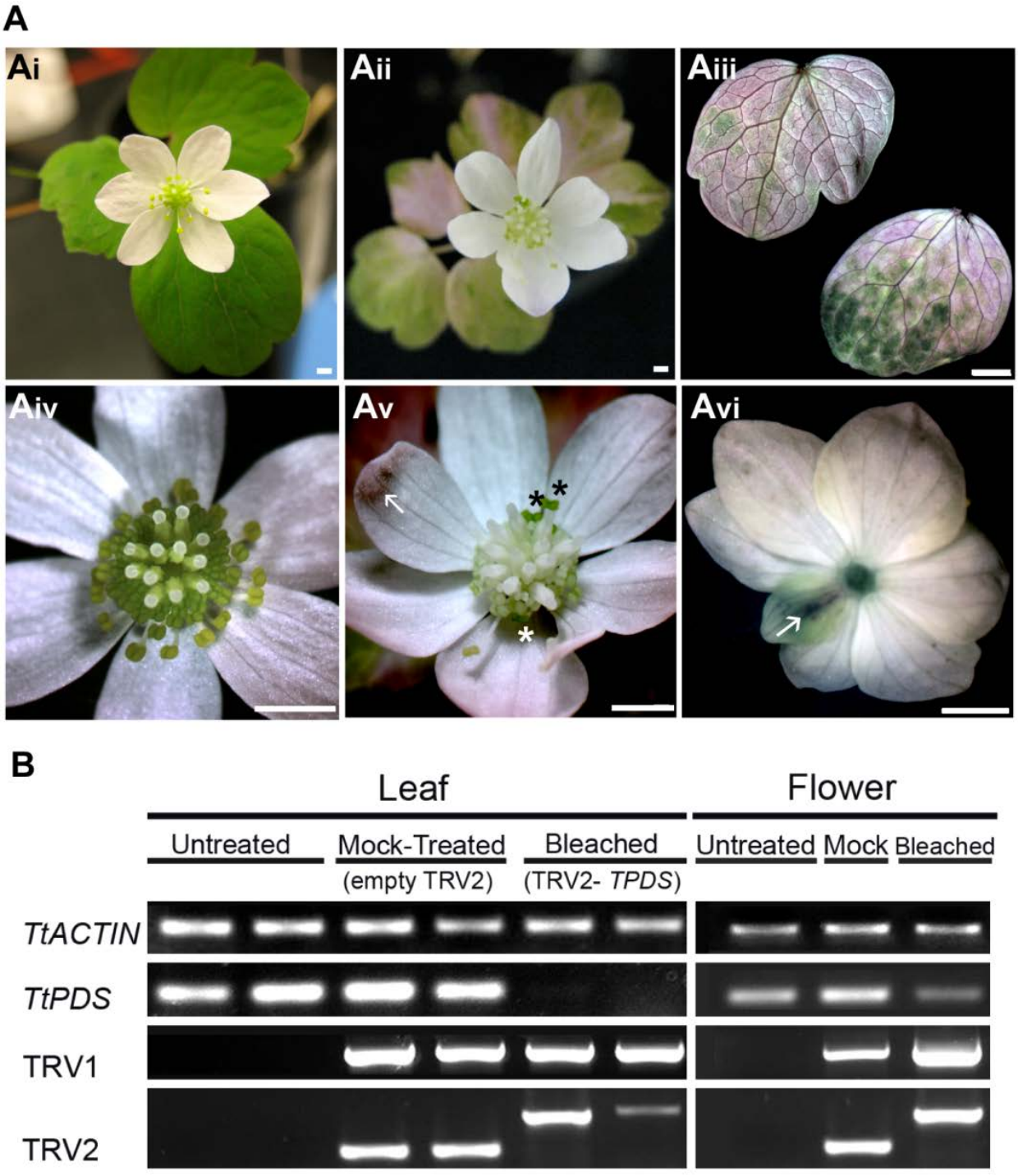

Figure 6.3 Virus-induced gene silencing of *TtPDS* causes photobleaching in leaves and flowers of *Thalictrum thalictroides*.

A: Flower and leaf *TtPDS* silencing phenotypes compared to controls.
Ai: Untreated flower of *T. thalictroides*, note green leaflets and green/yellow floral center; Aii: TRV2-*TPDS* treated plant, showing partial photobleaching of leaflets that appear variegated; Aiii: Detail of varying degrees of photobleaching in leaflets; Aiv: Detail of untreated flower, note that carpels and young stamens are normally photosynthetic (green); Av: Detail of treated flower showing silencing in stamens and carpels, three older stamens are not photobleached and therefore look green (asterisks), a patch of necrotic tissue (a viral effect) is indicated with an arrow; Avi: empty TRV2 mock-control flower showing background viral effects: arrow points to reduced sepal with patch of necrotic tissue. Scale bar = 1 mm.
B: Comparative expression of *TtPDS* in leaves and flowers of *T. thalictroides* plants treated with TRV2-*TPDS*, relative to controls.
Untreated and mock-treated (empty TRV2) plants are compared to TRV2-*TPDS* treated plants showing photobleached leaves (left panels) or flowers (right panels). Reverse-transcriptase PCR was performed with locus-specific primers to the housekeeping gene *TtACTIN* (loading control), to endogenous *TtPDS* and to the viral transcripts TRV1/TRV2. For TRV2: larger band results from the presence of insert, smaller band from an empty TRV2 (mock control).

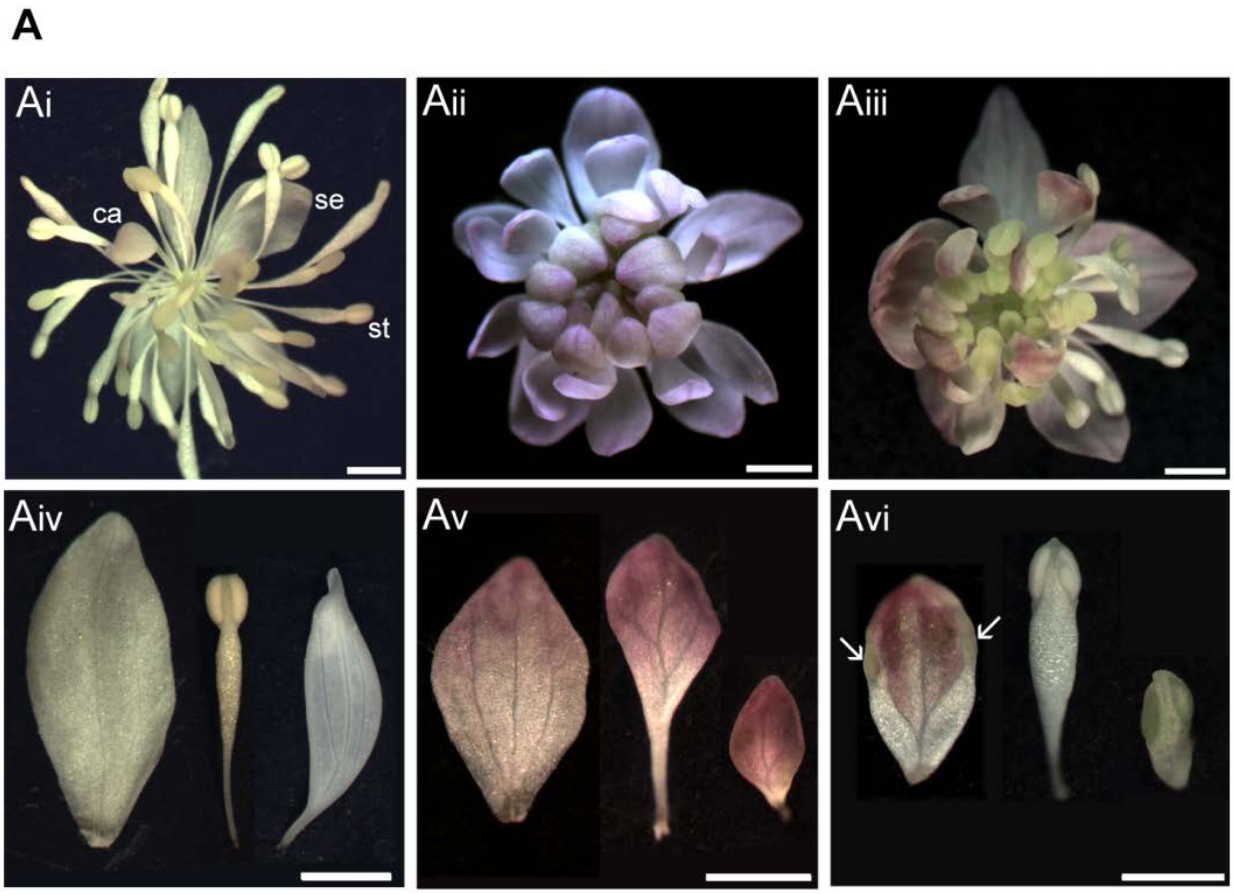
A
Ai
ca
se
st
Aii
Aiii
Aiv
Av
Avi

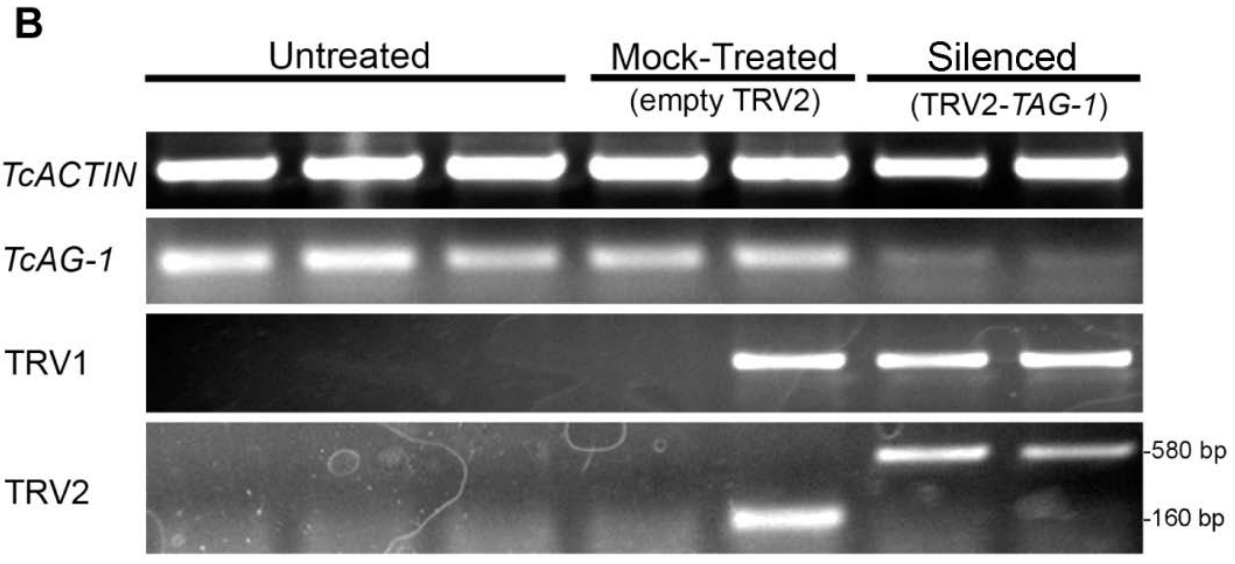
B
Untreated
Mock-Treated
(empty TRV2)
Silenced
(TRV2-TAG-1)
TcACTIN
TcAG-1
TRV1
TRV2
580 bp
160 bp

Figure 6.4 Virus-Induced Gene Silencing of *Thalictrum clavatum AGAMOUS* ortholog *TcAG-1* results in homeotic floral phenotypes.

A: Flower silencing phenotypes of *TcAG-1*, relative to controls.
Ai, Untreated flower of *T. clavatum* showing sepals (se), stamens (st) and carpels (ca); Aii: strongly silenced flower in TRV2-*TAG-1* treated plant, showing an array of sepals and no stamens nor carpels, all reproductive organs have been homeotically converted to sepals; Aiii: intermediate phenotype with partial conversion of organs and some normal ones; Aiv: detail of dissected organs in an untreated flower (sepal, stamen, carpel, from left to right); Av: detail of all sepaloid dissected organs from a strong *TcAG-1* silencing phenotype (from the outside to the inside of the flower, left to right); Avi: detail of sample chimeric organs, arrows point to anther tissue on the edges of an internal "sepal". Scale bar= 1 mm.
B: Gene expression by Reverse Transcriptase (RT)-PCR in *TcAG-1* silenced plants compared to controls. Untreated and mock-treated (empty TRV2) plants are compared to TRV2-*TAG-1* treated plants showing strong homeotic conversions (Aii, Av). RT-PCR was performed with locus-specific primers to the housekeeping gene *ACTIN* (loading control); to the MADS box gene *TcAG-1* and to the viral transcripts TRV1/TRV2. For TRV2: larger bands result from the presence of insert, the smaller band from an empty TRV2 (mock control).

6.6 Discussion

Thalictrum is one of the most species-rich genera in the family Ranunculaceae and has a key phylogenetic place at the base of the eudicots, which represent a smaller radiation nested within the major angiosperm radiation (Soltis and Soltis, 2004). This basal position, combined with the retention of ancestral floral features, provides a window into past scenarios of flower evolution. It is this particular combination of key phylogenetic position and floral diversity that makes *Thalictrum* a promising model plant lineage for evo-devo studies (Di Stilio *et al.*, 2005).

Recently, VIGS has been employed in a variety of plant systems as a reverse genetics approach (Galun, 2005). It is becoming a powerful tool in the area of evolution of plant development, allowing for functional studies of floral transcription factors across the angiosperm phylogeny, including early-diverging eudicots (Kramer *et al.*, 2007; Orashakova *et al.*, 2009). Our demonstration that VIGS can be implemented efficiently to silence a carotenoid pathway gene, as well as a floral transcription factor in three species of *Thalictrum*, provides proof of the value of this type of approach in evolutionary studies involving early-diverging eudicots.

The successful implementation of VIGS in leaves and flowers of *Thalictrum* species is a major step towards investigating gene function in this emerging model plant genus. Its amenability to vacuum infiltration of seedlings or dormant plants underscores the versatility of these herbaceous perennials. Post-treatment survival rates for *T. dioicum* seedlings were amongst the highest observed for this infiltration method (97%), comparable to those reported previously in *Papaver* (Hileman *et al.*, 2005) and higher than those in the closely related *Aquilegia* (Gould and Kramer, 2007). Further, we observed a higher percentage of the plants showing photobleaching at 42% compared with 12% and 23% in the above studies.

Implementation of VIGS in *Thalictrum* broadens the already wide host range of tobacco

rattle virus and further supports the use of VIGS in other, lesser known plant systems for which stable transgenic techniques are not yet available.

Moreover, *T. dioicum* is the only dioecious species emerging so far as a model system among basal eudicots (Di Stilio *et al.*, 2005). Comparative functional analyses within this genus, amongst hermaphroditic (*T. thalictroides* and *T. clavatum)* and dioecious species (*T. dioicum*), will facilitate studies of the genetic basis for the evolution of sexual dimorphism.

Most importantly, the use of VIGS has allowed us to carry out functional analyses within *Thalictrum* rather than relying on transformation into established model systems, with its inherent limitation to biochemically rather than physiologically informative results. A heterologous approach also deters the investigation of subtle functional differences amongst duplicated genes present in *Thalictrum* and widespread in the Ranunculaceae (Kramer *et al.*, 2003; Kramer *et al.*, 2004), due to the lack of a suitable molecular environment. The above limitations are widespread and would ultimately prevent a thorough investigation of the origin and evolution of key regulators of development that may have shaped the evolution of angiosperms using different pathways such as sub or neo-functionalization (Theissen *et al.*, 2000).

Certain species of *Thalictrum* are economically significant in the pharmacological (Khamidullina *et al.*, 2006) and horticultural industries (Hinkley, 2006). The development of this technique will facilitate the study of gene function of clinically relevant secondary metabolite biosynthesis in *Thalictrum.* Many species of *Thalictrum*, including the two hermaphrodites in this study, are sold as ornamentals. This study enables the exploration of the genetic basis of existing varieties and the creation of new, showier ones (such as the “double” flowers resulting from *AG* silencing, Figure 6.4Aii), a desirable goal for the floriculture industry.

In conclusion, we have shown that VIGS is an effective tool to assess gene function in three species of *Thalictrum*, resulting in leaf and floral phenotypes. Silencing of the floral MADS box gene *TAG-1* caused homeotic conversions of stamens and carpels into sepals, as predicted by the ABC model (Bowman *et al.*, 1991); silencing of *TPDS* produced the expected photobleached phenotype in leaves and flowers. The *Thalictrum* ortholog of *PDS* is a useful vegetative marker to quickly identify plants that are undergoing silencing, mainly in green leaves and additionally in species with green flowers (most of the wind-pollinated taxa), or green floral parts during early development (*T. thalictroides* and *T. clavatum*). Photobleaching can, however, be detrimental to plant growth and survival, especially in young plants. Therefore, the use of a marker gene in double constructs must be considered carefully, and may not be justified in cases where there is an expectation for a well-defined phenotype. With these caveats, high survival rates in seedlings and potentially improved ones on older tubers, combined with high infiltration efficiency and silencing rates, make VIGS promising for functional studies in these and related species.

With the prospect of a full-length transcriptome for *T. thalictroides* through the 1KP project (Univ. of Alberta, Canada), the ability to test genes or whole gene families by VIGS in this genus is especially timely (Becker and Lange, 2010). In order to build a toolbox for an emerging model system, it is indispensable to have a mechanism to assess gene function (Abzhanov *et al.*, 2008). Here, we have successfully adapted a tool for functional studies, which is rapid, relatively simple to implement and shows high promise for a comparative functional approach in *Thalictrum* and beyond.

6.7 Acknowledgments

We thank Dr. Dinesh-Kumar for allowing us to use the TRV vectors developed in his lab,

and Dr. Elena Kramer and Billie Gould for assistance with protocols and training. We would also like to thank Doug Ewing and the UW Botany Greenhouse staff, as well as student assistant George Abeyta for caring for the experimental plants. Student assistants Parisa Aalami-Monelli and Caitlin Connelly contributed to the cloning of *TdPDS*; Anjelique Schulfer sequenced *TtPDS*. Dr. Aaron Liston was consulted for botanical terminology.

BIBLIOGRAPHY

Abzhanov A, Extavour CG, Groover A, Hodges SA, Hoekstra HE, Kramer EM, Monteiro A. 2008. Are we there yet? Tracking the development of new model systems. *Trends Genet* **24**, 353-360.

Arimura S, Yamamoto J, Aida GP, Nakazono M, Tsutsumi N. 2004. Frequent fusion and fission of plant mitochondria with unequal nucleoid distribution. *Proc Natl Acad Sci U S A* **101**, 7805-7808.

Arthofer W, Schuler S, Steiner FM, Schlick-Steiner BC. 2010. Chloroplast DNA-based studies in molecular ecology may be compromised by nuclear-encoded plastid sequence. *Molecular Ecology* **19**, 3853-3856.

Ayliffe MA, Scott NS, Timmis JN. 1998. Analysis of plastid DNA-like sequences within the nuclear genomes of higher plants. *Mol Biol Evol* **15**, 738-745.

Backert S, Börner T. 2000. Phage T4-like intermediates of DNA replication and recombination in the mitochondria of the higher plant *Chenopodium album* (L.). *Curr Genet* **37**, 304-314.

Backert S, Dörfel P, Börner T. 1995. Investigation of plant organellar DNAs by pulsed-field gel electrophoresis. *Curr Genet* **28**, 390-399.

Backert S, Lurz R, Borner T. 1996. Electron microscopic investigation of mitochondrial DNA from Chenopodium album (L.). *Curr Genet* **29**, 427-436.

Backert S, Lurz R, Oyarzabal OA, Börner T. 1997. High content, size and distribution of single-stranded DNA in the mitochondria of *Chenopodium album* (L.). *Plant Mol Biol* **33**, 1037-1050.

Balk J, Chew SK, Leaver CJ, McCabe PF. 2003. The intermembrane space of plant mitochondria contains a DNase activity that may be involved in programmed cell death. *Plant J* **34**, 573-583.

Balk J, Pilon M. 2011. Ancient and essential: the assembly of iron-sulfur clusters in plants. *Trends Plant Sci* **16**, 218-226.

Barkan A. 2011. Expression of plastid genes: organelle-specific elaborations on a prokaryotic scaffold. *Plant Physiol* **155**, 1520-1532.

Baumgartner BJ, Rapp JC, Mullet JE. 1989. Plastid transcription activity and DNA copy number increase early in barley chloroplast development. *Plant Physiology* **89**, 1011-1018.

Baumgartner BJ, Rapp JC, Mullet JE. 1993. Plastid Genes Encoding the Transcription/Translation Apparatus Are Differentially Transcribed Early in Barley (Hordeum vulgare) Chloroplast Development (Evidence for Selective Stabilization of psbA mRNA). *Plant Physiol* **101**, 781-791.

Becker A, Lange M. 2010. VIGS--genomics goes functional. *Trends Plant Sci* **15**, 1-4.

Bendich AJ. 1987. Why do chloroplasts and mitochondria contain so many copies of their genome? *Bioessays* **6**, 279-282.

Bendich AJ. 1993. Reaching for the ring: the study of mitochondrial genome structure. *Curr Genet* **24**, 279-290.

Bendich AJ. 1996. Structural analysis of mitochondrial DNA molecules from fungi and plants using moving pictures and pulsed-field gel electrophoresis. *J Mol Biol* **255**, 564-588.

Bendich AJ. 2010. Mitochondrial DNA, chloroplast DNA and the origins of development in eukaryotic organisms. *Biol Direct* **5**, 42.

Bendich AJGLP. 1984. Morphometric analysis of cucurbit mitochondria: The relationship

between chondriome volume and DNA content. *Protoplasma Protoplasma* **119**, 1-7.
Bensasson D, Zhang DX, Hartl DL, Hewitt GM. 2001. Mitochondrial pseudogenes: evolution's misplaced witnesses. *Trends in Ecology & Evolution* **16**, 314-321.
Bergthorsson U, Adams KL, Thomason B, Palmer JD. 2003. Widespread horizontal transfer of mitochondrial genes in flowering plants. *Nature* **424**, 197-201.
Bino RJ, Lanteri S, Verhoeven HA, Kraak HL. 1993. Flow Cytometric Determination of Nuclear Replication Stage in Seed Tissues. *Annals of Botany* **72**, 181-187.
Bowman JL, Drews GN, Meyerowitz EM. 1991. Expression of the Arabidopsis floral homeotic gene AGAMOUS is restricted to specific cell types late in flower development. *Plant Cell* **3**, 749-758.
Bowsher CG, Tobin AK. 2001. Compartmentation of metabolism within mitochondria and plastids. *J Exp Bot* **52**, 513-527.
Braschi E, McBride HM. 2010. Mitochondria and the culture of the Borg: understanding the integration of mitochondrial function within the reticulum, the cell, and the organism. *Bioessays* **32**, 958-966.
Brigneti G, Martin-Hernandez AM, Jin H, Chen J, Baulcombe DC, Baker B, Jones JD. 2004. Virus-induced gene silencing in Solanum species. *Plant J* **39**, 264-272.
Burch-Smith TM, Anderson JC, Martin GB, Dinesh-Kumar SP. 2004. Applications and advantages of virus-induced gene silencing for gene function studies in plants. *Plant Journal* **39**, 734-746.
Burger G, Gray MW, Lang BF. 2003. Mitochondrial genomes: anything goes. *Trends Genet* **19**, 709-716.
Bustin SA, Benes V, Garson JA, Hellemans J, Huggett J, Kubista M, Mueller R, Nolan T, Pfaffl MW, Shipley GL, Vandesompele J, Wittwer CT. 2009. The MIQE guidelines: minimum information for publication of quantitative real-time PCR experiments. *Clin Chem* **55**, 611-622.
Butow RA, Avadhani NG. 2004. Mitochondrial signaling: the retrograde response. *Mol Cell* **14**, 1-15.
Cahoon AB, Cunningham KA, Bollenbach TJ, Stern DB. 2003. Maize BMS cultured cell lines survive with massive plastid gene loss. *Curr Genet* **44**, 104-113.
Cankar K, Stebih D, Dreo T, Zel J, Gruden K. 2006. Critical points of DNA quantification by real-time PCR--effects of DNA extraction method and sample matrix on quantification of genetically modified organisms. *BMC Biotechnol* **6**, 37.
Carling PJ, Cree LM, Chinnery PF. 2011. The implications of mitochondrial DNA copy number regulation during embryogenesis. *Mitochondrion* **11**, 686-692.
Carrie C, Small I. 2013. A reevaluation of dual-targeting of proteins to mitochondria and chloroplasts. *Biochim Biophys Acta* **1833**, 253-259.
Chang YM, Liu WY, Shih AC, Shen MN, Lu CH, Lu MY, Yang HW, Wang TY, Chen SC, Chen SM, Li WH, Ku MS. 2012. Characterizing regulatory and functional differentiation between maize mesophyll and bundle sheath cells by transcriptomic analysis. *Plant Physiol* **160**, 165-177.
Chew O, Whelan J, Millar AH. 2003. Molecular definition of the ascorbate-glutathione cycle in Arabidopsis mitochondria reveals dual targeting of antioxidant defenses in plants. *J Biol Chem* **278**, 46869-46877.
Clifton SW, Minx P, Fauron CMR, Gibson M, Allen JO, Sun H, Thompson M, Barbazuk WB, Kanuganti S, Tayloe C, Meyer L, Wilson RK, Newton KJ. 2004. Sequence and

comparative analysis of the maize NB mitochondrial genome. *Plant Physiology* **136**, 3486-3503.
Coleman AW. 1979. Use of the fluorochrome 4'6-diamidino-2-phenylindole in genetic and developmental studies of chloroplast DNA. *J Cell Biol* **82**, 299-305.
Collura RV, Auerbach MR, Stewart C-B. 1996. A quick, direct method that can differentiate expressed mitochondrial genes from their nuclear pseudogenes. *Current Biology* **6**, 1337-1339.
Cox MM. 2007. Regulation of bacterial RecA protein function. *Crit Rev Biochem Mol Biol* **42**, 41-63.
Cunningham FX, Gantt E. 1998. Genes and enzymes of carotenoid biosynthesis in plants. *Annual Review of Plant Physiology and Plant Molecular Biology* **49**, 557-583.
Cvetkovska M, Vanlerberghe GC. 2012. Alternative oxidase modulates leaf mitochondrial concentrations of superoxide and nitric oxide. *New Phytol* **195**, 32-39.
Dai H, Lo YS, Litvinchuk A, Wang YT, Jane WN, Hsiao LJ, Chiang KS. 2005. Structural and functional characterizations of mung bean mitochondrial nucleoids. *Nucleic Acids Res* **33**, 4725-4739.
Dai Z, Ku M, Edwards GE. 1995. C4 Photosynthesis (The Effects of Leaf Development on the CO2-Concentrating Mechanism and Photorespiration in Maize). *Plant Physiol* **107**, 815-825.
Day A, Madesis P. 2007. DNA replication, recombination, and repair in plastids. *Cell and Molecular Biology of Plastids*, 65-119.
Deaconescu AM, Artsimovitch I, Grigorieff N. 2012. Interplay of DNA repair with transcription: from structures to mechanisms. *Trends Biochem Sci* **37**, 543-552.
Deng XW, Wing RA, Gruissem W. 1989. The chloroplast genome exists in multimeric forms. *Proc Natl Acad Sci U S A* **86**, 4156-4160.
Di Stilio VS, Kramer EM, Baum DA. 2005. Floral MADS box genes and homeotic gender dimorphism in Thalictrum dioicum (Ranunculaceae) - a new model for the study of dioecy. *Plant Journal* **41**, 755-766.
Di Stilio VS, Martin C, Schulfer AF, Connelly CF. 2009. An ortholog of MIXTA-like2 controls epidermal cell shape in flowers of Thalictrum. *New Phytol* **183**, 718-728.
Dinesh-Kumar S, Anandalakshmi R, Marathe R, Schiff M, Liu Y. 2003. Virus-Induced Gene Silencing. *Plant Functional Genomics* **236**, 287 - 293.
du Buy HG, Riley FL. 1967. Hybridization between the nuclear and kinetoplast DNA's of Leishmania enriettii and between nuclear and mitochondrial DNA's of mouse liver. *Proc Natl Acad Sci U S A* **57**, 790-797.
Eberhard S, Drapier D, Wollman FA. 2002. Searching limiting steps in the expression of chloroplast-encoded proteins: relations between gene copy number, transcription, transcript abundance and translation rate in the chloroplast of Chlamydomonas reinhardtii. *Plant J* **31**, 149-160.
Elo A, Lyznik A, Gonzalez DO, Kachman SD, Mackenzie SA. 2003. Nuclear genes that encode mitochondrial proteins for DNA and RNA metabolism are clustered in the Arabidopsis genome. *Plant Cell* **15**, 1619-1631.
Emanuel C, Weihe A, Graner A, Hess WR, Börner T. 2004. Chloroplast development affects expression of phage-type RNA polymerases in barley leaves. *Plant J* **38**, 460-472.
Endress P. 1995. Floral structure and evolution in Ranunculanae. In: Jensen U, Kadereit J, eds. *Systematics and Evolution of the Ranunculiflorae*, Vol. 9: Springer Vienna, 47-61.
Epshtein V, Kamarthapu V, McGary K, Svetlov V, Ueberheide B, Proshkin S, Mironov A, Nudler E. 2014. UvrD facilitates DNA repair by pulling RNA polymerase backwards. *Nature* **505**, 372-377.

Erdei N, Barta C, Hideg E, Boddi B. 2005. Light-induced wilting and its molecular mechanism in epicotyls of dark-germinated pea (*Pisum sativum* L.) seedlings. *Plant Cell Physiol* **46**, 185-191.
Evans IM, Rus AM, Belanger EM, Kimoto M, Brusslan JA. 2010. Dismantling of Arabidopsis thaliana mesophyll cell chloroplasts during natural leaf senescence. *Plant Biol (Stuttg)* **12**, 1-12.
Falkenberg M, Larsson NG, Gustafsson CM. 2007. DNA replication and transcription in mammalian mitochondria. *Annu Rev Biochem* **76**, 679-699.
Fauron C, Casper M, Gao Y, Moore B. 1995. The maize mitochondrial genome: dynamic, yet functional. *Trends Genet* **11**, 228-235.
Fernie AR, Carrari F, Sweetlove LJ. 2004. Respiratory metabolism: glycolysis, the TCA cycle and mitochondrial electron transport. *Curr Opin Plant Biol* **7**, 254-261.
Foyer CH, Noctor G. 2003. Redox sensing and signalling associated with reactive oxygen in chloroplasts, peroxisomes and mitochondria. *Physiologia Plantarum* **119**, 355-364.
Frahm T, Mohamed SA, Bruse P, Gemünd C, Oehmichen M, Meissner C. 2005. Lack of age-related increase of mitochondrial DNA amount in brain, skeletal muscle and human heart. *Mech Ageing Dev* **126**, 1192-1200.
Friedberg EC, Walker GC, Siede W, Wood RD, Schultz RA, Ellenberger T. 2006. *DNA repair and mutagenesis*. Washington, D.C.: Washington, D.C. : ASM Press.
Friso G, Majeran W, Huang M, Sun Q, van Wijk KJ. 2010. Reconstruction of metabolic pathways, protein expression, and homeostasis machineries across maize bundle sheath and mesophyll chloroplasts: large-scale quantitative proteomics using the first maize genome assembly. *Plant Physiol* **152**, 1219-1250.
Fu DQ, Zhu BZ, Zhu HL, Jiang WB, Luo YB. 2005. Virus-induced gene silencing in tomato fruit. *Plant Journal* **43**, 299-308.
Fujie M, Kuroiwa H, Kawano S, Kuroiwa T. 1993. Studies on the behavior of organelles and their nucleoids in the root apical meristem of Arabidopsis thaliana (L.) Col. *Planta* **189**, 443-452.
Fujie M, Kuroiwa H, Kawano S, Mutoh S, Kuroiwa T. 1994. Behavior of organelles and their nucleoids in the shoot apical meristem during leaf development in Arabidopsis thaliana L. *Planta* **194**, 395-405.
Galbraith DW, Harkins KR, Knapp S. 1991. Systemic Endopolyploidy in Arabidopsis thaliana. *Plant Physiol* **96**, 985-989.
Galun E. 2005. RNA silencing in plants. *In Vitro Cellular & Developmental Biology-Plant* **41**, 113-123.
Golczyk H, Greiner S, Wanner G, Weihe A, Bock R, Borner T, Herrmann RG. 2014. Chloroplast DNA in mature and senescing leaves: a reappraisal. *Plant Cell* **26**, 847-854.
Gould B, Kramer E. 2007. Virus-induced gene silencing as a tool for functional analyses in the emerging model plant Aquilegia (columbine, Ranunculaceae). *Plant methods* **3**, 6.
Gould SB, Waller RF, McFadden GI. 2008. Plastid evolution. *Annu Rev Plant Biol* **59**, 491-517.
Gray MW. 2011. The incredible shrinking organelle. *EMBO Rep* **12**, 873.
Griffiths LM, Swartzlander D, Meadows KL, Wilkinson KD, Corbett AH, Doetsch PW. 2009. Dynamic Compartmentalization of Base Excision Repair Proteins in Response to Nuclear and Mitochondrial Oxidative Stress. *MOLECULAR AND CELLULAR BIOLOGY* **29**, 794-807.
Guo FQ, Crawford NM. 2005. Arabidopsis nitric oxide synthase1 is targeted to mitochondria and protects against oxidative damage and dark-induced senescence. *Plant Cell* **17**, 3436-3450.

Guo W, Jiang L, Bhasin S, Khan SM, Swerdlow RH. 2009. DNA extraction procedures meaningfully influence qPCR-based mtDNA copy number determination. *Mitochondrion* **9**, 261-265.
Gutman BL, Niyogi KK. 2009. Evidence for base excision repair of oxidative DNA damage in chloroplasts of Arabidopsis thaliana. *J Biol Chem* **284**, 17006-17012.
Hashimoto K, Kokubun S, Itoi E, Roach HI. 2007. Improved quantification of DNA methylation using methylation-sensitive restriction enzymes and real-time PCR. *Epigenetics* **2**, 86-91.
Hazkani-Covo E, Zeller RM, Martin W. 2010. Molecular Poltergeists: Mitochondrial DNA Copies *(numts)* in Sequenced Nuclear Genomes. *Plos Genetics* **6**, e1000834.
Heinze B. 2007. A database of PCR primers for the chloroplast genomes of higher plants. *Plant methods* **3**, 4.
Hibberd JM, Sheehy JE, Langdale JA. 2008. Using C4 photosynthesis to increase the yield of rice-rationale and feasibility. *Curr Opin Plant Biol* **11**, 228-231.
Hileman LC, Drea S, de Martino G, Litt A, Irish VF. 2005. Virus-induced gene silencing is an effective tool for assaying gene function in the basal eudicot species Papaver somniferum (opium poppy). *Plant Journal* **44**, 334-341.
Hinkley D. 2006. Thalictrum: an overview. *Plantsman* **5**, 178-184.
Hotto AM, Germain A, Stern DB. 2012. Plastid non-coding RNAs: emerging candidates for gene regulation. *Trends Plant Sci* **17**, 737-744.
Huang CY, Grunheit N, Ahmadinejad N, Timmis JN, Martin W. 2005. Mutational decay and age of chloroplast and mitochondrial genomes transferred recently to angiosperm nuclear chromosomes. *Plant Physiology* **138**, 1723-1733.
Hunt S. 2003. Measurements of photosynthesis and respiration in plants. *Physiol Plant* **117**, 314-325.
Hunter SE, Jung D, Di Giulio RT, Meyer JN. 2010. The QPCR assay for analysis of mitochondrial DNA damage, repair, and relative copy number. *Methods* **51**, 444-451.
Jacqmard A, De Veylder L, Segers G, de Almeida Engler J, Bernier G, Van Montagu M, Inze D. 1999. Expression of CKS1At in Arabidopsis thaliana indicates a role for the protein in both the mitotic and the endoreduplication cycle. *Planta* **207**, 496-504.
Jasbeer K SRMGFCYK. 2009. Real-time PCR evaluation of seven DNA extraction methods for the purpose of GMO analysis. *ASEAN Food J. ASEAN Food Journal* **16**, 329-341.
Jeon H, Jin YM, Choi MH, Lee H, Kim M. 2013. Chloroplast-targeted bacterial RecA proteins confer tolerance to chloroplast DNA damage by methyl viologen or UV-C radiation in tobacco (Nicotiana tabacum) plants. *Physiol Plant* **147**, 218-233.
Kanai R, Edwards GE. 1973. Separation of mesophyll protoplasts and bundle sheath cells from maize leaves for photosynthetic studies. *Plant Physiology* **51**, 1133-1137.
Karki S, Rizal G, Quick WP. 2013. Improvement of photosynthesis in rice (Oryza sativa L.) by inserting the C4 pathway. *Rice (N Y)* **6**, 28.
Kelliher T, Walbot V. 2014. Maize germinal cell initials accommodate hypoxia and precociously express meiotic genes. *Plant J*.
Khamidullina EA, Gromova AS, Lutsky VI, Owen NL. 2006. Natural products from medicinal plants: non-alkaloidal natural constituents of the Thalictrum species. *Natural Product Reports* **23**, 117-129.
Kim M, Christopher DA, Mullet JE. 1993. Direct evidence for selective modulation of psbA, rpoA, rbcL and 16S RNA stability during barley chloroplast development. *Plant Mol Biol* **22**,

447-463.
Kleine T, Maier UG, Leister D. 2009. DNA Transfer from Organelles to the Nucleus: The Idiosyncratic Genetics of Endosymbiosis. *Annual Review of Plant Biology* **60**, 115-138.
Kramer E, Holappa L, Gould B, Jaramillo M, Setnikov D, Santiago P. 2007. Elaboration of B gene function to include the identity of novel floral organs in the lower eudicot Aquilegia (Ranunculaceae). *Plant Cell* **Epub ahead of print**.
Kramer EM, Di Stilio VS, Schluter PM. 2003. Complex patterns of gene duplication in the APETALA3 and PISTILLATA lineages of the Ranunculaceae. *International Journal of Plant Sciences* **164**, 1-11.
Kramer EM, Jaramillo MA, Di Stilio VS. 2004. Patterns of gene duplication and functional evolution during the diversification of the AGAMOUS subfamily of MADS box genes in angiosperms. *Genetics* **166**, 1011-1023.
Ku SB, Gutierrez M, Kanai R, Edwards GE, Ku SB. 1974. Photosynthesis in mesophyll protoplasts and bundle sheath cells of various types of C4 plants II. Chlorophyll and hill reaction studies. *Zeitschrift Fur Pflanzenphysiologie* **72**, 320-337.
Kumagai MH, Donson J, Della-Cioppa G, Harvey D. 1995. Cytoplasmic inhibition of carotenoid biosynthesis with virus-derived RNA. *Proceedings-National Academy of Sciences, USA* **92**, 1679.
Kumar RA, Bendich AJ. 2011. Distinguishing authentic mitochondrial and plastid DNAs from similar DNA sequences in the nucleus using the polymerase chain reaction. *Curr Genet* **57**, 287-295.
Kumar RA, Oldenburg DJ, Bendich AJ. 2014. Changes in DNA damage, molecular integrity, and copy number for plastid DNA and mitochondrial DNA during maize development. *J Exp Bot, in press*.
Kuroiwa T. 1991. The replication, differentiation, and inheritance of plastids with emphasis on the concept of organelle nuclei. *International Review of Cytology-a Survey of Cell Biology* **128**, 1-162.
Kuroiwa T, Fujje M, Kuroiwa H. 1992. Studies on the Behavior of Mitochondrial DNA: Synthesis of Mitochondrial DNA Occurs Actively in a Specific Region just above the Quiescent Center in the Root Meristem of *Pelargonium Zonale*. *J Cell Sci* **101**, 483-493.
Lamppa G, Bendich A. 1984. Changes in mitochondrial DNA levels during development of pea (*Pisum sativum* L.). *Planta* **162**, 463-468.
Lamppa GK, Bendich AJ. 1979. Chloroplast DNA Sequence Homologies among Vascular Plants. *Plant Physiol* **63**, 660-668.
Langdale JA. 2011. C4 cycles: past, present, and future research on C4 photosynthesis. *Plant Cell* **23**, 3879-3892.
Lawrence ME, Possingham JV. 1986. Direct measurement of femtogram amounts of DNA in cells and chloroplasts by quantitative microspectrofluorometry. *J Histochem Cytochem* **34**, 761-768.
Li P, Ponnala L, Gandotra N, Wang L, Si Y, Tausta SL, Kebrom TH, Provart N, Patel R, Myers CR, Reidel EJ, Turgeon R, Liu P, Sun Q, Nelson T, Brutnell TP. 2010. The developmental dynamics of the maize leaf transcriptome. *Nat Genet* **42**, 1060-1067.
Li WM, Ruf S, Bock R. 2006. Constancy of organellar genome copy numbers during leaf development and senescence in higher plants. *Molecular Genetics and Genomics* **275**, 185-192.
Liere K, Weihe A, Börner T. 2011. The transcription machineries of plant mitochondria and chloroplasts: Composition, function, and regulation. *J Plant Physiol* **168**, 1345-1360.

Liscombe DK, Ziegler J, Schmidt J, Ammer C, Facchini PJ. 2009. Targeted metabolite and transcript profiling for elucidating enzyme function: isolation of novel N-methyltransferases from three benzylisoquinoline alkaloid-producing species. *Plant J* **60**, 729-743.
Liu P, Demple B. 2010. DNA repair in mammalian mitochondria: Much more than we thought? *Environ Mol Mutagen* **51**, 417-426.
Liu Y, Nakayama N, Schiff M, Litt A, Irish VF, Dinesh-Kumar SP. 2004. Virus induced gene silencing of a DEFICIENS ortholog in Nicotiana benthamiana. *Plant Molecular Biology* **54**, 701-711.
Liu YL, Schiff M, Dinesh-Kumar SP. 2002. Virus-induced gene silencing in tomato. *Plant Journal* **31**, 777-786.
Livak KJ, Schmittgen TD. 2001. Analysis of relative gene expression data using real-time quantitative PCR and the 2(-Delta Delta C(T)) method. *Methods* **25**, 402-408.
Lo YS, Hsiao LJ, Cheng N, Litvinchuk A, Dai H. 2011. Characterization of the structure and DNA complexity of mung bean mitochondrial nucleoids. *Mol Cells* **31**, 217-224.
Logan DC. 2006. Plant mitochondrial dynamics. *Biochim Biophys Acta* **1763**, 430-441.
Lonsdale DM, Hodge TP, Fauron CM-R. 1984. The physical map and organization of the mitochondrial genome from the fertile cytoplasm of maize. *Nucleic Acids Research* **12**, 9249-9261.
Lough AN, Roark LM, Kato A, Ream TS, Lamb JC, Birchler JA, Newton KJ. 2008. Mitochondrial DNA transfer to the nucleus generates extensive insertion site variation in maize. *Genetics* **178**, 47-55.
Lucchesi JC. 1973. Dosage Compensation in Drosophila. *Annual Review of Genetics* **7**, 225-237.
Lutskii V, Gromova A, Khamidullina E, Owen N. 2005. Structural Studies and Biological Activity of Plant Triterpenoids from the Thalictrum Genus. *Chemistry of Natural Compounds* **41**, 117-140.
M T. 1995. *Ranunculaceae*. Berlin: Duncker & Humblot.
Maier RM, Neckermann K, Igloi GL, Kossel H. 1995. Complete sequence of the maize chloroplast genome: gene content, hotspots of divergence and fine tuning of genetic information by transcript editing. *Journal of Molecular Biology* **251**, 614-628.
Majeran W, Cai Y, Sun Q, van Wijk KJ. 2005. Functional differentiation of bundle sheath and mesophyll maize chloroplasts determined by comparative proteomics. *Plant Cell* **17**, 3111-3140.
Majeran W, Friso G, Asakura Y, Qu X, Huang M, Ponnala L, Watkins KP, Barkan A, van Wijk KJ. 2012. Nucleoid-enriched proteomes in developing plastids and chloroplasts from maize leaves: a new conceptual framework for nucleoid functions. *Plant Physiol* **158**, 156-189.
Majeran W, van Wijk KJ. 2009. Cell-type-specific differentiation of chloroplasts in C4 plants. *Trends in Plant Science* **14**, 100-109.
Majeran W, Zybailov B, Ytterberg AJ, Dunsmore J, Sun Q, van Wijk KJ. 2008. Consequences of C-4 differentiation for chloroplast membrane Proteomes in maize mesophyll and bundle sheath cells. *Molecular & Cellular Proteomics* **7**, 1609-1638.
Manning JE, Richards OC. 1972. Synthesis and turnover of *Euglena gracilis* nuclear and chlorplast deoxyribonucleic acid. *Biochemistry* **11**, 2036-2043.
Maurino VG, Peterhansel C. 2010. Photorespiration: current status and approaches for metabolic engineering. *Curr Opin Plant Biol* **13**, 249-256.
Millar AH, Whelan J, Soole KL, Day DA. 2011. Organization and Regulation of Mitochondrial Respiration in Plants. *Annual Review of Plant Biology* **62**, 79-104.

Miller-Messmer M, Kuhn K, Bichara M, Le Ret M, Imbault P, Gualberto JM. 2012. RecA-dependent DNA repair results in increased heteroplasmy of the Arabidopsis mitochondrial genome. *Plant Physiol* **159**, 211-226.
Miyamura S, Kuroiwa T, Nagata T. 1990. Multiplication and Differentiation of Plastid Nucleoids during Development of Chloroplasts and Etioplasts from Proplastids in Triticum aestivum. *Plant and Cell Physiology* **31**, 597-602.
Miyamura S, Nagata T, Kuroiwa T. 1986. Quantitative fluorescence microscopy on dynamic changes of plastid nucleoids during wheat development. *Protoplasma* **133**, 66-72.
Moller IM. 2001. Plant mitochondria and oxidative stress: Electron Transport, NADPH Turnover, and Metabolism of Reactive Oxygen Species. *Annu Rev Plant Physiol Plant Mol Biol* **52**, 561-591.
Mulo P, Sakurai I, Aro EM. 2012. Strategies for psbA gene expression in cyanobacteria, green algae and higher plants: from transcription to PSII repair. *Biochim Biophys Acta* **1817**, 247-257.
Naciri Y, Manen JF. 2009. Potential DNA transfer from the chloroplast to the nucleus in Eryngium alpinum. *Molecular Ecology Resources* **10**, 728-731.
Nagamatsu A, Masuta C, Senda M, Matsuura H, Kasai A, Hong S, Kitamura K, Abe J, Kanazawa A. 2007. Functional analysis of soybean genes involved in flavonoid biosynthesis by virus-induced gene silencing. *Plant Biotechnology Journal* **5**, 778-790.
Nelson T. 2011. The grass leaf developmental gradient as a platform for a systems understanding of the anatomical specialization of C4 leaves. *Journal of Experimental Botany* **62**, 3039-3048.
Noutsos C, Richly E, Leister D. 2005. Generation and evolutionary fate of insertions of organelle DNA in the nuclear genomes of flowering plants. *Genome Research* **15**, 616-628.
O P. 1995. *Pollination biology*. Berlin: Duncker & Humblot.
Oda K, Yamato K, Ohta E, Nakamura Y, Takemura M, Nozato N, Akashi K, Kanegae T, Ogura Y, Kohchi T, Ohyama K. 1992. Complete nucleotide sequence of the mitochondrial DNA from a liverwort,Marchantia polymorpha. *Plant Molecular Biology Reporter* **10**, 105-163.
Oldenburg DJ, Bendich AJ. 1996. Size and Structure of Replicating Mitochondrial DNA in Cultured Tobacco Cells. *Plant Cell* **8**, 447-461.
Oldenburg DJ, Bendich AJ. 1998. The structure of mitochondrial DNA from the liverwort, Marchantia polymorpha. *J Mol Biol* **276**, 745-758.
Oldenburg DJ, Bendich AJ. 2001. Mitochondrial DNA from the liverwort Marchantia polymorpha: circularly permuted linear molecules, head-to-tail concatemers, and a 5' protein. *J Mol Biol* **310**, 549-562.
Oldenburg DJ, Bendich AJ. 2004a. Changes in the structure of DNA molecules and the amount of DNA per plastid during chloroplast development in maize. *J Mol Biol* **344**, 1311-1330.
Oldenburg DJ, Bendich AJ. 2004b. Most chloroplast DNA of maize seedlings in linear molecules with defined ends and branched forms. *J Mol Biol* **335**, 953-970.
Oldenburg DJ, Kumar RA, Bendich AJ. 2013. The amount and integrity of mtDNA in maize decline with development. *Planta* **237**, 603-617.
Oldenburg DJ, Rowan BA, Kumar RA, Bendich AJ. 2014. On the fate of plastid DNA molecules during leaf development: response to the Golczyk et al. Commentary. *Plant Cell* **26**, 855-861.
Oldenburg DJ, Rowan BA, Zhao L, Walcher CL, Schleh M, Bendich AJ. 2006. Loss or retention of chloroplast DNA in maize seedlings is affected by both light and genotype. *Planta* **225**, 41-55.
Orashakova S, Lange M, Lange S, Wege S, Becker A. 2009. The CRABS CLAW ortholog

from California poppy (Eschscholzia californica, Papaveraceae), EcCRC, is involved in floral meristem termination, gynoecium differentiation and ovule initiation. *Plant J* **58**, 682-693.
Palmer JD, Herbon LA. 1986. Tricircular mitochondrial genomes of Brassica and Raphanus: reversal of repeat configurations by inversion. *Nucleic Acids Res* **14**, 9755-9764.
Parent J-S, Lepage E, Brisson N. 2011. Divergent Roles for the Two PolI-Like Organelle DNA Polymerases of Arabidopsis. *Plant Physiology* **156**, 254-262.
Pesaresi P, Schneider A, Kleine T, Leister D. 2007. Interorganellar communication. *Curr Opin Plant Biol* **10**, 600-606.
Pfaffl MW. 2001. A new mathematical model for relative quantification in real-time RT-PCR. *Nucleic Acids Research* **29**, 6.
Poulton J, Chiaratti MR, Meirelles FV, Kennedy S, Wells D, Holt IJ. 2010. Transmission of mitochondrial DNA diseases and ways to prevent them. *PLoS Genet* **6**.
Preuten T, Cincu E, Fuchs J, Zoschke R, Liere K, Börner T. 2010. Fewer genes than organelles: extremely low and variable gene copy numbers in mitochondria of somatic plant cells. *Plant J* **64**, 948-959.
Prikryl J, Watkins KP, Friso G, van Wijk KJ, Barkan A. 2008. A member of the Whirly family is a multifunctional RNA- and DNA-binding protein that is essential for chloroplast biogenesis. *Nucleic Acids Research* **36**, 5152-5165.
Pyke K. 2009. *Plastid biology*. Cambridge, UK; New York: Cambridge University Press.
Quesada V, Sarmiento-Manus R, Gonzalez-Bayon R, Hricova A, Perez-Marcos R, Gracia-Martinez E, Medina-Ruiz L, Leyva-Diaz E, Ponce MR, Micol JL. 2011. Arabidopsis RUGOSA2 encodes an mTERF family member required for mitochondrion, chloroplast and leaf development. *Plant J* **68**, 738-753.
Ratcliff F, Martin-Hernandez AM, Baulcombe DC. 2001. Tobacco rattle virus as a vector for analysis of gene function by silencing. *Plant Journal* **25**, 237-245.
Ravi V KJPTAKKP. 2008. An update on chloroplast genomes. *Plant Syst. Evol. Plant Systematics and Evolution* **271**, 101-122.
Renner T, Bragg J, Driscoll HE, Cho J, Jackson AO, Specht CD. 2009. Virus-induced gene silencing in the culinary ginger (Zingiber officinale): an effective mechanism for down-regulating gene expression in tropical monocots. *Mol Plant* **2**, 1084-1094.
Rhoads DM, Umbach AL, Subbaiah CC, Siedow JN. 2006. Mitochondrial reactive oxygen species. Contribution to oxidative stress and interorganellar signaling. *Plant Physiol* **141**, 357-366.
Ribas-Carbo M, Flexas J, Robinson SA a, GGB. T. 2010. In vivo measurement of plant respiration. In: Taiz L, E Z, eds. *A companion to plant physiology*.
Richards OC, Ryan RS. 1974. Synthesis and turnover of *Euglena gracilis* mitochondrial DNA. *J Mol Biol* **82**, 57-75.
Richardson AO, Palmer JD. 2007. Horizontal gene transfer in plants. *J Exp Bot* **58**, 1-9.
Roark LM, Hui Y, Donnelly L, Birchler JA, Newton KJ. 2010. Recent and Frequent Insertions of Chloroplast DNA into Maize Nuclear Chromosomes. *Cytogenetic and Genome Research* **129**, 17-23.
Robertson D. 2004. VIGS vectors for gene silencing: Many targets, many tools. *Annual Review of Plant Biology* **55**, 495-519.
Rogers SO, Bendich AJ. 1988a. Extraction of DNA from plant tissues. *Plant Molecular Biology Manual*, Vol. A61, 10.
Rogers SO, Bendich AJ. 1988b. Extraction of DNA from plant tissues. *Plant Molecular*

Biology Manual **A6**, 1:10.
Roussell DL, Thompson DL, Pallardy SG, Miles D, Newton KJ. 1991. Chloroplast Structure and Function Is Altered in the NCS2 Maize Mitochondrial Mutant. *Plant Physiol* **96**, 232-238.
Rowan BA, Bendich AJ. 2009. The loss of DNA from chloroplasts as leaves mature: fact or artefact? *Journal of Experimental Botany* **60**, 3005-3010.
Rowan BA, Bendich AJ. 2011. Isolation, quantification, and analysis of chloroplast DNA. *Methods Mol Biol* **774**, 151-170.
Rowan BA, Oldenburg DJ, Bendich AJ. 2004. The demise of chloroplast DNA in Arabidopsis. *Current Genetics* **46**, 176-181.
Rowan BA, Oldenburg DJ, Bendich AJ. 2009. A multiple-method approach reveals a declining amount of chloroplast DNA during development in Arabidopsis. *BMC Plant Biol* **9**, 3.
Rowan BA, Oldenburg DJ, Bendich AJ. 2010. RecA maintains the integrity of chloroplast DNA molecules in Arabidopsis. *J Exp Bot* **61**, 2575-2588.
Sage RF, Khoshravesh R, Sage TL. 2014. From proto-Kranz to C4 Kranz: building the bridge to C4 photosynthesis. *Journal of Experimental Botany*.
Sakamoto W, Miyagishima SY, Jarvis P. 2008. Chloroplast biogenesis: control of plastid development, protein import, division and inheritance. *Arabidopsis Book* **6**, e0110.
Samanani N, Park SU, Facchini PJ. 2002. In vitro regeneration and genetic transformation of the berberine-producing plant, Thalictrum flavum ssp glaucum. *Physiologia Plantarum* **116**, 79-86.
Sawers R, Liu P, Anufrikova K, Hwang JG, Brutnell T. 2007. A multi-treatment experimental system to examine photosynthetic differentiation in the maize leaf. *BMC Genomics* **8**, 12.
Schnable PS, Ware D, Fulton RS, Stein JC, Wei FS, Pasternak S, Liang CZ, Zhang JW, Fulton L, Graves TA, Minx P, Reily AD, Courtney L, Kruchowski SS, Tomlinson C, Strong C, Delehaunty K, Fronick C, Courtney B, Rock SM, Belter E, Du FY, Kim K, Abbott RM, Cotton M, Levy A, Marchetto P, Ochoa K, Jackson SM, Gillam B, Chen WZ, Yan L, Higginbotham J, Cardenas M, Waligorski J, Applebaum E, Phelps L, Falcone J, Kanchi K, Thane T, Scimone A, Thane N, Henke J, Wang T, Ruppert J, Shah N, Rotter K, Hodges J, Ingenthron E, Cordes M, Kohlberg S, Sgro J, Delgado B, Mead K, Chinwalla A, Leonard S, Crouse K, Collura K, Kudrna D, Currie J, He RF, Angelova A, Rajasekar S, Mueller T, Lomeli R, Scara G, Ko A, Delaney K, Wissotski M, Lopez G, Campos D, Braidotti M, Ashley E, Golser W, Kim H, Lee S, Lin JK, Dujmic Z, Kim W, Talag J, Zuccolo A, Fan C, Sebastian A, Kramer M, Spiegel L, Nascimento L, Zutavern T, Miller B, Ambroise C, Muller S, Spooner W, Narechania A, Ren LY, Wei S, Kumari S, Faga B, Levy MJ, McMahan L, Van Buren P, Vaughn MW, Ying K, Yeh CT, Emrich SJ, Jia Y, Kalyanaraman A, Hsia AP, Barbazuk WB, Baucom RS, Brutnell TP, Carpita NC, Chaparro C, Chia JM, Deragon JM, Estill JC, Fu Y, Jeddeloh JA, Han YJ, Lee H, Li PH, Lisch DR, Liu SZ, Liu ZJ, Nagel DH, McCann MC, SanMiguel P, Myers AM, Nettleton D, Nguyen J, Penning BW, Ponnala L, Schneider KL, Schwartz DC, Sharma A, Soderlund C, Springer NM, Sun Q, Wang H, Waterman M, Westerman R, Wolfgruber TK, Yang LX, Yu Y, Zhang LF, Zhou SG, Zhu Q, Bennetzen JL, Dawe RK, Jiang JM, Jiang N, Presting GG, Wessler SR, Aluru S, Martienssen RA, Clifton SW, McCombie WR, Wing RA, Wilson RK. 2009. The B73 Maize Genome: Complexity, Diversity, and Dynamics. *Science* **326**, 1112-1115.
Schneider CA, Rasband WS, Eliceiri KW. 2012. NIH Image to ImageJ: 25 years of image

analysis. *Nat Methods* **9**, 671-675.
Schwarzlander M, Finkemeier I. 2013. Mitochondrial energy and redox signaling in plants. *Antioxid Redox Signal* **18**, 2122-2144.
Segui-Simarro JM, Coronado MJ, Staehelin LA. 2008. The mitochondrial cycle of Arabidopsis shoot apical meristem and leaf primordium meristematic cells is defined by a perinuclear tentaculate/cage-like mitochondrion. *Plant Physiol* **148**, 1380-1393.
Sellden G, Leech RM. 1981. Localization of DNA in Mature and Young Wheat Chloroplasts Using the Fluorescent Probe 4'-6-Diamidino-2-phenylindole. *Plant Physiol* **68**, 731-734.
Shaver JM, Oldenburg DJ, Bendich AJ. 2006. Changes in chloroplast DNA during development in tobacco, Medicago truncatula, pea, and maize. *Planta* **224**, 72-82.
Shaver JM, Oldenburg DJ, Bendich AJ. 2008. The structure of chloroplast DNA molecules and the effects of light on the amount of chloroplast DNA during development in Medicago truncatula. *Plant Physiol* **146**, 1064-1074.
Sheahan MB, McCurdy DW, Rose RJ. 2005. Mitochondria as a connected population: ensuring continuity of the mitochondrial genome during plant cell dedifferentiation through massive mitochondrial fusion. *Plant J* **44**, 744-755.
Shedge V, Arrieta-Montiel M, Christensen AC, Mackenzie SA. 2007. Plant mitochondrial recombination surveillance requires unusual RecA and MutS homologs. *Plant Cell* **19**, 1251-1264.
Shokolenko I, Venediktova N, Bochkareva A, Wilson GL, Alexeyev MF. 2009. Oxidative stress induces degradation of mitochondrial DNA. *Nucleic Acids Res* **37**, 2539-2548.
Singersam J, Lebon JM, Tanguay RL, Riggs AD. 1990. A quantitative HpaII-PCR assay to measure methylation of DNA from a small number of cells. *Nucleic Acids Research* **18**, 687-687.
Smith DR, Crosby K, Lee RW. 2011. Correlation between nuclear plastid DNA abundance and plastid number supports the limited transfer window hypothesis. *Genome Biol Evol* **3**, 365-371.
Soltis PS, Soltis DE. 2004. The origin and diversification of angiosperms. *Am J Bot* **91**, 1614-1626.
Solymosi K, Schoefs B. 2010. Etioplast and etio-chloroplast formation under natural conditions: the dark side of chlorophyll biosynthesis in angiosperms. *Photosynth Res* **105**, 143-166.
Song H, Buhay JE, Whiting MF, Crandall KA. 2008. Many species in one: DNA barcoding overestimates the number of species when nuclear mitochondrial pseudogenes are coamplified. *Proc Natl Acad Sci U S A* **105**, 13486-13491.
Sorenson MD, Quinn TW. 1998. Numts: A challenge for avian systematics and population biology. *Auk* **115**, 214-221.
Spitzer B, Ben Zvi MM, Ovadis M, Marhevka E, Barkai O, Edelbaum O, Marton I, Masci T, Alon M, Morin S, Rogachev I, Aharoni A, Vainstein A. 2007. Reverse genetics of floral scent: Application of tobacco rattle virus-based gene silencing in petunia. *Plant Physiology* **145**, 1241-1250.
Stern DB, Hanson MR, Barkan A. 2004. Genetics and genomics of chloroplast biogenesis: maize as a model system. *Trends in Plant Science* **9**, 293-301.
Stern DB, Palmer JD. 1986. Tripartite mitochondrial genome of spinach: physical structure, mitochondrial gene mapping, and locations of transposed chloroplast DNA sequences. *Nucleic Acids Res* **14**, 5651-5666.
Sylvester AW, Cande WZ, Freeling M. 1990. Division and differentiation during normal and liguleless-1 maize leaf development. *Development (Cambridge, England)* **110**, 985-1000.
Tahbaz N, Subedi S, Weinfeld M. 2012. Role of polynucleotide kinase/phosphatase in

mitochondrial DNA repair. *Nucleic Acids Res* **40**, 3484-3495.
Takano H, Onoue K, Kawano S. 2010. Mitochondrial fusion and inheritance of the mitochondrial genome. *J Plant Res* **123**, 131-138.
Theissen G, Becker A, Di Rosa A, Kanno A, Kim JT, Munster T, Winter KU, Saedler H. 2000. A short history of MADS-box genes in plants. *Plant Mol Biol* **42**, 115-149.
Timmis JN, Ayliffe MA, Huang CY, Martin W. 2004. Endosymbiotic gene transfer: Organelle genomes forge eukaryotic chromosomes. *Nature Reviews Genetics* **5**, 123-U116.
Timmis JN, Scott NS. 1983. Sequence homology between spinach nuclear and chloroplast genomes. *Nature* **305**, 65-67.
Toshoji H, Katsumata T, Takusagawa M, Yusa Y, Sakai A. 2012. Effects of chloroplast dysfunction on mitochondria: white sectors in variegated leaves have higher mitochondrial DNA levels and lower dark respiration rates than green sectors. *Protoplasma* **249**, 805-817.
Udy DB, Belcher S, Williams-Carrier R, Gualberto JM, Barkan A. 2012. Effects of reduced chloroplast gene copy number on chloroplast gene expression in maize. *Plant Physiol* **160**, 1420-1431.
Vinod K. 2004. Total genomic DNA extraction, quality check and quantitation. *training programme on "Classical and modern plant breeding techniques–A hands on training*, 109-121.
Wallace DC, Stugard C, Murdock D, Schurr T, Brown MD. 1997. Ancient mtDNA sequences in the human nuclear genome: A potential source of errors in identifying pathogenic mutations. *Proc Natl Acad Sci U S A* **94**, 14900-14905.
Wang X, Cao A, Yu C, Wang D, Wang X, Chen P. 2010. Establishment of an effective virus induced gene silencing system with BSMV in Haynaldia villosa. *Mol Biol Rep* **37**, 967-972.
Wege S, Scholz A, Gleissberg S, Becker A. 2007. Highly efficient virus-induced gene silencing (VIGS) in california poppy (Eschscholzia californica): An evaluation of VIGS as a strategy to obtain functional data from non-model plants. *Annals of Botany* **100**, 641-649.
Weigel DGJ. 2002. *Arabidopsis : a laboratory manual*. Cold Spring Harbor, N.Y.: Cold Spring Harbor Laboratory Press.
Williams BPASHJM. 2012. Molecular evolution of genes recruited into C4 photosynthesis. *Trends in Plant Science Trends in Plant Science* **17**, 213-220.
Woloszynska M. 2010. Heteroplasmy and stoichiometric complexity of plant mitochondrial genomes--though this be madness, yet there's method in't. *J Exp Bot* **61**, 657-671.
Woo KC, Pyliotis NA, Downton WJS. 1971. Thylakoid aggregation and chlorophyll-a/chlorophyll-b ratio in C4-plants. *Zeitschrift Fur Pflanzenphysiologie* **64**, 400-413.
Woodson JD, Chory J. 2008. Coordination of gene expression between organellar and nuclear genomes. *Nat Rev Genet* **9**, 383-395.
Wright AF, Murphy MP, Turnbull DM. 2009. Do organellar genomes function as long-term redox damage sensors? *Trends Genet* **25**, 253-261.
Yakes FM, Van Houten B. 1997. Mitochondrial DNA damage is more extensive and persists longer than nuclear DNA damage in human cells following oxidative stress. *Proc Natl Acad Sci U S A* **94**, 514-519.
Yamada M, Kawasaki M, Sugiyama T, Miyake H, Taniguchi M. 2009. Differential positioning of C4 mesophyll and bundle sheath chloroplasts: aggregative movement of C4 mesophyll chloroplasts in response to environmental stresses. *Plant Cell Physiol* **50**, 1736-1749.
Yao YG, Kong QP, Salas A, Bandelt HJ. 2008. Pseudomitochondrial genome haunts disease studies. *Journal of Medical Genetics* **45**, 769-772.
Ye J, Qu J, Bui HT, Chua NH. 2009. Rapid analysis of Jatropha curcas gene functions by

virus-induced gene silencing. *Plant Biotechnol J* **7**, 964-976.
Yoshida K, Terashima I, Noguchi K. 2011. How and why does mitochondrial respiratory chain respond to light? *Plant Signal Behav* **6**, 864-866.
Zelitch I, Schultes NP, Peterson RB, Brown P, Brutnell TP. 2009. High glycolate oxidase activity is required for survival of maize in normal air. *Plant Physiol* **149**, 195-204.
Zhelyazkova P, Sharma CM, Förstner KU, Liere K, Vogel J, Börner T. 2012. The primary transcriptome of barley chloroplasts: numerous noncoding RNAs and the dominating role of the plastid-encoded RNA polymerase. *Plant Cell* **24**, 123-136.
Zheng Q, Oldenburg DJ, Bendich AJ. 2011. Independent effects of leaf growth and light on the development of the plastid and its DNA content in *Zea* species. *J Exp Bot* **62**, 2715-2730.
Zoschke R, Liere K, Börner T. 2007. From seedling to mature plant: Arabidopsis plastidial genome copy number, RNA accumulation and transcription are differentially regulated during leaf development. *Plant Journal* **50**, 710-722.

VITA

Rachana Kumar was born and grew up in Pune, India where she attended school before graduating from University of Pune in 2002 with Masters in Botany. She was exposed to world of amazing plants by her mentor, Hema Sane, who also served as a role model for her. After graduation, she worked as a lecturer in Botany for undergraduates and later, served as a subject expert for a software company making educational software. She also gained research experience at International Crops Research Institute for Semi-Arid Tropics and Bhabha Atomic Research Center in India and in Carnegie Institution in USA, before being accepted into the Biology graduate program at the University of Washington in 2007. While in school, she served as a docent for green house and medicinal herb garden at University of Washington. She was very passionate about research and learning new things. Besides research, she enjoys spending time with her loving husband, Ajay Kumar and with her son, Ishan Kumar. She also enjoys hiking and gardening.